Isotopic tracing of fluids sources and transfer in the crust

Carolina Dantas Cardoso

Thèse

Présentée et soutenue publiquement pour l'obtention du titre de

Docteur de l'Université de Lorraine

Mention : Géosciences

par Carolina DANTAS CARDOSO

Sous la direction de Raphaël PIK

Isotopic tracing of fluids sources and transfer in the crust

Traçage isotopique des sources de fluides et des leur transfert dans la croûte

---

17 juillet 2023

Membres du jury :

Directeur(s) de thèse :
Dr. Raphaël PIK, CNRS, Centre de Recherches Pétrographiques et Géochimiques (France)

Co-encadrant :
Dr. Antonio CARACAUSI, Istituto Nazionale di Geofisica e Vulcanologia - Sezione di Palermo (Italia)
Prof. Bernard MARTY, Université de Lorraine, Centre de Recherches Pétrographiques et Géochimiques (France) (invité)

Président de jury :
Prof. Manuel MOREIRA, Université d'Orléans (France)

Rapporteurs :
Prof. Daniele PINTI, Université du Québec à Montréal (Canada)
Prof. Fin STUART, University of Glasgow (UK)

Examinateurs :
Dr. Evelyn FÜRI, CNRS, Centre de Recherches Pétrographiques et Géochimiques (France)
Prof. Manuel MOREIRA, Université d'Orléans (France)

Membres invités :
Prof. Bernard MARTY, Université de Lorraine, Centre de Recherches Pétrographiques et Géochimiques (France)

Acknowledgments

First, I'd like to thank my thesis supervisor (Raphaël) and co-supervisors (Bernard and Antonio) for the confidence when hiring me for this project and for all the guidance during the PhD - including the scientific discussions and orientations on how to communicate the findings.

I would like to thank Daniele Pinti, Fin Stuart, Evelyn Füri, and Manuel Moreira for accepting the invitation to be part of my jury.

I'm extremely grateful for Laurent's teachings and patience while helping me with the SFT Air line, since the beginning (when the method was still alien to me) until now. Bouch as well, for helping with the small and constant emergencies in the purification line, and Allan for the help with the Qtegra bugs.

I'm thankful for the whole CRPG staff, specially Bruno (Porcu) and Joëlle (Guerrier) for the help with the multiple shipments of samples and supplies to Iceland; Pierre (Baillot) for the welding of the thin copper tubes that I ended up not analysing; and Thomas (Rigaudier) for being patient with our last-time sampling and analyses schedules.

I'd like to thank Alasdair Skelton and Gabrielle Stockmann for the samples from HA-01 for the baseline data of the time-series. A special thanks to Saemi and Andri, from the University of Iceland, who sampled multiple sites in North Iceland for us, when we couldn't travel due to the pandemic, and also maintained the SPARTAH machines in the field.

I'm extremely grateful for my friends at CRPG and GeoRessources, specially Yujin, Emma, Belen, and my office mates, Nicolas and Gabriel, with whom I had great exchanges about life and science. Outside of CRPG I found a family with other PhD candidates in a similar situation and political alignment as me, who made the stay in this lovely town way more interesting: Melike, Melissa, and Rama (in alphabetical order to avoid drama :p). On

that note, I suppose I should thank Nancy for the weather condition during most of my stay: rain and wind is always a sweet combination.

I'm also thankful for the support given by my sister, mother, and specially my father, who passed away before I started my PhD but always supported my (non-profitable) career.

Résumé

L'objectif principal de cette thèse était de détecter les sources de fluides crustaux et géothermiques dans différents contextes géologiques et géotectoniques avec un accent particulier sur la précision des processus de transport dans la croûte - ceci afin d'optimiser l'utilisation de la géochimie isotopique des gaz rares pour le monitoring des fluides associés aux contextes sismiques/volcaniques dans le nord de l'Islande (**Chapitre 4**) ou pour des implications sociétales directes liées à des projets d'exploitation d'hélium (**Chapitre 5**) et géothermique (**Chapitre 6**).

Les gaz rares sont présents en faible concentration sur Terre et sont relativement inertes, ce qui en fait de bons traceurs des interactions fluides (Burnard et al., 2013). Contrairement à la plupart des isotopes stables ou des éléments majeurs couramment utilisés comme traceurs géochimiques, tels que C, S, H et O, les gaz rares sont moins sensibles aux modifications des interactions eau/roche. Dans la croûte continentale, les gaz rares proviennent principalement de l'atmosphère, du manteau et de la désintégration radioactive dans la croûte (Ballentine et Burnard, 2002). En raison de leurs rapports très variables entre ces réservoirs (Ballentine et Burnard, 2002 ; Graham, 2002), les systèmes isotopiques He et Ne sont particulièrement intéressants, fournissant des informations sur la source des fluides. Pour cette raison, leurs rapports ont été utilisés pour tracer les fluides (i) dans les bassins continentaux pour obtenir l'âge des eaux souterraines et estimer les flux d'hélium crustaux (par exemple, Torgersen et Clarke, 1985), ou dans le contexte des réservoirs de gaz (par exemple, Gilfillan et al., 2008); (ii) dans les systèmes hydrothermaux associés aux volcans et aux zones sismiques (par exemple, Caracausi et al., 2005) ; (iii) pour enquêter sur les fuites potentielles de stockage de CO2 (par exemple, Lafortune et al., 2009) ; et (iv) pour estimer l'âge et la circulation de l'eau des systèmes géothermiques (par exemple, Saby et al., 2020). Ainsi, les

isotopes de l'hélium sont utilisés depuis des décennies dans l'étude des sources de fluides dans la croûte et pour comprendre les processus de transport dans des bassins standard bien structurés avec des travaux pionniers sur la circulation horizontale de l'eau et le vieillissement de l'eau associés au flux radiogénique basal de la croûte (Torgersen et Clarke, 1985). Dans cette thèse, j'essaie d'aborder et d'élargir la compréhension du transport et de la circulation des fluides dans d'autres contextes géotectoniques où le schéma de circulation des fluides et ses contrôles sont plus complexes. Dans ce but, j'ai utilisé les isotopes de l'hélium alliés à d'autres traceurs hydrochimiques (par exemple, δ^{18}O and δ^{2}H) dans différents contextes tectoniques : (i) bassin continental abritant un réservoir de gaz dans le centre de la France, (ii) zones sismiquement actives et volcaniquement inactives dans le nord de l'Islande, et (iii) une zone géothermique insérée dans un système de rift actif dans la dépression Afar(lac Abhe, Djibouti).

Dans les fluides géothermiques islandais (**Chapitre 4**), les rapports ^{3}He/^{4}He présentent une large gamme qui n'est pas nécessairement liée à l'activité volcanique actuelle. À Vestfirðir, à plus de 110 km des zones de rift actives les plus proches, les rapports ^{3}He/^{4}He les plus élevés dans les fluides géothermiques ont été décrites (3 à 29 Ra), montrant l'influence de la composante du panache mantellique islandais. À l'exception de Vestfirðir, les régions hors rifts actifs n'ont pas été étudiées de manière approfondie, ce qui est le cas du nord de l'Islande. Cette région, bien que volcaniquement inactive, a enregistré des tremblements de terre avec des magnitudes allant jusqu'à environ M 7 liés à la zone de transfert entre la dorsale médio- atlantique et la Zone du Rift Nord icelandais (NRZ). Ses derniers tremblements de terre de grande magnitude ont détruit les maisons de Húsavík en 1872, rendant la surveillance de l'ensemble du système tectonique-hydrogéochimique d'une importance sociétale. Les séries chronologiques précédentes de mesures d'isotopes stables et d'éléments majeurs des fluides géothermiques provenant d'un forage à Hafralækur ont suggéré une relation entre les événements sismiques (M $>$ 5) et la variabilité de ces traceurs géochimiques. Ces traceurs sont sensibles aux interactions eau-roche et renseignent ainsi sur de tels types de processus alors que les gaz nobles sont chimiquement inertes et peuvent éclairer les sources de fluides profonds (croûte vs manteau) et/ou les processus de mélange qui peuvent modifier leurs contributions dans les fluides émis en surface, ceci en dehors de l'influence des processus

secondaires actifs dans la croûte. Notre étude visait à réduire le déficit de données pour les isotopes de l'hélium dans les fluides géothermiques du nord de l'Islande et à détecter les variations de la signature isotopique de l'hélium des eaux souterraines potentiellement liées aux séismes dans la région. Nous rapportons ici les résultats d'une étude isotopique du nord de l'Islande ainsi que des données de séries chronologiques obtenues de juin 2020 à octobre 2022 sur les isotopes de l'hélium pour les fluides géothermiques du forage à Hafralækur. Les résultats indiquent une forte variabilité régionale des rapports isotopiques de l'hélium (4 à 27 Ra) pouvant provenir de processus régionaux et locaux : (i) influence d'un flux mantellique global, mis en évidence par un dégazage enrichi en composants du manteau via les systèmes de failles, (ii) la libération d'hélium radiogénique potentiellement liée à des événements sismiques le long du linéament/zone de transfert de Dalvík, et (iii) le mélange des eaux souterraines à l'échelle locale à Hafralækur, documenté sur une période caractérisée par des événements sismiques de $M > 5$. Le flux de volatiles magmatiques global estimé est comparable à ceux des zones de rift actives voisines en Islande, où les magmas intrudés dans la croûte dégazent toujours activement. De plus, la signature isotopique de l'hélium des fluides géothermiques (> 8 Ra) indique l'influence du panache mantellique islandais. Des processus localisés induits par la sismicité se produisent également. Le long du linéament de Dalvík, les rapports $^3He/^4He$ (< 8 Ra) indiquent la libération de ^4He radiogénique des roches hôtes, ceci sur des périodes courtes et discrètes plutôt que dans des conditions d'état stable, potentiellement liées aux tremblements de terre le long de cette zone de transfert majeure. Bien que nous n'ayons trouvé aucune évidence de mélange des eaux souterraines à l'échelle régionale, notre série chronologique d'isotopes d'hélium (2020 à 2022) indique qu'un transport latéral pourrait se produire à l'échelle locale dans la vallée d'Aðaldalur, entre Hafralækur et la frontière ouest de la NRZ, apparemment partiellement contrôlée ou renforcée par des séismes de forte magnitude ($M \geq 5$).

Déterminer la ou les sources d'hélium dans les régions de la croûte où des anomalies de ^3He se produisent peut être difficile lorsqu'aucune manifestation d'activité magmatique en surface ou un régime d'extension actif clair ne sont présents (**Chapitre 5**). C'est le cas du Bassin parisien (France), où les rapports isotopiques $^3He/^4He$ des fluides géothermiques et des huiles ont été documentés antérieurement allant de 0,02 Ra à 0,14 Ra (Marty et al., 1993

; Pinti et Marty, 1995, 1998), tandis que les gaz naturels au sud du Bassin parisien (près du Massif central) montrent sans ambiguïté la contribution de l'hélium du manteau, avec $^{3}He/^{4}He$ jusqu'à 6,4 Ra (Bräuer et al., 2017). Cependant, un $^{3}He/^{4}He$ plus élevé que le pôle standard de la croûte (0,01 Ra), comme observé dans le Bassin parisien, pourrait être le signe soit (i) d'une faible contribution de l'He du manteau (enrichi en ^{3}He primordial) soit (ii) de l'apport de ^{3}He produit naturellement par les réactions nucléaires du lithium, pour lequel des concentrations commercialement exploitables ont été signalées dans les granites riches en métaux rares. Une façon de faire la distinction entre ces deux possibilités est de combiner la systématique des isotopes He avec d'autres traceurs de gaz rares d'apports du manteau, tels que les isotopes du xénon. Nous rapportons ici les compositions isotopiques de l'hélium et du xénon, mesurées respectivement par spectrométrie de masse statique et dynamique, dans des échantillons de gaz prélevés dans le département de la Nièvre, entre le Massif central et le Bassin parisien. Les rapports $^{3}He/^{4}He$ varient entre 0,16 et 0,22 Ra. Combinées à des études antérieures, nos données sont cohérentes avec une augmentation vers le sud des rapports isotopiques de He le long des principaux systèmes de failles du Bassin parisien (0,02 Ra) vers le Massif Central (6,4 Ra). Cette tendance géographique, associée aux mesures haute précision des isotopes du Xe présentant un excès de ^{129}Xe du manteau, montre un apport clair du manteau qui est très probablement limité aux principaux systèmes de failles du centre de la France. La présence d'hélium et de xénon d'origine mantellique dans le centre de la France met en évidence la présence de magmatisme cryptique dans des zones sans manifestations volcaniques apparentes.

Dans le champ géothermique du lac Abhe (**Chapitre 6**), les caractéristiques du système et les processus physico-chimiques sont différents de ceux de la région du bassin parisien et du nord de l'Islande. Ce champ géothermique à basse température ($< 150°C$) est positionné à proximité d'un système volcanique actif (Dama Ali, $\sim$ 30 km W), qui est probablement sa source de volatils, avec donc un apport de volatiles du manteau attendu. Le transport de cette composante, contrairement à ce que nous avons observé pour les fluides de la région du bassin parisien et du nord de l'Islande, semble se produire latéralement via l'écoulement des eaux souterraines puisque le système du lac Abhe est alimenté par un aquifère régional. Dans ce système géothermique, le dégazage se produit dans deux domaines communément

appelés « petites cheminées » et « grandes cheminées » ; cependant, les deux affichent des compositions des gaz et des signatures isotopiques similaires qui indiquent un système hydrothermal commun et homogène en profondeur, dominé par une source magmatique, ce qui est une information importante pour les objectifs du projet de « Geothermal Village » et l'enjeu pour l'emplacement du futur puits d'exploitation . Ce résultat est en accord avec le modèle précédemment proposé par Awaleh et al. (2015), dans lequel les auteurs proposent un réservoir commun aux deux zones basé sur le transport de chaleur depuis la profondeurs, le système hydrothermal étant alimenté par les eaux météoriques de l'aquifère régional. De plus, l'eau souterraine profonde a une signature compatible avec le mélange entre un composant du manteau (proche de 9 Ra) et l'ASW, sans preuve claire de l'influence d'un composant de type panache riche en ^{3}He. La source de ces volatiles étant très probablement le système volcanique de Dama Ali, à environ 30 km à l'ouest des sources chaudes du lac Abhe, l'étude future de ce système volcanique est cruciale pour mieux contraindre le pôle local du système géothermique du lac Abhe et l'origine de la composante 7-9 Ra en Afar Central associée à la composante panache.

Bien que les isotopes de l'hélium alliés à d'autres systèmes isotopiques puissent fournir des réponses sur la source des fluides, des ambiguïtés subsistent souvent. C'est le cas de la source de N_2 et de CO_2 dans le gisement de gaz de la Nièvre, puisqu'ils peuvent provenir de processus biogéniques (N_2), de matière organique (CO_2) ou être sensibles à des processus secondaires (CO_2) (e.g., Favara et al., 2002 ; Wada et al., 1975). Les rapports $^{3}He/^{4}He$ sont indépendants de la composition du gaz, étant donné que $^{3}He/^{4}He$ est à peu près le même pour les sources proches de SP4, dont Fontaine des Vertus, alors que ses teneurs en hélium et N_2 sont beaucoup plus élevées que pour le autres sources du groupe. Les résultats de $\delta^{15}N$, pour tous les groupes d'échantillons, sont comparables et indiquent une source crustale commune. L'azote dans la croûte se trouve principalement dans les minéraux silicatés sous forme de NH_4 (minéraux argileux, mica, feldspath, grenat, wadsleyite et bridgmanite ; Mysen, 2019). Une source commune indique que la variation des teneurs en N_2 est liée à des processus secondaires tels que la précipitation des carbonates et la dissolution du CO_2. Ces processus conduisent à un fractionnement du CO_2 entre la phase aqueuse et la phase gazeuse. La dissolution préférentielle du CO_2 dans l'eau par rapport au N_2 et à l'hélium entraîne des

teneurs plus faibles du premier en phase gazeuse, ce qui explique les concentrations élevées en N_2 et en hélium à Fontaine des Vertus, Bourbon-Lancy et Fontaines Salées. Établir la source de CO_2 est plus difficile. Considérant que les $\delta^{13}C$ du CO_2 de nos sources étudiées près du Bassin parisien sont distincts de la valeur régionale du manteau (Massif Central), le CO_2 est probablement principalement d'origine crustale. Cependant, un mélange entre les composants crustaux ou biogéniques et le manteau est attendu, d'autant plus que le CO_2 serait très probablement la phase porteuse du composant hélium du manteau et que les rapports $CO_2/^3He$ (entre 8 x 10^9 et 1 x 10^{10}) sont proches de la valeur MORB.

Pour la zone géothermique du lac d'Abhe, le N_2 est la principale phase gazeuse mais contrairement à la région de la Nièvre, il n'est pas concentré dans la phase gazeuse en raison de la dissolution préférentielle du CO_2 dans la phase aqueuse, mais au contraire très probablement en raison de la production locale à partir de NH_4 présent dans les argiles, silicates formés par altération hydrothermale des basaltes (Chapitre 6). Ainsi, la phase porteuse de l'hélium du manteau est le CO_2 comme pour les autres domaines d'étude de cette thèse.

D'après les résultats rapportés dans cette thèse, les isotopes de l'hélium montrent que l'apport mantellique est présent dans différents contextes géotectoniques, pas nécessairement liés au volcanisme actif ou à l'extension, comme le cas du Bassin parisien (**Chapitre 5**) et des Pyrénées (Annexe), tous en contexte de croûte continentale, ou de zones hors rift en Islande (**Chapitre 4**), et qui nécessitent des processus identiques de transfert vertical direct depuis le manteau.

Abstract

Noble gases occur in low concentration on Earth and are relatively inert, making them good tracers of fluid interactions. Contrary to most stable isotopes or major elements commonly used as geochemical tracers, such as C, S, H, and O, noble gases are less susceptible to water/rock interactions modifications. Due to their widely variable ratios among the three main Earth reservoirs (mantle, continental crust, and atmosphere), the He and Ne isotopic systems are of particular interest, providing information on the source of fluids. The main goal of this thesis was to detect the sources of crustal and geothermal fluids in different geological and geotectonic settings with a specific emphasis on precising transport processes in the crust – this, in order to optimize the use of noble gas isotopic geochemistry for monitoring fluids associated to seismic/volcanic contexts in Northern Iceland (**Chapter 4**) or for direct societal implications linked to helium (**Chapter 5**) and geothermal (**Chapter 6**) exploitation projects.

From the results reported in this thesis, helium isotopes show that mantle input is present in different geotectonic contexts, not necessarily linked to active volcanism or extension, such as the case of off-rift zones in Iceland (Vestfdir and North Iceland, **Chapter 4**) and of the Paris Basin (**Chapter 5**), the latter inserted in a continental crust setting. In the Lake Abhe geothermal system (**Chapter 6**), the helium isotopic signature is below the one expected for this segment of the East African Rift System (EARS), where an enriched plume-like endmember was anticipated, as observed a few kilometres away, in SW Afar ($\sim$ 55 km) and Tendaho Graben ($\sim$ 110 km NW). Thus, helium isotopes are a powerful tool to trace the mantle influence and transport complexities at different geological settings.

This thesis is organized in seven chapters; the first three of them give background information on the different studies and the the next ones deal with the results and conclusions

of such studies.

Chapter 1 presents the context of the thesis, the helium isotopes systematics, and target areas. I detail the principle of helium and neon isotopes, the different applications of these systems in the study of fluids in the crust, finalizing with the presentation of the objectives of each case study: (i) isotopic monitoring and survey in North Iceland, (ii) tracing the source of He in a continental basin in Central France, and (iii) tracing the source of He in the Lake Abhe geothermal field (Djibouti). **Chapter 2** lists the main sampling procedures I followed and **Chapter 3** describes the different steps of helium isotope analyses, the main methodology I employed in this thesis.

Chapter 4 presents the results of the investigation in North Iceland - both the isotopic survey of various systems ($^3He/^4He$, $^4He/^{20}Ne$, δ^2H, $\delta^{18}O$, $\delta^{34}S$, $\delta^{13}C_{TDIC}$, TDIC, major and trace elements analyses) and the time series of $^3He/^4He$ and $^4He/^{20}Ne$ of groundwater samples from a borehole (HA-01). The results show the influence of an enriched and plume-like endmember in this off-rift zone of Iceland, via vertical transport along extinct fissure swarms. One of the fjords exhibit lower $^3He/^4He$ ratios than expected for typical mantle values in such a context, which we attribute to $^4He^*$ (radiogenic) release enhanced by seismic activity along the Dalvík lineament. We interpret the small variations we observed in the time series as a result of a local scale lateral mixing of groundwater during periods of unrest ($M \geq 5$ earthquakes).

Chapter 5 presents the main results of our study of the gas reservoir and its nearby springs in Nièvre, Central France. It includes the $^3He/^4He$, $^3He/^{20}Ne$, major gas composition, stable isotopes of CO_2 ($\delta^{13}C$) and N2 ($\delta^{15}N$), and Ar, Ne, and Xe isotopes. Our findings indicate a clear yet limited mantle input ($\sim 2.5\%$) in this segment of the continental crust, along N-S fault systems in Central France, reaching the Paris Basin.

Chapter 6 reports results from the isotopic investigation performed at the Lake Abhe geothermal field (Djibouti) and nearby regions (SW Afar and Tendaho Graben). We collected gas and water samples for gas chromatography, $^3He/^4He$, $^4He/^{20}Ne$, $\delta^{13}C_{CO_2}$, $\delta^{13}C_{CH_4}$, $\delta^2H_{CH_4}$, $\delta^{15}N$, $\delta^{18}O$, δD, $\delta^{34}S_{SO_4}$, $\delta^{33}S_{SO_4}$, $\delta^{34}S_{H_2S}$, and $\delta^{33}S_{H_2S}$. From the results, we infer the Lake Abhe geothermal field source of heat is the Dama Ali volcano ($\sim$ 30km), source of the mantle signal observed in helium and CO_2, both transported by a regional aquifer fed

by meteoric water.

Chapter 7 summarizes the main results and conclusions of this thesis, along with the remaining questions and potential future studies.

Contents

Chapter 1

Introduction

Contents

1.1 General context

Noble gases occur in low concentration on Earth and are chemically inert, making them good tracers of fluid interactions (Burnard et al., 2013). Contrary to most stable isotopes or major elements commonly used as geochemical tracers, such as C, S, H, and O, noble gases are less susceptible to water/rock interactions modifications.

In the continental crust, noble gases originate mainly from the atmosphere, mantle, and radioactive decay within the crust (Ballentine and Burnard, 2002) (Figure 1.1). Due to their widely variable ratios among these reservoirs (Ballentine and Burnard, 2002; Graham, 2002), the He and Ne isotopic systems are of particular interest, providing information on the source of fluids. For this reason, their ratios have been used to trace fluids (i) in continental basins to obtain water age and estimate crustal helium fluxes (e.g., Torgersen and Clarke, 1985), or in the context of gas reservoirs (e.g., Gilfillan et al., 2008); (ii) in hydrothermal systems associated with volcanoes and seismic zones (e.g., Caracausi et al., 2005); (iii) to investigate potential CO_2 storage leakage (e.g., Lafortune et al., 2009); and (iv) to estimate the age and water circulation of geothermal systems (e.g., Saby et al., 2020).

Thus, helium isotopes have been used for decades in the study of fluid sources in the crust and to understand transport processes in standard well structured basins with pioneer work of horizontal water circulation and ageing of water associated with basal radiogenic flux from the crust (Torgersen and Clarke, 1985). In the current thesis, I try to address and expand the understanding of fluid transport and circulation in other geotectonic contexts where the pattern of fluid circulation and its controls are more complex. With that intent, I employed helium isotopes allied with other hydrochemical tracers (e.g., $\delta^{18}O$ and $\delta^{2}H$) at different tectonic settings: (i) continental basin hosting a gas reservoir in Central France, (ii) seismically active and volcanically inactive zones in North Iceland, and (iii) a geothermal area inserted in an active rift system in Lake Abhe (Djibouti). Additionally, I was involved in collaborations; one with Gaetan Milesi (GeoRessources) aiming to investigate the regional helium source in the Pyrenees (annex) and another focused on potential helium and hydrogen reservoirs in Corsica in the context of Hugo Dutoit's PhD thesis (ISTerre Grenoble). The latter will not be discussed further since the work is still undergoing. In total, I analysed $\sim$

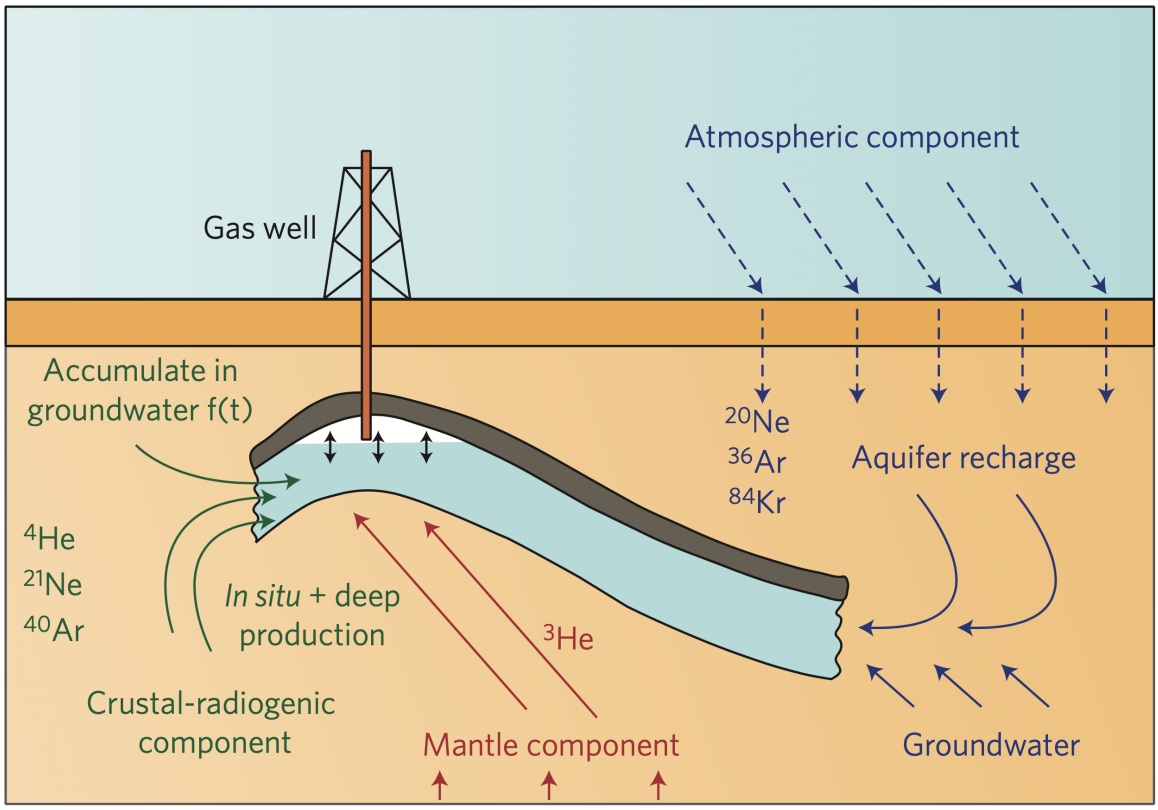

Figure 1.1: Sketch showing the three sources of noble gases in crustal fluids: atmosphere, mantle, and crust. The different isotopes are either primordial (present since Earth's accretion) and located in the atmosphere and mantle or produced in the crust by radiogenic decay. The latter are accumulated in groundwater as function of time and can give information on residency ages. Extracted from Lollar and Ballentine (2009).

225 samples for helium isotopic analysis, including 5 samples from Corsica.

Besides the study of transport in regional scale, the initial goal of this thesis was on high resolution monitoring of fluids in seismic and volcanic areas. Although this was not achieved due to travel constraints during the pandemic, in this thesis I also report time variations at a seismic zone in North Iceland via discrete weekly sampling (see Chapter 4).

1.2 He and Ne isotopes systematics

1.2.1 Helium

In the Earth system, the two helium isotopes, ^{3}He and ^{4}He, are found in the atmosphere, crust, and mantle in different proportions. ^{3}He is mainly of primordial origin and stored

mainly in the mantle, where it has been able to be preserved since Earth's accretion (Craig and Lupton, 1976). ^{4}He is mainly of radiogenic origin, from decay of U, Th, and Sm, produced predominantly in the continental crust where the contents of these elements are higher (Ballentine and Burnard, 2002).

In the atmosphere, helium is supplied by volcanic activity, faults, erosion, and groundwater cycle; its concentration in the atmosphere, however, is not cumulative as it also escapes to space due to its low mass (Burnard et al., 2013). There are other sources of ^{3}He to the Earth's atmosphere, such as auroral precipitation of solar wind, cosmic dust and meteorites, and direct accretion of cosmic rays (Lupton, 1983), yet these sources are insignificant in the whole He budget. The content of ^{4}He in the atmosphere has been demonstrated to variate over time in certain industrial regions due to anthropic activities (e.g., Sano et al., 2010). However, the ^{3}He/^{4}He ratio can be regarded as constant, on a global scale, at (1.382 $\pm$ 0.005) x 10^{-6}, an average of analyses from the literature (Burnard et al., 2013), although the value of 1.39 x 10^{-6} seems to remain the most used (e.g., Graham, 2002; Moreira, 2013). In the terrestrial system, the notation of the ^{3}He/^{4}He ratio is usually given as a function of Ra where Ra is the atmospheric ^{3}He/^{4}He ratio.

In the crust, production of ^{4}He mainly occurs by α-decay of the ^{235,238}U and ^{232}Th decay chains and it thus depends on the concentration of these two elements (Ballentine and Burnard, 2002). ^{4}He in situ production from α-decay of ^{147}Sm is negligible due to its long half-life, being orders of magnitude lower than U and Th. Production of ^{3}He can also occur in the crust depending, among other factors, on the presence of Li as it is produced by the thermal neutron capture by ^{6}Li by the reaction ^{6}Li(n,α) ^{3}H $\rightarrow^{3}$He (Morrison and Pine, 1955). Ballentine and Burnard (2002) present the following ^{3}He/^{4}He ratios, based on the production rates of the two isotopes in the crust, for the average lower, middle, and upper continental crust, respectively: 3.71 x 10^{-9} (0.003 Ra), 3.99 x 10^{-9} (0.003 Ra), and 1.08 x 10^{-8} (0.008 Ra). The authors remark how these values differ from the measured in the literature due to other sources of ^{3}He (mantle, cosmogenic), error of analysis, and possible fractionation. In general, rocks of crustal source present ^{3}He/^{4}He ratios inferior to that of the atmosphere and, consequently, inferior to that of rocks with mantellic source (Figure 1.2); the ^{3}He/^{4}He of the continental crust is usually regarded as < 0.02 Ra.

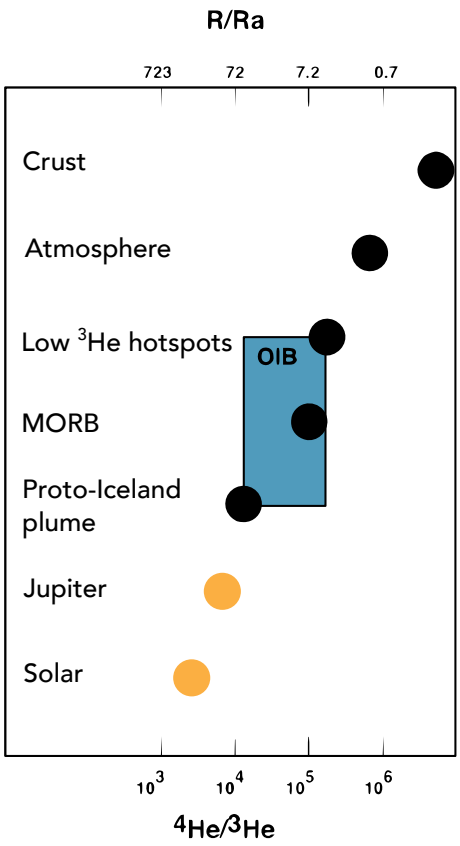

Figure 1.2: Isotopic ratios of the Earth system compared to Jupiter and solar. Modified from Moreira (2013).

The account of the mantle $^3He/^4He$ ratios are mostly given by the study of basalts, both MORBs and OIBs, and some works on mantle xenoliths (e.g., Tolstikhin et al., 1974). MORBS, as a result of partial melting of the mantle at spreading ridges, are viewed as a representation of the upper mantle. OIBs, however, are more complex and could represent mantle anomalies; it is debated in the literature whether or not they represent upwellings of the deep mantle (e.g., Graham, 2002). The variation in $^3He/^4He$ ratios in MORBs are small compared to OIBs, and can be considered as relatively homogeneous (Graham, 2002; Moreira, 2013). According to Graham (2002), the average ratio of MORBs is 8.75 $\pm$ 2.14 Ra while 9.58 $\pm$ 2.94 Ra for the Atlantic Ridge alone, 8.13 $\pm$ 0.98 for the Pacific Ridge, and 8.49 $\pm$ 1.62 for the Indian Ridge. The $^3He/^4He$ ratio of the Mid-Atlantic Ridge "popping rock" (8.14 $\pm$ 0.06 Ra; Sarda and Graham, 1990), however, is considered to be the closest to that of the upper mantle due to its high helium concentration and consequently high analytical precision (Graham, 2002). In the case of OIBs, they display lower and higher $^3He/^4He$

ratios compared to MORBs (Figure 1.2). Most hot spots display higher $^{3}He/^{4}He$ ratios, such as in Iceland, Hawaii, Réunion, Samoa, Yellowstone, and Ethiopian Rift, the highest being the Baffin Island picrites (50 Ra; Stuart et al., 2003). Other OIBs do not display these primitive helium signature and in fact show $^{3}He/^{4}He$ ratios lower or close to those of MORBs, raising into question whether they represent their mantle source or shallow processes (e.g., magma chamber degassing, crustal assimilation) (Moreira, 2013). This author discusses the possibility of mixture of a primitive mantle source enriched in ^{3}He and recycled material (subducting oceanic crust and/or sediments) or a MORB source.

1.2.2 Neon

There are three neon isotopes, ^{20}Ne, ^{21}Ne, and ^{22}Ne, in which ^{20}Ne and ^{22}Ne are mainly primordial and most abundant in the Earth, and ^{21}Ne nucleogenic (Porcelli and Turekian, 2014). However, only ^{20}Ne can be safely regarded as exclusively primordial in the Earth, since ^{22}Ne can be produced by the reaction $^{19}F(\alpha, n)^{22}Na(T_{1/2} = 2.605\ a) \rightarrow ^{22}Ne$ and ^{21}Ne is produced by $^{18}O(\alpha, n)^{21}Ne$ (Ozima and Podosek, 2002).

The atmosphere is enriched in ^{20}Ne compared to ^{22}Ne and ^{21}Ne with percent molar abundances of 90.5, 9.23, and 0.268, respectively (Porcelli et al., 2002). The relative abundances of ^{20}Ne and ^{21}Ne are given as a function of ^{22}Ne and are, respectively, 9.80 ± 0.08 and 0.0290 ± 0.0003 (Eberhardt et al., 1965; Porcelli et al., 2002). For a mantle source, $^{20}Ne/^{22}Ne$ ratios are larger than that of the atmosphere, approaching the value of the solar wind (13.8) (Porcelli and Turekian, 2014), with an approximated value of 13.2. This signature points to the presence of a primordial reservoir in the mantle, still not completely degassed. The $^{21}Ne/^{22}$ ratios vary between the value of air and 0.0697, the latter being the established value for the mantle endmember. For the average crust, the values used are 0.47 for $^{21}Ne/^{22}Ne$ and 0.3 for $^{20}Ne/^{22}Ne$, considering a uniform production rate (Ballentine and O'Nions, 1992).

1.2.3 He-Ne systematics in source determination

A fluid sample at the Earth surface can have contribution of the three Earth reservoirs – mantle, atmosphere, and crust (radiogenic). In order to quantify their contributions, the

$^4He/^{20}Ne$ ratio is largely employed associated to the $^3He/^4He$. The $^3He/^4He$ versus $^4He/^{20}Ne$ plot (Figure 1.3) is used to distinguish mixing between the three main sources of fluids. In groundwater samples, the atmospheric source is represented by air-saturated water (ASW) instead of air.

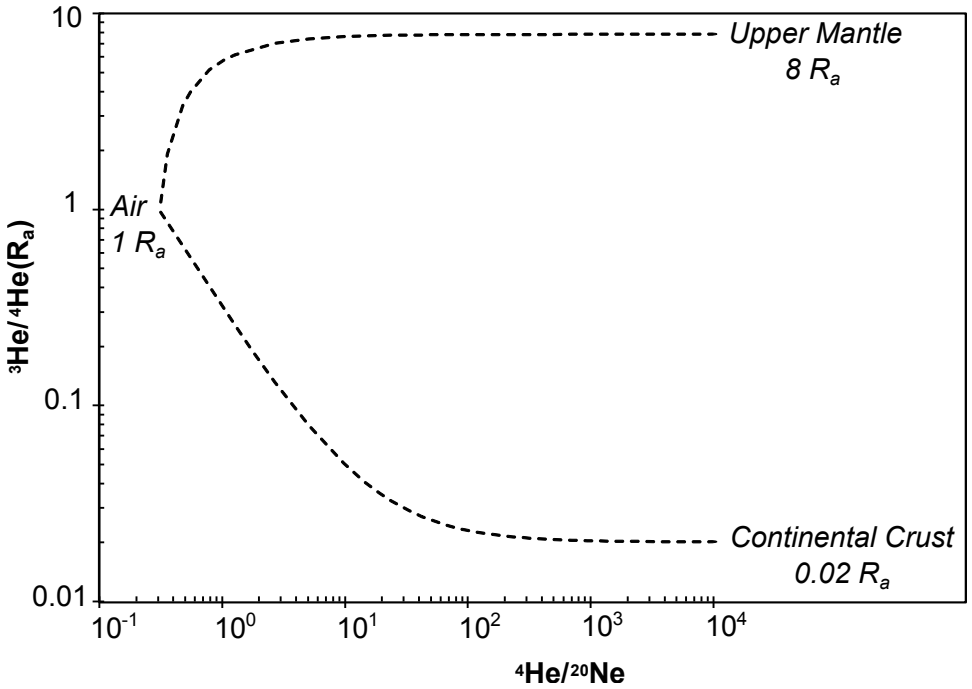

Figure 1.3: Classic $^3He/^4He$ versus $^4He/^{20}Ne$ plot. In this diagram, the three main earth reservoirs are represented: upper mantle (or MORB), continental crust, and the atmosphere (air or ASW). The hyperbolic curves represent mixing between these three sources.

In most studies, the measured $^3He/^4He$ ratios is corrected to air contributions using the formula given by Craig (1978):

$$(^3He/^4He)_{\mathrm{c}} = \frac{(^3He/^4He)_{\mathrm{m}} \times (^4He/^{20}Ne)_{\mathrm{m}}}{(^4He/^{20}Ne)_{\mathrm{air}} - (^3He/^4He)_{\mathrm{air}}} \div \left[\frac{(^4He/^{20}Ne)_{\mathrm{m}}}{(^4He/^{20}Ne)_{\mathrm{air}}} - 1\right] \tag{1.1}$$

Where the subscripts "m" and "c" refer to the measured and corrected ratios, respectively.

For fluid samples, Hilton (1996) recommends the following formula for air correction, which takes into account He and Ne solubility in water:

$$X = [(^4He/^{20}Ne)_{\mathrm{sample}}/(^4He/^{20}Ne)_{\mathrm{air}} \times (\beta Ne/\beta He)] \tag{1.2}$$

Where β_{He} and β_{Ne} are the Bunsen solubility coefficient at a given temperature and

salinity of the water; for pure water at 10°C βNe/βHe= 1.25.

These corrections are commonly applied when the target of such studies is the isotopic signature of the mantle component. In the context of groundwater, unlike when studying rocks and minerals, the air is not a contaminant but its main initial component acquired during aquifers recharge at the surface. Gas partitions between the water table and air in the soil at the transition zone between the saturated and unsaturated zones. In surface waters, the noble gas content is usually in equilibrium with that of the atmosphere, while for groundwaters it is common to find the atmospheric component in higher concentration than the equilibrium; this is referred to as "excess air". Often, excess air is the atmospheric air, however, in a few cases the air is fractionated, being enriched in heavier noble gases (Kipfer et al., 2002). There are several models for excess air that need to be considered when calculating the air component. In cases where air-equilibrium is assumed, the ^{4}He/^{20}Ne for air at 10°C is employed (0.288) (Ballentine et al., 2002). In cases where the groundwater is old, for instance, the "corrected" value is usually close to the measured value – $(^3\mathrm{He}/^4\mathrm{He})_\mathrm{c} \approx (^3\mathrm{He}/^4\mathrm{He})_\mathrm{m}$ because ^{4}He/^{20}Ne is high due to radiogenic production of ^{4}He over time (Ballentine et al., 2002). After the air component is "corrected" from the measured ^{3}He/^{4}He, it is possible to obtain the crustal ^{4}He by the formula (Ballentine et al., 2002):

$$(^4He)_\mathrm{crust} = (^4He)_\mathrm{tot} \times \left[\frac{(^3He/^4He)_\mathrm{mantle} - (^3He/^4He)_\mathrm{c}}{(^3He/^4He)_\mathrm{mantle} - (^3He/^4He)_\mathrm{crust}}\right] \tag{1.3}$$

The mantle ^{3}He/^{4}He can vary significantly regionally, thus an average value may not apply, for instance where the influence of a mantle plume occurs. In Iceland, Füri et al. (2010) measured ^{3}He/^{4}He of up to $\sim$ 22 Ra in groundwater showing a clear presence of the mantle component. For the ^{3}He/^{4}He of the crust, Ballentine et al. (2002) suggest the ratio of 1x10^{-8} (0.008 Ra) obtained by Ballentine and Burnard (2002) for the upper continental crust. However, for regions such as Iceland, the ^{4}He production might yield different values, and will depend on the local content of U and Th. The ^{4}He production can be given by (Ballentine and Burnard, 2002):

$$^4He\ atoms\ g^{-1}yr^{-1} = (3.115 \times 10^6 + 1.272 \times 10^5)[U] + 7.710 \times 10^5[Th] \tag{1.4}$$

Where the [U] and [Th] represent the contents of U and Th in ppm, respectively. Kipfer et al. (2002) also discuss the causes for the presence of "excess ^{4}He" in groundwater identified by the larger age obtained from ^{4}He than from ^{14}C. Some of the suggestions are a continuous flow of ^{4}He through the bulk crust to the surface, which is not generally accepted, ^{4}He diffusion from adjacent confining layers, ^{4}He release from minerals, sediment erosion, and weathering. As mentioned in section 1.2.1, ^{3}He can also be produced in the crust. The theoretical crustal ^{3}He/^{4}He ratio can be obtained through Equation 1.5 (Andrews, 1985), based on the production of ^{3}He and ^{4}He in the crust:

$$(P_3/P_4 = f(R, Na, Mg, Al, Si, Ca)F_{\mathrm{Li}}/(3.2108 \times 10^6 + 7.7633 \times 10^5 R) \qquad (1.5)$$

Where P_3/P_4 is the theoretical ^{3}He/^{4}He based on the ^{3}He and ^{4}He production rates, f(...) is the neutron production rate based on the rock composition, F_{Li} is the fraction of neutrons that are captured by ^{6}Li in the rock matrix, and R is the Th/U ratio. In continental basins with anomalously high ^{3}He/^{4}He signatures (e.g., Paris Basin with up to 0.14 Ra; Pinti and Marty, 1998), however, it has never been clearly shown that nucleogenic ^{3}He production alone could account for the helium isotopic ratios, mainly because the Li concentrations required (e.g., 600 ppm Li ro reach 0.17 Ra) are not common in basins.

1.3 Fluid transport in the crust: He and Ne isotopes applications

1.3.1 Continental basins and gas reservoirs

^{3}He/^{4}He are employed worldwide to detect the source of fluids in continental basins (e.g. Lollar et al., 1994; Marty et al., 1992; Ballentine and O'Nions, 1992). In European basins of various ages, ^{3}He/^{4}He values range between 0.01 and 3.9 Ra, reaching ∼0.1 Ra in the western Alps (Marty et al., 1992; Oxburgh et al., 1986). Oxburgh et al. (1986) suggested that this wide range in Neogene basins was related to their tectonic setting. Helium isotope compositions in the Pannonian basin reach values up to 3.9 Ra consistent with an extension

regimen and clear mantle input while the Molasse and Po basins show a range of $^3He/^4He$ between 0.02 and 0.09 Ra (Marty et al., 1992; Oxburgh et al., 1986), which, for the Molasse basin, Oxburgh et al. (1986) interpret as being of crustal origin despite the apparent small mantle contribution (up to 0.9%). In the Paris Basin, $^3He/^4He$ ratios are close to the range of values for the Molasse and Po basins (0.02 to 0.11 Ra), reaching 0.14 Ra at the basement in Couy (Pinti and Marty, 1998). These values are higher than the theoretical crustal $^3He/^4He$ ratio (0.001-0.02 Ra), based on the U-Th and Li values of the underlying sedimentary rocks (Pinti and Marty, 1998). These elevated $^3He/^4He$ values were therefore considered to be evidence for the input of mantle material with a higher than crustal $^3He/^4He$ (Pinti and Marty, 1998). However, with only small $^3He/^4He$ variations, up to 0.1 Ra, it is difficult to fully discriminate this component from variation in the crustal $^3He/^4He$ ratio. In addition, these areas show no evidence of igneous manifestations, and there is the possibility that ^3He could be produced in the crust without mantle input (see section 1.2). In the Vienna Basin, Ballentine and O'Nions (1992) identified higher $^3He/^4He$ in hydrocarbon reservoirs than in the Paris Basin, ranging from 0.11 to 2.26 Ra highlighting mantle contribution of up to 28% in this basin.

In the context of gas reservoirs, CO_2 accumulations can originate from mantle degassing, which is the source of various reservoirs worldwide (e.g., Gilfillan et al., 2008; Sherwood Lollar et al., 1997). CO_2 is prone to fractionation resultant of dissolution into the water phase and/or carbonate precipitation (e.g., Holland and Gilfillan, 2013) and thus, noble gases can shed light into the sources of deep fluids aside the influence of secondary processes in the crust. Additionally, carbon isotopes ranges for volcanic gases, non-marine carbonates, and graphites overlap, rendering the distinction between these sources not possible (Figure 1.4). This ambiguity can be solved with helium isotopes. When ^3He is known to be of mantle origin, that is, if nucleogenic production can be discarded on the basis of low lithium contents in the host rocks, the $CO_2/^3He$ ratio is a useful tool to detect the sources of CO_2. According to Holland and Gilfillan (2013), any CO_2 with $CO_2/^3He$ up to 1 x 10^{10} has a magmatic origin; above this value, CO_2 is considered of crustal origin. However, mixing of different components is possible; the $CO_2/^3He$ vs $\delta^{13}C$ plot (Sano and Marty, 1995) distinguishes mixing between marine limestone, organic sediments, and the upper mantle (Figure 1.5).

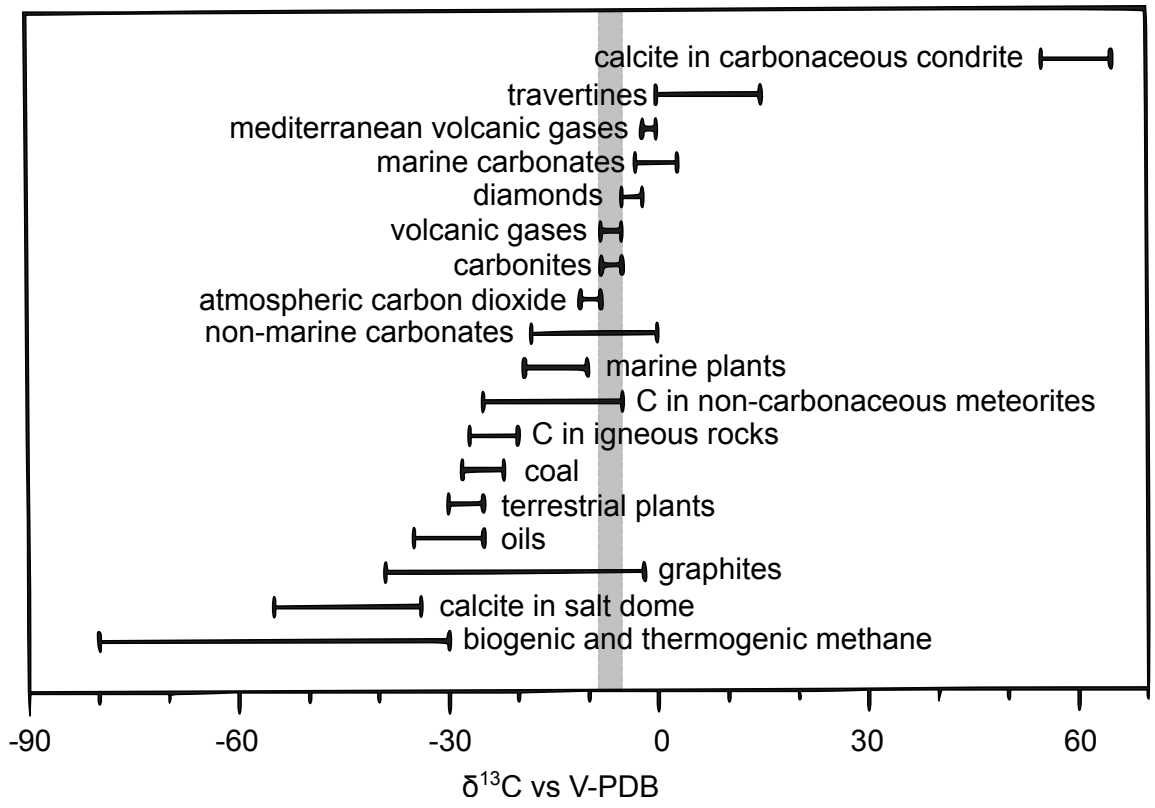

Figure 1.4: Ranges of carbon isotopic composition in natural systems. The grey field represents the range for volcanic gases and its overlap with continental carbonates (non-marine) and sediments (graphites). Redrawn from Favara et al. (2002).

Besides the source of fluids, noble gases give information on the processes of transport and entrapment of volatiles in the crust through partition between the water and gas phases (Ballentine et al., 2002; Holland and Gilfillan, 2013). This principle can be applied in hydrocarbon exploration to identify the transporting medium; if the natural gas shows evidence of groundwater-like signatures (air-equilibrated), then water was crucial to the transport and accumulation of the reservoir gas (Ballentine et al., 2002).

More recently, helium commercial reservoirs ($> 0.3\%$) are becoming prominent exploration targets due to increasing global demand, and are usually discovered as by-products of oil/gas exploration (Halford et al., 2022). As the lightest noble gas, its chemical inertness, small atomic radius, high thermal conductivity, ionization potential, and low boiling point make it fundamental to various industry sectors – from medical instruments and aerospace engineering to electronics. Since it is not possible to chemically synthesize helium, natural reservoirs are of global importance. Currently, world reserves are identified in Qatar, Russia,

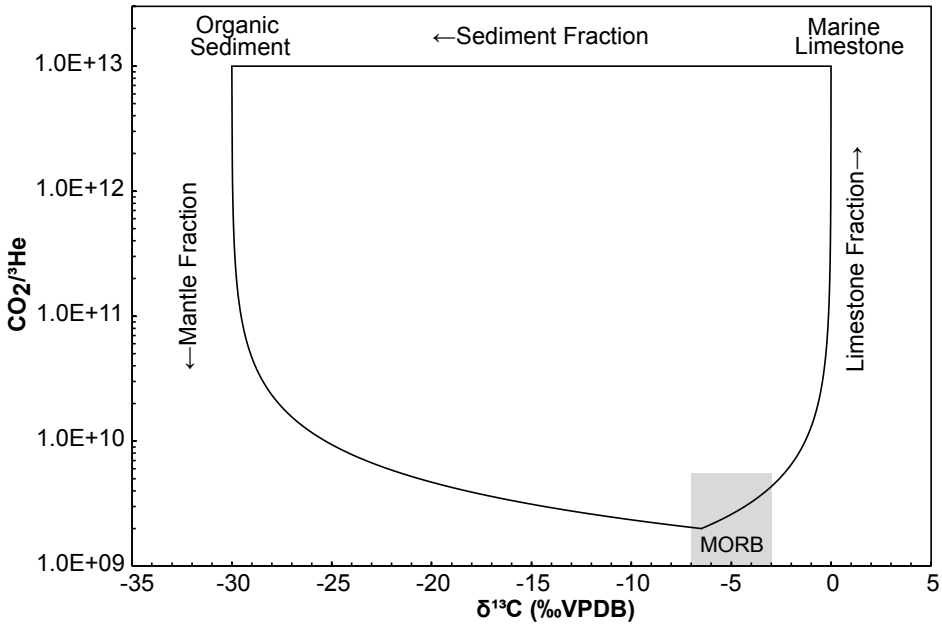

Figure 1.5: $CO_2/^3He$ versus $\delta^{13}C$ plot (Sano and Marty, 1995). This plot allows distinction of mixing between MORB (upper mantle), marine limestone, and organic sediments. The grey field represents the MORB range from Marty and Zimmermann (1999).

Canada, China, and USA (USGS, 2023). When talking of such reservoirs, we mostly speak of helium produced and accumulated in the crust, which is ^4He, however, ^3He has been coveted for the development of textsuperscript3He-based fuel for fusion technology (e.g., Wittenberg et al., 1992). In the context of reservoirs, it is important to identify the sources of helium to better constrain the system and eventually find analogous ones worldwide. In the last years, studies started to focus on characterizing helium reservoirs to identify its sources and transport/storing mechanisms (e.g., Halford et al., 2022; Brown, 2019). In the East African Rift System (EARS), for instance, a potential helium reservoir has been identified in the Rukwa Rift Basin, Tanzania (2.4-6.9% He; James, 1967; Danabalan, 2017; Mtili et al., 2021). Mtili et al. (2021) employed noble gases to detect the source and mechanisms involved in the gas accumulation; they established that the main source of helium was the continental crust with small mantle contribution (0.16-0.20 Ra) and that migration via the water phase occurred for long distances.

1.3.2 Groundwater monitoring

In the crust, groundwater can display mixing between the three different Earth reservoirs (continental crust, mantle, and atmosphere) and thus potential disturbances in the system triggered by seismic or volcanic activity can be detected via helium isotopes monitoring. Sano et al. (1998) identified the potential of $^3He/^4He$ monitoring with pioneer work in the context of natural hazards. For the Kobe earthquake (Japan, 1995), which caused over 6,000 deaths, no geophysical precursors were detected. However, Sano et al. (1998) observed that groundwater samples showed different isotopic ratios prior (1993) and immediately after the seismic events whereas $\delta^{18}O$ and δ^2H were identical. These authors attributed the changes in helium isotopic ratios to the release of ^4He due to microfracturing.

Aiming to detect possible changes in groundwater systems linked to volcanic and seismic activity, $^3He/^4He$ ratios from groundwater in Italy are monitored by the INGV (Istituto Nazionale di Geofisica e Vulcanologia) through discrete sampling. From the data collected, researchers identified correlations between variations in $^3He/^4He$ ratios and earthquakes/eruptions (e.g., Caracausi et al., 2005; Rizzo et al., 2006).

During the Umbria-Marche seismic crisis of 1997-1998 (Central Apennines, Italy), Caracausi et al. (2005) identified an increase in $^3He/^4He$ ratios, highlighting mantle contribution, coinciding with higher CO_2 degassing and a pH-drop due to CO_2 dissolution. The authors associated these variations to changes in rock permeability triggered by the extensional movement and crustal deformation. In Etna, increase in $^3He/^4He$ ratios, measured from gas samples, prior to the eruptions of 2001 and 2002 are correlated to magma ascent, while the stagnation of these ratios during the 2004-2005 eruption indicate a different trigger (Rizzo et al., 2006). For the eruptive period of 2011-2012, Paonita et al. (2016) identified an increase in $^3He/^4He$ (in the order of $\sim$0.5 Ra) that started, progressively, in 2010 and peaked at the beginning of volcanic activity (Figure 1.6) indicating the variations observed in 2010-2012 were related to one single magmatic recharge event. Thus, these studies point to the importance of the He isotopic system in the monitoring of natural hazards. Currently, the sampling frequency in the seismic zone of the Umbria-Marche region varies from seasonal or monthly to weekly at most (Caracausi et al., 2005). During periods of unrest, groundwa-

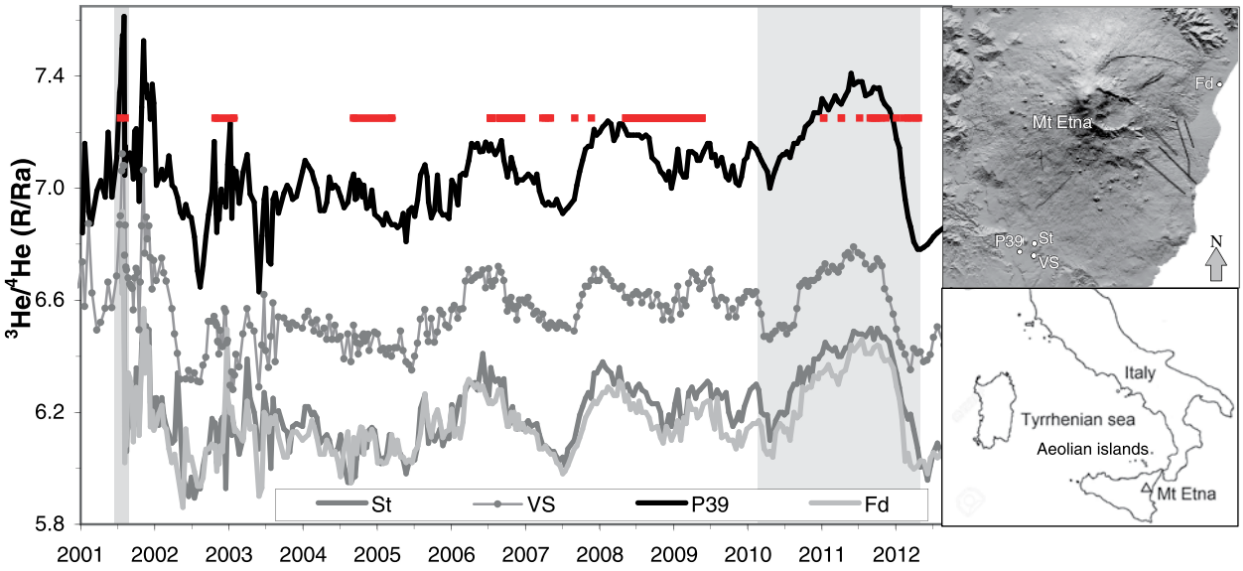

Figure 1.6: Time series of $^3He/^4He$ for gas vents of Mount Etna during the period 2001–2012 Sampling times are the same for all sites. Red lines highlight the eruptive phases; gray areas indicate the period Paonita et al. (2016) modeled. The authors attributed the changes in helium isotopic ratios from 2010 to 2012 to a single magmatic recharge event. Figure from Paonita et al. (2016).

ter at Stromboli and gas from soil, mud volcanos, and a water canal at Etna, are sampled twice a week. At Etna, during periods of quiescence, sampling is performed twice a month (Rizzo et al., 2006; Paonita et al., 2012), and once a month at Stromboli (Rizzo et al., 2009). However, for the case of Etna, for instance, the variations are very small (~ 0.5 R_a) and to improve the time series, the sampling frequency must be enhanced.

Helium isotopes can also be applied for monitoring of CO_2 storage leakage (Holland and Gilfillan, 2013; Lafortune et al., 2009). Surface water is equilibrated with the atmosphere (ASW) and has a known $^3He/^4He$ ratio (1 Ra); since ^4He is produced in the crust by α-decay of $^{235,238}U$ and ^{232}Th, changes in groundwater isotopic signatures can be due to migration of deeper fluids towards the surface. Noble gases can be either present in the system or injected as spike for tracing. The essential is to have the baseline measurements before CO_2 injection for storage. This method is being developed focusing on the study of natural reservoirs for future application in engineered storage sites (e.g., Lafortune et al., 2009; Wilkinson et al., 2009; Battani et al., 2010; Gilfillan et al., 2011). Gilfillan and Haszeldine (2011) investigated potential leakage of a CO_2 in the Weyburn-Midale Monitoring and Storage

Project in Saskatchewan (Canada) using $^{3}He/^{4}He$ and $^{4}He/^{20}Ne$ finding no evidence of the process by the signatures observed in groundwater.

1.3.3 Geothermal system characterization

He isotopic ratios have been employed vigorously to detect magmatic end-members and the influence of mantle plumes (e.g., Hilton et al., 1998; Graham, 2002; Harðardóttir et al., 2018). In such studies, they disregard the air end-member, considering it a contamination. However, air contribution is not always from sampling error but also due to equilibration of water bodies with the atmosphere from the recharge area. In the latter case, it is indicative of mixing processes between water bodies of different ages and sources. When investigating geothermal and groundwater systems, such distinctions are important to constrain not only the groundwater system but to identify the different inputs of helium, whether it is due to lateral transport of groundwater or from vertical flux through the crust. Allying helium isotopes with $\delta^{2}H$ and $\delta^{18}O$ can give information on such processes and sources of fluids.

In geothermal systems, $\delta^{2}H$ and $\delta^{18}O$ are important tools in investigating the source of water, giving information on recharge and potential secondary processes under the surface. Geothermal waters tend to exhibit similar signatures to that of meteoric water, indicating that magmatic fluids play a small role (e.g., Nicholson, 2012). The $\delta^{2}H$ and $\delta^{18}O$ composition of magmatic waters has been proposed by Sheppard et al. (1971) and White (1974) to be between -80 to -10‰ and +6 to +10‰, respectively. In the context of meteoric water, $\delta^{2}H$ and $\delta^{18}O$ fractionate, at low temperatures, to the condensed phase rendering the vapour phase (and consequent precipitation) more depleted in these isotopes towards the poles and high altitudes. Craig (1961) established that, at a global scale, this $\delta^{2}H$ and $\delta^{18}O$ relationship was represented by Equation 1.6:

$$\delta^{2}H = 8\delta^{18}O + 10 \tag{1.6}$$

Shifts in $\delta^{2}H$ and $\delta^{18}O$ are possible resulting of secondary processes (Figure 1.7). Water-rock interactions lead to fluids more enriched in $\delta^{18}O$ relative to meteoric water, since rocks are rich in O and not in H. In low temperature fluids, boiling is not a relevant process,

but in high temperature systems, fractionation between the steam and water phases lead to complex δ^2H and δ^{18}O signatures (Figure 1.7). For lakes situated in arid environments, surface evaporation plays an important role in δ^2H and δ^{18}O signatures, and mixing of meteoric and lake water generate a 4.6 slope instead of 8 (Figure 1.7), as proposed by Fontes and Gonfiantini (1967) for Saharian desert water and also demonstrated by Boschetti et al. (2007) and Awaleh et al. (2015) for the Atacama and Djibouti deserts springs, respectively.

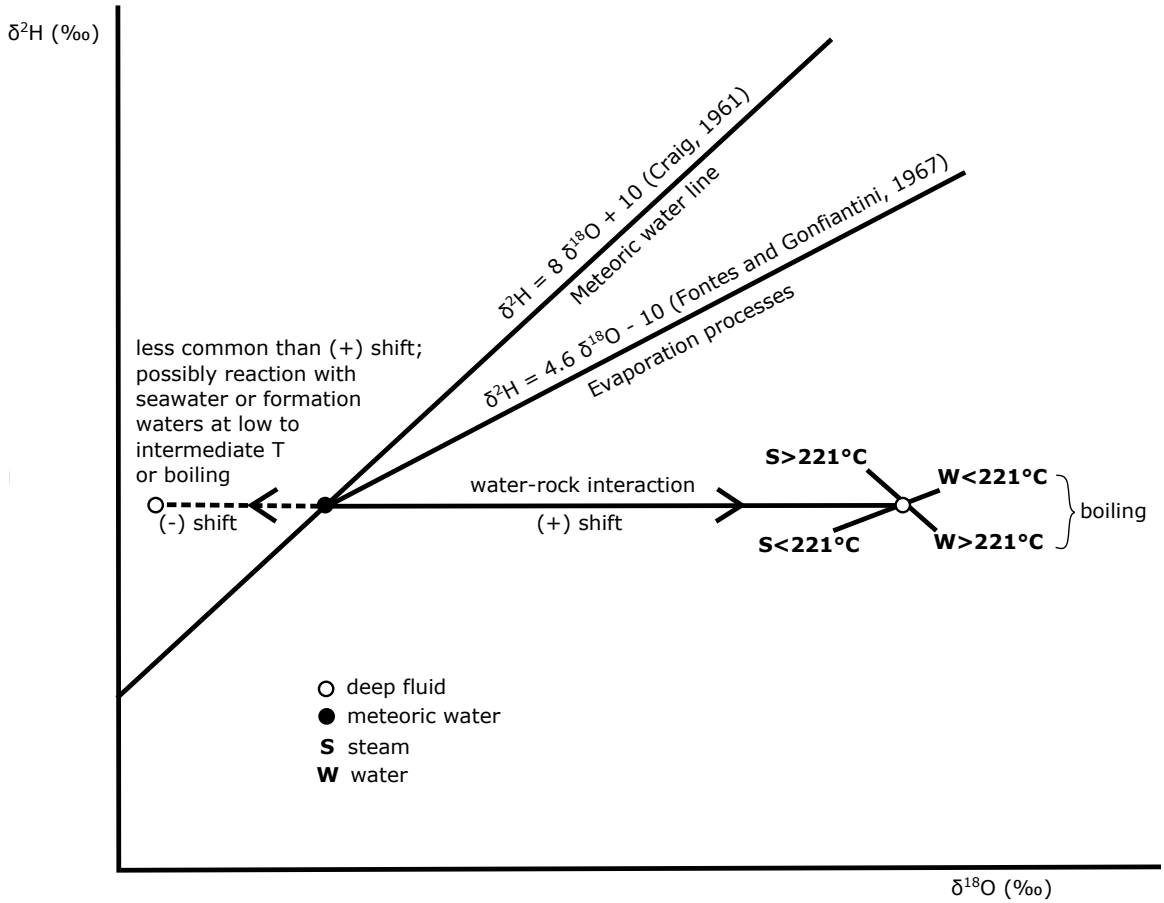

Figure 1.7: Schematic trends in δ^2H and δ^{18}O for geothermal fluids and meteoric water. Water-rock interactions lead to changes in δ^{18}O and not in δ^2H whereas evaporation in arid environments lead to changes in both isotopes. Trends due to boiling depend on fluid temperature and phase. Modified from Nicholson (2012).

An example of a study combining He, H_2, and O_2 isotopic systems is the one from Saby et al. (2020). These authors characterized the high-T Theistareykir geothermal field and identified multiple sources of fluids evidenced by small variations in different isotopic systems signatures. Coupled changes in ^{3}He/^{4}He and δ^{18}O showed mixing of meteoric and magmatic water, and influence of radiogenic helium (^{4}He*) paired with water-rock interaction.

1.4 Target areas and case studies

Helium isotopes are an excellent tool in detecting the sources and transport mechanisms of fluids in the crust. In this thesis, I employ helium isotopes, and other hydrochemical tracers, to decipher sources and transport processes at different timescales at various geotectonic contexts: (i) continental basin hosting a gas reservoir in Central France, (ii) seismically active and volcanically inactive zones in North Iceland, and (iii) a geothermal area inserted in an active rift system in Lake Abhe (Djibouti). In the case of North Iceland, the project was readapted due to the pandemic; for that reason, the next section explains the original and updated projects related to this target area.

1.4.1 Isotopic monitoring and survey in North Iceland

The initial goal of this thesis was to improve the sampling resolution of groundwater at seismically and volcanically active zones (mainly in Iceland and Italy) in order to comprehend the exchange and transfer of fluids to the surface in short timescales. Unlike the continuous CO_2 monitoring networks installed at various volcanoes and seismic regions, real-time analysis of isotopic ratios in the field remains unattainable. Continuous sampling, however, is possible using SPARTAH, an apparatus designed by Barry et al. (2009) for automatic groundwater sampling aiming future He analysis in the laboratory (Figure 1.8). SPARTAH consists mainly of a high-power motor, an uninterrupted power supply for eventual backup power, and a syringe pump linked to coils of Cu tubes. Before pumping, the Cu tubes are filled with deionized (DI) water which is drawn into the syringe at a rate established by the user. The space previously occupied by DI water is thus replaced by water from the well (Barry et al., 2009).

However, due to the pandemic, there were many travel restrictions and installation of machines in the field was severely impacted, with only one SPARTAH successfully installed in Hafralækur (North Iceland). Subsequent analyses of the samples at INGV Palermo were not possible. Nonetheless, the machine in North Iceland had to be installed inside the building due to weather conditions. In that case, SPARTAH was connected to a tank reservoir which was compromised due to re-equilibration of the water and gas phases, rendering the helium

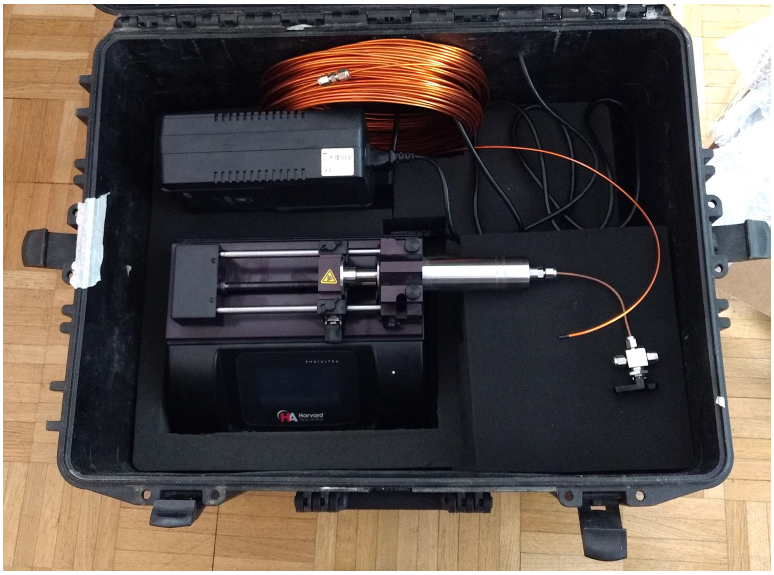

Figure 1.8: SPARTAH with all of its components: the Harvard syringe apparatus with syringe, Cu tubes, and power source inside a Pelican case.

isotopic ratios averaged values, and consequently non indicative of real-time changes. For these reasons, the SPARTAH project will not be reported or further discussed in this study.

Although a time series using SPARTAH was not achieved, weekly sampling of the same site was possible and groundwater was extracted directly from the well-head (borehole HA-01; Figure 1.10); these results are presented in Chapter 4. Even if changes in He isotopic ratios were detected, their interpretation could be biased if the different regional aquifers and isotopic end-members are not known. In order to support the He isotopes time series, we performed a thorough isotopic survey of North Iceland, where a data gap previously existed (Harðardóttir et al., 2018), including stable isotopes and major and trace elements. These different systems, sampled at the same time, can give information about mixing and secondary processes to identify if the helium isotopic variations, either in a spacial or temporal scale, are from degassing at depth or from lateral transport in the crust at subsurface depths, such as from mixing of different water bodies.

In Iceland geothermal fluids, $^{3}He/^{4}He$ ratios exhibit a wide range that are not necessarily connected to volcanic activity. In Vestfirðir, $>$ 110 km away from the closest active rift zones, the oldest rocks of Iceland are described (15.64 $\pm$ 0.15 Ma; Hardarson et al., 1997) along with its highest $^{3}He/^{4}He$ ratios, which have a high variability. Geothermal fluids in

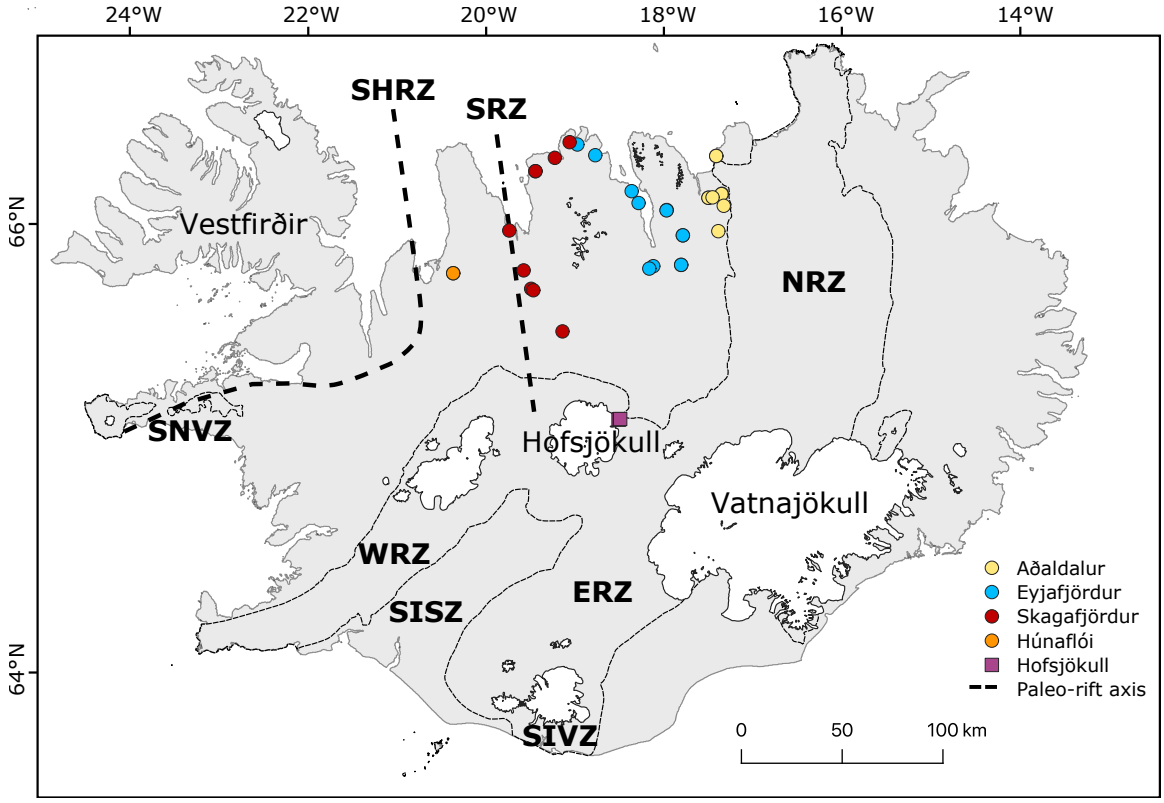

Figure 1.9: Iceland map with rift zones, regions of interest, and sampled sites.

Vestfirðir vary from 3 to 29 Ra (Füri et al., 2010; Hilton et al., 1998; Poreda et al., 1992), where Ra is the atmospheric $^{3}He/^{4}He$ (1.39 x 10^{-6}; Graham, 2002), displaying influence of the Icelandic plume component. Except for Vestfirðir, off-rift regions have not been investigated extensively, which is the case of North Iceland.

North Iceland, although volcanically inactive, registered earthquakes with magnitudes up to about 7 (Ms) (Einarsson, 2008; Stefansson et al., 2008). According to Barbieri et al. (2021) and Skelton et al. (2019, 2014), M > 5 events might trigger variations in hydrochemical parameters at Hafralækur, as observed in their time series for stable isotopes ($\delta^{18}O$ and $\delta^{2}H$), major, and trace elements. The variability of these geochemical tracers, nonetheless, is susceptible to water-rock interactions, unlike noble gases, which are chemically inert (Ballentine and Burnard, 2002). Helium isotopes can thus shed light on the sources of deep fluids (crust vs mantle) and/or the mixing processes that can modify their contributions in the fluids emitted at the surface, outside the influence of secondary processes in the crust (e.g., Caracausi et al., 2022).

Our study aims to diminish the helium isotopes data gap in North Iceland and to detect variations in groundwater helium isotopic signature potentially triggered by the tectonic earthquakes in the region. Our study area is limited in the east by the town of Húsavík in the Northern Rift Zone (NRZ), in the south by the Hofsjökull volcanic system, and in the west by Snæfellsnes-Húnaflói rift zone (SHRZ) ($\sim$ 50 km away from Vestfirðir) (Figure 1.9). This region is characterized by low temperature geothermal systems ($<$ 150°C), typical of off-rift regions in Iceland. To identify the sources of fluids and their transport mechanisms in the crust, we carried out an extensive survey of groundwater for $^{3}He/^{4}He$, $^{4}He/^{20}Ne$, $\delta^{2}H$, $\delta^{18}O$, $\delta^{34}S$, $\delta^{13}C_{TDIC}$, TDIC, major and trace elements analyses. Additionally, on June 28th, 2020 we started weekly sampling of groundwater from borehole HA-01 (Hafralækur) for $^{3}He/^{4}He$ and $^{4}He/^{20}Ne$ analyses.

Figure 1.10: HA-01; well head on the left and main building, where SPARTAH was connected and stored, on the right.

1.4.1.1 Hydrochemical background and monitoring at Hafralækur

North Iceland, although volcanically inactive, registered earthquakes with magnitudes up to 7 (M_s) (Einarsson, 2008; Stefansson et al., 2008). According to Barbieri et al. (2021) and Skelton et al. (2019, 2014), M $>$ 5 events might trigger variations in hydrochemical parameters at Hafralækur, as observed in their time series for stable isotopes (δ^{18} and $\delta^{2}H$), major, and trace elements (Figures 1.13 and 1.14). These geochemical tracers, nonetheless,

are susceptible to water-rock interactions, unlike noble gases, which are chemically inert (Ballentine and Burnard, 2002). Helium isotopes can thus shed light on the sources of deep fluids, outside the influence of secondary processes in the crust.

The borehole monitored in Hafralækur (HA-01) has a 100 m depth and its host rock is basalt and basalt-derived sediments (Figure Skelton et al., 2014; Andrén et al., 2016). These authors describe the water at 73-76 °C, pH of approximately 10.2, and 240 ppm of dissolved solids. Due to the seismic activity along and near the Húsavík-Flatey Fault, HA-01 has been monitored for dissolved major elements (Na, Si, Ca, and K) and stable isotopes (δ^{18}O and δ^{2}H) since 2008 (Skelton et al., 2019) and for dissolved trace elements since 2010 (Barbieri et al., 2021). This fault is highly active, registering earthquakes with magnitudes up to 7 (M_s) (Einarsson, 2008; Stefansson et al., 2008). Most earthquakes at this fault occur offshore; however, its last high magnitude (M_s 6.5) earthquakes on land destroyed the houses of Húsavík in 1872 (Stefansson et al., 2008). Three periods of earthquakes $M > 5$ occurred in the last decades in the area: in 2012-2013, 2020, and 2022.

Contribution from volcanism cannot be discarded. The nearest volcanic systems to HA-01 are towards the east (Figure 1.11): Theistareykir (or Þeistareykir) and Krafla. Theistareykir last eruption occurred c. 2.4 ka BP, producing the Theistareykjahraun lava flow. Southeast of Theistareykir, Krafla is composed of a central volcano and fissure swarms. Its largest known eruption, the Halarauður eruption, occurred c. 110 ka. The most recent eruption from this system consisted of a rifting event that started in December 1975 and ended in September 1984 (Sæmundsson, 1991; Thordarson and Larsen, 2007). The last eruption in the vicinity of HA-01 took place further south from Krafla and near the Vatnajökull ice cap, in the Bárðarbunga system, one of the most active, largest, and longest volcanic systems of Iceland (Thordarson and Larsen, 2007)). This eruption lasted from August 2014 until February 2015 and consisted of the reactivation of the Holuhraun eruptive fissure (Sigmundsson et al., 2015).

From the trace elements time series, Barbieri et al. (2021) identified changes in B, Al, and V concentrations before the $M > 5$ earthquake from 2012, variations in B, Al, V, Li, and Mo concentrations before the 2014 Bárðarbunga eruption (∼115 km from HA-01), and changes in some trace elements (Li, B, Ga, Mo, Sr, Rb, and Fe) before an $M > 5$ earthquake that

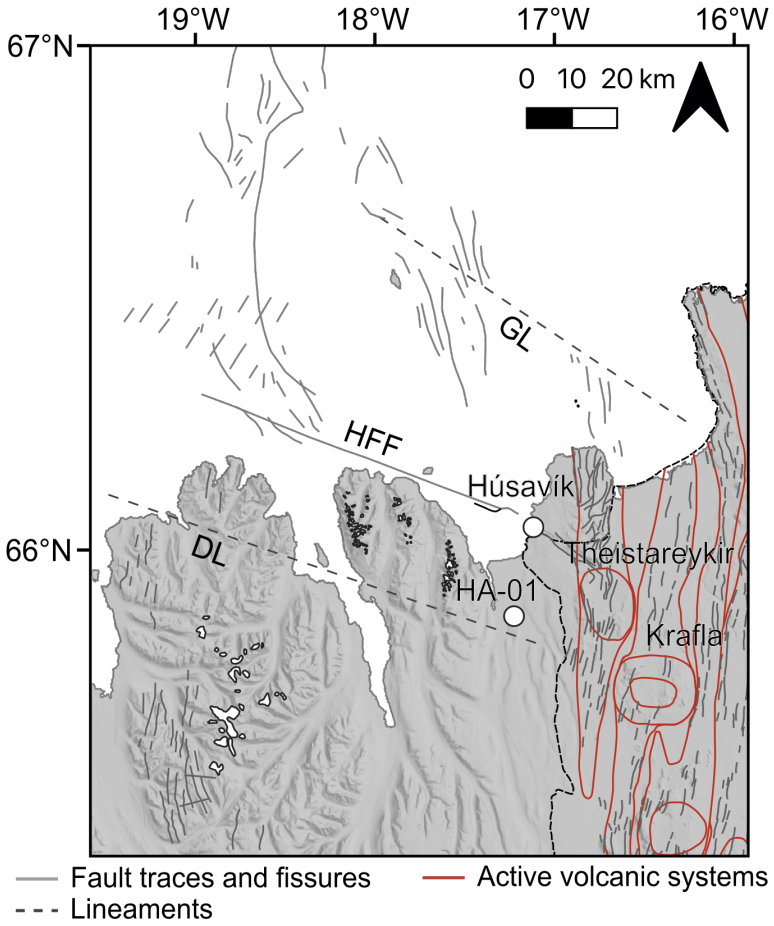

Figure 1.11: Main tectonic elements and volcanic centres near HA-01. DL refers to the Dalvík Lineament, HFF to Húsavík-Flatey Fault, and GL to Grímsey Lineament.

occurred in the north in 2018; however, the authors also describe changes in groundwater chemistry when no seismic (M $>$ 5) or volcanic events occurred.

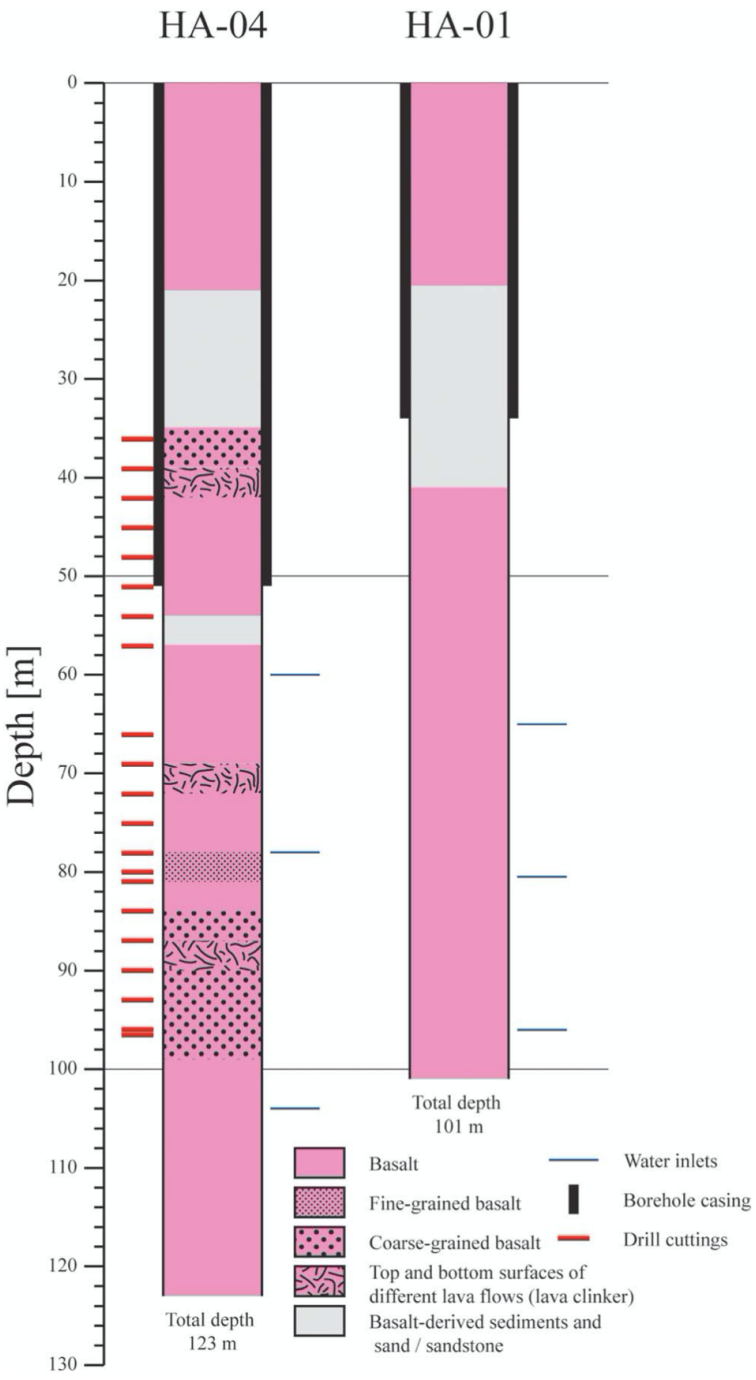

Figure 1.12: Profiles of the boreholes HA-04 and HA-01 (Andrén et al., 2016).

From dissolved major elements (Na, Si, Ca, and K) and stable isotope ratios of hydrogen (δ^2H) and oxygen (δ^{18}O) in groundwater, from 2008 to 2013, Skelton et al. (2014) proposed that the short-term chemical changes in the water of HA-01 were associated with M >5 earthquakes. δ^2H, Na, Si, and Ca maxima coincided with the M >5 earthquakes that oc-

curred during the investigated period. These peaks started before the earthquakes and lasted three months for δ2H and four for Na, Si, and Ca (Figure 1.13).

However, it remains to establish the source of the fluids and which mechanisms lead to the chemical changes. There are two main theories as to which mechanisms can cause them: (i) mixing of chemically different aquifers or (ii) water-rock interactions due to increase in reactive surface (Claesson et al., 2007). Skelton et al. (2014) explains the variations in δ^2H at Hafralækur through mixing of different groundwater components. Their samples plot in separate clusters parallel to the Icelandic meteoric water line (IMWL) and Global meteoric water line (GMWL), displaying highly negative δ^2H related to the presence of a pre-Holocene component (Figure 1.14). Skelton et al. (2019) interprets that clusters to the right of the GMWL and IMWL are probably controlled by a fluid-rock interaction whereas clusters to the left of the meteoric lines could be due to degassing or deuterium excess related to seasonal effects. δ^2H maxima were preceded by gradual increases towards Holocene values six to two months before the earthquakes and gradually returned to pre-Holocene values after the earthquakes. On the other hand, the sample clusters are separated by a δ^{18}O control that indicates, according to these authors, a component influenced by water-rock interactions since rocks contain large amounts of oxygen and minor of hydrogen.

Andrén et al. (2016) studied host rocks and secondary minerals from HA-04, a borehole nearby HA-01. These authors suggested that the observed long-term changes in major elements in the water, prior to earthquakes, are due to precipitation and dissolution processes resulted from water-rock interactions. The model proposed contains two stages: (i) constant replacement of labradorite by analcime and (ii) precipitation of other zeolite minerals in vesicles and/or fractures. Regarding the changes related to earthquakes, Andrén et al. (2016) attempted to explain the abrupt Na maxima that started only two months before the earthquakes, by a different process than that of δ^2H maxima since Holocene groundwater most likely contains less Na than pre-Holocene groundwater due to restrict time to interact with the host rocks. These authors propose a nonstoichiometric dissolution of analcime, mainly along fractures, with preferential release of Na because the stoichiometric reactions of labradorite, analcime, and zeolites can only explain Na absorption from the water. Andrén et al. (2016) also discussed the possibility that the water-rock chemical equilibrium

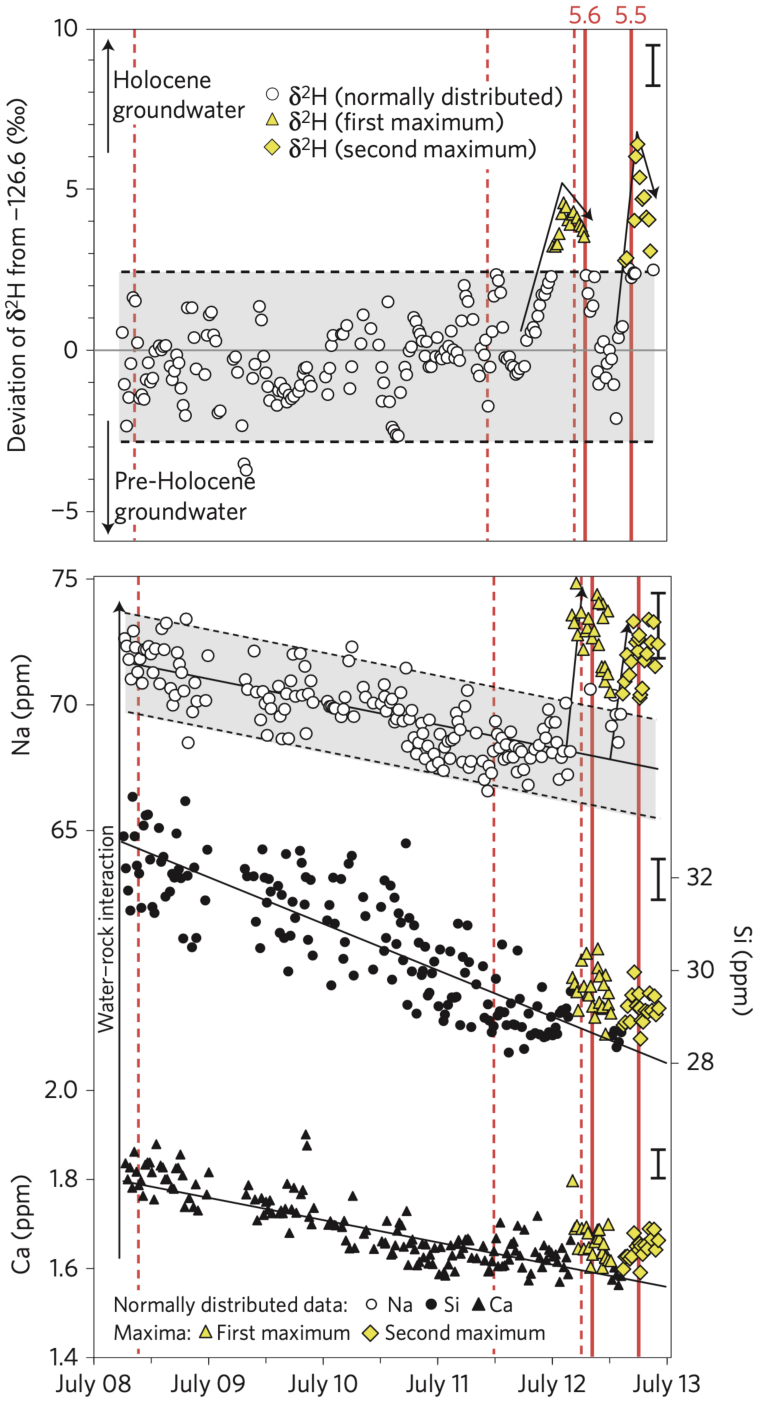

Figure 1.13: Time series for Ca, Si, and Na concentrations and δ^2H deviation from -126.6‰ of groundwater from 2008 to 2013 collected at borehole HA-01. Earthquakes are shown by solid (M $>$ 5) and dashed (M $<$ 5) red lines. Normally distributed data are shown by open circles (δ^2H, δ^{18}O, Na), black circles (Si) and triangles (Ca) with mean values (thin solid line) and 2σ envelopes (thin dashed lines and shading). Pre-seismic maxima are shown by yellow symbols. Pre- and co-seismic changes are shown by arrows. Analytical errors are shown above the top right of the data. Figure modified from Skelton et al. (2014).

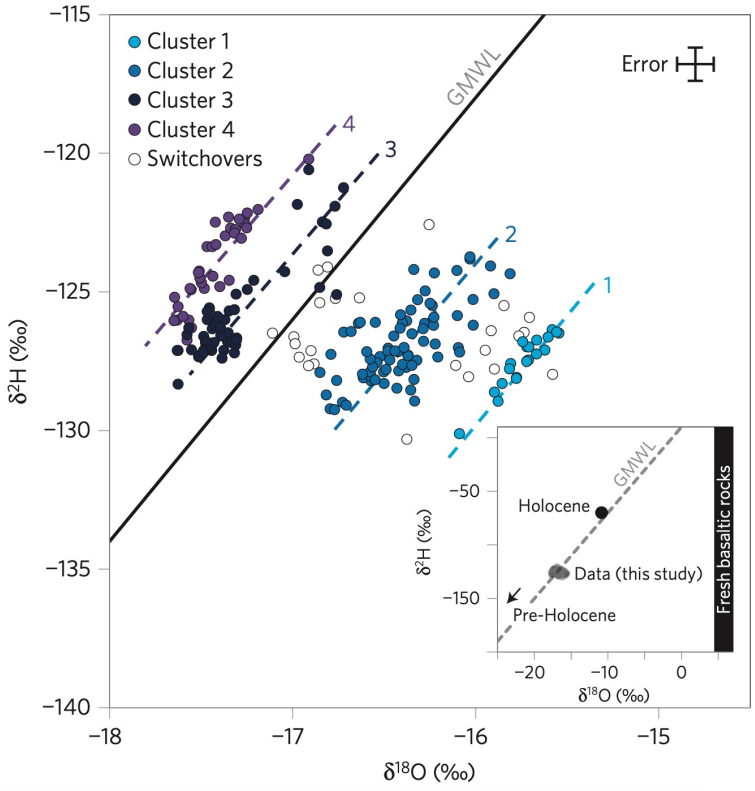

Figure 1.14: Plot of δ^2H vs δ^{18}O of groundwater from 2008 to 2013 collected at borehole HA-01. Clusters of analyses compared to the Global Meteoric Water Line (GMWL). Data and figure from Skelton et al. (2014).

was shifted by mixing of different groundwater components causing a variation in pH or temperature that could have triggered the nonstoichiometric reactions.

Based on the remarks of Andrén et al. (2016), Skelton et al. (2019) proposes a model in which (i) the changes prior to the M >5 earthquakes would be due to groundwater mixing that lead to shift from equilibrium, triggering chemical changes via water-rock interactions; (ii) the postseismic variations were due to fast mixing between different groundwater sources; and (iii) the long-term hydrochemical changes observed by Andrén et al. (2016) would be caused by both mixing and mineral growth.

1.4.2 Tracing the source of He in a continental basin: the case of Central France

In some regions of the crust, interpretation of $^{3}He/^{4}He$ ratios can be ambiguous, such as in the Paris Basin (France), where no magmatic manifestations at the surface, or evidence for modern tectonic extension are present, yet helium isotope ratios show higher $^{3}He/^{4}He$ than expected for the continental crust (up to 0.14 Ra; Marty et al., 1993; Pinti and Marty, 1995, 1998). Helium isotopes have been investigated in groundwater and crude oil from the Paris Basin and in gas manifestations in the Massif Central, respectively (Bräuer et al., 2017; Marty et al., 1993; Pinti and Marty, 1995, 1998). While there is unequivocal evidence for a mantle contribution in the Massif Central, with $^{3}He/^{4}He$ ratios up to 6.4 Ra (where Ra is the atmospheric $^{3}He/^{4}He$ – 1.39 x 10^{-6}; Graham, 2002), a mantle contribution in the Paris Basin is less evident. Helium isotope ratios (0.02 – 0.11 Ra, reaching 0.14 Ra for basement-hosted groundwater) are close to the crustal end-member (0.001 – 0.02 Ra) as computed from average U+Th/Li abundances in related lithologies of the Paris Basin (Pinti and Marty, 1998). Because $^{3}He/^{4}He$ ratios of geothermal fluids and oils are higher than values predicted for a purely crustal origin, Pinti and Marty (1998) proposed a mantle contribution to gases hosted by basinal fluids. In agreement with this possibility, it was observed that the $^{3}He/^{4}He$ ratios increase with depth in the basin, suggesting injection of mantle-derived helium from the basement underlying the sedimentary units, and progressive dilution of this signal by radiogenic, ^{4}He-rich helium produced in the sedimentary pile (Torgersen, 1993). Helium isotope ratios also tend to be higher towards the southern margin of the basin (0.09 Ra in groundwater and 0.14 Ra at the basement; Pinti and Marty, 1998). This trend is possibly related to the North-South major fault system ("Sillon Houiller") in Central France, and to the addition of mantle-derived ^{3}He from the nearby Rhine rift magmatism at the eastern border of the Paris Basin in Lorraine (Marty et al., 2003). Alternatively, $^{3}He/^{4}He$ ratios higher than expected for the purely crustal end-member could reflect local enrichments of lithium-derived ^{3}He, with He isotope variations potentially tracking the occurrence of Li-rich lithologies of economical relevance.

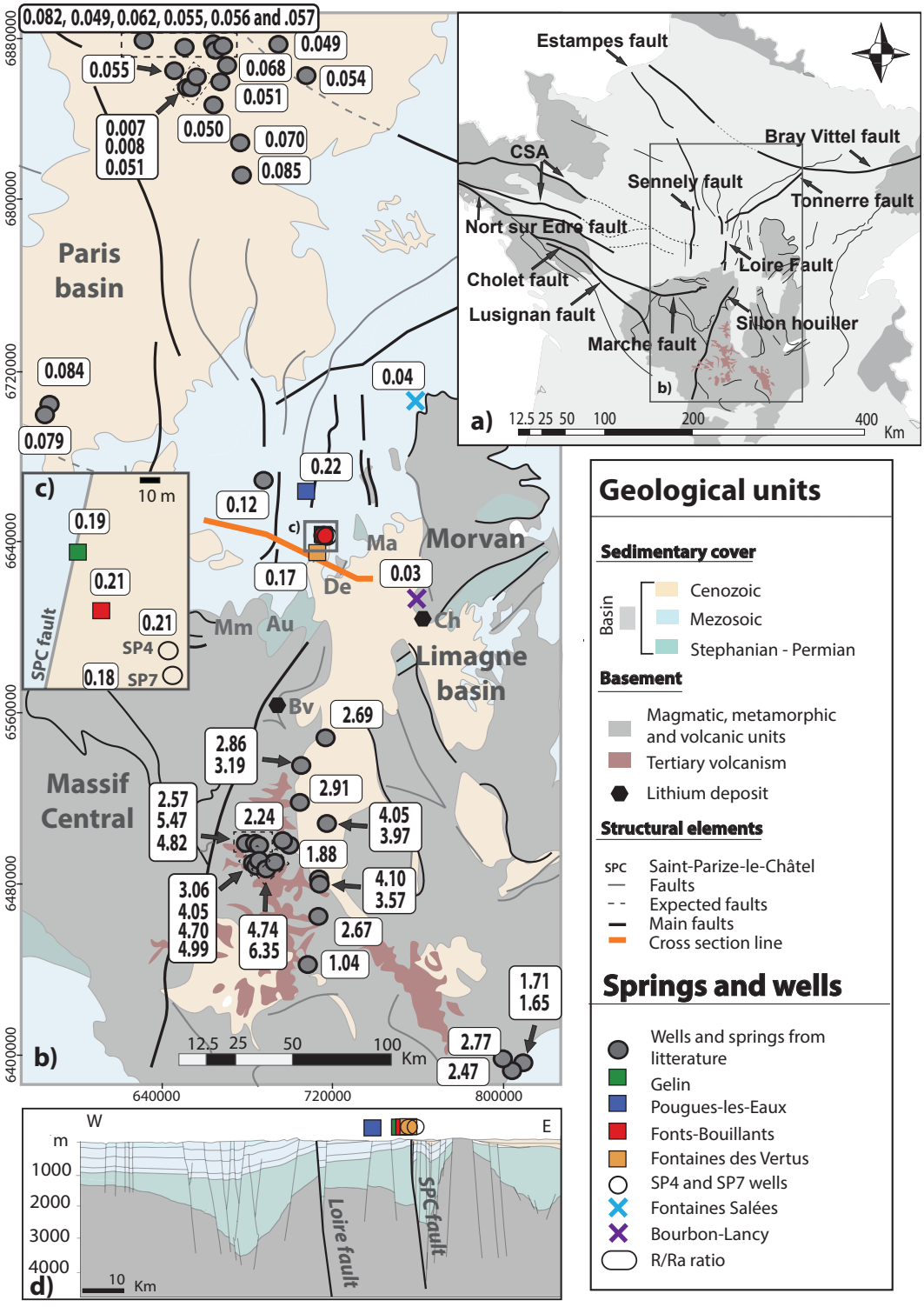

Figure 1.15: Geological map of the study area with helium isotope results (in Ra) and literature data. a) Structural map with major structures inherited from the Variscan orogeny (Baptiste, 2016). b) Simplified geological map (1/1,000,000 BRGM French geological map) with main geological structures of the area (Au: Aumance basin, De: Decize horst and Ma: Machine graben), location of the well SP4, SP7, springs and the lithium deposits of the area (Ch: Chanvence and Bv: Beauvoir; Gloaguen et al., 2018), and distribution of literature helium isotope data (Bräuer et al., 2017; Marty et al., 1993; Pinti and Marty, 1998). c) Focus on the Saint-Parize-le-Châtel area with location of the springs and wells. d) Simplified cross section line of the study area, with location on the map "b)" marked by the orange line.

Recently, a CO_2-rich gas reservoir with He concentration reaching 0.04% has been discovered while conducting helium exploration in the Nièvre County, between the Massif Central to the south and the southern border of the Paris Basin to the north (Figure 1.15). Although not reaching commercial concentrations for helium ($> 0.3\%$), its helium content is about 100 times higher than the atmosphere ($\sim 0.0005\%$; Glueckauf, 1946). This gas accumulation has the potential to shed light into the nature of the intermediate $^3He/^4He$ ratios, between typical mantle values and the crustal range, observed in the Paris Basin (e.g., Pinti and Marty, 1998). The geochemical description of this reservoir is still at an early stage, and so our paper focuses on the use of isotope geochemistry to identify the source(s) of the Nièvre gas.

Figure 1.16: Sampling station at the SP4 well. Cu tubes and Giggenbach bottles were connected to the same sampling train to avoid air contamination.

In the present study, we sampled bulk gas samples using two distinct approaches: copper tubes (dedicated to He isotope measurements) and Giggenbach bottles (dedicated to Ar-Ne-Xe isotope measurements) (Figures 1.16 and 1.17). The samples consist in free gases from two CO_2-rich wells (SP4 and SP7) and bubbling springs from the surrounding areas – Gelin, Fonts-Bouillants, Fontaine des Vertus, Pougues-les-Eaux, Fontaines Salées, and Bourbon-

Lancy (Figure 1.15). We also sampled SP4 every hour during the well test to detect potential disturbances in the reservoir (Figure 1.16). Most springs were cold (12-14°C; Boineau and Maisonneuve, 1972; Risler, 1974), apart from Bourbon-Lancy, which has a temperature of 52°C (Batard et al., 1982). To identify the different sources of helium, we analysed $^{3}He/^{4}He$ and $^{3}He/^{20}Ne$ on gas collected from all sites. We also analysed the major gas composition, stable isotopes of CO_2 ($\delta^{13}C$) and N2 ($\delta^{15}N$), and Ar, Ne, and Xe isotopes for the SP4 and SP7 well gas samples.

Figure 1.17: Sampling of gelin spring. Cu tubes and Giggenbach bottles were connected to the same sampling train to avoid air contamination.

1.4.3 Tracing the source of He in the Lake Abhe geothermal field, Djibouti

The East African Rift System (EARS) has a vast geothermal untapped resource, especially in remote regions where social challenges require it the most. The "Geothermal Village" project (LEAP-RE) aims to identify and characterize geothermal areas with potential for electric and thermal energy systems in the EARS for future implementation of independent geothermal power plants. One of the areas with such potential is Lake Abhe (Djibouti).

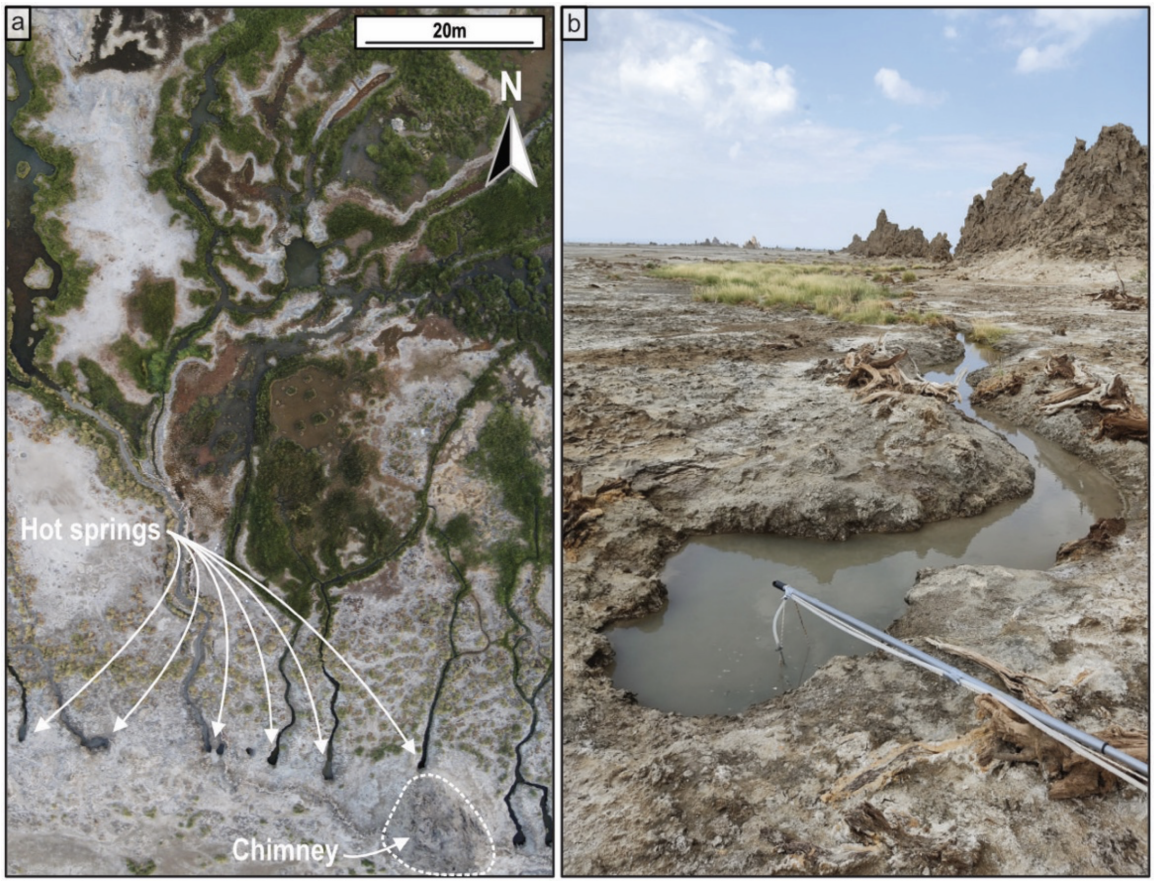

Figure 1.18: Hot springs in the Lake Abhe region. (a) Aerial view of hot springs flowing northward. (b) Hot spring hosted in the sedimentary flats near the travertine chimneys. Extracted from Walter et al. (2023).

Previous reports modelled the reservoir temperature at 110-154°C (Awaleh et al., 2015; Hersir et al., 2016) indicating that the low enthalpy geothermal system at Lake Abhe has potential for electricity production, although, according to Hersir et al. (2016), it would require large amounts of water for power production, which is a challenge for this arid

region. The "Geothermal Village" project aims to characterize better this reservoir in terms of geology and physical parameters. Our contribution was with the geochemical model via a survey (mainly stable and helium isotopes) in order to establish the source of gas and water dynamics.

The Lake Abhe geothermal area is $\sim$ 30 km from the Dama Ale volcano and $\sim$ 80 km from Lake Asal. Hot springs are located along WNW-ESE faults, emanating from carbonate chimneys (Figure 1.18). These springs range from 71 to 99.7 °C with pH from 7.61 to 8.80 and TDS of 1918 to 3795 mg/L (Awaleh et al., 2015). Awaleh et al. (2015) investigated the source of water in Lake Abhe (Djibouti) and its surrounding hot springs. These authors identified two main sources: one corresponding to young meteoric water from the surface and another from a deeper and older source, based on tritium ages. The latter indicates the presence of a regional groundwater system. Awaleh et al. (2015) proposed a model in which heat transport towards the surface mainly due to circulation of meteoric water through faults. Helium isotopes can shed light into the sources of deep fluids that could be associated with the hot springs emanations.

Lake Abhe is in a strategic location for helium isotopes studies. The helium isotopic signature in the Afar, Main Ethiopian Rift (MER), and Tadjoura gulf, for fluids and volcanic products, range up to 17 Ra (e.g., Marty et al., 1993, 1996; Scarsi and Craig, 1996), reaching values above the typical upper mantle signature (8 $\pm$ 1 Ra; Graham, 2002) which indicates the influence of a mantle plume. The plume centre was theorized to be near Lake Abhe (Rooney et al., 2011; Schilling et al., 1992), where helium isotopic data has not yet been reported in the literature.

We performed an isotopic survey of hot and cold springs near Lake Abhe to characterize the groundwater systems and identify the sources of fluids (Figure 1.19). We collected gas and water samples for gas chromatography, $^{3}He/^{4}He$, $^{4}He/^{20}Ne$, $\delta^{13}C_{CO_2}$, $\delta^{13}C_{CH_4}$, $\delta^{2}H_{CH_4}$, $\delta^{15}N$, $\delta^{18}O$, δD, $\delta^{34}S_{SO_4}$, $\delta^{33}S_{SO_4}$, $\delta^{34}S_{H_2S}$, and $\delta^{33}S_{H_2S}$. In our study we also combine data from SW Afar and Tendaho Grabben from surveys performed in 2015 and 2017.

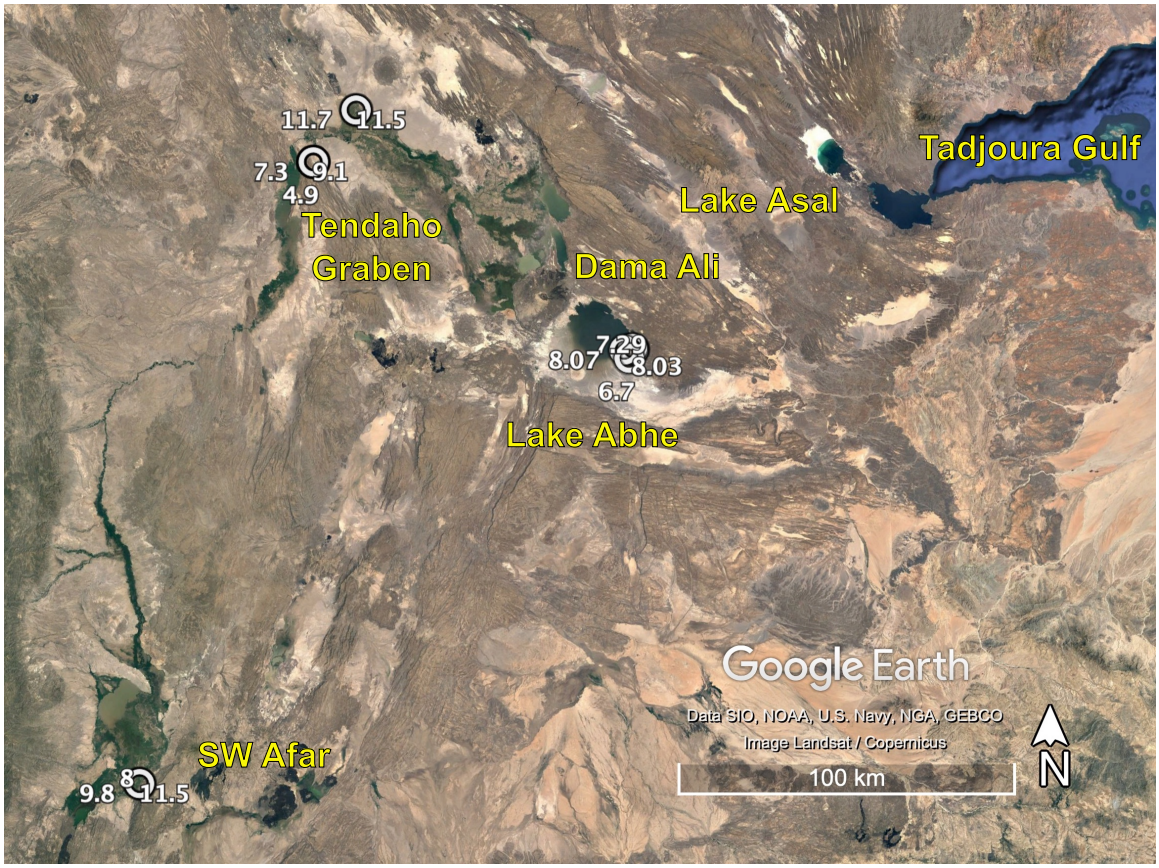

Figure 1.19: Sample locations with $^{3}He/^{4}He$ results (in Ra).

Chapter 2

Sampling

Sampling for helium isotopes analyses were performed using copper tubes as it has low helium diffusion and can be stored for years before analysis (e.g., Burnard et al., 2013). For other noble gas analyses (e.g., Ar, Xe), Giggenbach bottles were used since they allow the concentration of inert gases (mainly N_2 and noble gases, along with possible traces of CH_4, CO, H_2, etc) in the vacuum headspace above the NaOH solution (Giggenbach and Goguel, 1988). In the laboratory, the gaseous fraction from the Giggenbach bottles was equilibrated under vacuum with an evacuated metal bottle fitted with two metal valves (Nupro SS4H@), where the gas could be stored for long periods of time without diffusive leakage or exchange with atmospheric gases. For stable isotopes analyses and gas chromatography, I sampled the gas using evacuated glass bottles. The different types of samplers are shown in Figure 2.1.

The sampling containers are connected to the well (Figure 2.2) using hoses of different sizes and to a funnel when sampling a spring (Figures 2.3 and 2.4). "Flushing" of the air previously contained in the tubes (and funnel) is necessary before sampling; the duration depends on the volume of tubing and flow rate, but at least 30 minutes is recommended. When sampling gas, a container with water is added to the end of the sampling "train" to avoid atmospheric contamination. In the case of groundwater sampling, the water flow prevents air from entering the hoses.

In Iceland, sampling was performed from boreholes whereas in Djibouti I sampled exclusively from springs, most of them hot (up to 90°C). In Central France, most sites were cold springs with bubbles and only two of the sites were gas boreholes.

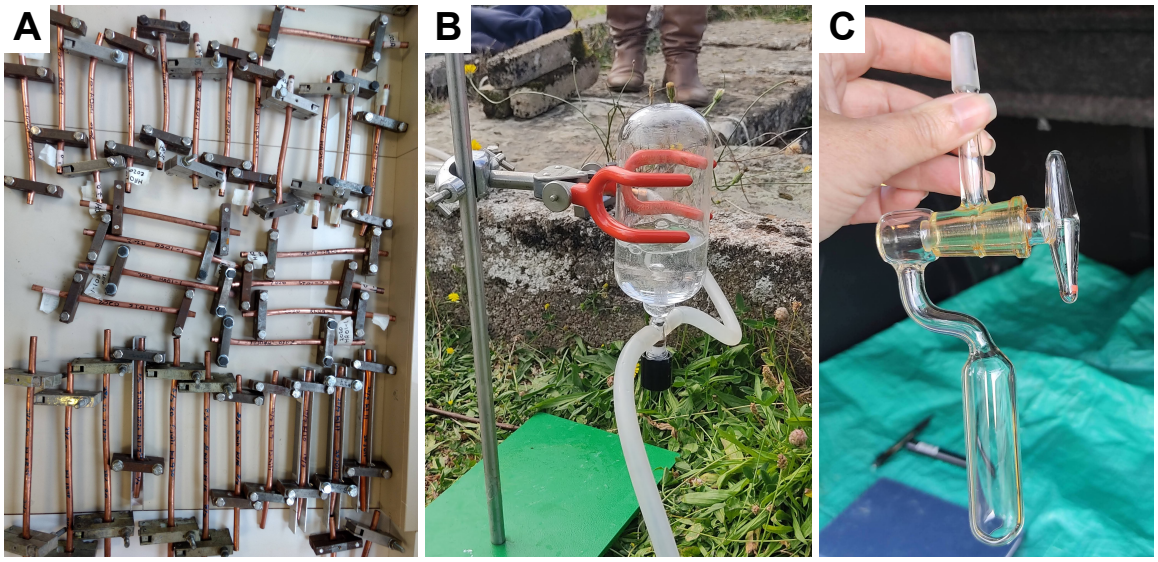

Figure 2.1: Main types of samplers used in this thesis. (a) Copper tubes for helium isotopes analyses, (b) Giggenbach bottles, and (c) glass bottles for stable isotopes analyses and gas chromatography.

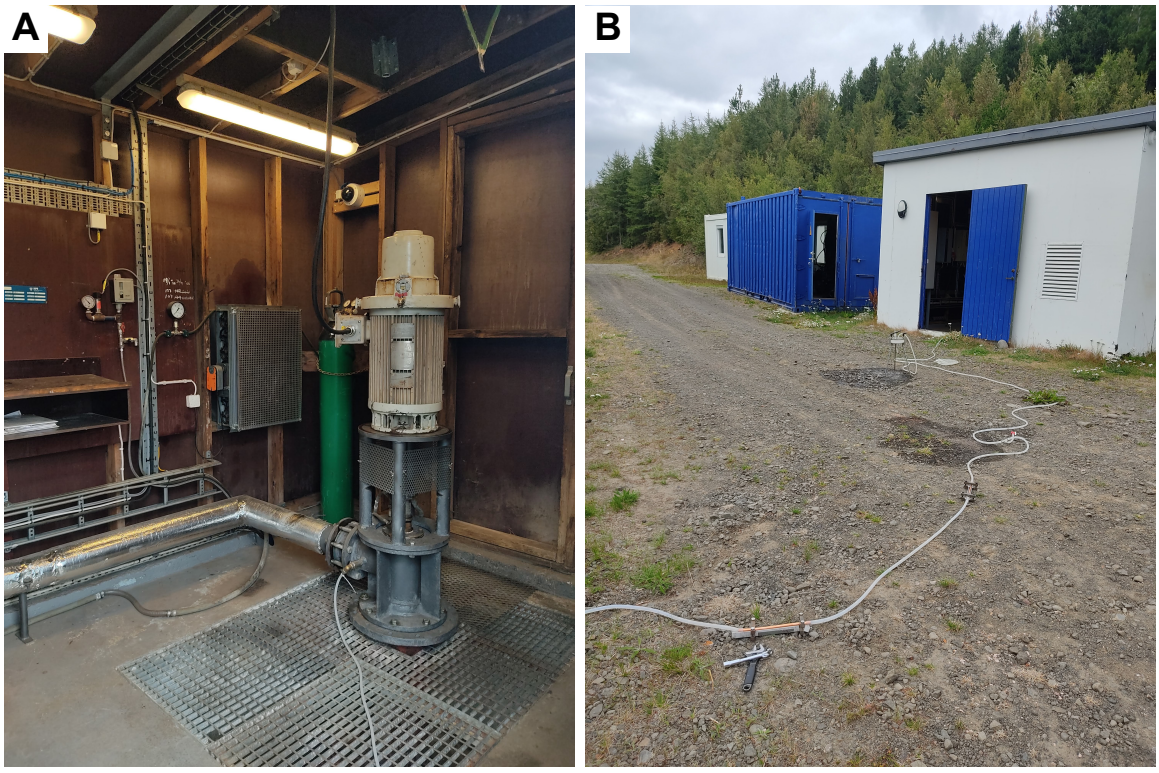

Figure 2.2: Sampling at BN-1, North Iceland. (a) Tubing connected to the water inlet of the borehole and (b) the copper tubes connected to several hoses for sampling.

Figure 2.3: Sampling at Fontaine des Vertus, Central France. The funnel is connected to the sampling containers by hoses.

Figure 2.4: Sampling at GVS4, Djibouti. The funnel is connected to the sampling containers by hoses.

Chapter 3

Helium isotopes analysis

Contents

In noble gas analyses, three main steps are followed: gas extraction, purification, and analysis (Figure 3.1). In this thesis, most samples were either water, glasses, or collected as free gas; for the latter, extraction is not required.

3.1 Gas extraction

Most samples described in this thesis were collected in copper tubes. First, a stainless steel vessel is required to connect the copper tube to the line and extract the sample (Figure 3.2). In this vessel, water is separated from gas so that the liquid does not contaminate the line. This container is referred to as an "extraction vessel". Before opening the tube at the lower clamp, the vessel is evacuated for 30 minutes. The sample is then equilibrated with the volume under static vacuum. In such conditions, noble gases will partition to the head-space above the liquid due to its low solubility. Water is contained in a stainless-steel

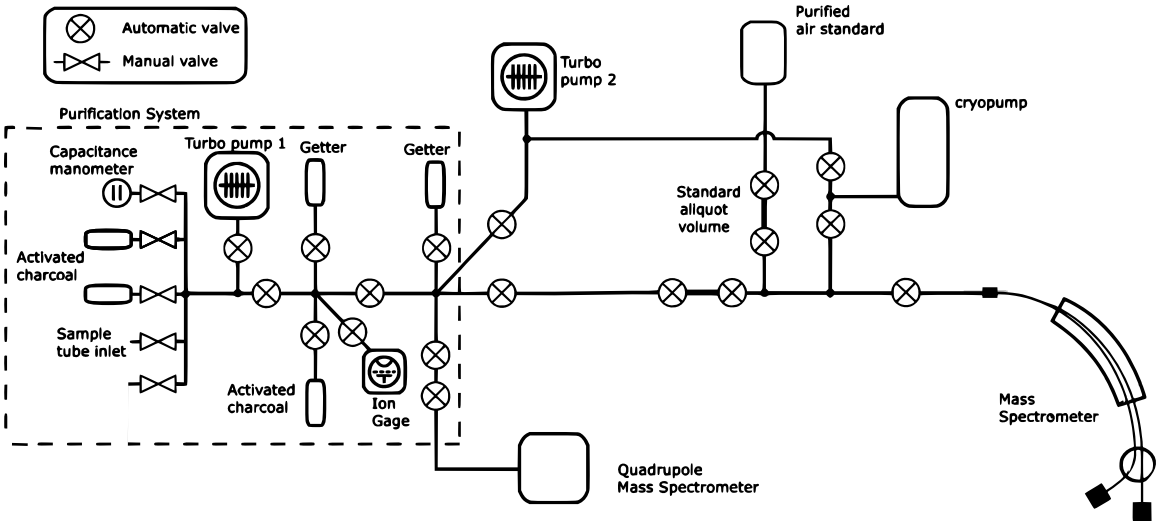

Figure 3.1: Schematics of the purification line and noble gas spectrometers. Modified from Mabry et al. (2013)

trap at liquid nitrogen temperature (77 K) before entering the line. The mass of water can be obtained by weighting the Cu tube before and after extraction.

For the glass samples, crushing under vacuum was employed to release gases trapped in fluid inclusions and vesicles following the procedures described in Burnard et al. (2013), pumping under ultra-high-vacuum and baked at 100-150°C for 12-24h.

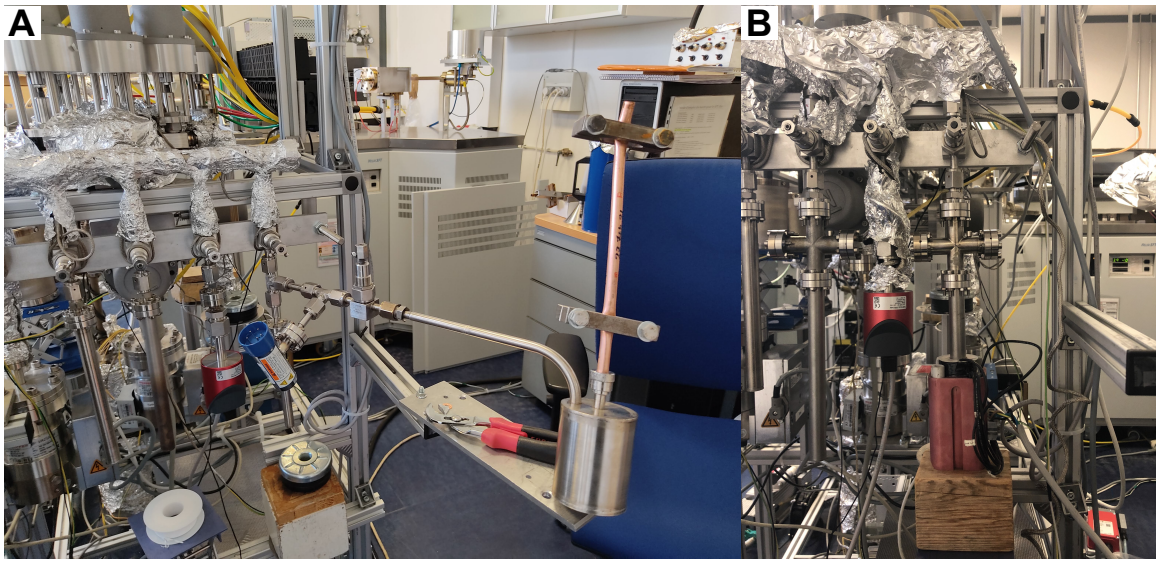

Figure 3.2: Extraction vessel for copper tube samples (A) and glass crusher (B) connected to the purification line.

3.2 Sample purification

The procedure to purify samples for noble gas analyses is described in Burnard et al. (2013) and Zimmerman et al 2015. The specific steps employed during this thesis are listed in the following paragraph.

Purification (Figure 3.1) begins with a charcoal trap at liquid nitrogen temperature to trap heavier noble gases. Then it is purified in the first getter at 600°C to trap active gas phases, such as CO_2, H_2O, SO_2, O_2, N_2, etc., and another charcoal trap at 77 K, simultaneously, to trap the heavier noble gases. Prior to being introduced in the quadrupole mass spectrometer (QMS) for ^{20}Ne and ^{4}He analyses, it goes through another set of getter and charcoal trap. After $^{4}He/^{20}Ne$ is analysed, the totality of the line is introduced in a cryogenic trap at 50 K to separate Ne and prevent competing ionization in the source. A charcoal trap at 77 K further purifies the sample, mainly from Ar at this point, and is introduced in a magnetic sector mass spectrometer, more specifically a split-flight-tube (SFT) mass spectrometer, for simultaneous ^{3}He and ^{4}He detection. Each purification step lasts 10 minutes. In the case of copper tubes containing only gas, the procedure is the same except it is not necessary to trap water.

3.3 Mass spectrometer

All helium isotopic analyses of this thesis were performed on a Thermofisher Helix SFT (split-flight-tube) at CRPG. It consists of a Nier-type ion source, a magnet to separate the two helium isotopes by mass, and two collectors, one for ^{4}He (Faraday cup) and another for ^{3}He (electron multiplier) simultaneous analyses (Figure 3.3). The electron multiplier has a mass resolution > 700, ensuring separation from its two interferences (HD and ^{3}H), and the Faraday cup > 400.

The source consists of a filament, current collector (trap), ionizing chamber (ion box), and multiple focalisation plates (Zimmermann and Bekaert, 2020). In the Nier-type source, ionization of the neutral gas occurs by electron impact; an electron beam is generated by applying a current to a metal filament (rhenium) (Figure 3.3). The filament is held at

high temperature (> 1500 °C) and the electrons produced are extracted from its surface and accelerated by potential difference. The electrons cross the ionizing chamber, where ionization of the gas happens, with its trajectory optimized by magnets, and are collected by the trap. The ions produced in the source are extracted by an electrostatic field and enter a magnetic field generated by an electro-magnet, inside the flight tube which allows transmission of ions from the source to the collectors. In the flight tube, the isotopes are separated by mass from their response to the changes in the magnetic field under a constant acceleration reference. In the Helix SFT, the split flight tube transmit the isotopes to multicollectors for analyses. Two types of collectors are commonly used in noble gas analyses: Faraday cup and electron multiplier. In a Faraday cup, the electrical charges brought by the ion beam are collected on its surface and accumulate generating a weak electric current proportional to the number of ions accumulated; this current is then amplified with a high resistance (10^{10} to 10^{12} Ω). This type of collector is adapted for analyses of noble gases abundant in nature, such as ^{4}He and ^{40}Ar; for low abundance isotopes, such as ^{3}He and Xe isotopes, an electron multiplier (Compact Discrete Dynode - CDD) is more adaptable, as it is more sensitive. A CDD consists of a system of plates (dynodes), similar to the ones in Faraday cups, parallel to each other, that convert the cations into electrons in an amplification chain of dynodes.

Before analyses, the source was tuned for high sensitivity, good peak shape (symmetric plateau) and alignment. The source parameters are reported in Table 3.1; small variations in the parameters occurred in the course of this thesis due to multiple power cuts.

Table 3.1: Source parameters for the Helix SFT measurements.

Source parameter	value	unit
Acceleration reference	∼4.5	kV
Trap voltage	24.82	V
Trap current	400.6	μA
Ion repeller	-5.8	V
Electron energy	94.0	V
Extraction lens	48.0	%
Horizontal symmetry	-5.11	%
Z-focus	47.0	%
Z-symmetry	6.0	%

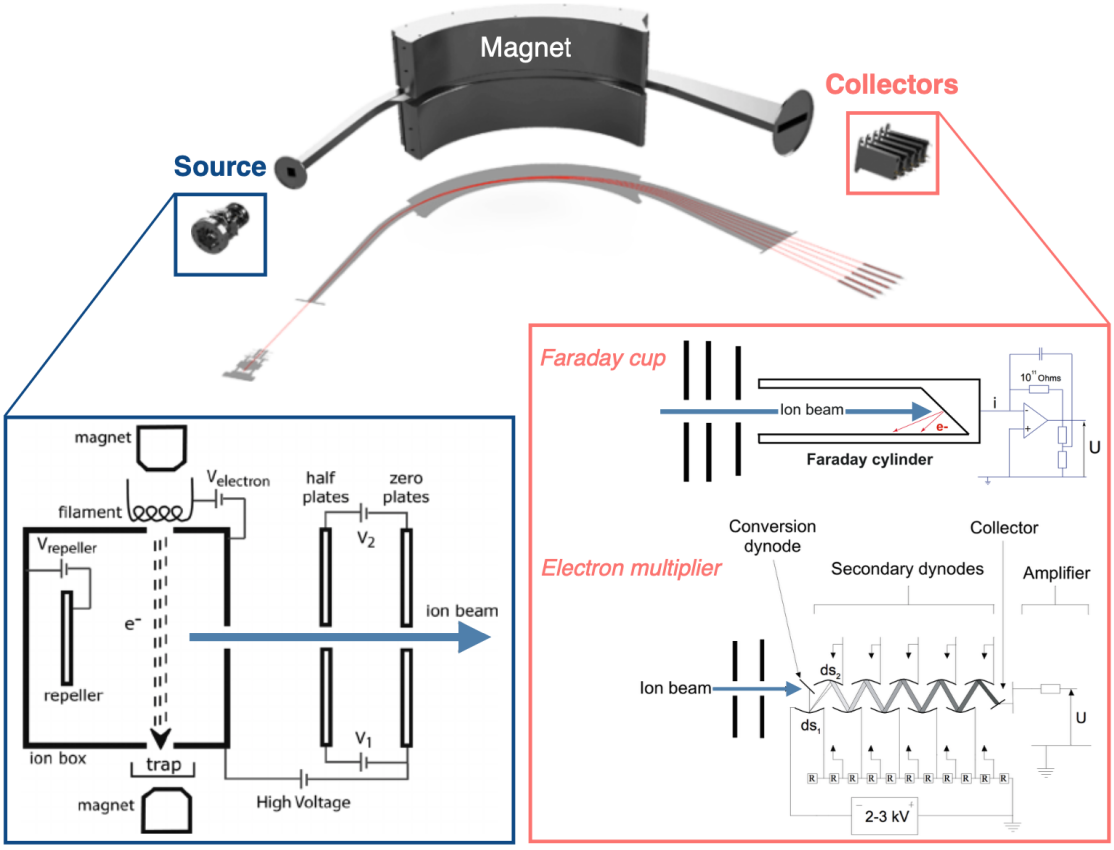

Figure 3.3: Main elements of the mass spectrometers for noble gas analyses: Nier-type source, a magnet for isotopes mass separation, and collectors. Extracted from Bekaert 2020.

3.4 Blanks and air standard measurements

Blanks are presented in Table 3.2, following chronological order. Line blanks are very close to the detection limit (3.6 x 10^{-16} mol ^{4}He), whereas blanks performed with the full extraction vessel are significantly higher (9.7 x 10^{-13} mol ^{4}He), but still remain very low compared to the He signal of typical samples (average of 5 x 10^{-9} mol ^{4}He). Even including the blanks with high ^{4}He signal, blank contribution is low (0.02%). Results reported in this thesis are corrected for the blanks.

In order to measure He and Ne abundance, the sensitivity method was employed. This method is based on the peak height of the most abundant noble gases, in this case, ^{4}He and ^{20}Ne. Its precision depends on the reproducibility of the standard gas (Burnard et al., 2013). The standard gas was atmospheric air calibrated at the laboratory considering no isotopic fractionation occurred. Standards were measured with 1, 5, and 10 pipettes, each

twenty times, in which the latter presented the best precision of $^3He/^4He$ ratios. The 10 pipettes standard "routines" (∼10 measurements each) yielded errors (relative repeatability = standard deviation /average) up to 3.89 %. During a period of stability of the mass spectrometers, $^3He/^4He$ ratios measured on samples were normalized to the average value of the 10 pipettes standard routine. After each power cut, a new standard routine is established. I adapted the dilution of each samples, when possible, to match the standard signal.

Table 3.2: Blanks for the line with ("Black tube Cu 'n'") and without ("Blank line 'n'") the extraction vessel for standard copper tubes.

Reference	$[^4He]$ (fA)	^4He (mol)	Dilution factor (10^{-2})
Blank line 1	0.08	7.2×10^{-16}	6.95
Blank line 2	0.05	4.5×10^{-16}	6.95
Blanc tube Cu 1	0.33	1.1×10^{-14}	0.69
Blanc tube Cu 2	0.29	9.5×10^{-15}	0.69
Blanc tube Cu 3	0.41	1.3×10^{-14}	0.69
Blank tube Cu 5	0.00	0.00	0.69
Blank line 4	0.09	1.6×10^{-16}	6.95
Blank tube Cu 7	0.37	2.4×10^{-15}	0.69
Blank line 5	0.06	1.1×10^{-16}	6.95
Blank tube Cu 8	63.34	1.6×10^{-12}	0.69
Blank tube Cu 9	22.12	5.8×10^{-13}	0.69
Blank tube Cu 10	23.34	6.1×10^{-13}	0.69
blank line 6	0.56	9.9×10^{-16}	6.95
blank tube Cu 11	0.24	3.3×10^{-14}	0.69
Blank tube Cu 12	0.24	3.2×10^{-14}	0.69
Blank tube Cu 13	0.21	3.5×10^{-14}	0.69
Blank tube Cu 14	5.76	9.4×10^{-13}	0.69
Blank tube Cu15	1.65	2.7×10^{-14}	0.69
Blank tube Cu16	0.34	5.5×10^{-14}	0.69
Blank tube Cu17	53.14	1.2×10^{-11}	0.69
Blank tube Cu18	0.49	1.0×10^{-13}	0.69
Blank tube Cu19	0.16	3.3×10^{-14}	0.69
Blank crusher 1	11.04	1.2×10^{-14}	1.49
Blank crusher 3	2.48	2.6×10^{-15}	1.49

Chapter 4

Regional and temporal helium isotopes variability in North Iceland geothermal fluids: evidence for off-rift mantle degassing and localized seismicity-induced processes

Manuscript to be submitted to GCA

Carolina Dantas Cardoso and collaborators

Abstract

In Iceland, the highest $^{3}He/^{4}He$ ratios for geothermal fluids are described in Vestfirðir (up to 29 Ra), >110 km away from the active rift zones. Other off-rift regions have not been investigated extensively, which is the case of North Iceland. This region, although volcanically inactive, registered earthquakes up to M 7; its last high magnitude earthquakes on land destroyed the houses of Húsavík in 1872, rendering the monitoring of the full tectonic-

hydrogeochemical system of societal importance. Helium is chemically inert and can shed light on the sources of deep fluids and their physical interactions. Our study aimed to diminish the helium isotopes data gap in North Iceland geothermal fluids and to detect variations in groundwater helium isotopic signature potentially triggered by the tectonic earthquakes in the region. Here we report results from an isotopic survey of North Iceland along with time series data from June 2020 to October 2022 of helium isotopes for geothermal fluids from a borehole in Hafralækur. The results indicate a high regional variability in helium isotopic ratios (4 to 27 Ra) that can originate from regional and local processes: (i) influence of a global mantellic flux evidenced by an enriched mantle component degassing via the fault systems, (ii) radiogenic helium release potentially triggered by seismic events along the Dalvík Lineament, and (iii) groundwater mixing in a local scale in Hafralækur, documented on a period characterized by M $>$ 5 seismic events. The estimated global magmatic flux is comparable to the ones of neighbouring active rift zones in Iceland, where melts intruded in the crust are still actively degassing. Moreover, the helium isotopic signature of the geothermal fluids ($>$ 8 Ra) indicates the influence of the Iceland mantle plume. Localized seismicity-induced processes also occur. Along the Dalvík Lineament, the $^3He/^4He$ ratios ($<$ 8 Ra) indicates release of radiogenic ^4He from the host rocks under short timescales rather than under steady-state conditions, potentially linked to the tectonic earthquakes along this major transfer zone. Although we found no evidence for groundwater mixing at the regional scale, our helium isotope time series (2020 to 2022) indicates that lateral transport could occur at a local scale in the Aðaldalur valley, apparently partially controlled or enhanced by high magnitude tectonic earthquakes (M $\geq$ 5).

Keywords: Helium isotopes; off-rift mantle degassing; Iceland plume; time series; geochemical monitoring

Contents

4.1 Introduction

The $^{3}He/^{4}He$ ratio is an essential tool for determining the source of fluids on Earth since its two isotopes, ^{3}He and ^{4}He, are found in the atmosphere, crust, and mantle in significatively different proportions. ^{3}He is mainly of primordial origin, occurring in higher proportions in the mantle, and ^{4}He radiogenic, being more concentrated in the continental crust (e.g., Ballentine and Burnard, 2002; Moreira, 2013). ^{4}He is continuously produced primarily by α-decay of $^{235,238}U$ and ^{232}Th (Ballentine and Burnard, 2002).

In Iceland geothermal fluids, $^3He/^4He$ ratios exhibit a wide range that are not necessarily connected to active volcanic activity. In Vestfirðir, $>$ 110 km away from the closest active rift zones, the oldest rocks of Iceland are described (15.64 $\pm$ 0.15 Ma; Hardarson et al., 1997) along with its highest $^3He/^4He$ ratios, which have a high variability. Geothermal fluids in Vestfirðir vary from 3 to 29 Ra (Füri et al., 2010; Hilton et al., 1998; Poreda et al., 1992), where Ra is the atmospheric $^3He/^4He$ (1.39×10^{-6}; Graham, 2002), displaying influence of the Icelandic plume component. Except for Vestfirðir, off-rift regions have not been investigated extensively, which is the case of North Iceland.

North Iceland, although volcanically inactive, registered earthquakes with magnitudes up to about 7 (Ms) (Einarsson, 2008; Stefansson et al., 2008) linked to the transfer zone between the Mid-Atlantic Ridge and the North-Rift Zone. Most earthquakes at this fault system occur offshore; however, its last high magnitude (M 6.5) earthquakes on land destroyed the houses in the town of Húsavík in 1872 (Stefansson et al., 2008), rendering the monitoring of the full tectonic-hydrogeochemical system of societal importance. According to Barbieri et al. (2021) and Skelton et al. (2019, 2014), M $>$ 5 events might trigger variations in hydrochemical parameters at Hafralækur, as observed in their time series for stable isotopes ($\delta^{18}O$ and δ^2H), major, and trace elements. The variability of these geochemical tracers is susceptible to water-rock interactions and can document this type of process in the crust. Noble gases, on another hand, are chemically inert (Ballentine and Burnard, 2002) and can thus shed light on the sources of deep fluids (crust vs mantle) and/or the mixing processes that can modify their contributions in the fluids emitted at the surface, outside the influence of secondary processes in the crust (e.g., Caracausi et al., 2022).

Our study aims to diminish the helium isotopes data gap in North Iceland geothermal fluids and to detect variations in groundwater helium isotopic signature potentially triggered by the tectonic earthquakes in the region. Our study area is limited in the east by the town of Húsavík in the Northern Rift Zone (NRZ), in the south by the Hofsjökull volcanic system, and in the west by Snæfellsnes-Húnaflói rift zone (SHRZ) ($\sim$ 50 km away from Vestfirðir) (Figure 4.1). This region is characterized by low temperature geothermal systems ($<$ 150°C), typical of off-rift regions in Iceland. To identify the sources of fluids and their transport mechanisms in the crust, we carried out an extensive survey of groundwater for

$^{3}He/^{4}He$, $^{4}He/^{20}Ne$, $\delta^{18}O$, $\delta^{2}H$, $\delta^{34}S$, $\delta^{13}C_{TDIC}$, TDIC, major and trace elements analyses. Additionally, on June 28th, 2020 we started weekly sampling of groundwater from borehole HA-01 (Hafralækur) for $^{3}He/^{4}He$ and $^{4}He/^{20}Ne$ analyses in order to complement the long-term geochemical monitoring performed by Skelton et al. (2019, 2014) and Barbieri et al. (2021) at this reference site.

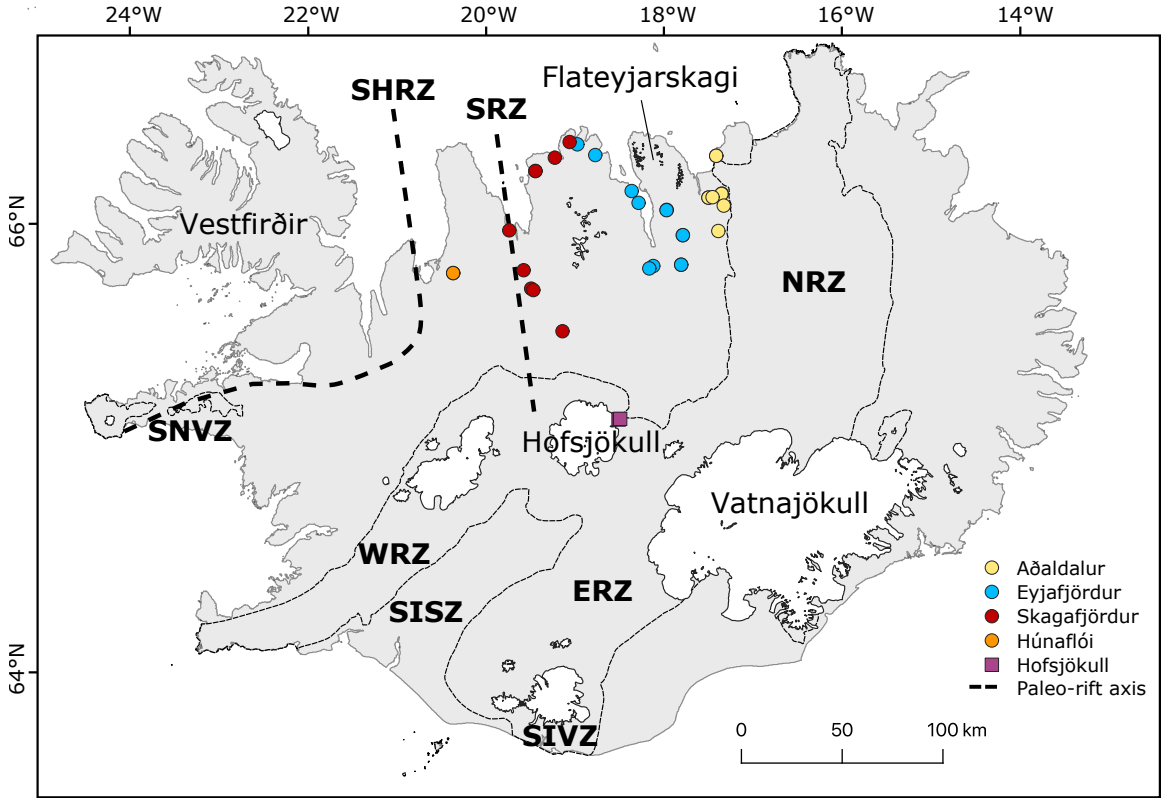

Figure 4.1: Rift zones of Iceland with sample groups and main sites discussed. NRZ: North Rift Zone, WRZ: West Rift Zone, ERZ: East Rift Zone, SNVZ: Snaefellsnes Volcanic Zone, SIVZ: South-Iceland Volcanic Zone, SISZ: South Iceland Seismic Zone, SRZ: Skagafjörður Rift Zone, SHRZ: Snæfellsnes-Húnaflói Rift Zone.

4.2 Geological setting

4.2.1 Geodynamic framework and volcanic history

Iceland is located in the plate boundary between the Eurasian and North American plates that here is segmented in different rift zones: the North Rift Zone (NRZ), West Rift Zone (WRZ), East Rift Zone (ERZ), South Iceland Seismic Zone (SISZ), South Iceland Volcanic

Zone (SIVZ) and the SnæfellsnesVolcanic Zone (SNVZ) (Figure 4.1).

In Iceland, the shift of the Mid-Atlantic Ridge toward the east is attributed to the presence of a mantle plume, which is hypothesized to be currently located under Vatnajökull (central-SE) (Darbyshire et al., 2000). Due to the very high magma production in such a context, the thickness of the crust in Iceland is anomalously high considering the typical values for the oceanic crust (<10 km; White et al., 1992). The thickest crust is found under the ERZ and Central Iceland (29 to 32 km) and its thinnest portions under the WRZ (19 +6/-1 km; Bjarnason and Schmeling, 2009) whereas in the NRZ, the crustal thickness ranges between 19 and 29 km (Bjarnason and Schmeling, 2009; Staples et al., 1997).

The three main chronological successions of Iceland volcanics are Tertiary (> 3.1 Ma), Plio-Pleistocene (0.7 to 3.1 Ma), and Upper Pleistocene (< 0.7 Ma) (Figure 4.2). In a general view, the axial rift zones contain basalts of the tholeiitic series and the off-axis volcanic regions alkalic to transitional-alkalic (Jakobsson et al., 2008). The oldest rocks of Iceland are in Vestfirðir with an age of 15.64 ± 0.15 Ma (Hardarson et al., 1997), and the oldest in North Iceland, in Flateyjarskagi (Flatey Penninsula), with an age of 11.9 ± 1.20 Ma (Jancin et al., 1985). The Tertiary successions cover most of our study area (Eyjafjördur and Skagafjörður groups), the Plio-Pleistocene only the Aðaldalur and Skagafjörður groups, and the Upper Pleistocene rocks host the Hofsjökull samples. The Hofsjökull central volcano had low volcanic activity in the Holocene (Einarsson, 2008). The main rocks identified in this volcanic system are hyaloclastites (< 0.7 Ma), postglacial basaltic lava (< 1100 years), and silicic lavas (> 10 ka) (Hjartarson et al., 2019).

Rift migration has been identified in North Iceland (Figure 4.1) based on geochronological and petrological evidence and seems directly linked to the interaction between the mantle plume and the ridge (Garcia et al., 2003; Hjartarson, 2003; Sæmundsson, 1974). The Snæfellsnes-Húnaflói rift zone (SHRZ) formed at 15 Ma and was active for 8 to 10 Ma. 6-7 Ma ago, the rift jumped again and formed the NRZ (Jóhannesson, 1980; Kristjánsson and Jónsson, 1998; Sæmundsson, 1974). Lastly, the Skagafjörður rift zone (SRZ) (Fig. 1) developed around 1.7 Ma, with activity in the Holocene restricted to the Hofsjökull Central Volcano (Hjartarson, 2003). Another argument in favour of a paleo-rift axis in Skagafjörður (Hjartarson, 2003) (Figure 4.1) is the high geothermal activity in this valley (Arnórsson,

1995) compared to its surrounding areas.

The causes for geothermal activity outside the active rift zones in Iceland are not clear, however, it seems linked to fault systems (Arnórsson, 1995). Although the average heat flow in the off-rift zones of Iceland is relatively high (130 mWm^{-2}; Flóvenz and Saemundsson, 1993), it is comparable to Tertiary basins in subduction zones (92 to 128 mWm^{-2}; da Silva Carvalho et al., 1980; Watanabe et al., 1977). The most accepted models for low-temperature geothermal systems in Iceland (up to 150°C) are of non-volcanic origin. One of them is based on hydraulic circulation bringing hot water from the highlands, either vertically through faults and fissures or horizontally through permeable rock formations led by hydrostatic pressure (Árnason, 1976). Bodvarsson (1983) proposes that low-temperature geothermal systems are formed by heat transfer from the rock to the water via fractures, but the source of heat is still open to debate. The source of fluids, however, based on $\delta^{18}O$ and $\delta^{2}H$, is mostly meteoric water with minor contribution of seawater in some cases (Arnórsson, 1995). In the active rift zones, however, the high temperature geothermal systems (> 150°C) are directly linked to volcanic activity (Arnórsson, 1995b). In an active volcanic context, magma degassing provides liberation of both ^{3}He and heat, rendering both parameters coupled and, consequently, they can act as tracers of magmatic activity at depth (e.g., Kennedy et al., 2000; Poreda and Arnórsson, 1992; Saby et al., 2020). In Icelandic high temperature geothermal systems, however, Poreda and Arnórsson (1992) observed that fractionation of ^{3}He occurs relative to heat, and young magmatic bodies tend to preferentially lose ^{3}He relative to heat, rending these systems with high ^{3}He/enthalpy whereas aging magmatic systems tend to trigger low ^{3}He/enthalpy. Drifting of high temperature geothermal systems out of the active rift zones has been proposed before to explain the low-T systems in Iceland (Arnórsson, 1995). This proposal is based on drill cores from low-T geothermal areas with mineral alteration consistent with rocks that once hosted a high-T hydrothermal system. This hypothesis aligns with the rift migration episodes observed in North Iceland.

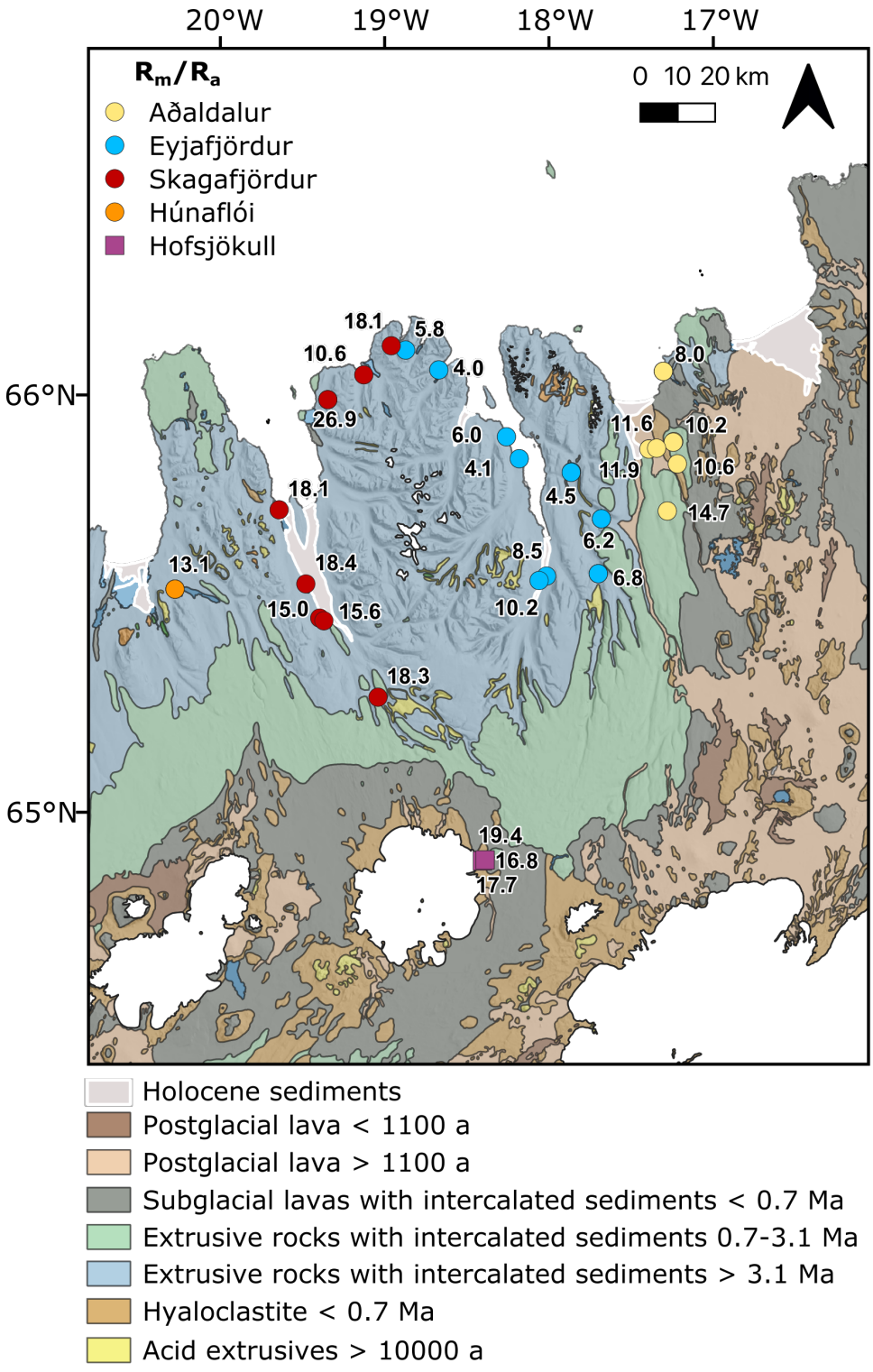

Figure 4.2: Location of samples in North Iceland with geology. Groups are separated according to geography and geotectonic setting. Circles represent groundwater samples and square glass samples. Helium isotopes are shown as measured values (Rm/Ra) and exhibit large variations (3.95 to 26.87 Ra) for geothermal fluids.

4.2.2 Helium isotopic signature in Iceland

Unlike mid-ocean ridge basalts (MORBs), which form by partial melting of the upper mantle and have a concise average $^3He/^4He$ of 8.75 ± 2.14 Ra (Graham, 2002), Iceland basalts show a complex helium isotopic signature and variability, comparable to other oceanic island basalts (OIBs), such as Hawaii, that coupled to other noble gases evidences (e.g., Ne-Xe systematics) a deep mantle plume source (Graham, 2002; Muhkophadhyay, 2012).

Volcanic glass and phenocrysts in Iceland (Figure 4.3a) (Brandon et al., 2007; Breddam et al., 2000; Burnard and Harrison, 2005; Burnard et al., 1994; Dixon et al., 2000; Eason et al., 2015; Ellam and Stuart, 2004; Füri et al., 2010; Halldórsson et al., 2016; Harðardóttir et al., 2018; Hilton et al., 1999, 1998, 1990; Kononov and Polak, 1976; Kurz et al., 1985; Licciardi et al., 2007; Macpherson et al., 2005; Marty et al., 1991; Moreira et al., 2001; Polak et al., 1975; Poreda et al., 1992; Sano et al., 1985; Torgersen and Jenkins, 1982; Trieloff et al., 2000) range from 7.6 to 34.3 Ra in the NRZ, from 14.6 to 25.9 Ra in the ERZ, and from 8.7 to 21.6 Ra in the WRZ. The highest $^3He/^4He$ ratios in Iceland are away from the active rift zones, in Vestfirðir (21.6 to 47.5 Ra; Ellam and Stuart, 2004; Füri et al., 2010; Harðardóttir et al., 2018; Hilton et al., 1999).

Iceland geothermal fluids exhibit a wide range in $^3He/^4He$ ratios that is not necessarily connected to present day volcanic activity (Fig. 4.3b); these values, however, resemble those of local volcanic rocks that give information on the active or paleo signature of the magmatic component. The highest $^3He/^4He$ ratios of geothermal fluids are found in Vestfirðir (6.2 to 29 Ra; Füri et al., 2010; Hilton et al., 1998; Poreda et al., 1992), followed by the ERZ (17 to 26 Ra; Füri et al., 2010; Hilton et al., 1990; Kononov and Polak, 1976; Polak et al., 1975; Poreda et al., 1992), the SISZ (14 to 23 Ra; Füri et al., 2010; Hauksson and Goddard, 1981; Hilton et al., 1990; Kononov and Polak, 1976; Poreda et al., 1992), and the WRZ (10 to 20 Ra; Füri et al., 2010; Hilton et al., 1990; Kononov and Polak, 1976; Marty et al., 1991; Polak et al., 1975; Poreda et al., 1992; Sano et al., 1985; Torgersen and Jenkins, 1982). The NRZ geothermal fluids have the lowest helium isotopic signature among the rift zones, ranging from 6.2 to 10.7 Ra (Füri et al., 2010; Hilton et al., 1990; Kononov and Polak, 1976; Marty et al., 1991; Polak et al., 1975; Poreda et al., 1992; Sano et al., 1985; Torgersen and Jenkins,

1982). Hilton et al. (1998) associated the helium isotopic signature at Vestfirðir fluids with a direct mantle source (mantle degassing from incipient melting) rather than from secondary processes such as water/rock interactions or lateral transport of groundwater.

4.2.3 Hydrochemical monitoring at Hafralækur and tectonic-volcanic activity

North Iceland is an area of interest due to its tectonic activity that registered M $\leq$ 7 earthquakes (Einarsson, 2008; Stefansson et al., 2008) along the transfer zone between the mid-Atlantic ridge and the NRZ (Figure 4.4). Groundwater from borehole HA-01, in Hafralækur (Aðaldalur valley), and borehole HU-01, in Húsavík, has been monitored for hydrochemical parameters and showed variations possibly correlated to high magnitude tectonic events (M $>$ 5) (Barbieri et al., 2021; Skelton et al., 2019, 2014) and volcanic activity (Barbieri et al., 2021) (more details later in this section). The North Rift Zone (NRZ) is connected to the Kolbeinsey Ridge by the Tjörnes Fracture Zone (TFZ). This transform zone includes the Grímsey Lineament (or Grímsey Oblique Rift) and Húsavík-Flatey Fault, where most of the seismicity of the TFZ occurs, and the Dalvík Lineament (or Dalvík Zone). The latter is not evident at the surface but is defined by the clear epicentre alignment of earthquakes (up to M 7) (Einarsson, 2008). Borehole HA-01 is located near this lineament (Figure 4.4). The Húsavík-Flatey Fault is highly active, registering earthquakes with magnitudes up to 7 (Einarsson, 2008; Stefansson et al., 2008). Three periods of earthquakes M $>$ 5 occurred in the last decades in the area: in 2012-2013, 2020, and 2022.

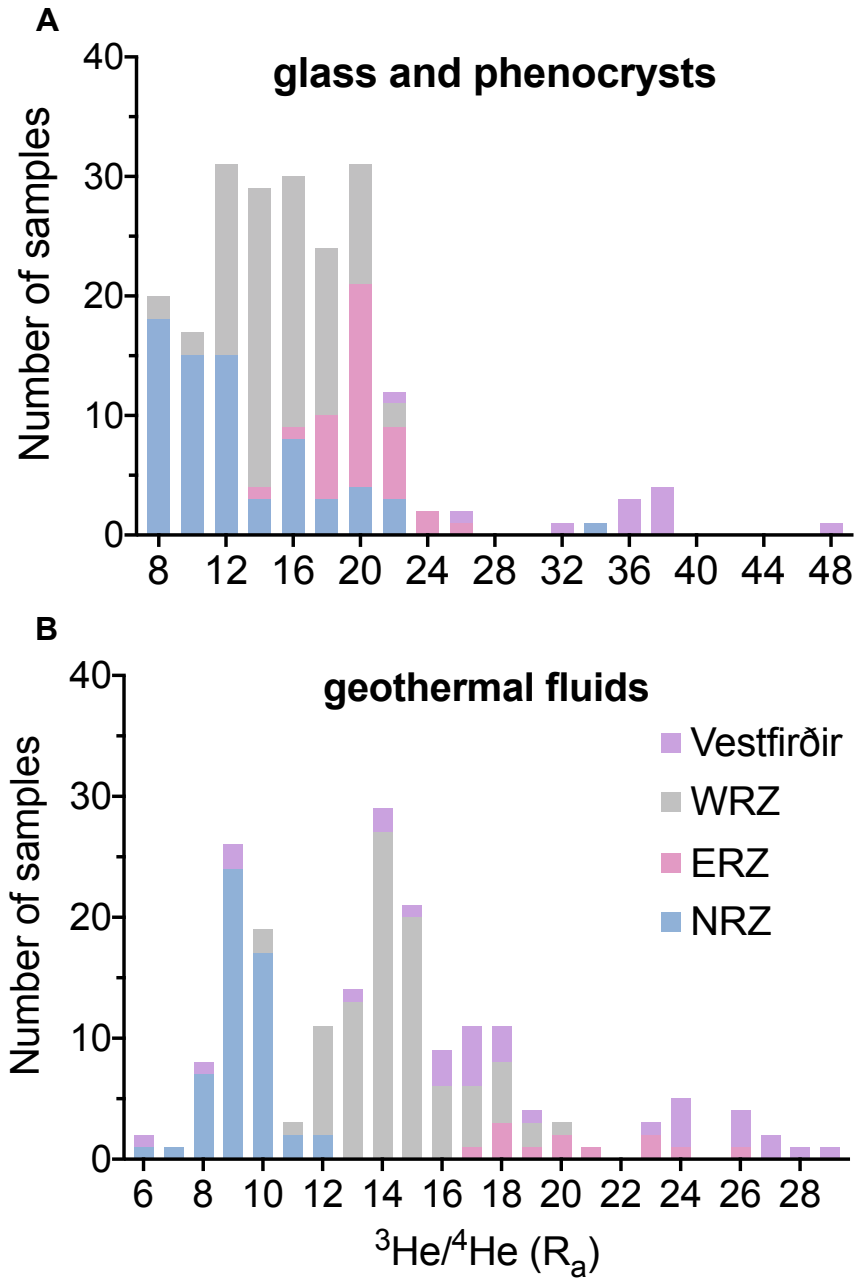

Figure 4.3: Histograms for previously published helium isotopes data from Iceland (a) glasses and phenocrysts and (b) geothermal fluids (Brandon et al., 2007; Breddam et al., 2000; Burnard and Harrison, 2005; Burnard et al., 1994; Dixon et al., 2000; Eason et al., 2015; Ellam and Stuart, 2004; Füri et al., 2010; Halldórsson et al., 2016; Harðardóttir et al., 2018; Hilton et al., 1999, 1998, 1990; Kononov and Polak, 1976; Kurz et al., 1985; Licciardi et al., 2007; Macpherson et al., 2005; Marty et al., 1991; Moreira et al., 2001; Polak et al., 1975; Poreda et al., 1992; Sano et al., 1985; Torgersen and Jenkins, 1982; Trieloff et al., 2000).

The nearest volcanic systems are east of HA-01, Theistareykir (or Þeistareykir) and Krafla. Theistareykir last eruption occurred c. 2.4 ka BP, producing the Theistareykjahraun

lava flow. Southeast of Theistareykir, Krafla is composed of a central volcano and fissure swarms. Its largest known eruption, the Halarauður eruption, occurred c. 110 ka. The most recent eruption from this system consisted of a rifting event that started in December 1975 and ended in September 1984 (Sæmundsson, 1991; Thordarson and Larsen, 2007). The last eruption in the vicinity of HA-01 took place further south from Krafla and near the Vatnajökull ice cap, in the Bárðarbunga system, one of the most active, largest, and longest volcanic systems of Iceland (Thordarson and Larsen, 2007). This eruption lasted from August 2014 until February 2015 and consisted of the reactivation of the Holuhraun eruptive fissure (Sigmundsson et al., 2014). Thus, even if, during the Holocene, lava flows originating from the Bárðarbunga or Mývatn areas invaded the Aðaldalur via the Laxárgljúfur and Bárðardalur long canyons, they represent a fine surficial formation emplaced on the older plio-pleistocene regional thick lava pile.

HA-01 has been monitored for dissolved major elements (Na, Si, Ca, and K) and stable isotope ratios of hydrogen (δ^2H) and oxygen (δ^{18}O since 2008 (Skelton et al., 2019) and for trace elements since 2010 (Barbieri et al., 2021). Skelton et al. (2014) proposed that the short-term δ^2H, Na, Si, and Ca maxima observed in the monitoring data coincided with the M $>$ 5 earthquakes from 2012 and 2013. Barbieri et al. (2021) identified changes in B, Al, and V concentrations before the M $>$ 5 earthquake from 2012, variations in B, Al, V, Li, and Mo concentrations before the 2014 Bárðarbunga eruption ($\sim$115 km from HA-01), and changes in some trace elements (Li, B, Ga, Mo, Sr, Rb, and Fe) before an M $>$ 5 earthquake that occurred in the north in 2018; however, the authors also describe changes in groundwater chemistry when no seismic (M $>$ 5) or volcanic events occurred. Skelton et al. (2019) propose a model in which (i) the changes before the M $>$ 5 earthquakes would be due to groundwater mixing that lead to shift from equilibrium, triggering chemical changes via water-rock interactions; (ii) the postseismic variations were due to fast mixing between different groundwater sources; and (iii) the long-term hydrochemical changes observed by Andrén et al. (2016) would be caused by both mixing and mineral growth.

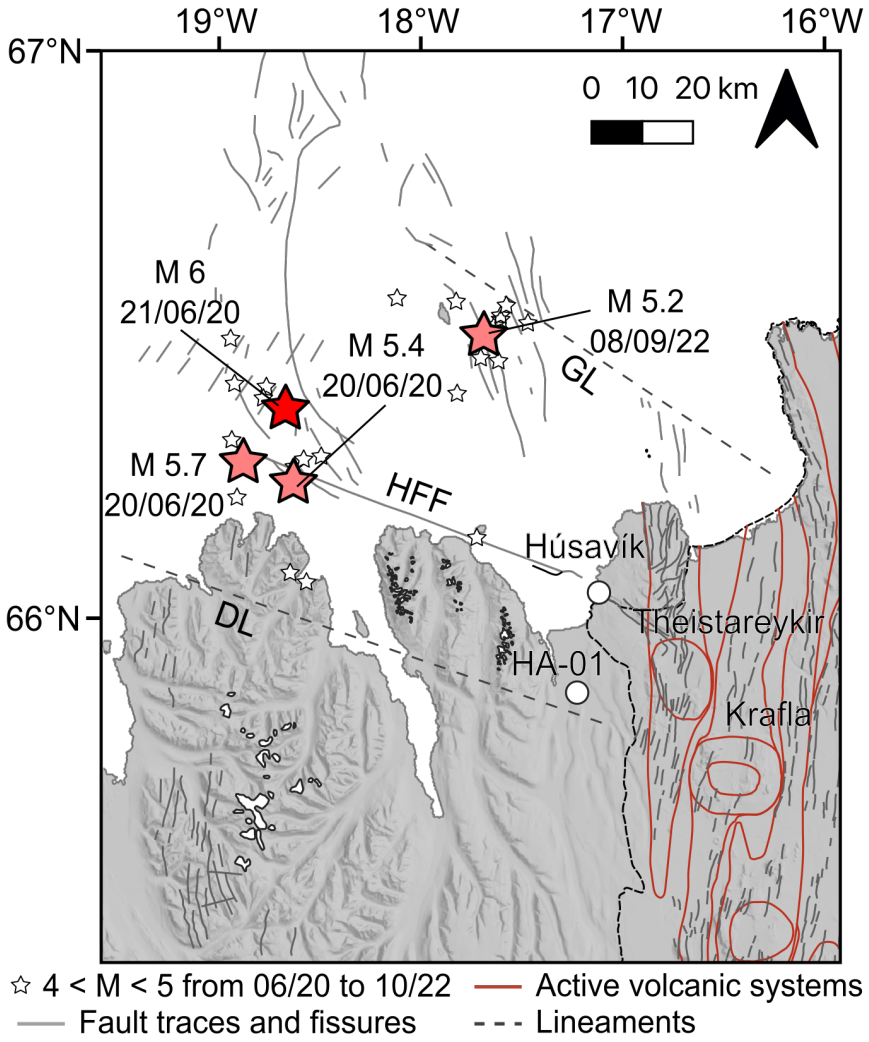

Figure 4.4: Map with location of HA-01 and earthquakes that occurred during the time series period. Only earthquakes M > 4 are shown and all for the period between June 2020 and October 2022. HFF: Húsavík-Flatey Fault and DL: Dalvík Lineament.

4.3 Methods and sampling

4.3.1 Sampling

Groundwater samples for helium isotopic analyses were collected using copper tubes (low He diffusion) and avoiding air contamination. For all sites, water samples were collected in the summer of 2020 and 2021 (Table 4.1). In addition, we present new data of He isotopic signature trapped within fluid inclusions in rocks from the Hofsjökull volcanic system where subglacial glass of pillow lavas and hyaloclastites were sampled in 20XX.

For the time series monitoring of the Hafralækur site (HA-01), samples were collected from July 2015 and February 2016 and interrupted until June 24th, 2020, when we started weekly sampling, shortly after an earthquake swarm of up to M 6. Even though we missed the seismic sequences of 2020, the results serve as a database for our current and any future monitoring in the area. Nonetheless, our time series covered the period of seismic activity of September 2022 with earthquakes up to M 5 (Figure 4.4). The period of 2015 and 2016 serve as a baseline of the time series since no earthquakes M $\geq$ 4 were recorded. Results of $^{3}He/^{4}He$ and $^{4}He/^{20}Ne$ analyses of the time series are on Table S2; the name of each sample corresponds to the date of sampling following the format day-month-year.

4.3.2 Helium and neon isotopes

Glass samples ($\sim$ 120 mg) of volcanics from Hofsjökull were selected for analyses avoiding surface alterations and phenocrysts and were prepared following the procedures described in Burnard et al., (2013).

The analyses of $^{4}He/^{20}Ne$ and $^{3}He/^{4}He$ ratios were performed, respectively, on a MKS Microvision 2 quadrupole mass spectrometer (QMS) and a split flight tube noble gas mass spectrometer (Helix SFT - Thermo Fisher Scientific) at the Centre de Recherches Pétrographiques et Géochimiques (CRPG) noble gas analytical facility following the procedure described in Mabry et al., (2013). The standard deviation of the $^{3}He/^{4}He$ ratios ranged from 1 to 3% based on the replicate analysis of standard He (atmospheric). Results are corrected for blanks, which contributed $< 0.1\%$ of the total He abundances of the groundwater samples and 1 to 10% for the glass samples.

Correction of $^{3}He/^{4}He$ ratios for atmospheric contribution follows the procedure described in Hilton (1996) (Table 4.1), considering the Bunsen coefficients, for the geothermal samples, assuming an air-equilibration temperature of 10 °C.

Table 4.1: List of groundwater and glass samples with coordinates and results for helium and stable isotopes. Sample prefix refers to year of collection (20 = 2020 and 21 = 2021). $_{a}X=[(^{4}He/^{20}Ne)m/(^{4}He/^{20}Ne)a] \times \beta Ne/\beta He$, where β represents the Bunsen coefficient from Weiss (1971), taken as 1.25 at 10 °C. $^{b}Rc/Ra$ is the air-corrected $^{3}He/^{4}He = [(Rm/Ra \times X) - 1)]/(X - 1)$. *The only glass samples of the study; in this case, X is not corrected for the Bunsen coefficient.

Sample	LAT (°N)	LONG (°E)	Rm/Ra	$^{4}He/^{20}Ne$	X[a]	Rc/Ra[b]	TDIC (mol/l)	$\delta^{13}C_{TDIC}$(‰)	$\delta^{2}H$ (‰)	$\delta^{18}O$ (‰)	$\delta^{34}S_{SO_4}$(‰)
Aðaldalur											
20-HUS-01-01B	66.0576	-17.3563	8.03 ± 0.11	1.36 ± 0.05	5.3	9.65	0.0008	-5.1			
21-HUS-01							0.0002	-4.5	-119.00	-14.56	
20-HA-01-01	65.8725	17.4526					0.0017	-7.8	-126.00	-16.71	6.8
20-HA-01-02B							0.0019		-126.20	-16.81	6.9
20-HA-01-03B			11.93 ± 0.20	1.47 ± 0.05	5.8	14.22	0.0014		-126.10	-16.37	6.9
20-HA-04-01B	65.8722	17.4528	11.13 ± 0.18	1.61 ± 0.05	6.3	13.03	0.0016	-8.2	-126.00	-16.90	6.9
21-HAFR-01							0.0010		-125.99	-16.86	
20-LAU-01-01B	65.7226	17.3546	14.73 ± 0.24	1.72 ± 0.05	6.8	17.10	0.0010	-11.0	-104.60	-14.51	5.1
21-LAUG-01											5.2
20-HVER-01-01	65.8885	17.3063					0.0029		-98.80	-13.71	5.6
21-HV-01C			10.21 ± 0.14	2.08 ± 0.08	8.2	11.49	0.0041		-100.43	-13.86	5.3
21-KL-01	65.8350	17.2886	10.56 ± 0.15	1.78 ± 0.05	7.0	12.16					5.1
21-AA-01C	65.8738	17.4077	11.55 ± 0.16	1.17 ± 0.05	4.6	14.48		-10.8			6.1
Eyjafjördur											
20-DS-01-01	65.8217	17.9088					0.0015	-11.7	-96.50	-13.44	2.8
21-DS-01B	65.8203	17.9108	4.50 ± 0.06	0.95 ± 0.04	3.7	5.78	0.0014	-12.1	-94.88	-13.37	2.6
20-ST-01-01	65.7077	17.7392	6.16 ± 0.05	5.13 ± 0.12	20.2	6.43	0.0017	-7.7	-84.50	-12.09	7.8

20-ST-01-01B			6.07 ± 0.08	5.07 ± 0.23	19.9	6.34					
20-RF-09-01	65.5763	17.7637	6.80 ± 0.11	4.75 ± 0.18	18.7	7.12	0.0018	-9.0	-97.10	-13.55	5.5
20-RF-09-01B			6.76 ± 0.11	2.45 ± 0.10	9.6	7.43					
21-OL-4	66.0693	18.6817	3.95 ± 0.06	0.66 ± 0.02	2.6	5.79	0.0011	-8.9	-81.75	-11.83	4.6
21-HJ-21C	65.8548	18.2134	4.05 ± 0.06	1.48 ± 0.06	5.8	4.69	0.0015	-7.2	-100.80	-14.31	4.0
21-SK11-01	66.11715	18.8775	5.79 ± 0.08	0.85 ± 0.02	3.3	7.84	0.0018	-3.2	-76.89	-11.35	2.3
21-YV-20C	65.9078	18.2870	6.02 ± 0.08	2.38 ± 0.08	9.4	6.62	0.0014	-11.1	-108.64	-14.96	5.1
21-LN-12	65.5727	18.0639	8.50 ± 0.12	3.99 ± 0.10	15.7	9.01	0.0015	-10.0	-94.91	-13.46	4.9
21-BN-1	65.5622	18.1071	10.17 ± 0.14	4.42 ± 0.15	17.4	10.73	0.0011	-9.2	-97.86	-13.84	2.5
Skagafjördur											
21-SDO1	66.12755	18.9625	18.09 ± 0.25	5.00 ± 0.20	19.6	19.01	0.0020	-5.7	-82.83	-12.08	4.5
21-LH04-01	66.05778	19.1248	10.58 ± 0.15	2.76 ± 0.11	10.8	11.55	0.0023	-6.8	-90.07	-12.77	7.3
21-BM13-01	65.73313	19.6166	18.13 ± 0.25	5.82 ± 0.19	22.9	18.91	0.0014	-10.0	-97.19	-13.36	5.9
21-HOFS-1	65.28506	19.0396	18.25 ± 0.26	14.34 ± 0.49	56.4	18.56	0.0022	-6.9	-119.64	-13.85	8.6
21-VH12-01	65.55608	19.4578	18.41 ± 0.26	3.40 ± 0.16	13.4	19.82	0.0034	-6.2	-108.50	-13.84	7.8
21-VARM-1	65.47440	19.3760	14.99 ± 0.21	0.81 ± 0.03	3.2	21.39	0.0018	-10.7	-103.19	-13.59	7.2
21-SK32-01	65.99812	19.3363	24.54 ± 0.55	41.69 ± 1.39	163.9	24.68	0.0012	-8.4	-107.04	-13.91	10.5
21-SK32-01B			26.87 ± 0.61	45.23 ± 1.59	177.8	27.02					
21-STE1-01B	65.46786	19.3522	15.60 ± 0.35	5.34 ± 0.18	21.0	16.33	0.0020	-13.8	-99.10	-13.32	5.4
Húnaflói											
21-RR22-01	65.53928	20.2144	13.13 ± 0.30	5.86 ± 0.27	23.0	13.68	0.0025	-9.6	-87.48	-12.31	2.4
21-RR22-01B			12.23 ± 0.28	4.00 ± 0.14	15.7	12.99					

*Hofsjökull**						
K-350b	64.89222	-18.4484	16.75 ± 0.35	4.10 ± 0.44	12.9	18.07
K351	64.89181	-18.4498	17.73 ± 0.37	4.76 ± 0.49	15.0	18.93
K354	64.89394	-18.4346	19.38 ± 0.40	30.62 ± 2.94	96.3	19.57

4.3.3 TDIC and $\delta^{13}C_{TDIC}$ isotopes

For total dissolved inorganic carbon (TDIC), thermal water samples were cooled down to avoid CO_2 degassing upon sample storage using an in-line cooling coil, collected into gas-tight amber glass bottles, and analysed using modified alkalinity titration (Stefánsson et al., 2007). $\delta^{13}C_{TDIC}$ were obtained using a Finnegan MAT251 isotope ratio mass spectrometer at the University of Iceland (Stefánsson et al., 2016). Results are reported in ‰ relative to the VPDB standard (Table 4.1). Replicate analysis of IVPDB reference material yielded a standard deviation of r = 0.15‰.

4.3.4 $\delta^{18}O$ and $\delta^{2}H$ isotopes

Water samples were collected using 60 ml gas-tight amber glass bottles. $\delta^{18}O$ was extracted by the method of Epstein and Mayeda (1953) and $\delta^{2}H$ analysis by the H_2-water equilibration method using a Pt-catalyst (Horita, 1988). Analysed were performed on a Finnegan MAT 251 ion ratio mass spectrometer (IRMS) at the University of Iceland and the results are reported in ‰ relative to the VSMOW standard (Table 4.1). Replicate analysis of the reference material yielded a standard deviation of 0.05‰ and 0.7‰ for oxygen and hydrogen, respectively.

4.3.5 $\delta^{34}S$ isotopes

We sampled water by filtering through 0.5 μm PTFE membranes into 15 ml HDPE bottles containing 0.15 ml of 1M ZnCl2 solution to precipitate sulfide as ZnS. In the lab, samples were centrifugated to separate the precipitated ZnS. A 1 ml aliquot of the liquid phase was taken for isotopic analyses. $\delta^{34}S$ was measured on a ThermoScientific Neptune Plus Multiple Collector – Inductively Coupled Plasma Mass Spectrometry (MC-ICPMS) at the Centre de Recherches Pétrographiques et Géochimiques (CRPG) (Paris et al., 2013) (Table 4.1). Errors (2σ) were estimated at ± 0.2‰ based on a seawater long-term consistency standard.

4.3.6 Major and trace elements

Samples were filtered on-site (0.2 μm cellulose acetate) into HDPE or PP bottles. Samples for major cation determination (Si, B, Na, K, Ca, Mg, Fe, Al) were acidified (1% HNO_3, Merck Suprapur®) followed by analysis by ICP-OES. Samples for determination of anions (F, Cl and SO4) were not further treated and analyzed using IC. Dissolved H_2S was analyzed on site using Hg titration with dithiozone as an indicator. Analyses were performed at the University of Iceland (Table S1). The analytical precision for major elements based on duplicate analyses was found to be<3% at the 95% confidence level.

4.4 Results

4.4.1 North Iceland survey of geothermal fluids

The surveyed area is separated into five groups based on geography from East to West, with the valleys of: Aðaldalur, Eyjafjörður, Skagafjörður, Húnaflói, and the southward Hofsjökull active volcanic center (Figures 4.1 and 4.2). Results for $^3He/^4He$ reported in figures and discussions refer to the measured $^3He/^4He$ (Rm/Ra) normalized to the He isotopic signature in air (Ra = $^3He/^4He$ in air, 1.39 x 10^{-6}), unless otherwise stated, since the aim of the study is not to detect and quantify precisely the initial mantle signature, but to investigate all possible sources of fluids and their interactions — air-saturated water (ASW), radiogenic and magmatic helium (Table 4.1).

In the $^3He/^4He$ (Rm/Ra) vs. $^4He/^{20}Ne$ plot (Figure 4.5), the five groups are within range of previously reported values for Iceland. This diagram is used to distinguish mixing between the three main sources of fluids – mantle, atmosphere, and crust (radiogenic); In groundwater samples, the atmospheric source is represented by air-saturated water (ASW). For our samples, this plot shows mixing between air-saturated water (ASW) and different magmatic endmembers ranging from $\sim$ 8 to 27 Ra, with potential addition of a small proportion of radiogenic component, which is not possible to assess directly for this range of isotopic values, except for the rare values which plot slightly below the ASW-8 Ra mixing line.

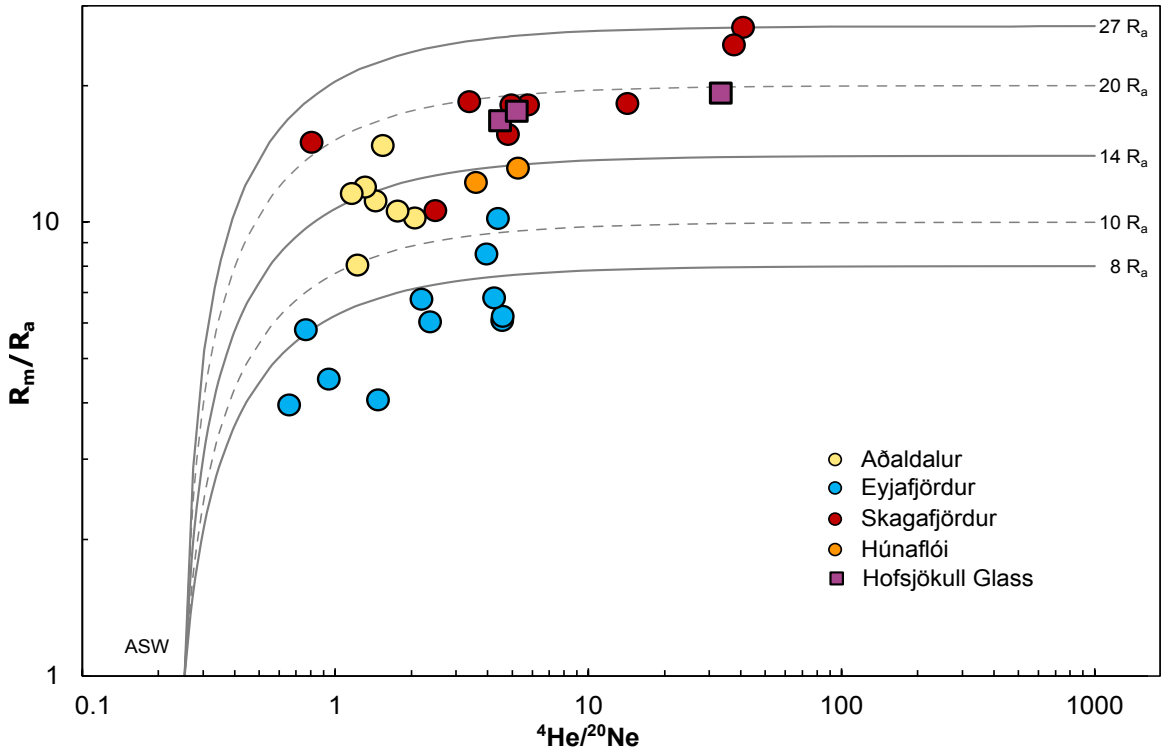

Figure 4.5: $^{3}He/^{4}He$ (Rm/Ra) vs. $^{4}He/^{20}Ne$ plot. Results populate two main regions, one with lower helium ratios (up to 14 Ra) including the Eyjafjörður and Aðaldalur groups and the other with the remaining groups reaching up to 27 Ra.

The Aðaldalur group ranges from 8.0 to 14.7 Ra (Table 4.1), and exhibits a coherent trend for most of the samples, ranging from 11.9 to 10.2 Ra (Figure 4.5). The samples from Hveravellir (HVER and HV in Table 4.1) show results lower than previously described (12.3 Ra; Kononov and Polak, 1976; Polak et al., 1975), when the authors assigned this site to the NRZ. Because of its clear geographic and geologic-tectonic context (Bourgeois et al., 2005), in our study we attribute this site to the Aðaldalur valley instead. Thus, later in the discussion, we consequently revise and restrict the range for the NRZ fluids to be from 6.2 to 10.7 Ra.

The Eyjafjörður group ranges from 4.0 to 10.2 Ra (Table 4.1) and encompasses the lowest values of our dataset, plotting below the 8 Ra mixing line with ASW, indicating possible $^{4}He^{*}$ (radiogenic ^{4}He) enrichment (Figure 4.5). The Skagafjörður sample group shows a wide range for helium isotopic ratios (10.6 to 26.9 Ra; Table 4.1), including the highest values from our survey. The westernmost sample, at Húnaflói, exhibits a higher ratio (13.1 Ra; Table 4.1, 4.2 and 4.5) than previously reported for the site (10.9 Ra; Kononov and Polak,

1976). For the glass samples of the southward Hofsjökull active volcanic center, results (16.8 to 19.4 Ra) are comparable to values previously reported for the SW portion of the Hofsjökull volcanic system (20 Ra; Kurz et al., 1985). In addition, we contributed the first $^{4}He/^{20}Ne$ values that allow to precisely confirm an endmember of $\sim$ 20 Ra with minimal atmospheric contribution for this site. For the whole new dataset, Rm/Ra does not follow a geographical trend and the highest signals are found in Skagafjörður, one of the furthest groups from the NRZ (Figure 4.6a).

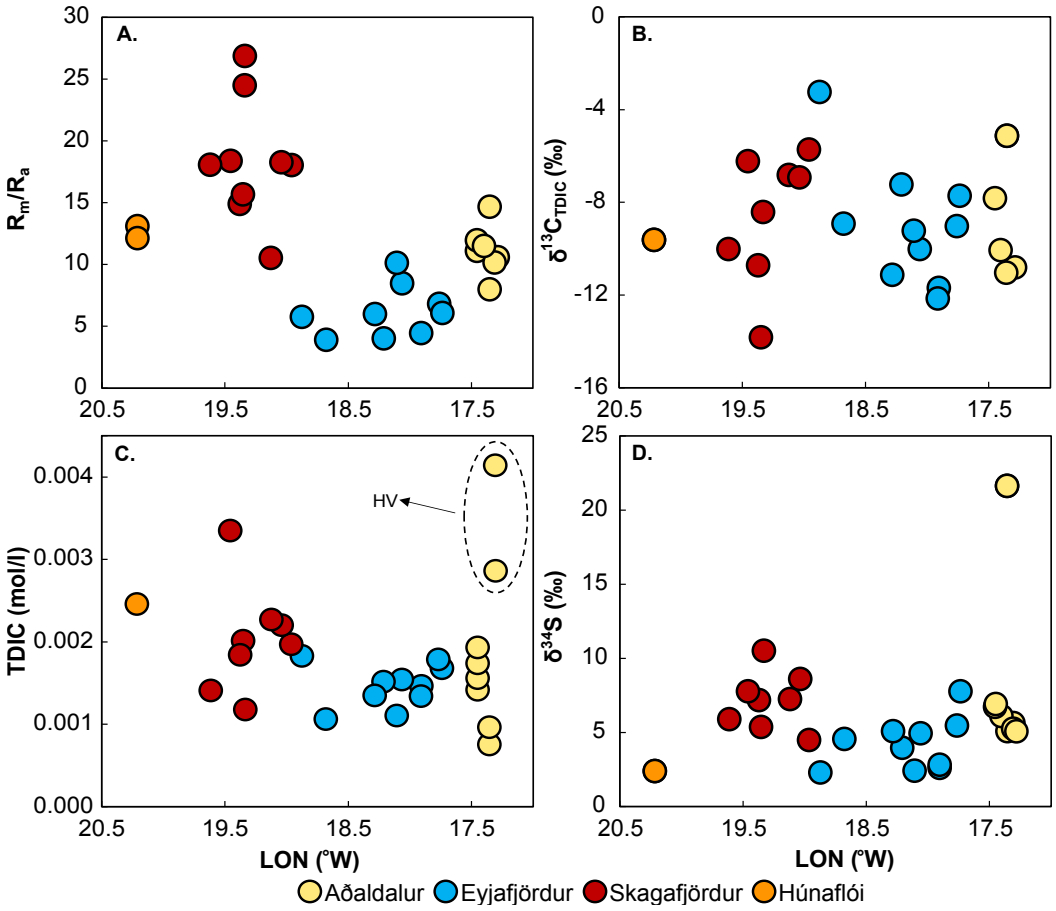

Figure 4.6: Variation of isotopes with longitude. (a) Rm/Ra, (b) $\delta^{13}C_{TDIC}$, (c) TDIC , and (d) $\delta^{34}S$ show no clear geographical patterns.

Tritium shows low values for all sample groups ($<$ 0.8 to 1 TU; Table S1). TDIC (total dissolved inorganic carbon) ranges from 0.0002 to 0.0041 mol/l for Aðaldalur, from 0.0011 to 0.0018 mol/l for Eyjafjörður, from 0.0012 to 0.0034 mol/l for Skagafjörður, and is 0.0025 for the Húnaflói sample (Table 4.1). For the C and S stable isotopes, the dataset shows

dispersion and no clear relationship between groups (Figs. 4.6 and S1). $\delta^{13}C_{TDIC}$ ranges from -11.0 to -4.5 ‰ for the Aðaldalur samples, from -12.1 to -3.2 ‰ for Eyjafjörður, from -13.8 to – 5.7 ‰ for Skagafjörður, and is -9.6 ‰ for the Húnaflói sample (Table 4.1). These ranges are compatible with several sources, including volcanic gases, graphite, and non-marine carbonates, the latter being the only one that covers the full isotopic range of our dataset (Favara et al., 2002). However, secondary processes are likely, especially considering the data dispersion and lack of correlation with TDIC contents (Fig S1).

δ^2H results range from -126.2 to -98.8 ‰ for the Aðaldalur group, from -108.6 to -76.9 ‰ for Eyjafjörður, from -119.6 to -82.8 ‰ for Skagafjörður, and is -87.5 ‰ for the Húnaflói sample (Table 4.1, Figure 4.7a). The depleted signature found in the Aðaldalur samples from the Hafralækur and Húsavík sites has been linked to a pre-Holocene water ("Ice Age water"; Skelton et al., 2019, 2014) whereas the samples least depleted in δ^2H, from all groups except Aðaldalur, are compatible with modern precipitation.

δ^{18}O results vary from -16.9 to -13.7 ‰ for the Aðaldalur samples, from -15.0 to -11.35 ‰ for Eyjafjörður, from -13.8 to -12.0 ‰ for Skagafjörður, and is -12.3 ‰ for the Húnaflói sample.

In the δ^2H versus δ^{18}O plot (Fig. 7a), all groups follow the meteoric line, except for some of the Aðaldalur and Skagafjörður samples, which present a δ^{18}O shift. In Hafralækur (HA-01 and HA-04 samples), this shift can be linked to water-rock interactions, as it has been proposed in previous studies (Skelton et al., 2019, 2014). In the Skagafjörður and Húsavík (HUS) samples, this shift is most likely due to seawater contribution, which is supported by the $\delta^{34}S_{SO_4}$ and Cl results (Tables 4.1 and S1, Figure 4.7c) that display values either close or with a trend towards the seawater signature (21‰ and 19,400 ppm, repectively; Bruland, 1983; Rees et al., 1978).

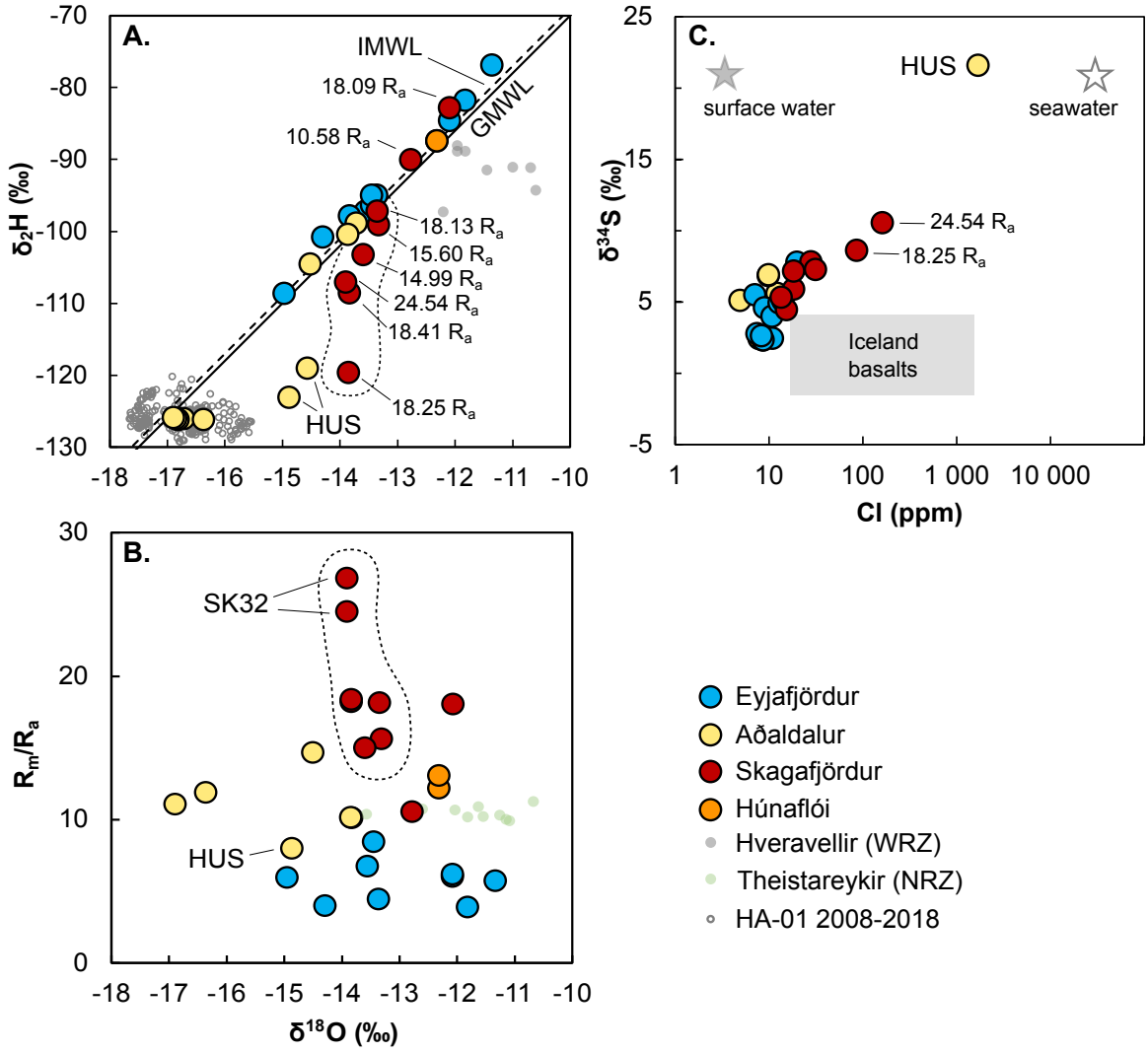

Figure 4.7: Relationships between isotopes and Cl contents for the survey area. a) Samples follow the global meteoric water line (GMWL; Craig, 1961) and Icelandic meteoric water line (IMWL; Sveinbjörnsdóttir et al., 1995) except for the NRZ and Skagafjörður groups and the samples from Hafralækur. Results for the latter are consistent with the timeseries of HA-01 reported by Skelton (2019). b) No clear relationship between helium and oxygen isotopes is present for the groups and the Skagafjörður δ^{18}O-shift is not associated with variations in $^{3}He/^{4}He$. Samples affected by the δ^{18}O-shift are shown within the dashed line. Small circles represent data from the literature (Arnórsson, 1985; Darling and Ármannsson, 1989; Saby et al., 2020; Skelton et al., 2019).

$\delta^{34}S_{SO_4}$ ranges from 5.1 to 21.6 ‰ for the Aðaldalur samples, from 2.3 to 7.8 ‰ for Eyjafjörður, from 4.5 to 10.5 ‰ for Skagafjörður, and is 2.4 ‰ for the Húnaflói sample. Except for the Húsavík sample (HUS), the remaining groups display δ^{34}S values close to the ones reported for geothermal waters from Krafla (3.40 to 13.37 ‰, (Stefánsson et al., 2015) and geothermal systems throughout Iceland (Gunnarsson-Robin et al., 2017), consistent with

SO_4 leaching from basalts (Iceland unaltered basalts -2.00 to 4.2 ‰ and pyrite from -4.2 to +7.9; Sakai et al., 1980; Torssander, 1989).

Regarding groundwater chemistry, limited variations can be observed between the Aðaldalur, Eyjafjörður, and Skagafjörður groups (Table S1; Fig. S2 and S3). Excluding the Húsavík sample (HUS), Aðaldalur has the highest Mg, Fe(t), Al, Ba, and V; Skagafjörður samples show the highest values for B, Na, Ca, F, and Cl; and the Eyjafjörður group has mostly intermediate ranges for these elements.

4.4.2 HA-01 time series

Our monitoring of $^3He/^4He$ and $^4He/^{20}Ne$ of borehole HA-01, in Hafralækur, started on June 28th, 2020, seven days after the M 6 event that occurred on June 21st, 2020, and comprises the period until October 14th, 2022. Samples collected in the period between July 2015 to February 2016 serve as the baseline for our time series since no earthquakes M $\geq$ 4 were registered in North Iceland according to the Global CMT Catalog Search (https://www.globalcmt.org) and USGS Earthquake (https://earthquake.usgs.gov/) databases.

For the baseline period, helium isotopes range from 10.1 to 11.8 Ra and $^4He/^{20}Ne$ from 1.20 to 1.95 (Table S2). Results from our time series range from 10.3 to 12.4 Ra for $^3He/^4He$ and from 1.4 to 1.9 for $^4He/^{20}Ne$ (Table S2). The time series results show limited variations compared with the baseline period; however, for the dataset of 2020 forwards, higher variations are observed, which could be tentatively separated into sub-periods with distinct slightly different signatures (see section 4.5.4).

4.5 Discussion

4.5.1 Regional isotopic variations

The geothermal fluids and glass samples from North Iceland show large ranges in helium isotopes (4 to 27 Ra), indicating that helium isotopic signatures higher than MORB values are not restricted to the rift zones, and as is the case for Vestfirðir, high $^3He/^4He$ ratios occur

in non-volcanically active regions (Figure 4.8). The variability of the He isotopic signature we report, although not associated with active volcanism, might be related to specific rock age and/or paleo-tectonic contexts (Figures 4.1 and 4.2).

In Figure 4.9, the regional Iceland dataset of geothermal fluids and volcanic products (glass and phenocrysts) is plotted. For the WRZ and ERZ (Figures 4.9b and c), both types of samples display similar signatures. In the NRZ (Figure 4.9a), however, geothermal fluids and volcanic products exhibit distinct variations; the former display a narrow range between 6.2 and 10.7 Ra (Füri et al., 2010; Hilton et al., 1990; Kononov and Polak, 1976; Marty et al., 1991; Polak et al., 1975; Poreda et al., 1992; Sano et al., 1985; Torgersen and Jenkins, 1982) whereas glasses and phenocrysts range from 7.6 to 34.3 Ra (Breddam et al., 2000; Burnard et al., 1994; Füri et al., 2010; Harðardóttir et al., 2018; Kurz et al., 1985; Licciardi et al., 2007; Macpherson et al., 2005; Moreira et al., 2001). The highest $^{3}He/^{4}He$ ratios described in the NRZ, for glasses and phenocrysts, are either located near Central Iceland (20.2 to 34.3 Ra; Macpherson et al., 2005), where the plume head is theorized to be (Vatnajökull; Darbyshire et al., 2000) and where geothermal fluids show comparable signature (Figure 4.8), or in the northernmost portion of the NRZ (21.0 to 22.7 Ra; Licciardi et al., 2007). In most of the NRZ, however, the glass and phenocrysts range between 8 and 14 Ra (Figure 4.8).

Such a global correspondence between the helium isotopic signature of volcanic products and geothermal fluids in the active rift zones is rather logical in a model for which the outgassing of helium is correlated with enthalpy and directly linked to the advection of magmas into the crust. However, this correspondence has also been described previously in non-active off-rift zones such as Vestfirðir (Figure 4.9d), where the highest $^{3}He/^{4}He$ ratios of Iceland are present in both volcanic products and geothermal fluids (up to 47.5 Ra), suggesting that the mantle plume influenced this region not only in the Tertiary, when volcanism was active, but also in the present (e.g., Harðardóttir et al., 2018; Hilton et al., 1998). This relationship is also what we can observe in our dataset, especially in the westward Húnaflói and Skagafjörður geothermal fluids, which exhibit values ranging from $\sim$ 14 to 27 Ra, with isotopic ratios as high as the ones of the Vestfirðir region. Data from the former is also compatible with the magmatic sources identified in the volcanic products and geothermal fluids of the nearest rift zones southward (Figure 4.9), as well as to the new data

we provide for the active Hofsjökull volcanic complex situated at the southern termination of the Skagafjörður valley, and which exhibit elevated values between 18 and 19.5 Ra.

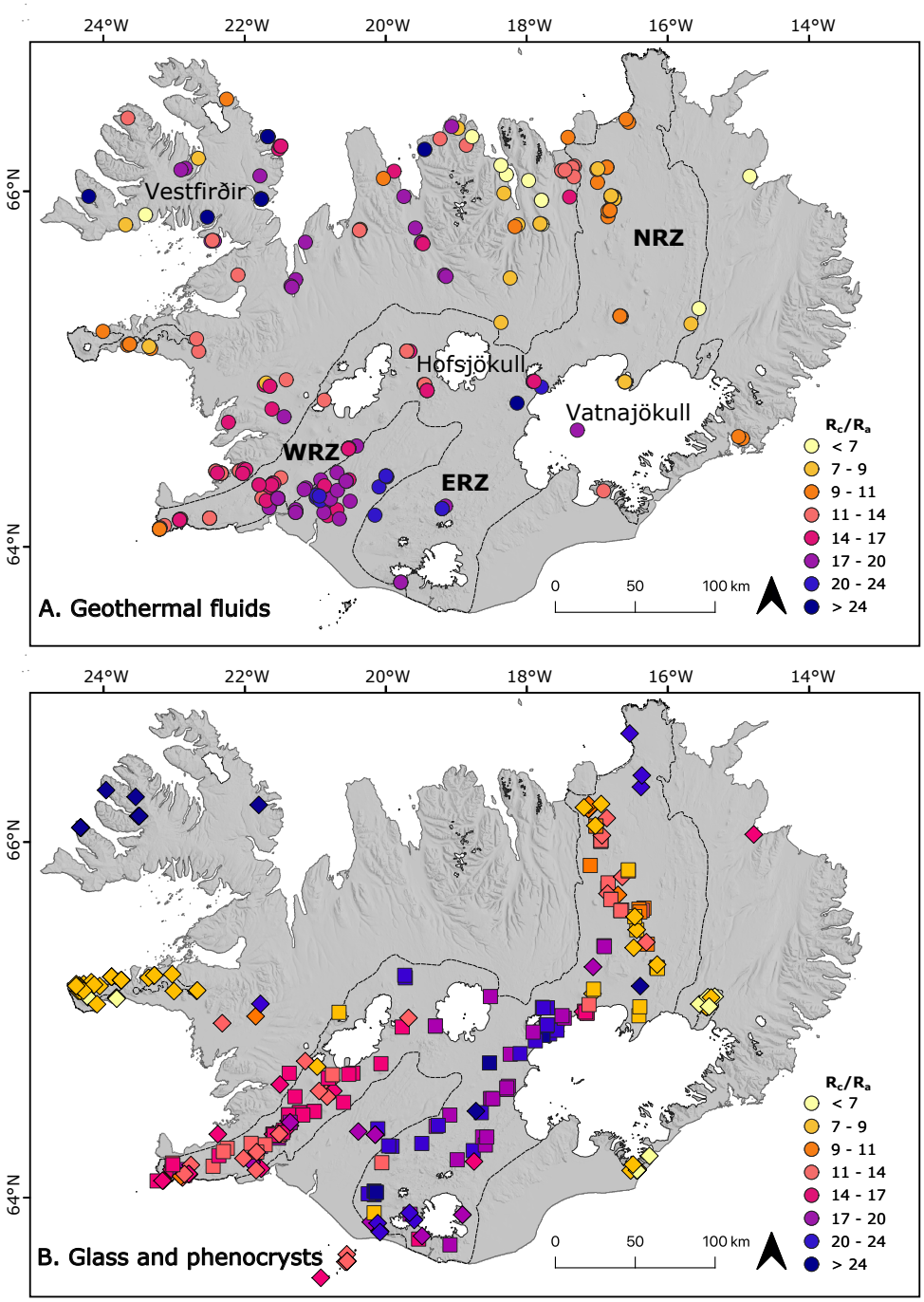

Figure 4.8: Distribution of helium isotope ratios in (a) geothermal fluids and (b) glass and mafic crystals of Iceland. The points are filtered data from Harðardóttir et al. (2018) and the current study. Rc/Ra is reported when $^4He/^{20}Ne$ is available, otherwise Rm/Ra is shown. The study area comprises some of the lowest helium isotope signals of Iceland (Eyjafjörður group).

Eastward, the Eyjafjörður and Aðaldalur geothermal fluids overall display lower values, ranging between 14 and 6-8 Ra, and which are more compatible with most of the volcanic products and geothermal fluids from the neighbouring NRZ in its central part (between 65.2 and 65.9°N). The Eyjafjörður group of geothermal fluids, which is emplaced in the oldest basalts in Northern Iceland, however, exhibits a maximum endmember at $\sim$ 11 Ra, and most samples plot below the ASW-8 Ra mixing line (Figures 4.5, 4.9, and 4.14), which is not compatible with a simple mantle origin, and may require additional sources for the helium concentration carried by those geothermal fluids (^{4}He* accumulation in the water phase over time; see section 4.5.3 for a complete discussion). Closest to the active NRZ, the Aðaldalur group of geothermal fluids exhibits a coherent variation trend (Figures 4.5 and 4.9) that can be linked to groundwater mixing at a local scale between a source with isotopic composition close to the NRZ geothermal fluids signature (up to 10.7 Ra; Poreda et al., 1992) and one with higher ^{3}He/^{4}He ($\sim$ 14.5 Ra), as also encountered in volcanic products of the NRZ (see section 4.5.4).

Overall, our new dataset for geothermal fluids from North Iceland complement the previously available information and allow to draw a clearer panorama of the off-rift helium isotopic signature. They confirm that a mantle component is carried by the geothermal fluids with isotopic compositions encompassing the full range of the Iceland active rift zones, with some potential discrete preferential clustering at 8-10, 14, 18-20, and 27 Ra. They also highlight a clear partitioning of those isotopic mantle signatures, with the highest one located in the west (14 to 29 Ra) from Vestfirðir to Skagafjörður and the lowest one (8 to 17 Ra) located in the East from Eyjafjörður to Aðaldalur, closest to the NRZ. This agrees with previous hypothesis/suggestions that the mantle plume is tilted towards N and NW Iceland based on geophysics and helium isotopes evidence (Harðardóttir et al., 2018; Mihalffy et al., 2008; Shen et al., 2002). In the next sections, we discuss the various possible processes responsible for the helium isotopic variability in North Iceland.

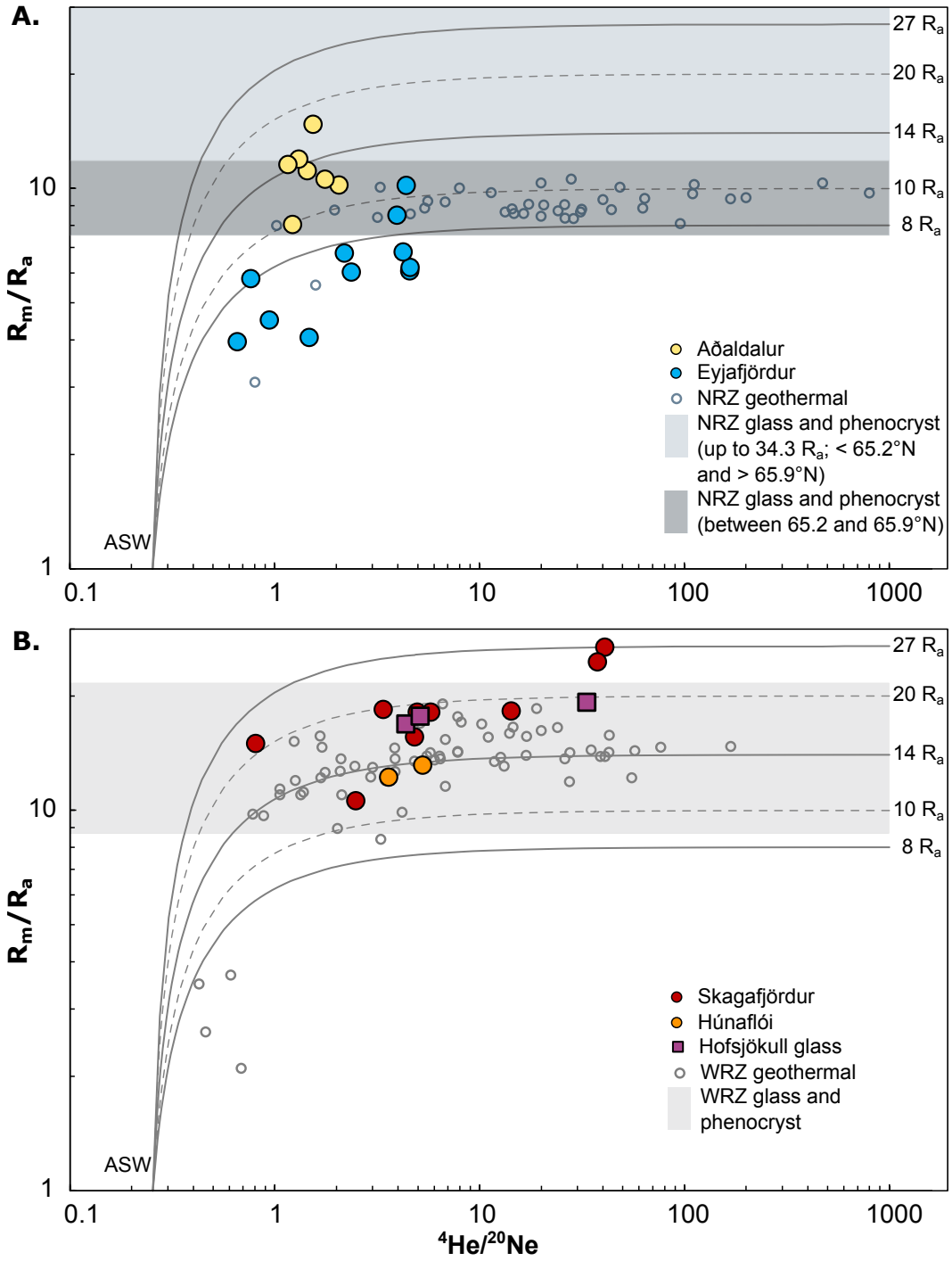
A.
27 Ra
20 Ra
14 Ra
10 Ra
8 Ra
10
1
Rm/Ra
ASW
Aðaldalur
Eyjafjördur
NRZ geothermal
NRZ glass and phenocryst (up to 34.3 Ra; < 65.2°N and > 65.9°N)
NRZ glass and phenocryst (between 65.2 and 65.9°N)
0.1
1
10
100
1000
B.
27 Ra
20 Ra
14 Ra
10 Ra
8 Ra
10
1
Rm/Ra
ASW
Skagafjördur
Húnaflói
Hofsjökull glass
WRZ geothermal
WRZ glass and phenocryst
0.1
1
10
100
1000
4He/20Ne

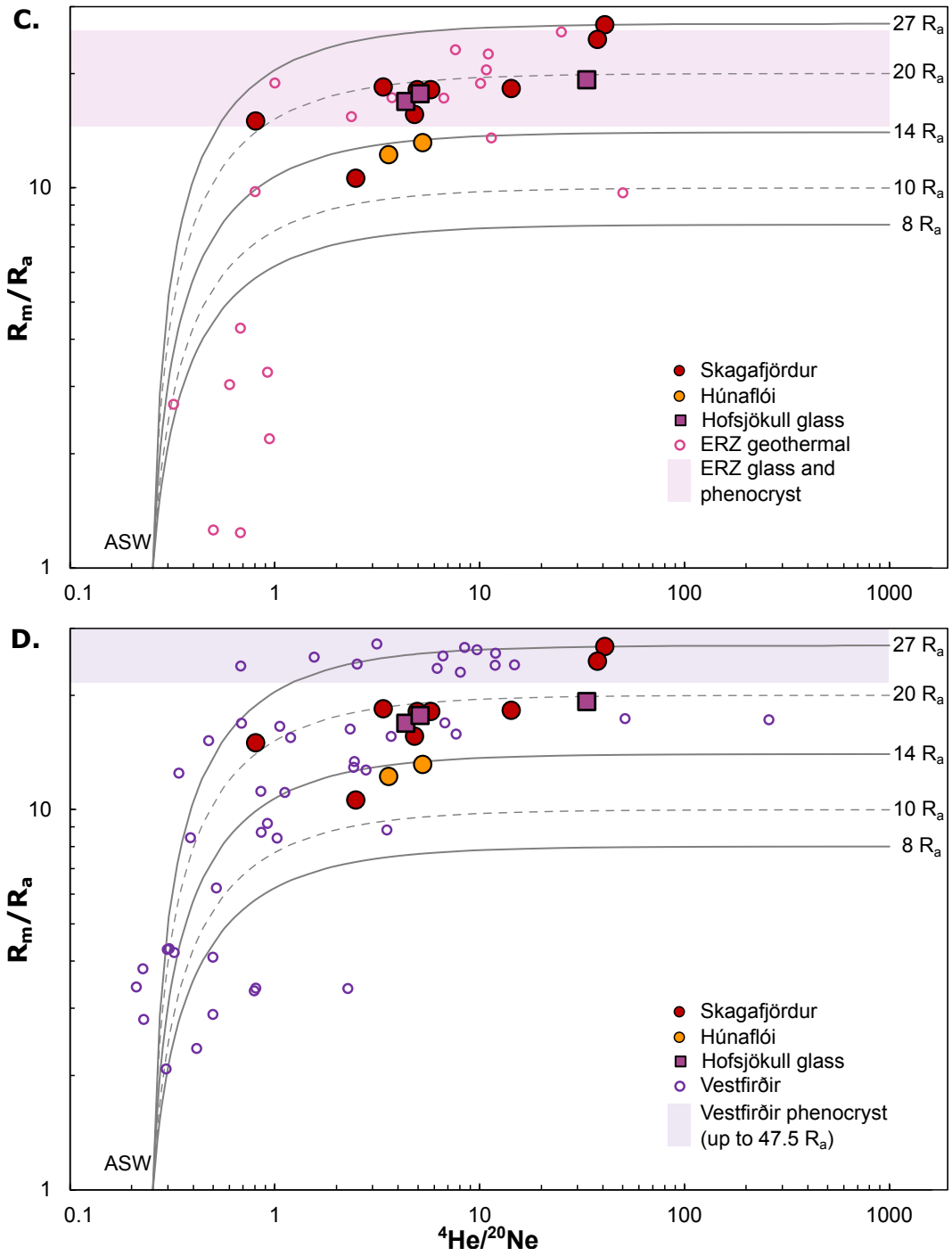

Figure 4.9: $^{3}He/^{4}He$ (Rm/Ra) vs. $^{4}He/^{20}Ne$ plot. Results populate two main regions, one with lower helium ratios (up to 14 Ra) including the Eyjafjörður and Aðaldalur groups and the other with the remaining groups reaching up to 27 Ra. The first region overlaps with previously published results of geothermal fluids from the NRZ (a) and the second region from those of the WRZ (b) and ERZ (c). Literature data of geothermal fluids from Vestfirðir (d) overlap with our full dataset. Open symbols and fields (without $^{4}He/^{20}Ne$ analyses) represent previously published data (Brandon et al., 2007; Breddam et al., 2000; Burnard and Harrison, 2005; Burnard et al., 1994; Dixon et al., 2000; Eason et al., 2015; Ellam and Stuart, 2004; Füri et al., 2010; Halldórsson et al., 2016; Harðardóttir et al., 2018; Hilton et al., 1999, 1998, 1990; Kononov and Polak, 1976; Kurz et al., 1985; Licciardi et al., 2007; Macpherson et al., 2005; Marty et al., 1991; Moreira et al., 2001; Polak et al., 1975; Poreda et al., 1992; Sano et al., 1985; Torgersen and Jenkins, 1982; Trieloff et al., 2000).

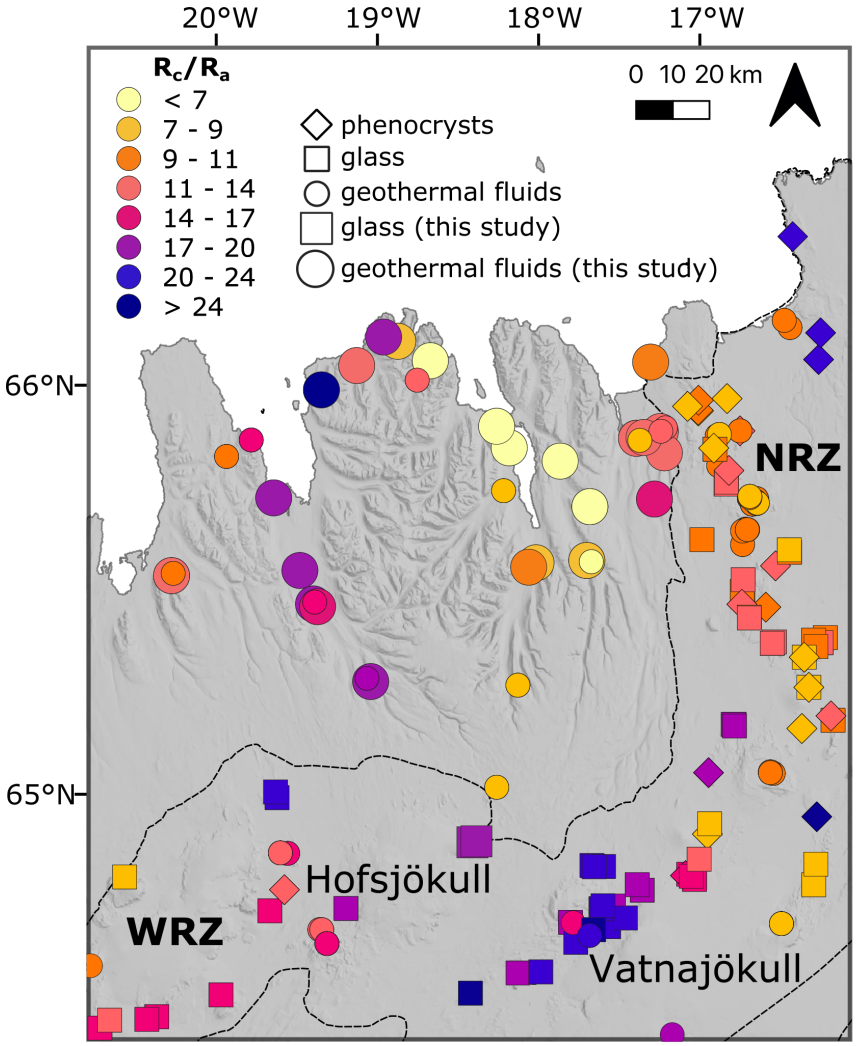

Figure 4.10: Distribution of helium isotope ratios in the study area and vicinity. The points are filtered data from Harðardóttir et al. (2018) and the current study (large symbols). The closest location, in the rift zones, with geothermal fluids showing helium isotopic signature compatible with the current study, is near Vatnajökull.

4.5.2 Fluid migration and the origin of the magmatic helium end-member in North Iceland

The geothermal fluids from our dataset are located along major valleys and low ground areas associated with globally S-N paleo-fault systems (Figures 4.1 and 4.2) that can facilitate fluid transfer either laterally or vertically. The magmatic imprint in those geothermal systems could therefore result from either (i) lateral transport via shallow aquifers from neighbouring active rift zones which are associated with fresh magma advected into the crust, or (ii) from

vertical transport alternatively transferring mantle helium directly from the deepest portions of the crust and its boundary with the mantle, or from scavenging/collecting mantle helium from alteration of the basaltic country rocks. We discuss these processes in next sub-sections.

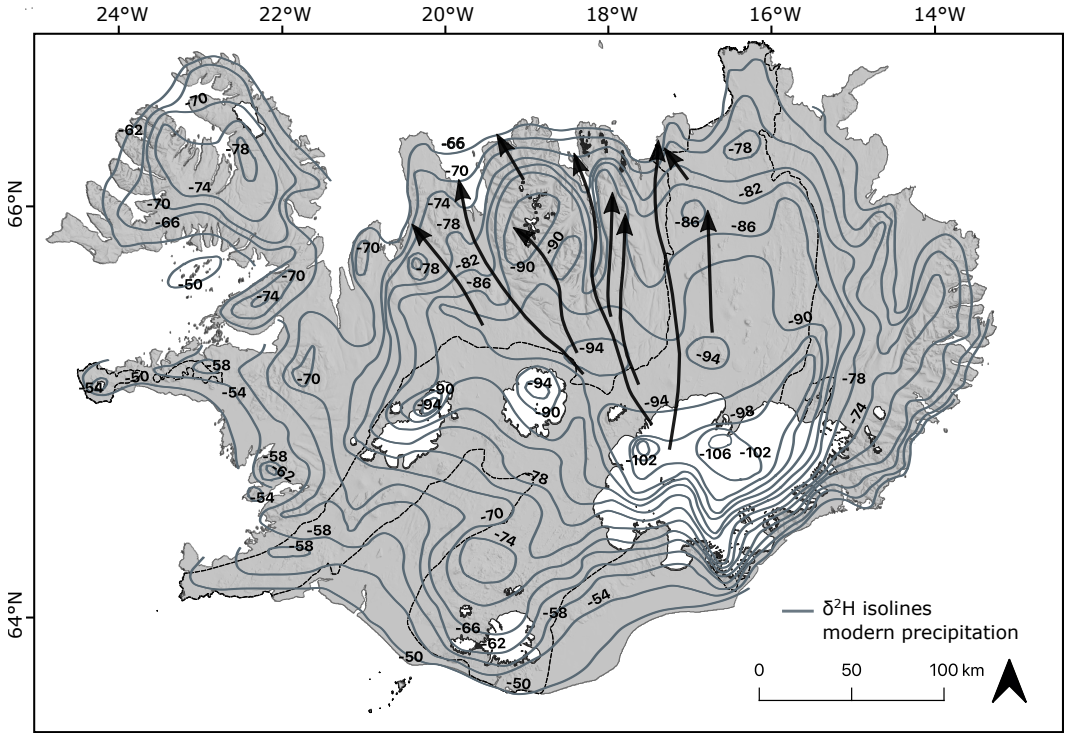

Figure 4.11: Map of Iceland with δ2H isolines for modern precipitation and groundwater flow patterns from the highlands (arrows) proposed by Árnason (1977).

4.5.2.1 Lateral transport of fluids

As discussed in section 4.5.1, our dataset for geothermal fluids, which contain mantle-derived He with an isotopic signature up to 27 Ra, is in the off-rift zone, as Vestfirðir, where no active volcanism is present, although part of our samples is hosted in younger domains (0.7 to 3.1 Ma) than in Vestfirðir ($>$ 3.1 Ma). Due to lack of active volcanism in such regions, Kurz et al. (1985) suggested that high $^3He/^4He$ ratios away from the rift zones in Iceland were due to groundwater circulation from the central highlands based on the patterns suggested by Árnason (1977) accounting for hydrostatic pressure estimations and fracture/fissure directions. These flow patterns overlap with all sample groups from the study area along the main N-S valleys (Fig. 11). Hilton (1998) refuted this model for the Vestfirðir geothermal fluids (3.14 – 30.4 Ra) on the basis that their δ^2H values reflected local

precipitation signature for most sites, not compatible with a remote source characterized by higher elevation and associated with more depleted δ^2H values. They thus concluded that the helium isotopic signature required a local source, not linked to groundwater transport and mixing. In the case of our eastward surveyed area, δ^2H values (-126 to -77 ‰; Table 4.1, Figures 4.11 and 4.12) are lower than those of modern-day precipitation for the region (-90 to -66 ‰; Árnason, 1977, 1976; Figure 4.8), and are therefore compatible with a potential recharge from the central highlands. However, most samples (mainly NRZ, Aðaldalur, and Skagafjörður groups) are even more depleted in δ^2H (minimum at -126 ‰) than the highlands (minimum at -106 ‰).

In systems where δ^2H is lighter than Iceland modern precipitation, the source of the water is linked to a period when the atmospheric temperature was colder and the precipitation had more depleted isotopic signatures ("Ice Age", $>$ 12 ka); these paleo-waters are found in areas with low groundwater flow, usually in altitudes close to sea level such as in valleys (e.g., Stefánsson et al., 2017). In Skagafjörður and Eyjafjörður, Stefánsson et al. (2019, 2017) attributed the depleted δ^2H (minimum at -118 ‰) in the low-ground regions to an "Ice Age water" component since the modern precipitation in the highlands near Skagafjörður only reaches a minimum of -94 ‰ (Árnason, 1977, 1976). This component is present in all sample groups from our dataset, except for Húnaflói (-88 ‰). Overall, the low tritium values observed for all sample groups ($<$ 1 TU; Table S1) are not compatible with modern meteoric water but are within the range described by Stefánsson et al. (2019) indicative of mixing between two endmembers: a $>$ 50 years old meteoric water and an "Ice Age" water.

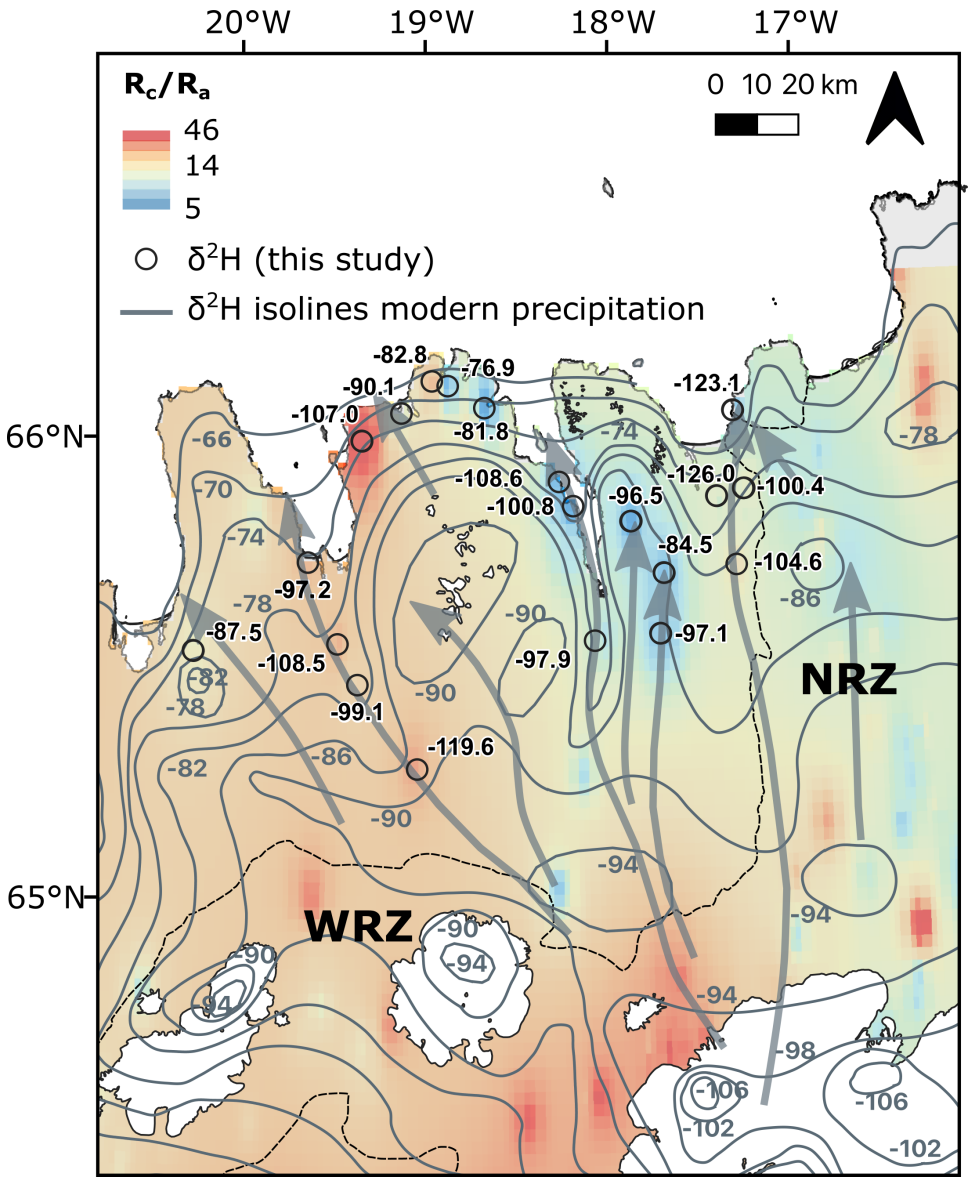

Figure 4.12: Map of the study area with δ^2H and helium isotope ratios results against the helium isotope map calculated with the Inverse Distance Weighted (IDW) interpolation method. δ^2H results are lighter than modern precipitation ranges and do not show a clear relationship with helium isotope signatures. Isolines for modern precipitation and groundwater flow patterns (grey arrows) from Árnason (1977).

Additionally, the helium isotopic signatures of geothermal fluids along those valleys are not fully compatible with the signature of their adjacent volcanic systems in the active rift zones from where they could potentially originate (Figures 4.10 and 4.12). In the western part, the Skagafjörður valley flow lines are anchored in the highlands close to the Hofsjökull active area, for which our new helium isotopic data (18 to 20 Ra) could acknowledge for

most of the values measured in the associated geothermal systems (Figures 4.5 and 4.9). However, this potential lateral source of helium would not explain the highest values of 25-27 Ra measured at its extreme termination in the north for the site of Skagafjörður. The lateral origin is even more problematic for the Eyjafjörður valley geothermal systems which exhibits measures below 11 Ra, whereas the flow lines are anchored in the highlands close to the Vatnajökull active magmatic area which displays isotopic values $>$ 17 Ra. The highest value measured in the southern part of the Aðaldalur valley (magmatic endmember of $\sim$17 Ra) could be compatible with the values measured in the northern part of the Vatnajökull active magmatic area (17-20 Ra). However, most of the remaining data from the geothermal systems of this valley (magmatic endmember of 10-14 Ra) are more compatible with values measured in the Krafla and Þeystareykir active areas (NRZ), from which the associated northward flow line does not seems to be connected to the main corridor of the Aðaldalur valley (Figures 4.11 and 4.12).

Thus, there does not seem to be a direct relationship between δ^2H-depleted waters and their helium isotope signatures, via northward migration of crustal fluid initiating from active rift zones where magmas are currently crystallising and degassing in the crust. The magmatic components observed in the off-rift north Iceland geothermal systems are therefore most likely due to a vertical flux via active tectonic discontinuities.

4.5.2.2 Vertical transport of fluids

Besides the isotopic signatures of geothermal fluids and their compatibility with potential sources and origins considered previously, the absolute concentration of helium dissolved into those fluids is also a key parameter to evaluate. The helium concentrations in groundwater from our dataset varies in a wide range (65 to 9325 $ncm^3g^{-1}H_2O$; Table 4.1), which is comparable with those observed at active rift zones in Iceland and at Vestfirðir (Figures 4.13 and 4.14). Such concentrations of helium in the fluids, mostly of magmatic origin, could either originates from (i) weathering of volcanic glass and mafic minerals which contain a certain amount of mantle volatiles, or from (ii) direct input of volatiles from fresh magmas stored into the underlying crustal column or from the mantle itself. Both hypotheses are considered below.

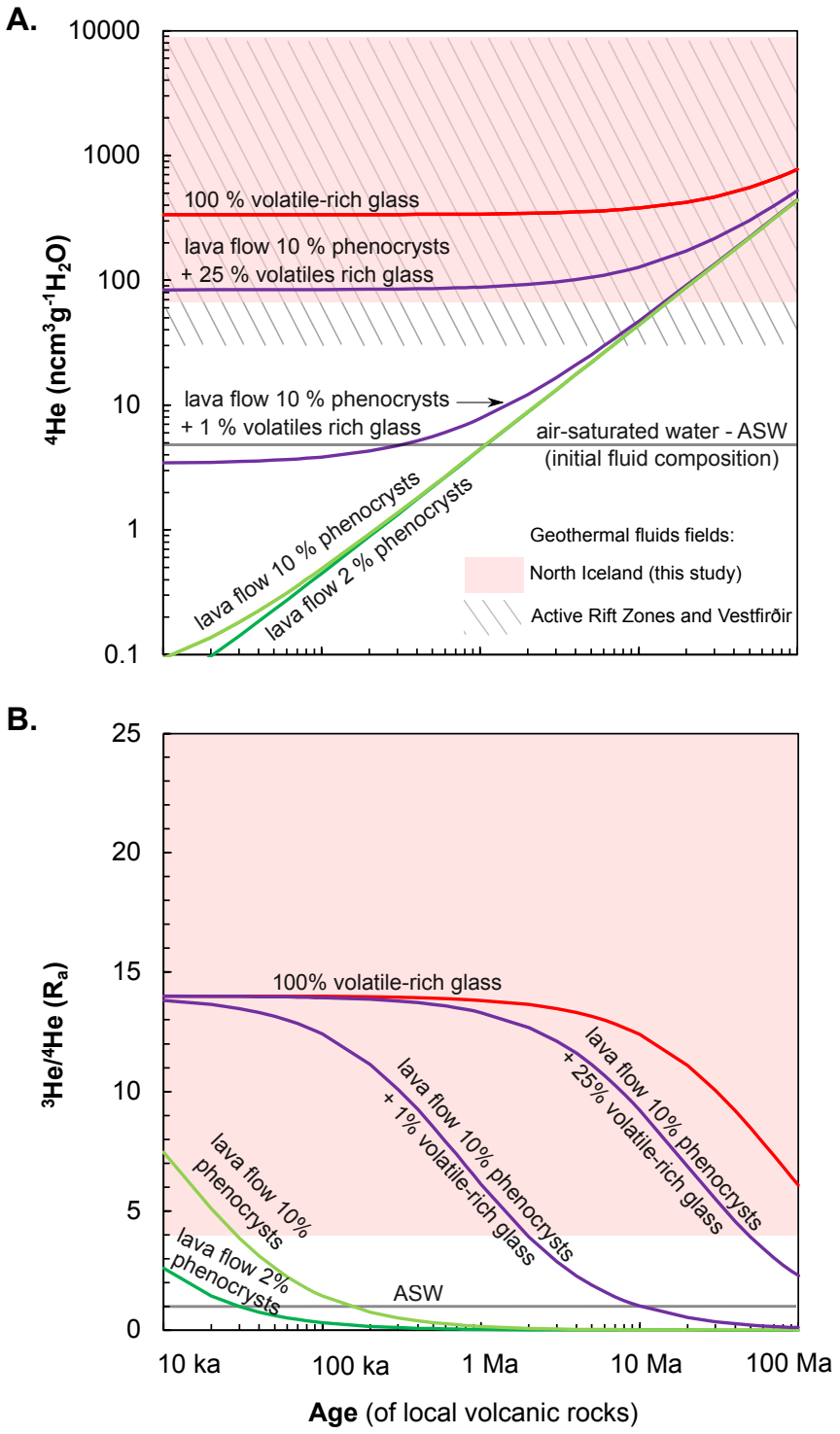

Figure 4.13: Composition (a) and helium isotopic signature (b) of geothermal fluids with modelled contribution from the rocks with various phenocrysts and glass rims proportions over time. Fields for geothermal fluids from Iceland active rift zones and Vestfirðir from the literature (Brandon et al., 2007; Breddam et al., 2000; Burnard and Harrison, 2005; Burnard et al., 1994; Dixon et al., 2000; Eason et al., 2015; Ellam and Stuart, 2004; Füri et al., 2010; Halldórsson et al., 2016; Harðardóttir et al., 2018; Hilton et al., 1999, 1998, 1990; Kononov and Polak, 1976; Kurz et al., 1985; Licciardi et al., 2007; Macpherson et al., 2005; Marty et al., 1991; Moreira et al., 2001; Polak et al., 1975; Poreda et al., 1992; Sano et al., 1985; Torgersen and Jenkins, 1982; Trieloff et al., 2000).

4.5.2.2.1 Release of helium from host rocks

The hypothesis of magmatic helium originating from the host rocks of hydrothermal fluids systems has already been investigated in the literature. For the Iceland case, and more specifically for the Vestfirðir fluids, Hilton et al. (1998) computed the budget of helium concentration that could be potentially liberated to the hydrothermal waters by weathering of mafic minerals contained in local basalts. The various parameters they considered (water/rock ratio, helium concentration in fluid inclusions, percentage of mafic minerals in basalts) allowed them to consider that such a process cannot account for the magmatic helium present in hydrothermal fluids because the maximum amount liberated would be orders of magnitudes below the one required to acknowledge the concentrations measured in the fluids. More recently, Méjean et al. (2020) modelled, for groundwater with limited mantle input in Canada, that a fossil magmatic source was preserved in the crust since its time of formation ($\sim$ 100 Ma; Monteregian Hills Igneous Province) and can transfer, via leaching, this typical aged magmatic signature into the modern/Holocene local groundwaters. At the base of their calculation, they considered potential initial helium concentrations of non-degassed quenched glass (6.7 x 10^{-6} cm^3g^{-1}rock; Torgersen et al., 1995).

In order to go beyond this apparent discrepancy regarding the hypothesis of host rock origin, we propose in Figure 4.13 a model which investigates the various key parameters controlling the amount of volatiles potentially liberated in the fluids and their helium isotopic ratio through time. In this scenario, both ^{3}He and ^{4}He are liberated from the rock and belong to (i) initial magmatic origin, with (ii) in situ addition trough time of radiogenic ^{4}He and nucleogenic ^{3}He; the latter being negligeable in the case of the low Li content of Icelandic basalts. The theoretical amounts of helium liberated in the fluids are computed for a water/rock ratio of 100:5 (average between the low-T and high-T geothermal systems ratios; (Gislason and Eljgster, 1987), and by ageing the rock with the helium in situ production ratios (Eqs. S1 and S2, supplementary material) for a range of time encompassing the maximum ages for North Iceland basalts ($<$ 10 Ma). We use different starting ^{4}He concentrations of the volcanic host rocks (Figure 4.13a) controlled by the amounts of either mafic minerals and/or volatiles-rich glass, with modulations that range from the initial conditions

considered by Hilton et al. (1998) (rather limited percentage of mafic minerals in the lavas) to the one considered by Méjean et. (2020) (100% volatiles-rich glass). This computation indicates that for typical host rock ages of Northern Iceland ($\sim$ 1 to 10 Ma), the amount liberated in the waters would not reach the ranges of concentrations measured in geothermal fluids ($>$ 60 $ncm^3g^{-1}H_2O$) for most of the starting rock compositions, except for rocks that contain large proportions of volatile-rich glass (50 to 100%). The computation of the associated isotopic ratios gives the same results (Figure 4.13b). It is only when the lavas contain high concentrations of magmatic volatiles that the initial typical mantle isotopic signatures can resist ageing and production of ^{4}He*.

Even if potentially occurring locally in sub-glacial volcanic contexts, such initial end-member compositions, with large proportions of volatile-rich glass, are not realistic for the entire crust in Iceland. As Hilton et al. (1998) already observed, mantellic He would only be reasonably preserved in a minor fraction of the lavas (glass rims and small proportions of phenocrysts) that do not provide enough mantle helium by weathering processes. Thus, leaching of the local lava pile cannot explain the helium isotopic ratios and He concentrations observed in datasets from North Iceland geothermal fluids.

4.5.2.2.2 Mantle degassing

Off-rift mantle degassing has been proposed in the past to explain the wide range of helium isotopes in Vestfirðir ($\sim$ 30 Ra; Hilton et al., 1998). The main issue with this theory is the lack of surface evidence of recent magmatic activity and of confirmation from other chemical and isotopic tracers besides noble gases. Stefánsson et al. (2016) computed the mantle CO_2 flux for off-rift low-temperature geothermal systems in Iceland and found it to be low in Skagafjörður and Vestfirðir ($<$ 5 mol $km^{-2}a^{-1}$), and thus incompatible with high CO_2 partial pressure typical of degassing of the Icelandic mantle. However, CO_2 is highly susceptible to secondary processes such as dissolution in groundwater and carbonate precipitation and thus its current signature might not reflect the initial source of the fluid. Additionally, the estimation of heat flow to the surface in off-rift zones in Iceland is relatively homogeneous for the survey area ($\sim$ between 100 and 150 mWm^{-2}; Flóvenz and Saemundsson, 1993), unlike the helium ratios (3.9 – 26.9 Ra). Temperature profiles and heat flow maps are necessary

to detect potential lateral and vertical variations that could be linked to the helium isotope heterogeneity in off-rift zones.

Some of the geothermal systems from Northern Iceland are located in areas identified as extinct fissure swarms (Aðaldalur; Bourgeois et al., 2005) and aborted rifts (Skagafjörður and Húnaflói; Garcia et al., 2003; Hjartarson, 2003; Sæmundsson, 1974). This constraint suggests a geotectonic control that can be related to degassing of residual melts at depth. The age of dykes from the Aðaldalur valley (Skjálfandi fissure swarm) and Skagafjörður are relatively young ($\sim$ 2 Ma Bourgeois et al., 2005; Hjartarson, 2003) and lavas from Skagafjörður show evidence for plume upwelling at 3 Ma, as seen presently at central Iceland (Walters et al., 2013). It is, however, difficult to determine how long residual melt survives in the crust. Crystal residence ages of volcanic systems give an estimate of how long magma can be stored in the crust before eruption. Worldwide, crystal residency ages reach up to 10^5 years (Cooper and Kent, 2014) and in Iceland between 10^3 and 10^4 years (Zellmer et al., 2008). Beyond such timescales, in new trans-crustal views of magma storage, magma bodies are stocked in sills at various depths, which can lead to faster heat loss, cooling rates, and crystallization compared to the traditional model of a single magmatic chamber (Maclennan, 2019).

Considering the age of the rocks in Northern Iceland, the magmatic bodies are then most probably fully crystallized and thus active degassing of residual intruded melts is unlikely. An alternative and potential source of mantle helium transported vertically in the geothermal fluids of North Iceland could be from a global flux originating below the crust from incipient melting. A vertical flux originating from the mantle/crust boundary can occur via advective flow controlled by faults due to improved permeability (Kennedy and van Soest, 2007; Kulongoski et al., 2013, 2005). In the model proposed by Kennedy and van Soest (2007), a vertical fault splay must penetrate the ductile lower crust and reach the mantle acting as a channel for fluid flow; strain localization must occur to generate vertical faults in depth. The areas where mantle input via advective flow have been described (Kennedy and van Soest, 2007; Kulongoski et al., 2013, 2005) are seismically active regions, which is the case of North Iceland.

We attempt to estimate such a flux, anchored by the age of the groundwater in North

Iceland, following the model of water age estimation of Zuber et al. (1997) (Equations 4.1 and 4.2) modified to account for both ^{4}He and ^{3}He fluxes (based on the helium isotopic ratio of the magmatic endmember considered), as well as the nucleogenic production of ^{3}He that occurs depending on the presence of lithium through the thermal neutron capture on ^{6}Li (Morrison and Pine, 1955).

$$S_{^n\mathrm{He}} = \rho_\mathrm{r}/\rho_\mathrm{f}\phi P_{^n\mathrm{He}} \tag{4.1}$$

$$t_{^n\mathrm{He}} = C_{^n\mathrm{He}}\phi h\rho_\mathrm{f}/(J_{^n\mathrm{He}} + \phi h\rho_\mathrm{f}\Lambda P_{^n\mathrm{He}}) \tag{4.2}$$

Where $S_{^n\mathrm{He}}$ is the rate in which the nHe produced in situ in porous rock (Equations S1 and S2; supplementary material) goes into the groundwater, $P_{^n\mathrm{He}}$ is the production rate, ρ_r the rock density, ρ_f the fluid density, ϕ the total interconnected porosity, tnHe the age, $C_{^n\mathrm{He}}$ the total ^{n}He content, h the aquifer thickness, Λ the gas phase escaping from the solid phase, and $J_{^n\mathrm{He}}$ the crustal flux to the system from underlying formations. $C_{^n\mathrm{He}}$ is the ^{n}He produced plus the initial ^{n}He from ASW ($\sim$ 4.7 x 10^{-8} and 6.5 x 10^{-14} cm_3STPg^{-1} for ^{4}He and ^{3}He, respectively; Kipfer et al., 2002).

In Figure 4.14, two distinct magmatic helium fluxes ($J_{^4\mathrm{He}}$: 1 x 10^{-8} and 1 x 10^{-7} $cm^3STPcm^{-2}a^{-1}$) have been used in the calculations to compute resulting isotopic ratios and concentrations in the geothermal waters. From Equation 4.1, for an arbitrary ϕ of 0.1, ρ_r of 2.9 gcm^{-3}, and ρ_f of 1 gcm^{-3} we reach a ^{4}He solution rate of 2.63 x 10^{-12} $cm^3STPa^{-1}H_2O$. The age of the fluid is given by Equation 4.2 where we employ an arbitrary aquifer thickness (h) of 100 m and Λ of 0, assuming all in situ produced isotopes are retained in the rock for those specific simulations (see next section for a detailed investigation of this parameter). For the two helium fluxes computed, the North Iceland dataset plots between the 1 and 250 ka groundwater age isolines, which is consistent with the age estimations previously proposed for the aquifers in the NRZ volcanic systems (up to 160 ka; Saby et al., 2020) and Eyjafjörður alike (up to 15 ka; Stefánsson et al., 2019). However, according to the δ^2H stable isotopes data (see section 4.5.2.1), the North Iceland hydrothermal systems are either fed by modern groundwaters or by fossil waters that could be of few tens of ka (Stefánsson et al., 2019)

which would be more compatible with the computed flux of 1 x 10^{-7} $cm^3STPcm^{-2}a^{-1}$.

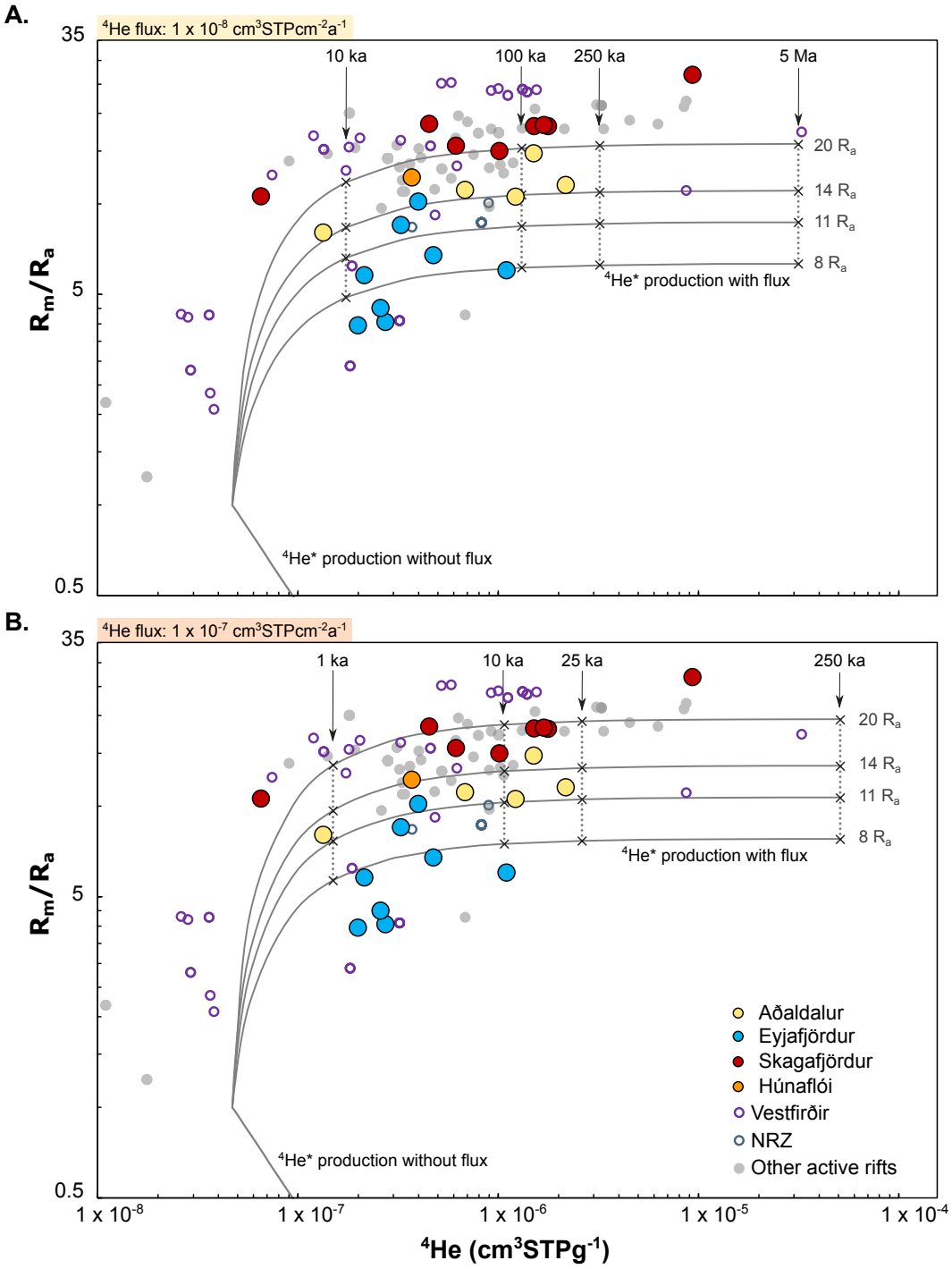

Figure 4.14: Water aging model based on ^{4}He* enrichment from an initial fluid composition of air-saturated water (ASW) with a regional ^{4}He flux of (a) 1 x 10^{-8} $cm^3STPcm^{-2}a^{-1}$ and (b) 1 x 10^{-7} $cm^3STPcm^{-2}a^{-1}$. The model for regional flux of zero is also represented.

Note that another crucial parameter in this model is the aquifer thickness (h); this

model has been built for traditional confined aquifers in continental basins settings where h corresponds to the vertical thickness of the active flow. In our study, we can transpose the system and envisage h represents the width of the faulted and weathered zone where the hydrothermal system if flowing. Any reduction of this width from 100 m to 10 m, for instance, will also decreases by $\sim$ one order of magnitude the associated helium flux to conserve the same range of water age and dissolved helium concentrations. Nonetheless, if one considers that most of the local groundwaters in one of those valleys could be characterized by clustered and similar ages, then the contrasted ^{4}He concentrations observed for each group on Figure 4.14 could reflect (i) distinct magmatic fluxes, which is also unlikely at that scale, or (ii) distinct width of each considered geothermal systems, which could be more probable and could depict the local diversity and complexity of the vertical pathways.

The range of global flux obtained (1 x 10^{-8} and 1 x 10^{-7} $cm^3STPcm^{-2}a^{-1}$ ^{4}He) is lower than the one (Craig et al., 1975) calculated for the mid-ocean ridge ($\sim$ 4 x 10^{-7} $cm^3STPcm^{-2}a^{-1}$), which is reasonable considering recent magma production is not evident in North Iceland.

To explain the helium ratios above typical upper mantle values ($\sim$ 8 Ra) for these off-rift zones, the flux from the magmatic endmember could originate from degassing of a ^{3}He-rich mantle source. Although the plume head has been hypothesized to be currently located under Vatnajökull (central-SE) (Darbyshire et al., 2000), plume tilting has been suggested for Iceland as evidenced by geophysics and helium isotopes (Harðardóttir et al., 2018; Mihalffy et al., 2008; Shen et al., 2002). Shen et al. (2002) proposed that the plume conduit in Iceland is tilted towards the north in the upper mantle due to a northward or southward flow (of the asthenosphere and upper mantle, respectively). A tilted plume model has been proposed also in Hawaii (Farnetani and Hofmann, 2010; Hofmann et al., 2011) where, similar to Vestfirðir (e.g., Füri et al., 2010; Hilton et al., 1998) and Skagafjörður (Kononov and Polak, 1976; current study), high ^{3}He/^{4}He signals have been described at Loihi seamount ($>$ 30 Ra;, up to 100 km away from the current plume centre. A more recent geophysical model proposes that the Iceland plume extends under Greenland reaching higher depths into the transition zone (Celli et al., 2021). In their model, the low velocity anomaly, at 56 km depth, is located under North Iceland and Vestfirðir. Since no volcanism is evidenced in our study area, generation of melt from influence of the mantle plume is incipient.

4.5.3 Potential ^{4}He* enrichment of Eyjafjörður geothermal fluids

As mentioned in section 4.5.1, the Eyjafjörður samples show a maximum endmember (10.7 Ra; Table 4.1) compatible with NRZ fluids (6.2 to 10.7 Ra) (Figure 4.9). The variations within this sample group and their excursion below the ASW-8 Ra mixing line (if air contamination during sampling is discarded), could be associated with ^{4}He* (radiogenic ^{4}He) enrichment by in situ production since glass and phenocrysts samples from the NRZ (Figure 4.9) have a minimum helium isotopic signature of 7.6 Ra (Macpherson et al., 2005) compatible with upper mantle signature. Although even lower values are described in the SNVZ and ÖVZ (5.4 to 11.6 Ra; Sigmarsson et al., 1992; Williams, 2005; Debaille et al., 2009; Peate et al., 2010; Harðardóttir et al., 2018), in this model we consider the nearby NRZ endmembers.

Based on ^{4}He* in situ accumulation in groundwater (Equation 4.2; Zuber et al., 1997), we modelled that, for a system with a ^{4}He magmatic flux of 1 x 10^{-7} $cm^3STPcm^{-2}a^{-1}$, with an endmember signature of 11 and 8 Ra, the steady-state escape of all ^{4}He* produced in situ (Λ of 1) does not explain the variations found in the Eyjafjörður dataset (Figure 4.15b).

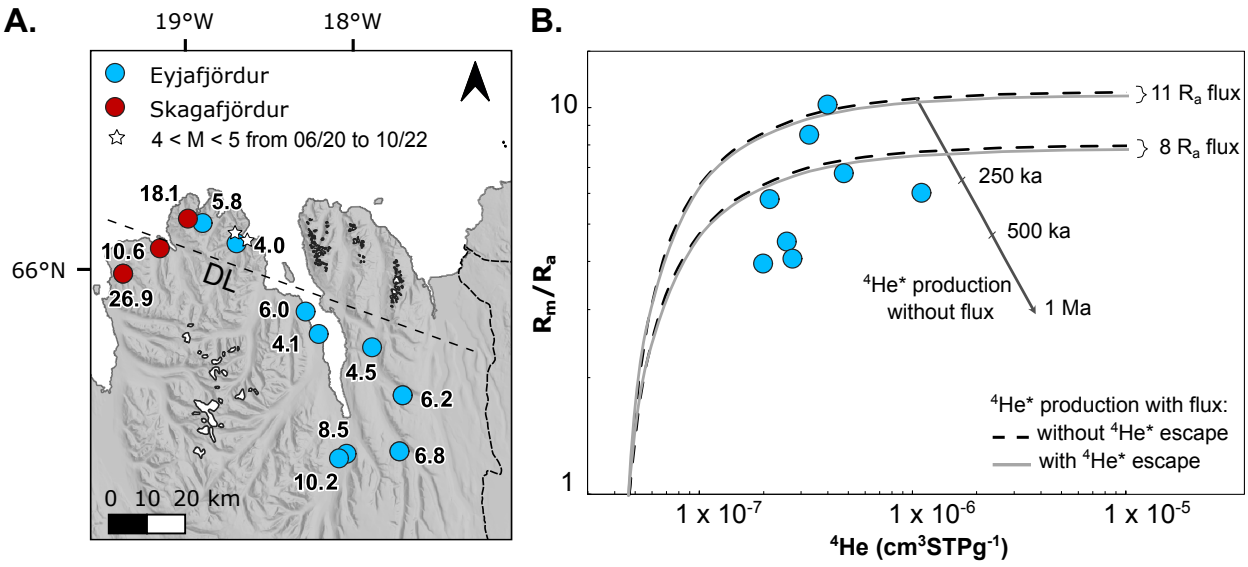

Figure 4.15: Eyjafjörður model. (a) Map with Eyjafjörður and other relevant samples with recent onshore earthquakes along the Dalvík Lineament (DL). (b) Water aging models: (i) with and (ii) without ^{4}He* enrichment for a ^{4}He flux of 1 x 10^{-7} $cm^3STPcm^{-2}a^{-1}$ with 8 and 11 Ra signatures and (iii) another without a regional helium flux and for a fluid with initial ^{4}He composition close to ones of the active rift zones ($\sim$ 1 x 10^{-6} $cm^3STPg^{-1}H_2O$).

If the ^{4}He* in situ accumulation in groundwater is decoupled from the continuous accu-

mulation of the magmatic flux, then starting from the composition of the magmatic source fluid (endmember at 11 Ra and 1 x 10-^{6} cm^{3}STPg^{-1} ^{4}He; Figure 4.15b), between 250 to 500 ka are necessary to produce the ^{4}He concentrations observed for the site exhibiting the lowest ^{3}He/^{4}He ratio of the group (Figure 4.15b). This is largely compatible with the host rock age which is frequently older than 1 Ma in Northern Iceland. If the host rock retains the ^{4}He* produced, which is released under non-steady state conditions to the water phase, in short timescales, then the water age might not coincide with its ^{4}He content. The Eyjafjörður samples are hosted in areas where earthquakes have been registered onshore, along the Dalvík Lineament (DL) (Figure 4.15a). In seismically active regions, release of noble gases, produced in rocks, can be increased due to dilatancy resultant of shear deformation and fracturing (Buttitta et al., 2020; Caracausi and Paternoster, 2015; Honda et al., 1982). According to Torgersen and O'Donnell (1991), this process can occur in short timescales ($<$ 1500 years) and fracturing can increase the helium flux by a factor of 10^2 to 10^4 times higher the steady state model. In Italy, Caracausi et al. (2022) observed that crustal ^{4}He* degassing under steady state conditions is diffusive and could not account for the ^{4}He contents in the natural reservoirs and that in contrast seismicity, instead, can optimize ^{4}He* release from rocks by triggering episodic and focused degassing that control the He isotopic signature in continental areas reducing the evidences of mantle derived degassing.

This type of non-steady state model was built for a crustal scenario characterized by degassing of crustal and subordinate mantle He. It might have different implications in an magmatic crust context such as the case of Iceland. Furthermore, another argument in favour of a non-steady state release of ^{4}He* from the rocks to the water phase, is the alignment of the samples from Eyjafjörður with the lowest ^{3}He/^{4}He ratios along the DL (Figure 4.15a). Moreover, one sample from Skagafjörður with much lower ratios (10.6 Ra) than the remaining of the group (from 15.0 to 26.9 Ra), which at first glance seems to be an outlier, is also hosted along the DL domain. The reason for the high signatures of the other two samples from Skagafjörður near the DL is not clear and might reflect complex magmatic processes at depth (see section 4.5.2.2.2).

^{4}He* enrichment can occur in other sampled groups, however, it is harder to distinguish it from other processes such as groundwater mixing between water systems with different

helium isotopic signatures or contribution of various magmatic sources since, above 8 Ra, variations in $^3He/^4He$ can reflect the distinct mantle signatures in Iceland due to influence of the plume. This is the case for the Aðaldalur group in which, besides groundwater mixing with distinct end-member compositions, release of $^4He^*$ under non-steady state conditions could also be envisaged, considering that most of the wells sampled in the valley are located near the DL (Figure 4.4). Although no evidence of this process is clear from the helium isotopes results, the apparent higher magmatic flux in the Aðaldalur valley (Figure 4.14) might overprint the $^4He^*$ contribution.

4.5.4 Groundwater mixing in Aðaldalur and the HA-01 time series

Most of the Aðaldalur group plots between the 14.5 Ra and 11.5 Ra mixing lines with ASW (Figure 4.16b) and displays a trend in the Rm/Ra vs. $^4He/^{20}Ne$ plot (Figure 4.9 and 4.16b) that could be associated with mixing of groundwater systems with different helium isotopic signatures in a local scale. Samples with the lowest $^3He/^4He$ (HV and KL) are the ones closest to the NRZ (Figure 4.16a) and their volcanic systems which have helium ratios of up to 10.7 Ra for geothermal fluids (e.g., Kononov and Polak, 1976) and volcanic endmembers approaching 12 Ra (glass samples; Breddam et al., 2000; Kurz et al., 1985).

Mixing of different groundwater bodies is also supported by the δ^2H signature. Although results of water chemistry and stable isotopes are only available for one of the wells closer to the NRZ (HV), it has higher δ^2H (-100.4 ‰), closer to modern precipitation values, lower V contents, and higher K, Cs, Ge, Li, Rb, and Sr contents than those of the remaining samples of the group. (Table 4.1 and S1). The overall groundwater water signature of HV (HVER) is compatible with geothermal areas in the NRZ (Krafla and Námafjall; Kaasalainen and Stefánsson, 2012; Stefánsson et al., 2017).

HA-01 is part of the Aðaldalur group (Figure 4.16a) and its time series $^3He/^4He$ data overlaps with the trend formed by the remaining samples of the group (Figure 4.16b); this relationship, added to their geographical proximity, suggests that the same processes are involved in both regional and periodic $^3He/^4He$ variations and balancing between potential water bodies endmembers.

The variation in helium isotope ratios over time at HA-01 is limited, granting there is a

$\sim$ 4-year data gap between the 2016 and 2020 samples that cannot account for the period just before the major earthquake swarm of June 2020. Considering the $^{4}He/^{20}Ne$ range for the time series is low (1.20 to 1.95, Table S2), discarding air contamination during sampling is difficult, and small variations of the isotopic ratio linked to micro-contaminations can still be present in the dataset. We could, however, observe and distinguish some distinct periods in Figure 4.16c. There is a slightly higher $^{3}He/^{4}He$ signature for the data from June 2020 to March 2021, which plot closer to the ASW-14Ra mixing line in Figure 4.16b (measured values close to 12 Ra in Figure 4.16c) compared to our baseline data from 2015-2016. The moving average plotted for this period ($^{3}He/^{4}He$ ratio at $\sim$ 11.5 Ra) on Figure 4.16c is also slightly, but significantly, distinct from the one of the following period which exhibits lower values from April 2021 to May 2022 ($\sim$ 10.9 Ra). After this second period, a new tendency with higher values seems to start again. The correspondence between those slight variations and the observed seismic events during the monitored period is not as clear as the one associated with the previous hydrochemical variations documented by Skelton et al. (2014, 2019).

However, it seems that the two periods associated with the seismic events with $M > 5$, such as the swarm from June 2020 following an initial $M \leq 6$ event, and the M 5 earthquake of September 2022, share the same higher $^{3}He/^{4}He$ ratio at $\sim$ 11.5 Ra, compared to the intermediate quiescent period which is characterized by a globally lower value of $\sim$ 10.9 Ra. The isotopic value of the quiescent period of our time series (which lasted $\sim$ nine months after the swarm of June 2020) is not strictly equivalent with the moving average value of the baseline period of 2015-2016, however they share variations of isotopic values in the same direction. Those limited variations detected in our time series, together with the mixing trend observed in most of the Aðaldalur valley samples, overall agree with the hypothesis of mixing of groundwater bodies, which has been previously proposed for the area based on shifts in stable isotopes and water chemistry (Skelton et al., 2019, 2014). Nonetheless, even if the transitions between the periods we document appear rather short and sharp, it is difficult to precisely determine the role of the seismic events in triggering such potential modifications via mixing of water bodies or potential liberation of $^{4}He^{*}$ (see previous section) and their subsequent relaxation toward stable quiescent periods, especially in the absence of

clear record before the major events of M > 6.

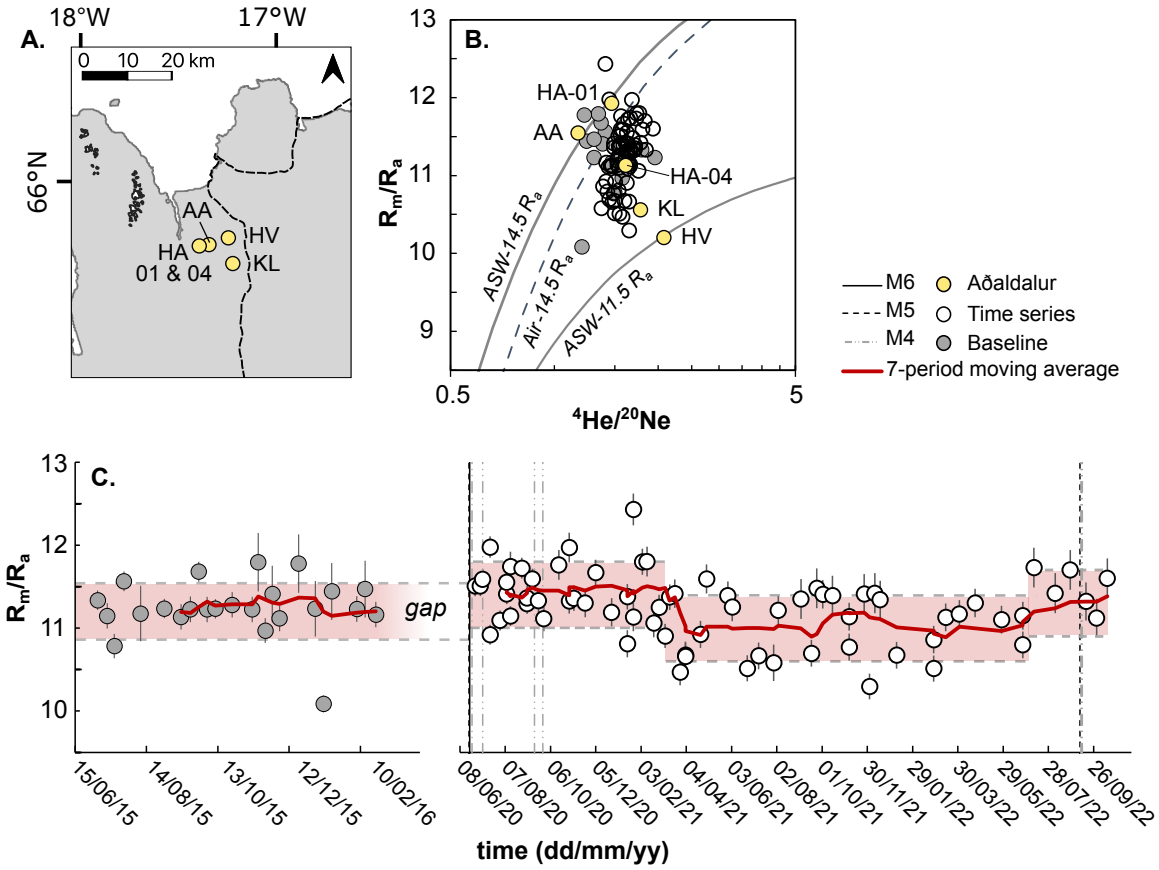

Figure 4.16: Time series results and relationship with the Aðaldalur dataset. (a) Location of Aðaldalur samples with HA-01 (HA). (b) Rm/Ra vs. $^{4}He/^{20}Ne$ plot of the HA-01 time series and the Aðaldalur samples. (d) Time series results for HA-01.

4.6 Conclusion

The results from our survey and time series in North Iceland geothermal fluids indicate a high regional variability in helium isotopic ratios (4 to 27 Ra) that can result from regional and local processes: (i) mantle degassing via fault systems, (ii) radiogenic helium release, and (iii) groundwater mixing; the latter two potentially triggered by seismic events.

High helium contents and isotopic ratios of geothermal fluids along fault zones in North Iceland require the presence of a global magmatic flux, with estimated value (1 x 10^{-7} $cm^3STPcm^{-2}a^{-1}$ ^{4}He) comparable to the ones of neighboring active rift zones in Iceland, where melts intruded in the crust are still actively degassing. Because lateral transport of

the magmatic component from those active rift zones or leaching of local magmatic country rocks are not satisfactory hypothesis to explain such a flux, the only alternative process that can be envisaged is direct transfer from the mantle itself. The helium ratios above typical upper mantle values ($\sim$ 8 Ra) for these off-rift zones may therefore be associated to a mantle flux originating from degassing of a ^{3}He-rich mantle source influenced by the Iceland mantle plume via cryptic and incipient melting.

Along the Dalvík Lineament, the helium isotopic signature indicates release of radiogenic ^{4}He from the host rocks, which is not compatible with continuous release coupled with the mantle flux. This ^{4}He* input is rather associated with additional short timescales processes, potentially linked to the tectonic earthquakes experienced along this major transfer zone between the mid-Atlantic ridge and the Northern Rift Zone of Iceland. Although we found no evidence for groundwater mixing at the regional scale, from the highlands towards the north, such a lateral transport seems to occur at local scale in the Aðaldalur valley, between Hafralækur and the NRZ western border. This process is probably partially controlled or enhanced by high magnitude tectonic earthquakes ($M \geq 5$), as shown by our helium isotope time series (2020 to 2022), confirming what Skelton et al. (2019, 2014) previously reported from stable isotopes shifts during the 2002, 2012, and 2012 $M > 5$ events. To confirm these observations, monitoring of borehole HA-01 should continue until capturing a major event, and associated new monitoring initiative(s) along the Dalvík Lineament should be envisaged.

References

Andrén, M., Stockmann, G., Skelton, A., Sturkell, E., Mörth, C.M., Gurúnardóttir, H.R., Keller, N.S., Odling, N., Dahrén, B., Broman, C., Balic-Zunic, T., Hjartarson, H., Siegmund, H., Freund, F., Kockum, I., 2016. Coupling between mineral reactions, chemical changes in groundwater, and earthquakes in Iceland. J Geophys Res Solid Earth 121, 2315–2337.

Árnason, B., 1976. Groundwater System in Iceland, Traced by Deuterium. Societas Scientiarum Islandica, Reykjavik 236.

Árnason, B., 1977. Hydrothermal systems in Iceland traced by deuterium. Geothermics 5, 125–151.

Arnórsson, S., 1995a. Geothermal systems in Iceland: Structure and conceptual models-II. Low-temperature areas. Geothermics 24, 603–629.

Arnórsson, S., 1995b. Geothermal systems in Iceland: Structure and conceptual models—I. High-

temperature areas. Geothermics 24, 561–602.

Ballentine, C.J., Burnard, P.G., 2002. Production, release and transport of noble gases in the continental crust. Rev Mineral Geochem 47.

Barbieri, M., Franchini, S., Barberio, M.D., Billi, A., Boschetti, T., Giansante, L., Gori, F., Jónsson, S., Petitta, M., Skelton, A., Stockmann, G., 2021. Changes in groundwater trace element concentrations before seismic and volcanic activities in Iceland during 2010–2018. Science of The Total Environment 793, 148635.

Bjarnason, I.T., Schmeling, H., 2009. The lithosphere and asthenosphere of the Iceland hotspot from surface waves. Geophys J Int 178, 394–418.

Bodvarsson, G., 1983. Temperature/flow statistics and thermomechanics of low-temperature geothermal systems in Iceland. Journal of Volcanology and Geothermal Research 19, 255–280.

Bourgeois, O., Dauteuil, O., Hallot, E., 2005. Rifting above a mantle plume: Structure and development of the Iceland Plateau. Geodinamica Acta 18, 59–80.

Brandon, A.D., Graham, D.W., Waight, T., Gautason, B., 2007. 186Os and 187Os enrichments and high-3He/4He sources in the Earth's mantle: Evidence from Icelandic picrites. Geochim Cosmochim Acta 71, 4570–4591.

Breddam, K., Kurz, M.D., Storey, M., 2000. Mapping out the conduit of the Iceland mantle plume with helium isotopes. Earth Planet Sci Lett 176, 45–55.

Bruland, K.W., 1983. CHAPTER 45 - Trace Elements in Sea-water. In: RILEY, J.P., CHESTER, R.B.T.-C.O. (Eds.), . Academic Press, pp. 157–220.

Burnard, P., Harrison, D., 2005. Argon isotope constraints on modification of oxygen isotopes in Iceland Basalts by surficial processes. Chem Geol 216, 143–156.

Burnard, P., Zimmermann, L., Sano, Y., 2013. The noble gases as geochemical tracers: History and background. Advances in Isotope Geochemistry 1–15.

Burnard, P.G., Stuart, F.M., Turner, G., Oskarsson, N., 1994. He mantle Ar isotopic composition. J Geophys Res 99, 17709–17715.

Buttitta, D., Caracausi, A., Chiaraluce, L., Favara, R., Gasparo Morticelli, M., Sulli, A., 2020. Continental degassing of helium in an active tectonic setting (northern Italy): the role of seismicity. Sci Rep 10, 1–5.

Caracausi, A., Buttitta, D., Picozzi, M., Paternoster, M., Stabile, T.A., 2022. Earthquakes control the impulsive nature of crustal helium degassing to the atmosphere. Commun Earth Environ 3, 224.

Caracausi, A., Paternoster, M., 2015. Radiogenic helium degassing and rock fracturing: A case study of the southern Apennines active tectonic region. J Geophys Res Solid Earth 120, 2200–2211.

Celli, N.L., Lebedev, S., Schaeffer, A.J., Gaina, C., 2021. The tilted Iceland Plume and its effect on the North Atlantic evolution and magmatism. Earth Planet Sci Lett 569, 117048.

Cooper, K.M., Kent, A.J.R., 2014. Rapid remobilization of magmatic crystals kept in cold storage. Nature 506, 480–483.

Craig, H., Clarke, W.B., Beg, M.A., 1975. Excess 3He in deep water on the East Pacific Rise. Earth Planet Sci Lett 26, 125–132.

da Silva Carvalho, H., Purwoko, Siswoyo, Thamrin, M., Vacquier, V., 1980. Terrestrial heat flow in the tertiary basin of central Sumatra. Tectonophysics 69, 163–188.

Darbyshire, F.A., White, R.S., Priestley, K.F., 2000. Structure of the crust and uppermost mantle of Iceland from a combined seismic and gravity study. Earth Planet Sci Lett 181, 409–428.

Debaille, V., Trønnes, R.G., Brandon, A.D., Waight, T.E., Graham, D.W. and Lee, C.T.A., 2009. Primitive off-rift basalts from Iceland and Jan Mayen: Os-isotopic evidence for a mantle source containing enriched subcontinental lithosphere. Geochimica et Cosmochimica Acta, 73(11), pp.3423-3449.

Dixon, E.T., Honda, M., McDougall, I., Campbell, I.H., Sigurdsson, I., 2000. Preservation of near-solar neon isotopic ratios in Icelandic basalts. Earth Planet Sci Lett 180, 309–324.

Eason, D.E., Sinton, J.M., Grönvold, K., Kurz, M.D., 2015. Effects of deglaciation on the petrology and eruptive history of the Western Volcanic Zone, Iceland. Bull Volcanol 77. Einarsson, P., 2008. Plate boundaries , rifts and transforms in Iceland. Jokull 58, 35–58.

Ellam, R.M., Stuart, F.M., 2004. Coherent He–Nd–Sr isotope trends in high 3He/4He basalts: implications for a common reservoir, mantle heterogeneity and convection. Earth Planet Sci Lett 228, 511–523.

Epstein, S., Mayeda, T., 1953. Variation of O18 content of waters from natural sources. Geochim Cosmochim Acta 4, 213–224.

Farnetani, C.G., Hofmann, A.W., 2010. Dynamics and internal structure of the Hawaiian plume. Earth Planet Sci Lett 295, 231–240.

Favara, R., Grassa, F., Inguaggiato, S., Pecoraino, G., Capasso, G., 2002. A simple method to determine the δ13C content of total dissolved inorganic carbon. Geofisica Internacional 41, 313–320.

Flóvenz, Ó.G., Saemundsson, K., 1993. Heat flow and geothermal processes in Iceland. Tectonophysics 225, 123–138.

Füri, E., Hilton, D.R., Halldórsson, S.A., Barry, P.H., Hahm, D., Fischer, T.P., Grönvold, K., 2010. Apparent decoupling of the He and Ne isotope systematics of the Icelandic mantle: The role of He depletion, melt mixing, degassing fractionation and air interaction. Geochim Cosmochim Acta 74, 3307–3332.

Garcia, S., Arnaud, N.O., Angelier, J., Bergerat, F., Homberg, C., 2003. Rift jump process in Northern Iceland since 10 Ma from 40Ar/ 39Ar geochronology. Earth Planet Sci Lett 214, 529–544.

Gislason, S., Eljgster, H., 1987. Meteoric water-basalt interactions. II: A field study in N.E. Iceland 212.

Graham, D.W., 2002. Noble gas isotope geochemistry of mid-ocean ridge and ocean island basalts: Characterization of mantle source reservoirs. Rev Mineral Geochem 47, 247–317.

Gunnarsson-Robin, J., Stefánsson, A., Ono, S., Torssander, P., 2017. Sulfur isotopes in Icelandic thermal fluids. Journal of Volcanology and Geothermal Research 346, 161–179.

Halldórsson, S.A., Hilton, D.R., Barry, P.H., Füri, E., Grönvold, K., 2016. Recycling of crustal material by the Iceland mantle plume: New evidence from nitrogen elemental and isotope systematics of subglacial

basalts. Geochim Cosmochim Acta 176, 206–226.

Harðardóttir, S., Halldórsson, S.A., Hilton, D.R., 2018. Spatial distribution of helium isotopes in Icelandic geothermal fluids and volcanic materials with implications for location, upwelling and evolution of the Icelandic mantle plume. Chem Geol 480, 12–27.

Hardarson, B.S., Fitton, J.G., Ellam, R.M., Pringle, M.S., 1997. Rift relocation - A geochemical and geochronological investigation of a palaeo-rift in northwest Iceland. Earth Planet Sci Lett 153, 181–196.

Hauksson, E., Goddard, J.G., 1981. Radon earthquake precursor studies in Iceland. J Geophys Res Solid Earth 86, 7037–7054.

Hilton, D.R., 1996. The helium and carbon isotope systematics of a continental geothermal system: Results from monitoring studies at Long Valley caldera (California, U.S.A.). Chem Geol 127, 269–295.

Hilton, D.R., Grönvold, K., Macpherson, C.G., Castillo, P.R., 1999. Extreme 3He/4He ratios in northwest Iceland: Constraining the common component in mantle plumes. Earth Planet Sci Lett 173, 53–60.

Hilton, D.R., Grönvold, K., O'Nions, R.K., Oxburgh, E.R., 1990. Regional distribution of 3He anomalies in the Icelandic crust. Chem Geol 88, 53–67.

Hilton, D.R., Gronvold, K., Sveinbjornsdottir, A.E., Hammerschmidt, K., 1998. Helium isotope evidence for off-axis degassing of the Icelandic hotspot. Chem Geol 149, 173–187.

Hjartarson, Á., 2003. The Skagafjörður unconformity, North Iceland, and its geological history: postglacial lava production in Iceland.

Hjartarson, Á., Kaldal, I., Sæmundsson, K., Sigurgeirsson, M.Á., Víkingsson, S., 2019. Geological Map of Central Iceland. 1:100.000.

Hofmann, A.W., Farnetani, C.G., Spiegelman, M., Class, C., 2011. Displaced helium and carbon in the Hawaiian plume. Earth Planet Sci Lett 312, 226–236.

Honda, M., Kurita, K., Hamano, Y., Ozima, M., 1982. Experimental studies of He and Ar degassing during rock fracturing. Earth Planet Sci Lett 59, 429–436.

Horita, J., 1988. Hydrogen isotope analysis of natural waters using an H2-water equilibration method: A special implication to brines. Chemical Geology: Isotope Geoscience section 72, 89–94.

Jakobsson, S.P., Jónasson, K., Sigurðsson, I. a., 2008. The three igneous rock series of Iceland. Jökull 58, 117–138.

Jancin, M., Young, K.D., Voight, B., Aronson, J.L., Saemundsson, K., 1985. Stratigraphy and K/AR ages across the west flank of the northeast Iceland Axial Rift Zone, in relation to the 7 MA volcano-tectonic reorganization of Iceland. J Geophys Res 90, 9961.

Jóhannesson, H., 1980. Jardlagaskipan of throun rekbleta a Vesturlandi.(Evolution of rift zones in western Iceland). Natturufraedingurinn Reykjavik 50, 13–31.

Kaasalainen, H., Stefánsson, A., 2012. The chemistry of trace elements in surface geothermal waters and steam, Iceland. Chem Geol 330–331, 60–85.

Kennedy, B.M., Fischer, T.P., Shuster, D.L., 2000. Heat and helium in geothermal systems. In: Twenty-

Fifth Workshop on Geothermal Reservoir Engineering Stanford University. Citeseer. Kennedy, B.M., van Soest, M.C., 2007. Flow of mantle fluids through the ductile lower crust: Helium isotope trends. Science (1979) 318, 1433–1436.

Kipfer, R., Aeschbach-Hertig, W., Peeters, F., Stute, M., 2002. Noble gases in lakes and ground waters. Rev Mineral Geochem 47.

Kononov, V.I., Polak, B.G., 1976. Indicators of abyssal heat recharge of recent hydrothermal phenomena.

Kristjánsson, L., Jónsson, G., 1998. Aeromagnetic results and the presence of an extinct rift zone in western Iceland. J Geodyn 25, 99–108.

Kulongoski, J.T., Hilton, D.R., Barry, P.H., Esser, B.K., Hillegonds, D., Belitz, K., 2013. Volatile fluxes through the Big Bend section of the San Andreas Fault, California: Helium and carbon-dioxide systematics. Chem Geol 339, 92–102.

Kulongoski, J.T., Hilton, D.R., Izbicki, J.A., 2005. Source and movement of helium in the eastern Morongo groundwater Basin: The influence of regional tectonics on crustal and mantle helium fluxes. Geochim Cosmochim Acta 69, 3857–3872.

Kurz, M.D., Meyer, P.S., Sigurdsson, H., 1985. Helium isotopic systematics within the neovolcanic zones of Iceland. Earth Planet Sci Lett 74, 291–305.

Licciardi, J.M., Kurz, M.D., Curtice, J.M., 2007. Glacial and volcanic history of Icelandic table mountains from cosmogenic 3He exposure ages. Quat Sci Rev 26, 1529–1546. Mabry, J., Lan, T., Burnard, P., Marty, B., 2013. High-precision helium isotope measurements in air. J Anal At Spectrom 28, 1903–1910.

Maclennan, J., 2019. Mafic tiers and transient mushes: Evidence from Iceland. Philosophical Transactions of the Royal Society A: Mathematical, Physical and Engineering Sciences 377. Macpherson, C.G., Hilton, D.R., Day, J.M.D., Lowry, D., Grönvold, K., 2005. High-3He/4He, depleted mantle and low-δ18O, recycled oceanic lithosphere in the source of central Iceland magmatism. Earth Planet Sci Lett 233, 411–427.

Marty, B., Gunnlaugsson, E., Jambon, A., Oskarsson, N., Ozima, M., Pineau, F., Torssander, P., 1991. Gas geochemistry of geothermal fluids, the Hengill area, southwest rift zone of Iceland. Chem Geol 91, 207–225.

Méjean, P., Pinti, D.L., Kagoshima, T., Roulleau, E., Demarets, L., Poirier, A., Takahata, N., Sano, Y., Larocque, M., 2020. Mantle helium in Southern Quebec groundwater: A possible fossil record of the New England hotspot. Earth Planet Sci Lett 545, 116352.

Mihalffy, P., Steinberger, B., Schmeling, H., 2008. The effect of the large-scale mantle flow field on the Iceland hotspot track. Tectonophysics 447, 5–18.

Moreira, M., 2013. Noble Gas Constraints on the Origin and Evolution of Earth's Volatiles. Geochem Perspect 2, 229–230.

Moreira, M., Breddam, K., Curtice, J., Kurz, M.D., 2001. Solar neon in the Icelandic mantle: New evidence for an undegassed lower mantle. Earth Planet Sci Lett 185, 15–23. Morrison, P., Pine, J., 1955. Radiogenic Origin of the Helium Isotopes in Rock. Ann N Y Acad Sci 62, 71–92.

Paris, G., Sessions, A.L., Subhas, A. V., Adkins, J.F., 2013. MC-ICP-MS measurement of δ34S and Δ33S in small amounts of dissolved sulfate. Chem Geol 345, 50–61.

Peate, D.W., Breddam, K., Baker, J.A., Kurz, M.D., Barker, A.K., Prestvik, T., Grassineau, N. and Skovgaard, A.C., 2010. Compositional characteristics and spatial distribution of enriched Icelandic mantle components. Journal of Petrology, 51(7), pp.1447-1475.

Polak, B.G., Kononov, V.I., Tolstikhin, I.N., Mamyrin, B., Khabarin, L. V, 1975. The helium isotopes in thermal fluids. In: Thermal and Chemical Problems of Thermal Waters, Proceedings of the Grenoble Symposium, August/September 1975. p 17-33

Poreda, R.J., Arnórsson, S., 1992. Helium isotopes in Icelandic geothermal systems: II. Helium-heat relationships. Geochim Cosmochim Acta 56, 4229–4235.

Poreda, R.J., Craig, H., Arnórsson, S., Welhan, J.A., 1992. Helium isotopes in Icelandic geothermal systems: I. 3He, gas chemistry, and 13C relations. Geochim Cosmochim Acta 56, 4221–4228.

Rees, C.E., Jenkins, W.J., Monster, J., 1978. The sulphur isotopic composition of ocean water sulphate. Geochim Cosmochim Acta 42, 377–381.

Saby, M., Pinti, D.L., van Hinsberg, V., Gautason, B., Sigurðardóttir, Á., Castro, C., Hall, C., Óskarsson, F., Rocher, O., Hélie, J.F., Méjean, P., 2020. Sources and transport of fluid and heat at the newly-developed Theistareykir Geothermal Field, Iceland. Journal of Volcanology and Geothermal Research 405, 107062.

Sæmundsson, K., 1974. Evolution of the axial rifting zone in northern Iceland and the Tjornes fracture zone. Geol Soc Am Bull 85, 495–504.

Sæmundsson, K., 1991. The geology of the Krafla system (Jarðfraeði Kröflukerfisins). Náttúra Mývatns. Hið íslenska náttúrufraeðifélag, Reykjavík 25–95.

Sakai, H., Gunnlaugsson, E., Tòmasson, J., Rouse, J.E., 1980. Sulfur isotope systematics in icelandic geothermal systems and influence of seawater circulation at Reykjanes. Geochim Cosmochim Acta 44, 1223–1231.

Sano, Y., Urabe, A., Wakita, H., Chiba, H., Sakai, H., 1985. Chemical and isotopic compositions of gases in geothermal fluids in Iceland. Geochem J 19, 135–148.

Shen, Y., Solomon, S.C., Bjarnason, I.T., Nolet, G., Morgan, W.J., Allen, R.M., Vogfjörd, K., Jakobsdóttir, S., Stefánsson, R., Julian, B.R., Foulger, G.R., 2002. Seismic evidence for a tilted mantle plume and north-south mantle flow beneath Iceland. Earth Planet Sci Lett 197, 261–272.

Sigmarsson, O., Condomines, M. and Fourcade, S., 1992. Mantle and crustal contribution in the genesis of recent basalts from off-rift zones in Iceland: constraints from Th, Sr and O isotopes. Earth and Planetary Science Letters, 110(1-4), pp.149-162.

Sigmundsson, F., Hooper, A., Hreinsdóttir, S., Vogfjörd, K.S., Ófeigsson, B.G., Heimisson, E.R., Dumont, S., Parks, M., Spaans, K., Gudmundsson, G.B., Drouin, V., Árnadóttir, T., Jónsdóttir, K., Gudmundsson, M.T., Högnadóttir, T., Fridriksdóttir, H.M., Hensch, M., Einarsson, P., Magnússon, E., Samsonov, S., Brandsdóttir, B., White, R.S., Ágústsdóttir, T., Greenfield, T., Green, R.G., Hjartardóttir, Á.R., Pedersen,

R., Bennett, R.A., Geirsson, H., la Femina, P.C., Björnsson, H., Pálsson, F., Sturkell, E., Bean, C.J., Möllhoff, M., Braiden, A.K., Eibl, E.P.S., 2014. Segmented lateral dyke growth in a rifting event at Bárðarbunga volcanic system, Iceland. Nature 517.

Skelton, A., Andrén, M., Kristmannsdóttir, H., Stockmann, G., Mörth, C.M., Sveinbjörnsdóttir, Á., Jónsson, S., Sturkell, E., Gudrúnardóttir, H.R., Hjartarson, H., Siegmund, H., Kockum, I., 2014. Changes in groundwater chemistry before two consecutive earthquakes in Iceland. Nat Geosci 7, 752–756.

Skelton, A., Liljedahl-Claesson, L., Wästeby, N., Andrén, M., Stockmann, G., Sturkell, E., Mörth, C.M., Stefansson, A., Tollefsen, E., Siegmund, H., Keller, N., Kjartansdóttir, R., Hjartarson, H., Kockum, I., 2019. Hydrochemical Changes Before and After Earthquakes Based on Long-Term Measurements of Multiple Parameters at Two Sites in Northern Iceland—A Review. J Geophys Res Solid Earth 124, 2702–2720.

Staples, K., White, S., Menke, W., Mcbride, H., 1997. Firoe-Iceland Ridge Experiment Other Major Seismic Profiles in Figure lb represent fissures . Bathymetry is shown offshore . (a) The NASP (North Atlantic 102, 7849–7866.

Stefánsson, A., Arnórsson, S., Sveinbjörnsdóttir, Á.E., Heinemaier, J., Kristmannsdóttir, H., 2019. Isotope (δD, δ18O, 3H, δ13C, 14C) and chemical (B, Cl) Constrains on water origin, mixing, water-rock interaction and age of low-temperature geothermal water. Applied Geochemistry 108, 104380.

Stefánsson, A., Gunnarsson, I., Giroud, N., 2007. New methods for the direct determination of dissolved inorganic, organic and total carbon in natural waters by Reagent-FreeTM Ion Chromatography and inductively coupled plasma atomic emission spectrometry. Anal Chim Acta 582, 69–74.

Stefánsson, A., Hilton, D.R., Sveinbjörnsdóttir, Á.E., Torssander, P., Heinemeier, J., Barnes, J.D., Ono, S., Halldórsson, S.A., Fiebig, J., Arnórsson, S., 2017. Isotope systematics of Icelandic thermal fluids. Journal of Volcanology and Geothermal Research 337, 146–164.

Stefánsson, A., Keller, N.S., Robin, J.G., Ono, S., 2015. Multiple sulfur isotope systematics of Icelandic geothermal fluids and the source and reactions of sulfur in volcanic geothermal systems at divergent plate boundaries. Geochim Cosmochim Acta 165, 307–323.

Stefánsson, A., Sveinbjörnsdóttir, Á.E., Heinemeier, J., Arnórsson, S., Kjartansdóttir, R., Kristmannsdóttir, H., 2016. Mantle CO2 degassing through the Icelandic crust: Evidence from carbon isotopes in groundwater. Geochim Cosmochim Acta 191, 300–319.

Stefansson, R., Gudmundsson, G.B., Halldorsson, P., 2008. Tjörnes fracture zone. New and old seismic evidences for the link between the North Iceland rift zone and the Mid-Atlantic ridge. Tectonophysics 447, 117–126.

Thordarson, T., Larsen, G., 2007. Volcanism in Iceland in historical time: Volcano types, eruption styles and eruptive history. J Geodyn 43, 118–152.

Torgersen, T., Drenkard, S., Stute, M., Schlosser, P., Shapiro, A., 1995. Mantle helium in ground waters of eastern North America: Time and space constraints on sources. Geology 23, 675–678.

Torgersen, T., Jenkins, W.J., 1982. Helium isotopes in geothermal systems: Iceland, The Geysers, Raft

River and Steamboat Springs. Geochim Cosmochim Acta 46, 739–748.

Torgersen, T., O'Donnell, J., 1991. The degassing flux from the solid earth: release by fracturing. Geophys Res Lett 18, 951–954.

Torssander, P., 1989. Sulfur isotope ratios of Icelandic rocks. Contributions to Mineralogy and Petrology 102, 18–23.

Trieloff, M., Kunz, J., Clague, D.A., Harrison, D., Allègre, C.J., 2000. The Nature of Pristine Noble Gases in Mantle Plumes. Science (1979) 288, 1036–1038.

Walters, R.L., Jones, S.M., Maclennan, J., 2013. Renewed melting at the abandoned Húnafloí Rift, northern Iceland, caused by plume pulsing. Earth Planet Sci Lett 377–378, 227–238.

Watanabe, T., Langseth, M.G., Anderson, R.N., 1977. Heat Flow in Back-Arc Basins of the Western Pacific. In: Island Arcs, Deep Sea Trenches and Back-Arc Basins, Maurice Ewing Series. pp. 137–161.

Weiss, R.F., 1971. Solubility of Helium and Neon in Water and Seawater. J Chem Eng Data 16, 235–241.

White, R.S., McKenzie, D., O'Nions, R.K., 1992. Oceanic crustal thickness from seismic measurements and rare earth element inversions. J Geophys Res Solid Earth 97, 19683–19715. Zellmer, G.F., Rubin, K.H., Grönvold, K., Jurado-Chichay, Z., 2008. On the recent bimodal magmatic processes and their rates in the Torfajökull-Veidivötn area, Iceland. Earth Planet Sci Lett 269, 388–398.

Williams, A.J., 2005. The nature of the chemically enriched components of the Iceland mantle plume (Doctoral dissertation, University of Edinburgh).

Zuber, A., Weise, S.M., Osenbriick, K., Mateńko, T., 1997. Origin and age of saline waters in Busko Spa (Southern Poland) determined by isotope, noble gas and hydrochemical methods: evidence of interglacial and pre-Quaternary warm climate recharges. Applied Geochemistry 12, 643–660.

Supplementary Material

The production rates of ^{4}He and ^{3}He are:

(Eq. S1) $P_{^4He} = 1.19 \times 10^{-13}[U] + 2.88 \times 10^{-14}[Th]$

(Eq. S2) $P_{^3He} = f(R,Na,Mg,Al,Si,Ca)F_{Li}$

Where f(...) is the neutron production rate based on the composition, F_{Li} is the fraction of neutrons that are captured by ^{6}Li in the rock matrix, and R is the Th/U ratio (Andrews, 1985). We use [U] 0.43 ppm and [Th] 1.37 ppm, which are average values based on compositions of Tertiary basalts from east of the NRZ (Kitagawa et al., 2008).

Table S1 Tritium, pH, and major and trace elements data for the survey area. *Temperature of pH measurement

Sample	20-HUS-01-01	21-HUS-01	20-HA-01-03B	20-HA-04-01B	21-HAFR-01	20-LAU-01-01B	20-HVER-01-01	21-HV-01C	20-DS-01-01
group	Aðaldalur	Aðaldalur	Aðaldalur	Aðaldalur	Aðaldalur	Aðaldalur	Aðaldalur	Aðaldalur	Eyjafjördur
LAT DD	66.0576	66.0576	65.8725	65.8722	65.8722	65.7226	65.8885	65.8872	65.8217
LONG DD	-17.3563	-17.3563	-17.4526	-17.4528	-17.4528	-17.3546	-17.3063	-17.3093	-17.9088
3H (TU)	1					<0.8	<0.8		
pH/°C*	8.97/21	9.06/21	10.22/21	10.15/21	10.18/21	10.52/21	9.42/21	9.42/21	9.99/21
SO4	87.9	76.3	23.9	23.4	23.77	13.2	29.9	31.51	15.88
H2S	0.11	0.07	<0.01	<0.01	0.11	<0.01	0.97	0.99	<0.01
SiO2	80	83.7	113.6	120	105.6	82.7	191.4	166.1	76
B	0.119	0.095	0.05	0.046	0.054	0.049	0.054	0.068	0.062
Na	730.64	724.93	57.75	57.89	55.79	49.62	60.13	54.28	37.77
K	25.84	28.24	0.77	0.79	0.61	0.5	3	2.38	0.45
Ca	205.49	210.12	2.05	1.59	1.98	2.13	1.92	1.79	2.73
Mg	0.04	0.014	0.016	0.011	0.007	0.005	0.006	0.007	0.01
Fe(tot)	0.007	0.017	0.013	0.007	0.018	0.004	0.035	0.016	0.028
Al	0.1	0.047	0.137	0.125	0.136	0.378	0.285	0.234	0.033
F	0.16	0.85	1.04	1.01	1.01	0.72	1.04	0.93	0.39
Cl	1710	1494.11	9.96	9.87	9.86	4.9	12.11	12.02	7.56
As	8.049	na	1.067	1.125	na	1.183	1.003	na	6.058
Ba	7.697	1.421	4.391	3.668	0.156	2.001	4.86	4.994	1.999
Be	-0.001	0.000	0.001	0.000	0.001	-0.001	0.010	0.019	0.000
Bi	0.001	0.001	0.001	0.001	0.001	0.001	0.001	0.004	0.000
Ce	0.006	0.000	0.003	0.008	0.000	0.002	0.004	0.000	0.002

Co	0.047	0.017	0.009	0.011	0.002	0.009	0.005	0.002	0.005
Cr	0.060	0.035	1.356	0.051	0.027	0.032	0.031	0.066	0.124
Cs	4.033	4.64	0.019	0.026	0.016	0.005	0.718	0.681	0.014
Cu	0.664	0.029	1.331	0.562	0.069	0.421	1.074	0.051	0.41
Dy	0.001	0.000	0.001	0.001	0.000	0.000	0.001	0.000	0.000
Er	0.001	0.000	0.000	0.001	0.000	0.000	0.000	0.000	0.000
Eu	0.001	0.000	0.000	0.001	0.000	0.000	0.000	0.000	0.000
Ga	1.347	1.393	7.078	6.122	8.695	10.885	5.765	7.221	2.539
Gd	0.001	0.000	0.001	0.001	0.000	0.000	0.001	0.000	0.000
Ge	2.045	2.204	2.065	2.101	2.008	1.274	4.586	4.560	0.829
Ho	0.000	0.000	0.000	0.000	0.000	0.000	0.000	0.000	0.000
La	0.003	0.000	0.005	0.004	0.000	0.001	0.002	0.000	0.002
Li	190.112	168.754	2.146	2.149	2.152	0.662	15.588	17.973	1.513
Lu	0.000	0.000	0.000	0.000	0.000	0.000	0.000	0.000	0.000
Mn	1.812	1.464	0.465	0.423	0.105	0.117	0.283	0.220	0.128
Mo	12.787	15.017	18.723	18.781	19.794	6.517	11.498	12.499	4.95
Nd	0.005	0.000	0.002	0.004	0.000	0.001	0.003	0.000	0.001
Ni	2.136	1.013	0.569	0.086	0.06	0.105	0.272	0.296	0.092
Pb	0.132	0.022	0.102	0.337	0.012	0.085	0.540	0.037	0.056
Pr	0.001	0.000	0.000	0.001	0.000	0.000	0.001	0.000	0.000
Rb	109.965	134.048	1.009	0.994	1.1	0.597	10.324	11.377	0.596
Sb	0.097	na	0.023	0.020	na	0.011	0.093	na	0.050
Sc	0.283	0.188	0.183	0.204	0.157	0.125	0.281	0.250	0.125
Se	0.039	na	0.005	0.005	na	0.000	0.001	na	0.016

Sm	0.002	0.000	0.001	0.001	0.000	0.001	0.001	0.000	0.000
Sr	634.363	774.007	1.953	1.745	1.770	1.176	6.818	7.725	1.443
Tb	0.000	0.000	0.000	0.000	0.000	0.000	0.000	0.000	0.000
Ti	170.873	0.480	2.050	3.058	0.311	1.713	1.459	0.301	2.164
Tm	0.000	0.000	0.000	0.000	0.000	0.000	0.000	0.000	0.000
V	0.429	0.613	5.361	4.934	5.724	21.805	1.737	2.034	5.112
W	0.464	na	2.218	2.244	na	0.978	2.064	na	1.221
Yb	0.000	0.000	0.000	0.001	0.000	0.000	0.000	0.000	0.000
Zn	5.802	6.398	1.926	3.193	3.142	1.095	3.422	7.404	1.053

Cont. Table S1

Sample	21-DS-01B	20-ST-01-01	20-RF-09-01	21-OL-4	21-HJ-21C	21-SK11-01	21-YV-20C	21-LN-12	21-BN-1
group	Eyjafjördur	Eyjafjördur	Eyjafjördur	Eyjafjördur	Eyjafjördur	Eyjafjördur	Eyjafjördur	Eyjafjördur	Eyjafjördur
LAT DD	65.8203	65.7077	65.5763	66.0693	65.8548	66.11715	65.9078	65.5727	65.5622
LONG DD	-17.9108	-17.7392	-17.7637	-18.6817	-18.2134	-18.8775	-18.287	-18.0639	-18.1071
3H (TU)		<0.8				1			
pH/°C*	10.14/21	9.78/21	9.89/21	10.23/21	10.05/21	9.98/21	10.04/21	9.63/21	9.77/21
SO4	15.63	32.5	17.2	6.54	18.15	10.44	17.48	39.23	49.94
H2S	na	<0.01	0.11	na	na	na	na	na	na
SiO2	71	111.1	118.7	77.6	117.6	97.7	115.8	101.5	92.2
B	0.071	0.11	0.064	0.039	0.214	0.032	0.189	0.166	0.179
Na	37.88	53.35	47.95	37.11	56.49	45	55.07	51.69	50.69
K	0.38	1.11	1.03	0.42	1.04	0.75	1.01	1.09	1.02
Ca	2.63	2.64	1.78	2.65	1.96	1.89	1.79	2.94	4.14

Mg	0.010	0.009	0.007	0.002	0.002	0.000	0.002	0.005	0.004
Fe(tot)	0.007	0.027	0.023	0.005	0.002	0.001	0.004	0.012	0.002
Al	0.032	0.042	0.262	0.11	0.138	0.075	0.113	0.184	0.222
F	0.35	0.67	0.41	0.16	1.74	0.38	1.23	0.48	0.58
Cl	8.36	19.9	7.1	8.93	10.87	8.61	13.94	12.86	10.97
As	na	6.711	3.682	na	na	na	na	na	na
Ba	0.317	2.179	4.307	0.082	0.113	0.285	0.083	0.258	0.234
Be	0.000	0.001	0.001	0.000	0.003	0.002	0.002	0.002	0.002
Bi	0.003	0.001	0.001	0.001	0.009	0.012	0.000	0.000	0.002
Ce	0.000	0.007	0.004	0.000	0.000	<0.001	0.000	0.000	0.000
Co	0.005	0.008	0.007	0.001	0.003	0.003	0.003	0.002	0.003
Cr	0.122	0.062	0.055	0.029	0.037	0.031	0.026	0.018	0.052
Cs	0.011	0.084	0.109	0.019	0.18	0.007	0.114	0.19	0.227
Cu	0.092	0.991	1.453	0.265	0.028	0.116	0.028	0.032	0.026
Dy	0.000	0.001	0.000	0.000	0.001	<0.001	0.000	0.000	0.000
Er	0.000	0.000	0.000	0.000	0.001	<0.001	0.000	00.000	0.000
Eu	0.000	0.001	0.000	0.000	0.000	<0.001	0.000	0.000	0.000
Ga	2.974	5.663	5.937	7.03	7.799	6.707	7.958	6.526	6.582
Gd	0.000	0.002	0.001	0.000	0.001	<0.001	0.000	0.000	0.001
Ge	0.951	2.700	1.250	0.709	2.358	1.232	1.68	0.843	0.854
Ho	0.000	0.000	0.000	0.000	0.000	<0.001	0.000	0.000	0.000
La	0.000	0.004	0.002	0.000	0.001	<0.001	0.002	0.000	0.000
Li	1.603	6.371	4.246	1.348	6.15	1.597	5.13	6.464	6.204
Lu	0.000	0.000	0.000	0.000	0.000	<0.001	0.000	0.000	0.000

Mn	0.163	0.352	0.194	0.067	0.061	0.181	0.104	0.132	0.112
Mo	5.448	14.564	8.974	2.681	7.766	4.791	10.305	11.989	13.562
Nd	0.000	0.005	0.002	0.000	0.001	<0.001	0.000	0.000	0.000
Ni	0.449	0.156	0.400	0.021	0.026	0.042	0.031	0.039	0.048
Pb	0.13	0.136	0.249	0.178	0.026	0.19	0.064	0.176	0.031
Pr	0.000	0.001	0.000	0.000	0.001	<0.001	0.000	0.000	0.000
Rb	0.679	3.16	2.581	1.514	3.893	1.324	3.095	3.773	3.928
Sb	na	0.289	0.04	na	na	na	na	na	na
Sc	0.106	0.177	0.178	0.112	0.192	0.146	0.151	0.152	0.133
Se	na	0.000	0.006	na	na	na	na	na	na
Sm	0.000	0.001	0.001	0.000	0.001	<0.001	0.000	0.000	0.000
Sr	1.519	4.509	6.929	9.909	15.065	2.53	10.914	25.11	33.069
Tb	0.000	0.000	0.000	0.000	0.000	<0.001	0.000	0.000	0.000
Ti	0.143	3.047	1.798	0.135	0.145	0.198	0.221	0.295	0.235
Tm	0.000	0.000	0.000	0.000	0.000	<0.001	0.000	0.000	0.000
V	5.51	2.692	1.353	2.278	0.653	5.369	1.725	1.238	0.573
W	na	2.55	1.754	na	na	na	na	na	na
Yb	0.000	0.001	0.000	0.000	0.001	<0.001	0.000	0.000	0.000
Zn	22.993	3.188	2.041	5.788	3.117	4.498	4.028	3.749	2.949

Cont. Table S1

Sample	21-SDO1	21-LH04-01	21-BM13-01	21-HOFS-1	21-VH12-01	21-VARM-1	21-SK32-01	21-STE1-01B	21-RR22-01
group	Skagafjördur	Skagafjördur	Skagafjördur	Skagafjördur	Skagafjördur	Skagafjördur	Skagafjördur	Skagafjördur	Húnaflói
LAT DD	66.12755	66.05778	65.73313	65.28506	65.55608	65.4744	65.99812	65.46786	65.53928

LONG DD	-18.9625	-19.1248	-19.6166	-19.0396	-19.4578	-19.376	-19.3363	-19.3522	-20.2144
3H (TU)	<0.8	<0.8	<0.8		<0.8	0.8352832	<0.8	<0.8	<0.8
pH/°C*	9.87/21	9.71/21	9.95/21	9.30/21	9.55/21	10.20/21	9.38/21	10.13/21	9.64/21
SO4	23.96	56.09	39.02	89.8	48.84	21.94	131.15	18.4	57.57
H2S	na	na	na	na	na	na	na	na	na
SiO2	122.2	153.9	69.5	112.1	123.3	90.4	104.6	86.3	105.5
B	0.038	0.075	0.149	1.554	0.467	0.317	0.202	0.277	0.024
Na	54.6	80.18	55.01	114.28	78.27	59.47	162.11	56.78	65.14
K	1.27	2.93	0.78	2.44	2.11	0.63	4.07	0.54	1.9
Ca	2.4	2.12	3.25	4.83	1.69	1.66	14.82	1.6	2.73
Mg	0.001	0.001	0.001	0.004	0.001	0.004	0.003	0.034	0.002
Fe(tot)	0.002	0.016	0.02	0.001	0.001	0.001	0.004	0.006	0.001
Al	0.034	0.131	0.074	0.037	0.104	0.132	0.053	0.131	0.025
F	0.52	0.59	1.55	1.29	2.19	1.38	0.56	1.04	5.32
Cl	15.44	31.57	18.32	86.81	28	18.41	164.13	13.48	7.91
As	na	na	na	na	na	na	na	na	na
Ba	0.124	1.874	0.134	1.13	0.129	0.13	0.47	0.158	0.216
Be	0.001	<0.001	0.001	0.005	0.008	0.002	0.003	0.002	0.011
Bi	<0.001	<0.001	0.004	<0.001	<0.001	<0.001	0.017	0.002	<0.001
Ce	<0.001	<0.001	<0.001	<0.001	<0.001	<0.001	0.001	0.004	<0.001
Co	0.004	0.012	0.005	0.003	0.003	0.005	0.009	0.01	0.003
Cr	0.043	0.035	0.048	0.037	0.04	0.02	0.049	0.062	0.028
Cs	0.187	0.715	0.087	0.217	0.785	0.007	0.543	0.008	0.777
Cu	0.229	3.113	0.148	0.08	0.089	0.159	0.042	0.178	1.306

Dy	<0.001	<0.001	<0.001	<0.001	<0.001	<0.001	0.001	<0.001	<0.001
Er	<0.001	<0.001	<0.001	<0.001	<0.001	<0.001	0.001	<0.001	<0.001
Eu	<0.001	<0.001	<0.001	<0.001	<0.001	<0.001	<0.001	<0.001	<0.001
Ga	4.701	6.991	3.923	2.997	3.945	8.071	2.692	7.992	3.57
Gd	<0.001	<0.001	<0.001	<0.001	<0.001	<0.001	0.004	0.002	<0.001
Ge	1.52	1.858	1.941	8.272	6.254	1.526	1.465	1.359	3.022
Ho	<0.001	<0.001	<0.001	<0.001	<0.001	<0.001	<0.001	<0.001	<0.001
La	<0.001	<0.001	<0.001	<0.001	<0.001	<0.001	0.002	0.002	<0.001
Li	10.589	18.381	6.102	23.21	20.735	3.973	24.032	2.854	20.987
Lu	<0.001	<0.001	<0.001	<0.001	<0.001	<0.001	<0.001	<0.001	<0.001
Mn	0.204	0.523	0.39	0.274	0.202	0.166	0.449	0.255	0.26
Mo	8.733	16.268	16.361	138.623	39.64	16.964	44.939	12.228	14.092
Nd	<0.001	<0.001	<0.001	<0.001	<0.001	<0.001	0.001	0.002	<0.001
Ni	0.114	0.628	0.124	0.074	0.07	0.048	0.112	0.074	0.234
Pb	0.029	0.652	0.896	0.018	0.043	0.902	0.11	0.239	0.348
Pr	<0.001	<0.001	<0.001	<0.001	<0.001	<0.001	0.001	<0.001	<0.001
Rb	4.588	11.171	2.563	7.777	9.424	1.429	11.2	0.986	9.268
Sb	na	na	na	na	na	na	na	na	na
Sc	0.171	0.212	0.108	0.191	0.184	0.128	0.2	0.156	0.142
Se	na	na	na	na	na	na	na	na	na
Sm	<0.001	<0.001	<0.001	<0.001	<0.001	<0.001	0.001	<0.001	<0.001
Sr	8.067	15.836	18.137	11.81	12.296	1.384	48.759	1.342	40.981
Tb	<0.001	<0.001	<0.001	<0.001	<0.001	<0.001	<0.001	<0.001	<0.001
Ti	0.221	0.306	0.382	0.538	0.394	0.26	0.676	0.778	0.552

Tm	<0.001	<0.001	<0.001	<0.001	<0.001	<0.001	0.001	<0.001	<0.001
V	1.109	0.537	0.201	1.507	0.573	2.296	2.985	2.25	0.084
W	na	na	na	na	na	na	na	na	na
Yb	<0.001	<0.001	<0.001	<0.001	<0.001	<0.001	<0.001	<0.001	<0.001
Zn	4.354	5.12	11.083	21.351	2.884	5.438	5.68	2.805	8.214

Table S2 List of samples of the HA-01 time series with $^{3}He/^{4}He$ and $^{4}He/^{20}Ne$ results. Baseline period is also included.

Sample	Date (dd/mm/yyyy)	$^{4}He/^{20}Ne$	error	$^{3}He/^{4}He$	error	^{4}He (mol/g.H_2O)
ICE 4-7-15	04/07/2015	1.79	0.07	11.33	0.12	4.88E-11
ICE 12-7-15	12/07/2015	1.66	0.06	11.15	0.15	3.07E-11
ICE 18-7-15	18/07/2015	1.49	0.07	10.78	0.15	5.37E-11
ICE 26-7-15	26/07/2015	1.40	0.02	11.56	0.12	1.9E-07
ICE 9-8-15	09/08/2015	1.47	0.06	11.17	0.33	1.19E-10
ICE 29-8-15	29/08/2015	1.53	0.04	11.23	0.12	6.76E-11
ICE 12-9-15	12/09/2015	1.55	0.04	11.13	0.15	3.22E-11
ICE 20-9-15	20/09/2015	1.53	0.06	11.22	0.15	4.14E-11
ICE 27-9-15	27/09/2015	1.37	0.01	11.68	0.12	3.6E-06
ICE 4-10-15	04/10/2015	1.53	0.06	11.22	0.15	9.06E-11
ICE 11-10-15	11/10/2015	1.95	0.08	11.23	0.12	2.95E-11
ICE 25-10-15	25/10/2015	1.62	0.07	11.28	0.15	5.78E-11
ICE 11-11-15	11/11/2015	1.53	0.07	11.22	0.15	3.22E-11
ICE 16-11-15	16/11/2015	1.34	0.01	11.79	0.35	3.78E-07
ICE 22-11-15	22/11/2015	1.57	0.08	10.97	0.15	3.78E-11
ICE 28-11-15	28/11/2015	1.38	0.06	11.41	0.34	3.34E-11
ICE 4-12-15	04/12/2015	1.47	0.06	11.11	0.15	3.88E-11
ICE 20-12-15	20/12/2015	1.22	0.00	11.78	0.35	3.41E-07
ICE 3-1-16	03/01/2016	1.30	0.04	11.23	0.34	1.6E-11
ICE 10-1-16	10/01/2016	1.20	0.05	10.08	0.10	4.86E-11
ICE 17-1-16	17/01/2016	1.24	0.05	11.44	0.34	3.41E-11
ICE 7-2-16	07/02/2016	1.63	0.07	11.23	0.15	3.19E-11
ICE 14-2-16	14/02/2016	1.30	0.05	11.47	0.34	2.75E-11
ICE 23-2-16	23/02/2016	1.58	0.06	11.16	0.15	3.23E-11
ICE 28-6-20	28/06/2020	1.53	0.05	11.51	0.12	6.83E-12
ICE 5-7-20	05/07/2020	1.56	0.06	11.51	0.12	1.23E-11
ICE 8-7-20B2	08/07/2020	1.58	0.05	11.59	0.13	3.49E-11
ICE 18-7-20	18/07/2020	1.45	0.03	11.97	0.13	2.74E-09
ICE 18-7-20B	18/07/2020	1.50	0.05	10.92	0.12	3.41E-11
ICE 31-7-20B	31/07/2020	1.63	0.06	11.09	0.12	3.39E-11
ICE 9-8-20	09/08/2020	1.49	0.05	11.41	0.12	1.26E-11
ICE 9-8-20B	09/08/2020	1.62	0.07	11.55	0.12	2.04E-11
ICE 14-8-20	14/08/2020	1.63	0.06	11.14	0.12	1.73E-11

ICE 14-8-20B	14/08/2020	1.66	0.05	11.74	0.18	2.19E-11
ICE 29-8-20B	29/08/2020	1.63	0.04	11.72	0.13	1.26E-09
ICE 5-9-20	05/09/2020	1.63	0.06	11.29	0.12	1.69E-11
ICE 5-9-20B	05/09/2020	1.55	0.05	11.36	0.15	2.71E-11
ICE 12-9-20	12/09/2020	1.80	0.05	11.59	0.13	6.84E-11
ICE 20-09-20	20/09/2020	1.84	0.05	11.33	0.15	8.87E-10
ICE 27-09-20B	27/09/2020	1.44	0.07	11.11	0.15	2.57E-11
ICE 17-10-20	17/10/2020	1.56	0.04	11.76	0.18	8.87E-10
ICE 31-10-20	31/10/2020	1.71	0.09	11.32	0.15	2.45E-11
ICE 31-10-20B	31/10/2020	1.68	0.04	11.97	0.18	8.41E-11
ICE 6-11-20	06/11/2020	1.49	0.07	11.36	0.15	1.84E-11
ICE 21-11-20	21/11/2020	1.66	0.04	11.30	0.17	2.53E-11
ICE 05-12-20	05/12/2020	1.59	0.03	11.67	0.16	5.75E-09
ICE 26-12-20	26/12/2020	1.52	0.04	11.19	0.17	2.37E-11
ICE 16-01-21	16/01/2021	1.54	0.08	11.38	0.15	1.61E-11
ICE 16-01-21B	16/01/2021	1.54	0.04	10.81	0.16	4.78E-11
ICE 24-01-21	24/01/2021	1.41	0.03	12.43	0.19	1.08E-07
ICE 24-01-21C	24/01/2021	1.47	0.05	11.13	0.17	4.84E-09
ICE 5-02-21	05/02/2021	1.73	0.05	11.80	0.16	1.98E-09
ICE 11-02-21	11/02/2021	1.77	0.05	11.80	0.18	4.87E-11
ICE 20-02-21	20/02/2021	1.75	0.06	11.06	0.17	2.8E-10
ICE 27-02-21B	27/02/2021	1.54	0.08	11.25	0.15	2.9E-11
ICE 07-03-21	07/03/2021	1.62	0.07	10.90	0.15	4.02E-11
ICE 13-03-21	13/03/2021	1.55	0.06	11.37	0.15	3.53E-11
ICE 20-03-21	20/03/2021	1.61	0.04	11.41	0.17	2.93E-11
ICE 27-03-21	27/03/2021	1.58	0.04	10.47	0.16	4.53E-11
ICE 03-04-21	03/04/2021	1.50	0.05	10.67	0.16	
ICE 03-04-21B	03/04/2021	1.48	0.03	10.66	0.16	4.22E-11
ICE 23-04-21	23/04/2021	1.41	0.03	10.92	0.16	
ICE 01-05-21	01/05/2021	1.56	0.03	11.59	0.17	5.27E-11
ICE 29-05-21	29/05/2021	1.59	0.05	11.39	0.17	
ICE 04-06-21	04/06/2021	1.56	0.04	11.25	0.17	2.88E-11
ICE 24-06-21	24/06/2021	1.50	0.04	10.51	0.16	2.91E-11
ICE 09-07-21	09/07/2021	1.65	0.04	10.66	0.16	1.9E-11
ICE 29-07-21	29/07/2021	1.37	0.03	11.58	0.22	2.35E-11
ICE 04-08-21B	04/08/2021	1.61	0.07	11.21	0.17	5.51E-11

ICE 03-09-21B	03/09/2021	1.71	0.05	11.35	0.24	1.73E-11
ICE 17-09-21	17/09/2021	1.44	0.04	10.69	0.16	4.89E-11
ICE 24-09-21	24/09/2021	1.69	0.04	11.48	0.24	2.06E-11
ICE 02-10-21	02/10/2021	1.56	0.05	11.41	0.17	3.93E-11
ICE 15-10-21	15/10/2021	1.71	0.05	11.39	0.24	3.41E-11
ICE 06-11-21	06/11/2021	1.49	0.04	10.77	0.16	1.73E-11
ICE 06-11-21B	06/11/2021	1.53	0.06	11.14	0.17	4.19E-11
ICE 26-11-21	26/11/2021	1.64	0.03	11.41	0.24	3.44E-11
ICE 03-12-21	03/12/2021	1.65	0.04	10.30	0.15	4.97E-11
ICE 10-12-21	10/12/2021	1.61	0.04	11.42	0.24	4.46E-11
ICE 17-12-21	17/12/2021	1.66	0.04	11.34	0.23	1.11E-10
ICE 08-01-22	08/01/2022	1.60	0.06	10.67	0.16	1.03E-10
ICE 26-02-22	26/02/2022	1.55	0.05	10.51	0.16	3.92E-11
ICE 26-02-22B	26/02/2022	1.38	0.04	10.86	0.16	1.2E-11
ICE 14-03-22	14/03/2022	1.45	0.05	11.13	0.17	3.45E-11
ICE 01-04-22	01/04/2022	1.41	0.03	11.17	0.17	4.86E-11
ICE 22-04-22	22/04/2022	1.62	0.06	11.30	0.17	1.13E-11
ICE 27-05-22	27/05/2022	1.55	0.04	11.10	0.17	1.86E-11
ICE 24-06-22	24/06/2022	1.65	0.06	11.15	0.17	3.2E-11
ICE 24-06-22B	24/06/2022	1.42	0.03	10.80	0.16	4.17E-11
ICE 09-07-22	09/07/2022	1.73	0.04	11.73	0.24	5.11E-11
ICE 06-08-22	06/08/2022	1.78	0.05	11.42	0.24	5.55E-11
ICE 26-08-22	26/08/2022	1.83	0.06	11.70	0.24	5.4E-11
ICE 16-09-22	16/09/2022	1.63	0.04	11.32	0.23	4.69E-11
ICE 30-09-22	30/09/2022	1.66	0.05	11.12	0.23	2.97E-11
ICE 14-10-22	14/10/2022	1.93	0.04	11.60	0.24	4.67E-11

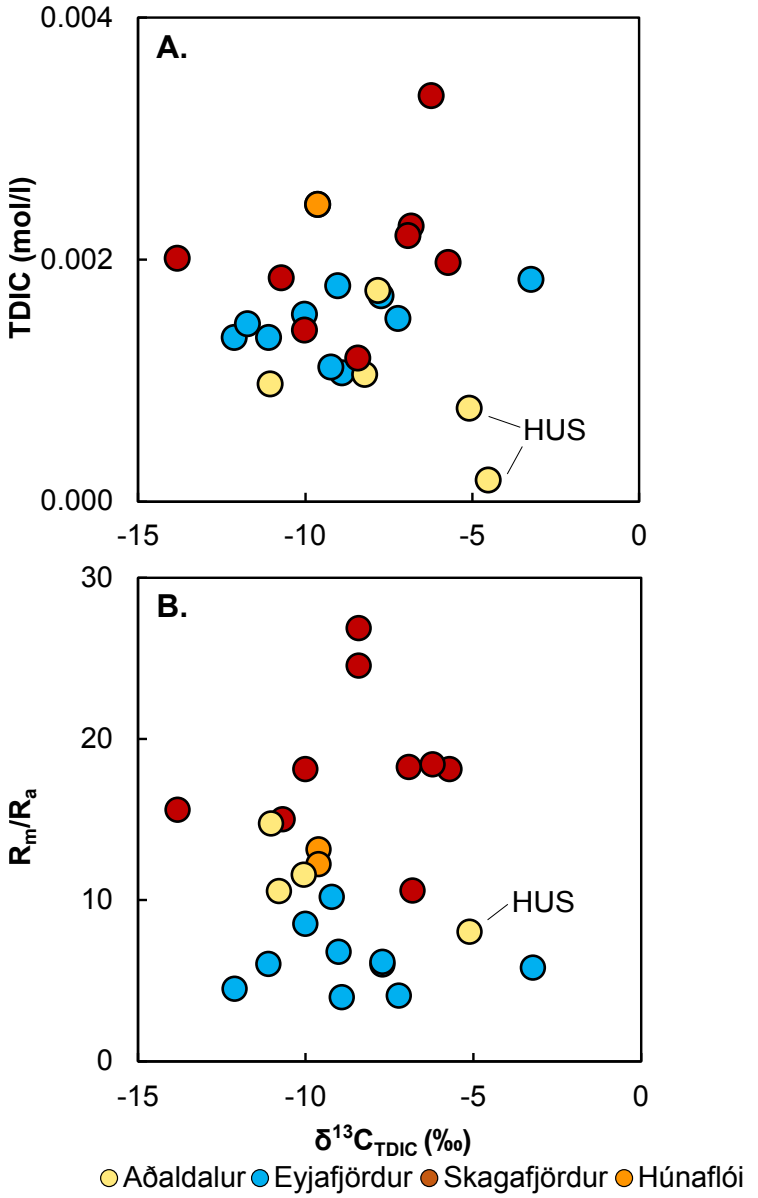

Figure S1 Relationships between $\delta^{13}C_{TDIC}$ and (a) TDIC and (b) Rm/Ra. There are no clear links between helium and carbon isotopes.

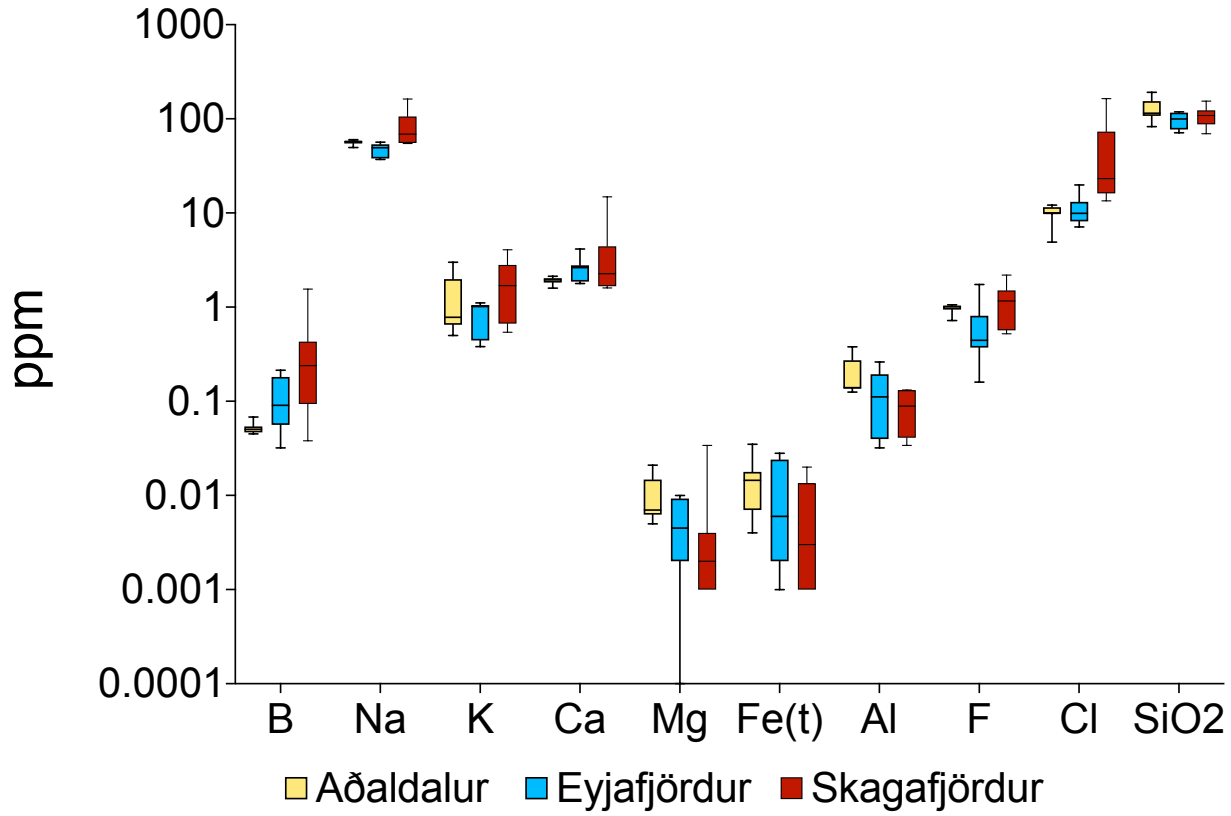

Figure S2 Box-and-whiskers diagram showing the concentration ranges (in ppm) of major elements in groundwater from the study area. Small regional trends are observed in B, Ca, Mg, Fe(t), Al, and Cl. The sample from Húsavík is not included in this plot due to its seawater signature.

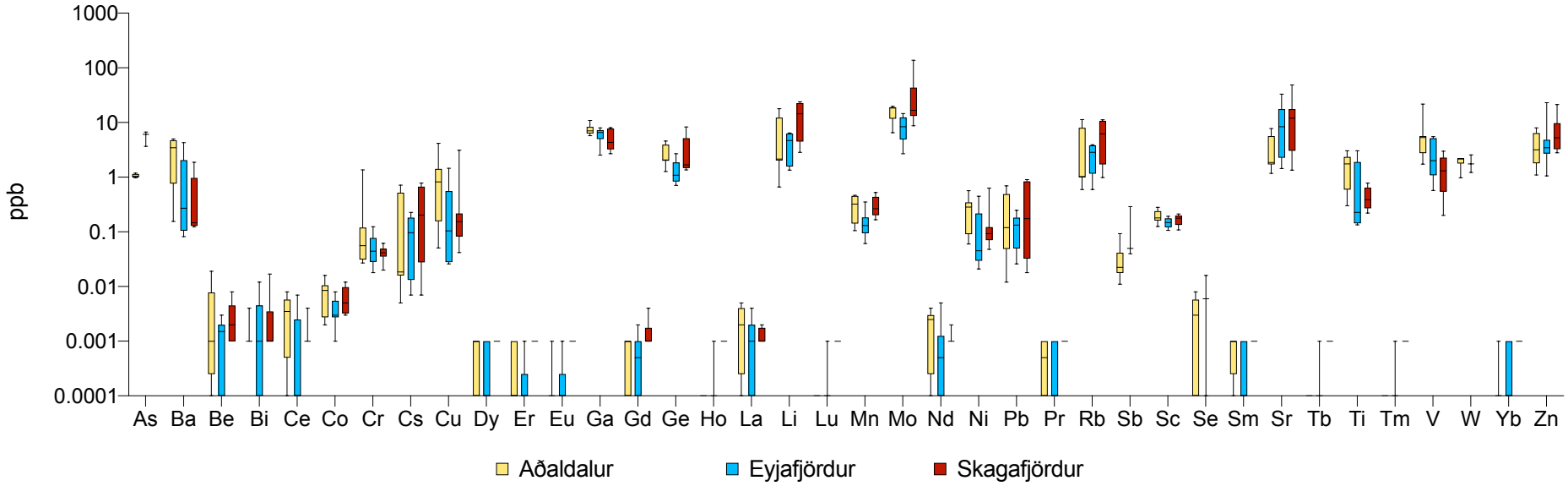

Figure S3 Box-and-whiskers diagram showing the concentration ranges (in ppb) of trace elements in groundwater from the study area. Small regional trends are observed in Ba and V. The sample from Húsavík is not included in this plot due to its seawater signature.

Chapter 5

Helium isotope evidence for cryptic magmatism along Central France

This study was performed in the farmework of a collaboration with GeoRessources (Université de Lorraine) and 45-8 Energy, in parallel with the PhD thesis of Emma Russier (*"Caractérisation des systèmes géologiques de l'Hélium en Europe Continentale – Evaluation du potentiel exploratoire de la ressource"*).

Published at Chemical Geology

Authors

Carolina Dantas Cardoso[a,*], Emma Russier[b,c], Bernard Marty[a], Raphaël Pik[a], David V. Bekaert[a,d], Alan Seltzer[d], Michael W. Broadley[a], David Byrne[a], Thomas Rigaudier[a], Yves Géraud[b], Alexandre Tarantola[b], Benoît Hauville[c]

Affiliations

[a]Université de Lorraine, CNRS, CRPG, F-54000 Nancy, France

[b]Université de Lorraine, CNRS, GeoRessources, F-54000 Nancy, France

[c]45-8 Energy, Metz 57000, France

[d]Marine Chemistry and Geochemistry Department,Woods Hole Oceanographic Institu-

tion, Woods Hole, Massachusetts 02543, USA.

Abstract

Determining the source(s) of helium in regions of the crust where ^{3}He anomalies occur can be challenging when no surface manifestations of magmatic activity or a clear active extension regime are present. This is the case of the Paris basin (France), where geothermal fluids and oils ^{3}He/^{4}He have been previously shown to range from 0.02 Ra up to 0.14 Ra (Marty et al., 1993; Pinti and Marty, 1995, 1998), whereas natural gases to the south of the Paris Basin (near the Massif central) show unambiguous evidence for mantle helium contribution, with ^{3}He/^{4}He up to 6.4 Ra (Bräuer et al., 2017). However, higher ^{3}He/^{4}He than the crustal endmember ($\sim$ 0.01 Ra), as observed in the Paris Basin, could be a sign of either (i) a weak contribution of mantle He (enriched in primordial ^{3}He) or (ii) the contribution of ^{3}He naturally produced by nuclear reactions of lithium, for which commercially exploitable concentrations have been reported in rare-metal-rich granites. One way to distinguish between these two possibilities is to combine He isotope systematics with other noble gas tracers of mantle inputs, such as xenon isotopes. Here, we report the isotope compositions of helium and xenon, measured by static and dynamic mass spectrometry, respectively, in gas samples collected in the Nièvre County, between the Massif Central and the Paris Basin. ^{3}He/^{4}He ratios range between 0.16 and 0.22 Ra. Combined with previous studies, our data are consistent with a southward increase of He isotope ratios along major fault systems from the Paris Basin ($\sim$ 0.02 Ra) towards the Massif Central (6.4 Ra). This geographical trend, paired with high precision Xe isotopes exhibiting an excess of mantle ^{129}Xe, shows a clear mantle input that is most likely restricted to the major fault systems in Central France. The occurrence of mantle-derived helium and xenon in Central France highlights the presence of cryptic magmatism in areas with no apparent volcanic manifestations.

Keywords: noble gases; helium isotopes; xenon isotopes; mantle input; CO_2 reservoir

Contents

5.1 Introduction

On Earth, the two helium isotopes, ^{3}He and ^{4}He, are found in the atmosphere, crust, and mantle in different proportions. ^{3}He is mainly of primordial origin, occurring in higher proportions in the mantle, where it has been able to be preserved since Earth's accretion (Craig and Lupton, 1976). ^{4}He on the other hand is primarily of radiogenic origin and is concentrated in the continental crust (Ballentine and Burnard, 2002). The production of ^{4}He primarily occurs by α-decay of ^{235,238}U and ^{232}Th, and is thus dependent on the concentration of these two parent elements (Ballentine and Burnard, 2002). However, production of ^{3}He can also occur in the crust produced through the thermal neutron capture on ^{6}Li by the reaction ^{6}Li (n,α) ^{3}H (β-) $\rightarrow$ ^{3}He (Morrison and Pine, 1955).

The ^{3}He/^{4}He ratio is thus an essential tool for determining the origin of different gas reservoirs. In some regions of the crust, the interpretation of ^{3}He/^{4}He can be ambiguous, such as in the Paris Basin (France), where no magmatic manifestations at the surface, or evidence for modern tectonic extension are present, yet helium isotope ratios show higher

$^{3}He/^{4}He$ than expected for the continental crust (up to 0.14 Ra; Marty et al., 1993; Pinti and Marty, 1995, 1998). Helium isotopes have been investigated in groundwater and crude oil from the Paris Basin and in gas manifestations in the Massif Central, respectively (Bräuer et al., 2017; Marty et al., 1993; Pinti and Marty, 1995, 1998). While there is unequivocal evidence for a mantle contribution in the Massif Central, with $^{3}He/^{4}He$ ratios up to 6.4 Ra (where Ra is the atmospheric $^{3}He/^{4}He$ – 1.39 x 10^{-6}; Graham, 2002), a mantle contribution in the Paris Basin is less evident. Helium isotope ratios (0.02 – 0.11 Ra, reaching 0.14 Ra for basement-hosted groundwater) are close to the crustal end-member (0.001 – 0.02 Ra) as computed from average U+Th/Li abundances in related lithologies of the Paris Basin (Pinti and Marty, 1998). Because $^{3}He/^{4}He$ ratios of geothermal fluids and oils are higher than values predicted for a purely crustal origin, Pinti and Marty (1998) proposed a mantle contribution to gases hosted by basinal fluids. In agreement with this possibility, it was observed that the $^{3}He/^{4}He$ ratios increase with depth in the basin, suggesting injection of mantle-derived helium from the basement underlying the sedimentary units, and progressive dilution of this signal by radiogenic, ^{4}He-rich helium produced in the sedimentary pile (Marty et al., 1993). Helium isotope ratios also tend to be higher towards the southern margin of the basin (0.09 Ra in groundwater and 0.14 Ra at the basement; Pinti and Marty, 1998). This trend is possibly related to the North-South major fault system ("Sillon Houiller") in Central France, and to the addition of mantle-derived ^{3}He from the nearby Rhine rift magmatism at the eastern border of the Paris Basin in Lorraine (Marty et al., 2003). Alternatively, $^{3}He/^{4}He$ ratios higher than expected for the purely crustal end-member could reflect local enrichments of lithium-derived ^{3}He, with He isotope variations potentially tracking the occurrence of Li-rich lithologies of economical relevance.

Recently, a CO_2-rich gas reservoir with He concentration reaching 0.04% has been discovered while conducting helium exploration in the Nièvre County, between the Massif Central to the south and the southern border of the Paris Basin to the north (Figure 5.1). Although not reaching commercial concentrations for helium ($> 0.3\%$), its helium content is about 100 times higher than the atmosphere ($\sim 0.0005\%$; Glueckauf, 1946). This gas accumulation has the potential to shed light into the nature of the intermediate $^{3}He/^{4}He$ ratios, between typical mantle values and the crustal range, observed in the Paris Basin (e.g., Pinti and

Marty, 1998). The geochemical description of this reservoir is still at an early stage, and so our paper focuses on the use of isotope geochemistry to identify the source(s) of the Nièvre gas. In the present study, we sampled bulk gas samples using two distinct approaches: copper tubes (dedicated to He isotope measurements) and Giggenbach bottles (dedicated to Ar-Ne-Xe isotope measurements). The samples consist in free gases from two CO_2-rich wells (SP4 and SP7) and bubbling springs from the surrounding areas – Gelin, Fonts-Bouillants, Fontaine des Vertus, Pougues-les-Eaux, Fontaines Salées, and Bourbon-Lancy (Figure 5.1). Most springs were cold (12-14°C; Boineau and Maisonneuve, 1972; Risler, 1974), apart from Bourbon-Lancy, which has a temperature of 52°C (Batard et al., 1982). To identify the different sources of helium, we analysed $^3He/^4He$ and $^4He/^{20}Ne$ on gas collected from all sites. We also analysed the major gas composition, stable isotopes of CO_2 ($\delta^{13}C$) and N_2 ($\delta^{15}N$), and Ar, Ne, and Xe isotopes for the SP4 and SP7 well gas samples.

5.2 Geological setting

The study area is located between the southern border of Paris Basin and the north of the Massif Central and Limagne basin, west of the Morvan massif (Figure 5.1). The Massif Central and Morvan belong to the Hercynian belt. The basement of the basin is made up of Hercynian granites, migmatites, gneisses and mica schists that outcrop in the Decize horst (Clozier and Turland, 1982; Roger et al., 2010). The study zone is also likely to contain uranium-rich carboniferous and permian deposits, mostly alternating clay and sandstone, that formed during the dismantling of the Variscan belt under the Mesozoic and Cenozoic cover (Beccaletto et al., 2015; Farjanel, 1989; Mercuzot et al., 2021).

The area underwent magmatic and volcanic activity during the Hercynian period and Paleogene (Baptiste, 2016; Farjanel, 1989). The emplacement of the Decize and Montmarault granitic intrusion (321 ± 2 Ma U-Th-Pb dating on monazite; Joly, 2007) and rare metal-enriched granites in the Morvan and Massif Central took place as the belt began dismantling (Gloaguen et al., 2018; Roger et al., 2010). The most recent volcanic activity occurred during the Paleogene, at ∼90 km to the South of the Paris Basin, in "Chaîne des Puys" related to the Alpine orogeny and the Cenozoic extension regime (Barruol and Granet, 2002). The origin

of volcanism in the area is still debated (Nehlig et al., 2003). On the one hand, it could reflect the surface expression of a mantle plume (Coisy and Nicolas, 1978; Froidevaux et al., 1974), as potentially suggested by seismic tomography (Mazabraud et al., 2005), originating from the asthenosphere related to the activity of a hot spot (Froidevaux et al., 1974) or to a passive rift (Merle and Michon, 2001). On the other hand, volcanism may result from crustal extension and melting of the lithospheric material (Gautheron et al., 2005). One last possibility is that a deep plume led to the formation of shallower plumes in the Sub Continental Lithospheric Mantle (SCLM) and/or in the old oceanic lithosphere crust ($\sim$ 400 Ma subduction during the Hercynian orogeny) (Buikin et al., 2005; Gautheron et al., 2005). Noble gas data from the Massif Central, namely Xe and Ne isotopes, indicate a MORB-like source, discarding the influence of a mantle plume (Moreira et al., 2018).

Seismicity is not restricted to the Massif Central and seismic events have been recorded along the major structures of the area (Marche and Sillon Houiller faults). Most faults appear to be related to the complex geodynamic history of the area (Variscan subduction, collision, and exhumation) and are deeply embedded in the basement, such as the Sillon Houiller and Loire faults (Baptiste, 2016; Regorda et al., 2020; Roger et al., 2010; Vanderhaeghe et al., 2020). The Magnetic Paris Anomaly follows the same N-S orientation as the Loire fault in the North of Massif Central. Even if its origin is debated, this anomaly could be linked to a deep major structure, such as a main strike-slip fault or an oceanic suture covered by the Paris Basin sediments (Baptiste, 2016). Variscan faults oriented N20-30 have been reactivated into shear and then normal faults during the formation of the Carbonifereous pull-out and Permian hemi-graben (Beccaletto et al., 2015; Farjanel, 1989). They were also reactivated by extension and compression at the end of the Jurassic (E-W) during the opening of the Tethys, amid the Cretaceous (SW-NE extension and N-S compression) and the W-E extension in the Tertiary (Guillocheau et al., 2000; Jolivet et al., 2021; Manatschal et al., 2021; Roger et al., 2010). Gas-rich springs and drillings are located along faulted areas with mainly N-S directions. SP4, SP7, Gelin, Fonts-Bouillants, and Fontaine des Vertus follow a single fault, the Saint-Parize-le-Châtel fault while Pougues-les-Eaux is located in an area affected by multiple normal faults. Bourbon-Lancy and Fontaines Salées are situated along Morvan bounding fault.

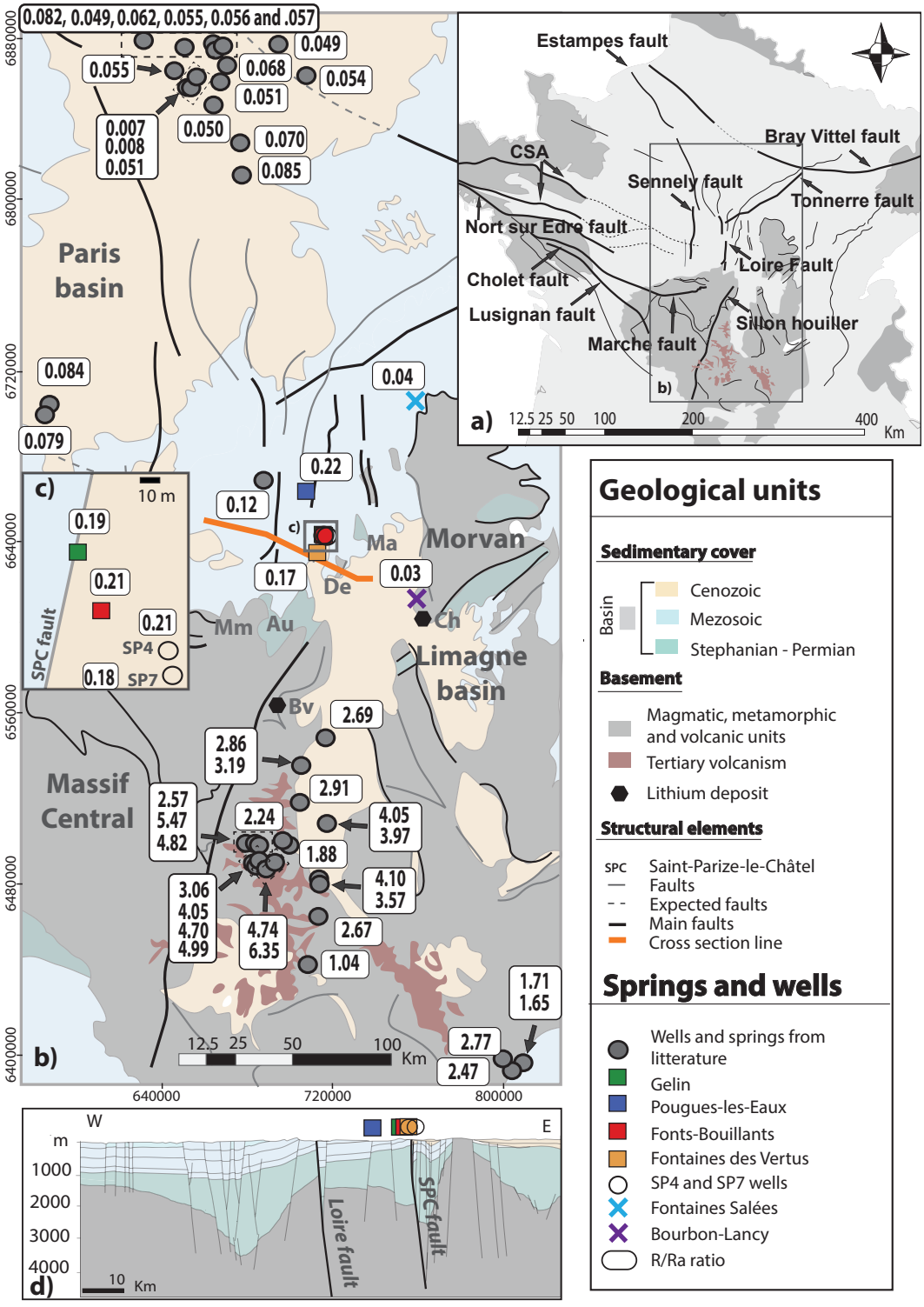

Figure 5.1: Geological map of the study area with helium isotope results (in Ra) and literature data. a) Structural map with major structures inherited from the Variscan orogeny (Baptiste, 2016). b) Simplified geological map (1/1,000,000 BRGM French geological map) with main geological structures of the area (Au: Aumance basin, De: Decize horst and Ma: Machine graben), location of the well SP4, SP7, springs and the lithium deposits of the area (Ch: Chanvence and Bv: Beauvoir; Gloaguen et al., 2018), and distribution of literature helium isotope data (Bräuer et al., 2017; Marty et al., 1993; Pinti and Marty, 1998). c) Focus on the Saint-Parize-le-Châtel area with location of the springs and wells. d) Simplified cross section line of the study area, with location on the map "b)" marked by the orange line.

5.3 Methods

5.3.1 Bulk gas compositions

Gases occur either as bubbles in springs (Gelin, Fonts-Bouillants, Fontaine des Vertus, Pougues-les-Eaux, Bourbon-Lancy and Fontaines Salées) or as free CO_2-rich gas in two drill holes (SP4 and SP7). Samples were collected during three field campaigns and/or well testing operations, in August-September, 2021, February and May-June, 2022 (Table 1). SP4 and SP7 drill holes are rooted in the Triassic sediments and cross the Saint-Parize-le-Châtel fault. Gases were sampled in evacuated vials or Tedlar Bags after purging the tubes connecting them to the wellheads. The springs near SP4 (Gelin, Fonts-Bouillants, Pougues-les-Eaux, and Fontaine des Vertus) were sampled before and after the well test to detect potential variations in helium isotopes. Bubbling gases from springs were collected through funnel and Teflon tubing in previously evacuated vials (Pasquet et al., 2021) or Tedlar bags (Battani et al., 2010). Finally, the gas composition was measured by gas chromatography (GC) (Supplementary material; Pasquet et al., 2021).

5.3.2 Noble gases

5.3.2.1 $^{3}He/^{4}He$ and $^{4}He/^{20}Ne$

The analyses of $^{4}He/^{20}Ne$ and $^{3}He/^{4}He$ ratios of gases sampled in copper tubes were performed, respectively, on a MKS Microvision 2 quadrupole mass spectrometer (QMS) and a split flight tube noble gas mass spectrometer (Helix SFT - Thermo Fisher Scientific) at the Centre de Recherches Pétrographiques et Géochimiques (CRPG) noble gas analytical facility (Mabry et al., 2013). The standard deviation of the $^{3}He/^{4}He$ ratios ranged from 1.4 to 3.7% based on the replicate analysis of standard He (atmospheric). Results are corrected for blanks, which contributed $< 0.1\%$ of the total He abundances (Table 2).

5.3.2.2 Ar, Ne, and Xe isotopes

Gases were collected in 1.5 L Giggenbach bottles (Giggenbach and Goguel, 1988; Bekaert et al. 2019) containing 4N NaOH solution in which CO_2 and other reactive species (e.g., S

compounds) can be trapped. This method permits the concentration of inert gases (mainly N2 and noble gases and possible traces of CH_4, CO, H_2, etc) in the vacuum headspace above the solution. In the laboratory, the gaseous fraction was equilibrated under vacuum with an evacuated metal bottle fitted with two metal valves (Nupro SS4H@), where the gas could be stored for long periods of time without diffusive leakage or exchange with atmospheric gases. Aliquots of gas were expanded in a vacuum line and the abundances of He and Ar as well as Ar isotopic ratios were measured after purification via static mass spectrometry on a GV Helix MC mass spectrometer. Two aliquots of the SP4 well gas were also sampled from the metal bottles and analysed for all noble gases (Table 3). Gases were purified using hot (600°C) and cold (25°) Ti-getters and, after cryogenic separation (Broadley et al., 2022), noble gas abundances and isotopic ratios were analysed with a Helix MC+ mass spectrometer at the Centre de Recherches Pétrographiques et Géochimiques (CRPG) noble gas analytical facility (Bekaert et al., 2019; Broadley et al., 2020).

At last, argon and xenon isotope ratios were measured in the Seltzer Lab at Woods Hole Oceanographic Institution via dynamic isotope-ratio mass spectrometry (Bekaert et al., 2023; Seltzer and Bekaert, 2022) for one sample of the SP7 well gas collected in a large Giggenbach bottle (1.5 L) following the sampling procedure detailed by Bekaert et al. (2019). With a dynamic mass spectrometer, often called an "isotope ratio mass spectrometer," the rapid switching between analysis of sample and reference gas streams reduces the effect of instrumental drift (McKinney et al., 1950) and allows for many comparable measurements of purified sample gas and standard gas of known isotopic composition over the course of an analysis, hence ensuring accurate and unbiased isotopic ratio determination at the sub-per mil level. Results are in permil (‰) and notated as δ following $\delta R=[(R_{sample}/R_{atmosphere})-1]\times 1000$; where R is a Xe isotope ratio. Raw measurements were corrected for diffusive transport fractionation (DTF; light isotope enrichment due to physical subsurface fractionation; Bekaert et al., 2023) using $\delta^{128}Xe/^{130}Xe$, yielding a mass-dependent correction of 0.504 ± 0.157 ‰ u-1. Our reported uncertainties on Xe isotope data reflect both analytical and DTF-correction sources of uncertainty (Table 3)

5.3.3 Stable isotopes

The carbon and nitrogen isotopic compositions of CO_2 and N_2, respectively, were measured with a Thermo Scientific MAT 253 Mass Spectrometer at the Centre de Recherches Pétrographiques et Géochimiques (CRPG) stable isotopes analytical facility. Sampling was performed using Giggenbach bottles and evacuated glass bottles.

5.3.3.1 δ^{13}C

For the δ^{13}C measurements of the CO_2, CO_2 and H_2O were trapped into liquid nitrogen and then cryogenically separated. All values are reported in the delta notation in permil (‰) relative to PDB, with error below 0.2‰ (Table 2).

5.3.3.2 δ^{15}N

Nitrogen isotope measurements were done using the non-condensable fraction of the Giggenbach bottles, which consists mainly of N_2, CO, and noble gases since CO_2 has been removed. Both CO and N_2 gases were transferred in a sealed pyrex tube containing CuO and Cu_2O grains to be oxidized into N_2 and CO_2 at 450°C for 1 hour. Prior to being used, the CuO and Cu_2O grains have been heated few minutes under vacuum at 350°C and pumped overnight at room temperature to remove adsorbed gases. The produced CO_2 was then cryogenically trapped and N_2 was collecting using a Toepler pump. All values are reported using the delta notation, in permil (‰) relative to air, with error ∼0.5 ‰ calculated from the reproducibility of duplicates (Table 2).

5.4 Results

5.4.1 Wells

During the main flow of the SP4 well test, which lasted approximately 10h, samples were collected for $^3He/^4He$ and $^4He/^{20}Ne$ measurements every hour. Sample names follow the format “site name-sampling order + copper tube number” and duplicate samples have an “M1” at the end; sampling order is “100” when before well test, “200” during, and “300” if

sampled after the well test (Table 5.1). For the SP7 well, only one sample was collected for noble gas measurements. SP4 and SP7 are CO_2-dominated, consisting of $\sim$ 94% CO_2 and 6% N_2 and only traces of CH_4 ($< 0.6\%$); helium contents range from 394 to 426 ppm vol. The δ13C value of the SP4 sample is -10.1 ‰, which is compatible with a primarily organic source of CO_2 or non-marine carbonates (Table 5.2).

Throughout the SP4 well test, no significant change on helium abundance or isotopic ratios was detected. $^3He/^4He$ ratios range from 0.17 to 0.21 ($\pm$ 0.01) Ra, with no temporal variation (Table 5.2). $^4He/^{20}Ne$ ratios are consistently > 2000, however, measurements are not precise due to the low content of ^{20}N relative to ^4He, with the former showing values very close to the baseline. During the SP7 well test, we only collected one sample, which shows similar results with a $^3He/^4He$ ratio of 0.18 ($\pm$ 0.01) Ra and $^4He/^{20}Ne > 2000$. The $^{40}Ar/^{36}Ar$ ratios, measured for two aliquots of the SP4 well gas, are 2866 $\pm$ 5 and 2574 $\pm$ 11, respectively, with the $^{38}Ar/^{36}Ar$ ratios being indistinguishable from atmosphere (Table 3). The $^{20}Ne/^{22}Ne$ (9.40 $\pm$ 0.05) and the $^{21}Ne/^{22}Ne$ ratios (0.0621 $\pm$ 0.0011) deviate slightly from the atmospheric Ne value, indicating contribution of crustal (and possibly mantle) neon (see section 5.5.2). Analyses of SP7 show $^{40}Ar/^{36}Ar$ (696.6 $\pm$ 0.2) above the air value, but still lower than the SP4 well, indicating possible atmospheric contamination during drilling operations. Xenon isotopic ratios of SP7 by dynamic mass spectrometry (Table 5.3) indicate contribution of fissiogenic and mantle Xe (see section 5.5.2).

5.4.2 Springs

Fontaines Salées and Bourbon-Lancy are N_2-dominated (93% and 97%, respectively) while Fontaine des Vertus is comprised of 63% CO_2 and 39% N_2 (Table 5.1). The remaining springs are CO_2-dominated ranging from 95 to 97%. For all springs, only traces of CH_4 are identified ($< 0.6\%$). Helium contents range from 245 to 426 ppm vol for the CO_2-dominated sites, and from 2874 to 45794 ppm vol for Fontaine des Vertus, Fontaines Salées, and Bourbon-Lancy.

The springs near SP4 (Gelin, Fonts-Bouillants, and Fontaine des Vertus) present $^3He/^4He$ ratios similar to those of SP4, ranging from 0.16 to 0.21 ($\pm$ 0.01) Ra, as well as the Pougues-les-Eaux spring which is 25 km north from SP4 (0.22 $\pm$ 0.01 Ra) (Table 5.2). Fontaines Salées and Bourbon-Lancy which are located 80 km NE and 50 km SE of SP4, have distinct

$^3He/^4He$ signatures (0.04 ± 0.00 and 0.03 ± 0.00 Ra, respectively) that are close to the purely radiogenic end-member. $^3He/^4He$ variations do not correlate with gas compositions, with similar $^3He/^4He$ for springs near SP4 (including Fontaine des Vertus) despite much higher helium and N_2 contents.

$\delta^{13}C$ of CO_2 values show little variation among the springs, ranging from -11.8 to -10 ‰ (vs. PDB), except for Fontaines Salées (-20 ‰), which suggests either different sources of CO_2 or different processing in the crust. Weinlich (2005) reported comparable values of -13.9 ‰ for a N_2-dominated spring at Pougues-les-Eaux (74% N_2) and of -20.4 ‰ at Saint Père (94% N_2), near Fontaines Salées. The Pougues-les-Eaux spring in the present study is dominated by CO_2 (95 vol.%) and has a very similar $\delta^{13}C$ (-10.3 ‰) to the one described in Weinlich (2005). Moreover, the springs with lower CO_2 contents tend to present lighter $\delta^{13}C$ values (Figure S1) that could indicate chemical processes during transport in the crust due to solution of CO_2 in the water phase and/or carbonate precipitation, concentrating helium and N_2 in the gas phase. $\delta^{15}N$ results for the springs from both groups display similar values (+6.1 to +8.4 ‰) compatible with a primarily crustal source.

Table 5.1: List of samples with coordinates, sampling dates, and average of main gas phase results from GC measurements. *A second sampling campaign occurred in May-June/2022 for δ^{15}N analyses.

Site	type	Date	Sample	map ref	LAT (°N)	LONG (°E)	CO_2(vol.%)	N_2(vol.%)	He (ppmV)
SP4	well	Aug-Sept/2022	SP4-200 CTN3 SP4-200 CTN3 M1 SP4-200 CTN4 SP4-200 CTN9 SP4-200 CTN11 M1	1	46.85979	3.19336	93	5.6	394
SP7	well	Feb/2022	SP7	2	47.82861	4.18083	94	5.6	426
Gelin	spring	Aug-Sept/2022	GEL-100 CTN1 GEL-300 CTN1 M1	3	46.86035	3.19268	91	6.1	416
Fonts-Bouillants	spring	Aug-Sept/2022	FBO-100 CTN1 M1 FBO-300 CTN1 M1	4	46.86008	3.19284	92	5.7	393
Fontaine des Vertus	spring	Aug-Sept/2022*	VER-100 CTN1 VER-200 CTN1 M1	5	46.82025	3.17123	60	36.3	2874
Pougues-les-Eaux	spring	Aug-Sept/2022*	POU-100 CTN1 M1	6	47.07635	3.09240	94	4	245
Fontaines Salées	spring	Aug-Sept/2022	FON-100 CTN1 M1	7	47.44900	3.77680	0.9	92.5	45794
Bourbon-Lancy	spring	May-June/2022	B-LANCY A	8	46.61786	3.76974	2.6	91.3	20644

Table 5.2: $^{3}He/^{4}He$, $^{4}He/^{20}Ne$, $CO_2/^{3}He$, and stable isotopes results. $^{3}He/^{4}He$ are normalized by the atmospheric $^{3}He/^{4}He$ ratio (Ra – 1.39 x 10-6; Graham, 2002). *Average $\delta^{15}N$ values from multiple measurements; SP4 value from two measurements performed on the same day (6.3 and 8.3 ‰) and Gelin from three measurements on different days (7.9, 8.5, and 8.9 ‰).

Site	Sample	$^{4}He/^{20}Ne$	$^{3}He/^{4}H$ (Ra)	$CO_2/^{3}He$	$\delta^{13}C$ (‰ vs PDB)	$\delta^{15}N$ (‰ vs Air)
SP4	SP4-200 CTN3	62080 ± 4724	0.21 ± 0.01	8.16E+09	-10.1	7.3*
	SP4-200 CTN3 M1	≤ 1656612	0.19 ± 0.01	8.96E+09		
	SP4-200 CTN4	35291 ± 3003	0.21 ± 0.00	7.99E+09		
	SP4-200 CTN9	66651 ± 5465	0.17 ± 0.01	1.00E+10		
	SP4-200 CTN11 M1	1975 ± 55	0.20 ± 0.01	8.71E+09		
SP7	SP7	180114 ± 34276	0.18 ± 0.01	8.66E+09	-	-
Gelin	GEL-100 CTN1	9509 ± 354	0.19 ± 0.00	8.37E+09	-10.0	8.4*
	GEL-300 CTN1 M1	2222 ± 72	0.17 ± 0.01	9.09E+09		
Fonts-Bouillants	FBO-100 CTN1 M1	776 ± 22	0.21 ± 0.00	8.00E+09	-10.0	-
	FBO-300 CTN1 M1	7525 ± 281	0.21 ± 0.01	8.18E+09		
Fontaine des Vertus	VER-100 CTN1	10240 ± 336	0.16 ± 0.01	9.26E+08	-11.8	7.5
	VER-200 CTN1 M1	9042 ± 476	0.17 ± 0.00	9.06E+08		
Pougues-les-Eaux	POU-100 CTN1 M1	1170 ± 35	0.22 ± 0.01	1.22E+10	-10.3	6.1
Fontaines Salées	FON-100 CTN1 M1	2587 ± 66	0.04 ± 0.00	-	-20.0	7.1
Bourbon-Lancy	B-LANCY A	960 ± 20	0.03 ± 0.01	-	-	-

Table 5.3: Ne, Ar, and Xe isotope results. Xe ratios are reported in the delta notation relative to the atmospheric isotope composition. "corr" refers to data corrected for physical fractionation. Errors shown at 1 sigma.

Sample	$^{20}Ne/^{22}Ne$	$^{21}Ne/^{22}Ne$	$^{40}Ar/^{36}Ar$	$^{38}Ar/^{36}Ar$	δ vs Air, ‰					
					$^{128}Xe/^{130}Xe$	$^{129}Xe/^{130}Xe$	$^{131}Xe/^{130}Xe$	$^{132}Xe/^{130}Xe$	$^{134}Xe/^{130}Xe$	$^{136}Xe/^{130}Xe$
SP4-200-GB1	9.40 ± 0.05	0.0621 ± 0.0011	2866 ± 5	0.189 ± 0.001	-	-	-	-	-	-
SP4-100-GB1	-	-	2574 ± 11	0.179 ± 0.001	-	-	-	-	-	-
SP7 (raw)	-	-	696.6 ± 0.2	0.18840 ± 0.00002	0.996 ± 0.311	1.865 ± 0.145	-0.042 ± 0.179	1.463 ± 0.145	6.554 ± 0.167	9.464 ± 0.195
SP7 (corr)	-	-	-	-	0 ± 0.311	1.371 ± 0.212	0.445 ±0.235	2.430 ± 0.335	8.462 ± 0.619	12.286 ± 0.902

5.5 Discussion

5.5.1 Source of helium

In European basins of various ages, $^3He/^4He$ values range between 0.01 and 3.9 Ra, reaching ∼0.1 Ra in the western Alps (Marty et al., 1992; Oxburgh et al., 1986). Oxburgh et al. (1986) suggested that this wide range in Neogene basins was related to their tectonic setting. Helium isotope compositions in the Pannonian basin reach values up to 3.9 Ra consistent with an extension regimen and clear mantle input while the Molasse and Po basins show a range of $^3He/^4He$ between 0.02 and 0.09 Ra (Marty et al., 1992; Oxburgh et al., 1986), which, for the Molasse basin, Oxburgh et al. (1986) interpret as being of crustal origin despite the apparent small mantle contribution (up to 0.9%). In the Paris Basin, $^3He/^4He$ ratios are close to the range of values for the Molasse and Po basins (0.02 to 0.11 Ra), reaching 0.14 Ra at the basement in Couy (Pinti and Marty, 1998). These values are higher than the theoretical crustal $^3He/^4He$ ratio (0.001-0.02 Ra), based on the U-Th and Li values of the underlying sedimentary rocks. These elevated $^3He/^4He$ values were therefore considered to be evidence for the input of mantle material with a higher than crustal $^3He/^4He$ (Pinti and Marty, 1998). However, with only small $^3He/^4He$ variations, up to 0.1 Ra, it is difficult to fully discriminate this component from variation in the crustal $^3He/^4He$ ratio. In addition, these areas show no evidence of igneous manifestations, and there is the possibility that ^3He could be produced in the crust without mantle input (see section 5.5.1.1).

In the $^3He/^4He$ versus $^4He/^{20}Ne$ plot (Figure 5.2), we identify two groups of samples: one of them contains Fontaines Salées and Bourbon-Lancy, and the other one contains SP4, SP7, surrounding springs, and Pougues-les-Eaux. Considering the typical values found in the various basins in Europe, the $^3He/^4He$ signature found at Fontaines Salées and Bourbon-Lancy is within the European crustal range (0.02 – 0.1 Ra). The remaining samples show significantly higher $^3He/^4He$ (0.16 – 0.22 Ra). However, in any case, the main source of helium in the basin is from the continental crust.

Using U, Th, and Li contents of lithologies from the Paris Basin (Pinti and Marty, 1998) (since rock chemistry data is not available for our target area), we calculated the theoretical $^3He/^4He$ signature to be between 0.001 and 0.016 Ra, based on radiogenic (^4He)

and nucleogenic (^{3}He) production equations (Equation 5.1; Andrews, 1985). For the SP4 sample group that includes SP4, SP7, nearby springs, and Pougues-les-Eaux, we compute that the higher ^{3}He/^{4}He ratios can either be accounted for by, (i) either nucleogenic ^{3}He production from the presence of high amounts of lithium in the host rocks, (ii) or by a 2.5% mantle input to the original crustal signature. In the next sections, we discuss both possibilities for the ^{3}He/^{4}He signature we find for the SP4 group.

$$P_3/P_4 = (f(R, Na, Mg, Al, Si, Ca)F_{\mathrm{Li}})/((3.2108x10^6 + 7.7633x10^5 R)) \quad (5.1)$$

Where P_3/P_4 is the theoretical ^{3}He/^{4}He based on the ^{3}He and ^{4}He production rates, f(...) is the neutron production rate based on the composition, FLi is the fraction of neutrons that are captured by 6Li in the rock matrix, and R is the Th/U ratio.

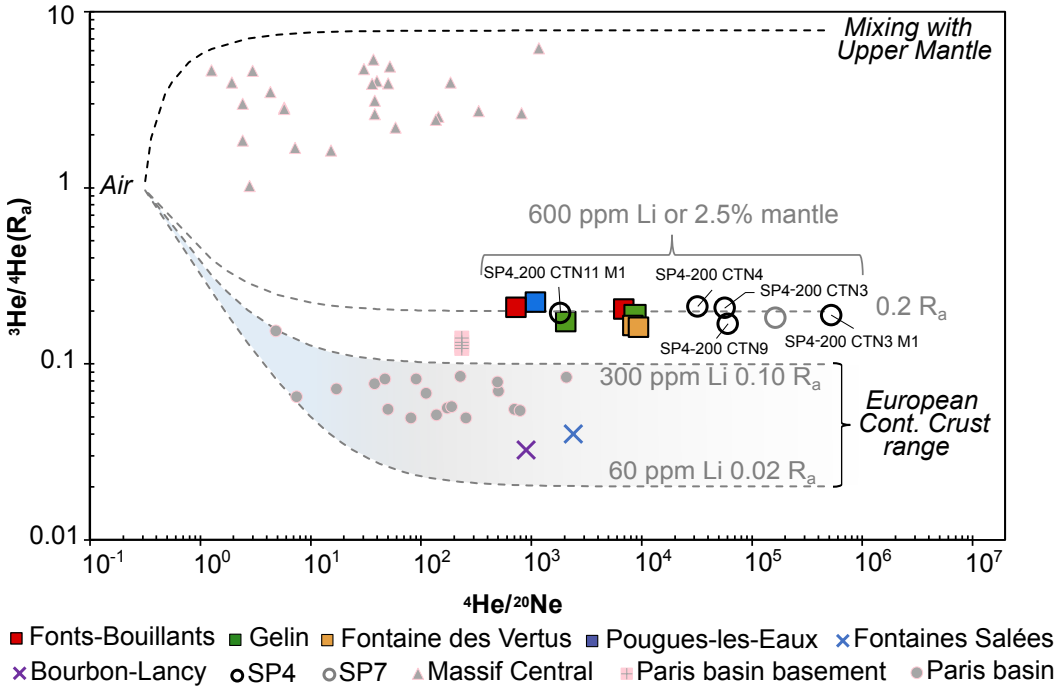

Figure 5.2: ^{4}He/^{20}Ne versus ^{3}He/^{4}He plot. Samples plot in two groups, one with signatures close to a crustal source and the other with either a 2.5% input of mantle or with nucleogenic ^{3}He production consistent with the presence of 600 ppm Li. Lithium contents for the lower and upper limits of the European continental crust range are based on average values of U-Th for the continental crust (1.8 and 7.2 ppm, respectively; Krauskopf and Bird, 1967). ^{4}He/^{20}Ne values for SP4 are not precise due to ^{20}Ne abundances indistinguishable from baseline measurement. Massif Central and Paris Basin data are from the literature (Bräuer et al., 2017; Marty et al., 1993; Pinti and Marty, 1998).

5.5.1.1 Nucleogenic ^{3}He production

As previously stated, one potential production pathway to increase the ^{3}He/^{4}He from crustal values to that measured in the SP4, SP7, surrounding springs, and Pougues-les-Eaux samples is through the localised production of nucleogenic helium (^{3}He) via thermal neutron capture on 6Li via the reaction ^{6}Li (n,α) ^{3}H (β-) $\rightarrow$ ^{3}He (Morrison and Pine, 1955). To raise the ^{3}He/^{4}He signatures of the SP4 sample group (Figure 5.2, Table 5.2) from an assumed original crustal signature (0.001 – 0.016 Ra) we calculate that it would require Li concentrations in the basement and/or host rocks to be on the order of 600 ppm (Andrews, 1985; Equation 5.1). This calculation assumes that all the excess ^{3}He within the samples is produced from the thermal neutron capture by 6Li and that the basement / host rock contains typical crustal U-Th concentrations (1.8 and 7.2 ppm, respectively; Krauskopf and Bird, 1967). Although this amount of Li is atypical in view of the average continental crust value (30 ppm Li), small proximal basins such as the ones in the Massif Central have the potential to accumulate lithium (Sun et al., 2022).

One of the major concentrated sources of lithium in the crust is surface and subsurface brines. Near the study region ($\sim$ 100 km), in the Massif Central, a geothermal brine with 81 ppm Li has been identified in the Limagne basin (Fonroche geothermie, 2019) but values higher than that have not yet been reported. Brines from the area were previously described with much lower lithium contents (e.g., Millot et al., 2007; 7 ppm). In the Paris Basin, lithium concentration is low, in brines associated with Triassic salt deposits (up to 60 ppm; Fontes and Matray, 1993a; Millot et al., 2011) and oil fields (4.8 ppm; Fontes and Matray, 1993b b).

Apart from brines and geothermal water, the main hard-rocks that are sources of lithium are rare-metal-rich granites such as the Beauvoir, Montebras, and Chavence granites, near our study area, LCT pegmatites, and greisen deposits produced by high-temperature hydrothermal alteration of the aforementioned types (Gourcerol et al., 2019). The lithium mineralizations in the Massif Central are usually located near important ductile faults (Gloaguen et al., 2018).

Considering the various sources of lithium with production potential (Gloaguen et al.,

2018) in the Massif Central, near the study area, it is possible to consider that a Li-rich granitic basement produces significant quantities of helium. The closest lithium sources are the Chavence (56 km SE) and Beauvoir granites (72 km SW), the latter containing lithium concentrations between 367 and 5,220 ppm in its upper units (Raimbault et al., 1995). Taking the U, Th, and Li contents from the Beauvoir granite (16.2 - 52.4, 1.15 - 5.63, and 367 - 5,220 ppm, respectively; Raimbault et al., 1995), the theoretical $^{3}He/^{4}He$ ratios would range between 0.12 and 1.66 Ra. In that case, helium could be produced in the basement, before migrating upwards to the basin and being stored in the sedimentary layers, acting as a reservoir. Another possibility is that, as a proximal basin, detrital material from the Li-rich rocks accumulates in the basin and ^{3}He is produced in the sedimentary layers. The Chavence granite is located near Bourbon-Lancy ($\sim$ 9 km) where we find a crustal signature for helium isotopes; however, at Bourbon-Lancy, the spring is directly on top of the basement and not in a sedimentary basin. To observe the same signatures as for the SP4 sample group at Bourbon-Lancy, a sedimentary basin that accumulates and traps the produced gas is required, as otherwise degassing from a Li-rich source would only occur locally and relatively far from the spring. There are also non-conventional sources of lithium that have recently been brought to light and that cannot be discarded, such as coal (e.g., Qin et al., 2015). Considering the regional geology, Stephanian-Permian basins in the Massif Central region have coal levels (Mercuzot et al., 2021) that could potentially provide the required amounts of lithium.

In the context of local production, Martel et al. (1990) found $^{3}He/^{4}He$ ratios (0.025 Ra) higher than the expected theoretical value (0.0033 Ra) for the Carnmenellis granite-hosted water (England). They explain this observation by presenting a model of preferential release of ^{3}He from the rocks, relative to ^{4}He. However, this model only works if some conditions are satisfied to retain ^{4}He within the minerals – i.e., U and Th get concentrated in accessory phases and the host rock has remained at low temperature since formation (hence limiting He loss through diffusion). In our current study, testing this model would require detailed mineralogical characterization, but currently the composition of underlying basement and host rock is not well known Furthermore, the Paris Basin has a relatively high heat flux (60 to 120 mW/m2; Dentzer et al., 2016; Torgersen, 1993) which makes this model unlikely.

5.5.1.2 Mantle contribution

The alternative explanation for $^3He/^4He$ ratios above typical crustal values is a contribution of mantle-derived ^3He. This could originate from an old magmatic source in the crust, put in place around the time of basin formation, or from more recent magma intrusions.

Méjean et al. (2020) proposed a model in which a fossil magmatic signal is diluted over time by radiogenic ^4He production in the crust. This model is appropriate to explain the mantle input observed in the Southern Quebec groundwater since a clear alignment of Cretaceous magmatic intrusions is present (Monteregian Hills Igneous Province). For the Paris Basin, however, no evidence of magma emplacement in such scale during its formation is found.

Pinti and Marty (1998) describe two possibilities for the minor mantle signature in the Paris Basin observed in He isotopes – either from Permo-Carboniferous intrusions in Couy (lamprophyre dykes) or from a deep-seated magmatic source. The former could explain localized variations in the $^3He/^4He$ ratios but is unlikely to explain the signatures observed across a broad area. Furthermore, if the mantle input was coming from magmatic bodies that have already crystallized, helium would need to be liberated from minerals. For such a process to happen, certain temperatures must be reached to release He from the mineral; in the case of olivine crystals, helium release from fluid inclusions seems to start at $\sim 500°C$ (Tolstikhin et al., 2010) while closure temperatures are between 143 and 244°C (Shuster et al., 2004; Wang et al., 2015). In this case, diffusion is the primary process, and will not only depend on the current isotherms but also on the age of the crystallized body. Furthermore, cooling rates may play a role in controlling the availability of He since, if the heat flux has been continuously high in the region and the minerals crystallized long ago, the majority of the helium would likely have been lost from the magmatic body. A deep-seated magmatic source could explain the vertical $^3He/^4He$ gradient observed (Marty et al., 1993; Pinti and Marty, 1998) from the basement-hosted groundwater with 0.12-0.14 Ra, going through the Triassic aquifer with 0.08 Ra, and terminating at the Middle Jurassic waters at 0.02 Ra.

In Figure 5.3, we observe a geographical trend with $^3He/^4He$ decreasing from the South (Massif Central) towards the north (Paris Basin) while the SP4 sample group shows inter-

mediate $^{3}He/^{4}He$ ratios. Considering that this trend coincides with the N-S orientation of the fault systems, it could point to a localized weakening of the crust that facilitates mantle input by degassing of a melt generated by decompression and partial melting. The horizontal transport of gases with a mantle signature from a relatively young magmatic system through faults is unlikely since the most recent active volcanic system in the region is located in the Chaîne des Puys (4040 BCE), 90 km south of our study area in the Massif Central (2.9- 3.2 Ra; Bräuer et al., 2017). Also, no evidence for transport of gas via groundwater is observed in the dataset: transport through large distances would entail gas-water interaction and the $^{4}He/^{20}Ne$ ratios are consistently above 2000 and far from the air-saturated water value ($\sim$ 0.28). For the eastern segment of the Paris Basin, further from our study area in the Lorraine region, Marty et al. (2003) proposed that the elevated signatures (0.4 Ra) might originate from nearby rifting in the Rhine graben (1.7 Ra; Griesshaber et al., 1992), which is up to 120 km away from their studied sites. Similarly, for the Drôme County, in the subalpine massifs (SE France), $^{3}He/^{4}He$ ratios have a wide range and can reach relatively high values (0.02 to 3.64 Ra; Marty et al., 1992) while being $\sim$ 70 km away from the nearest volcanic systems (Ardèche and Auvergne). In both studies, $^{4}He/^{20}Ne$ and $^{3}He/^{4}He$ ratios of groundwater samples plot along a mixing line between ASW and a crust/mantle component and thus water could work as the transport medium of the magmatic $^{3}He/^{4}He$ component.

The input of mantle ^{3}He in some of our sample sites may therefore come directly from the mantle underlying the continental crust. In the Pannonian basin and Rhine graben, the crustal thickness is low, around 25 km and heat flow is on the order of 80 mW/m^2 (Čermák, 1982). Similarly, the current crustal thickness of the Paris Basin varies between 29 and 41 km (Lefort and Agarwal, 1996; Prijac et al., 2000) while the heat flux is between 60 and 120 mW/m^2 (Dentzer et al., 2016; Torgersen, 1993). However, in the Morvan, the crustal thickness is lower at between 27 and 29 km (Lefort and Agarwal, 1996) despite the typical crustal $^{3}He/^{4}He$ signatures (up to 0.04 Ra; current study). This suggests that crustal thickness and diffusive transport of mantle material through the crust is unlikely to be the dominant source of mantle ^{3}He within these systems. Therefore, Marty et al. (1993) interpret the anomalous $^{3}He/^{4}He$ signatures as the result of degassing of partial melts at depth, which explains the vertical ^{3}He flux.

Although the commonly known processes by which mantle helium enters the crust are via magmatic intrusions, degassing of magma, or diffusion, in areas without recent volcanism and under either extension or compression regimes, mantle input can also occur via advective flow controlled by faults due to improved permeability (Kennedy and van Soest, 2007; Kulongoski et al., 2005, 2013). In the model proposed by Kennedy and van Soest (2007), a vertical fault splay must penetrate the ductile lower crust and reach the mantle acting as a channel for fluid flow. To satisfy this model, strain localization must occur to generate vertical faults in depth; Kennedy and van Soest (2007) propose this process is possible with increased dextral shear strain. The areas where mantle input via advective flow have been described (Kennedy and van Soest, 2007; Kulongoski et al., 2005, 2013) are seismically active regions, however, which is not the case for the Paris Basin. Slow deforming areas can present seismicity such as in the Armorican Massif or the Massif Central, west and south of the Paris Basin, respectively; the main difference between them, in a tectonic context, is the presence of a thick unfaulted Meso-Cenozoic sedimentary pile that acts as a "patch" and protects the basement rocks in the Paris Basin from brittle movement by improving the cohesion and decreasing the thickness of the breakable portion of the upper crust (Petit et al., 2019). Our study area, nonetheless, is at the border of the basin and contains a series of faults. Further South, closer to the Massif Central, earthquakes with magnitudes up to M4.4 have been recorded (Mazabraud et al., 2005). The closest to the study area ($\sim$ 40 km south) was an M4.1 in 1977, near Vieure (46.52°N, 2.93°E; Mazabraud et al., 2005). To test if mantle input occurs via advective flow controlled by faults, a detailed structural and geophysical study of the region is necessary.

In any case, the anomalous $^{3}He/^{4}He$ signatures – above typical crustal values for this part of the crust – seem to be focused along the N-S fault systems with an apparent decreasing gradient starting at the Massif Central volcanic area up to the Paris Basin. This trend, coupled with the vertical $^{3}He/^{4}He$ gradient observed at the Paris Basin $^{3}He/^{4}He$ (Marty et al., 1993; Pinti and Marty, 1998), seem to point to a localized and limited mantle input along these faults, which is endorsed by the ^{129}Xe excess observed at SP7 (see section 5.5.2).

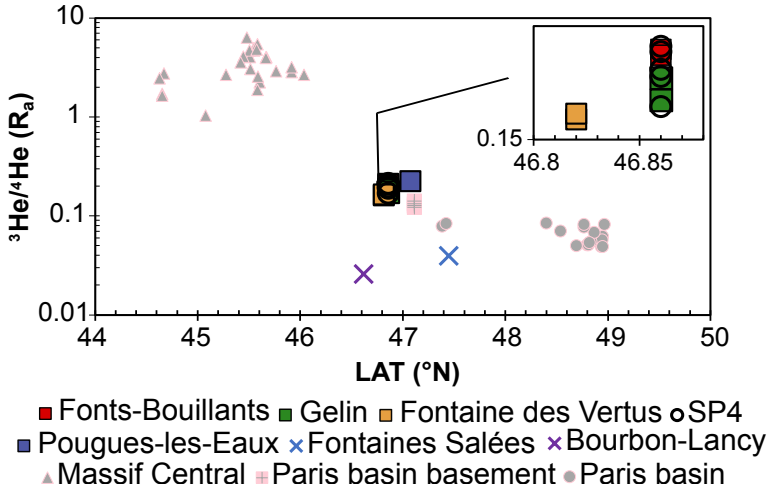

Figure 5.3: Variation of helium isotope ratios with latitude. There is an apparent trend with decreasing ^{3}He/^{4}He ratios from south, starting at the Massif Central, to north, ending in the Paris Basin. Helium contents are higher for our dataset. Massif Central and Paris Basin data are from the literature (Bräuer et al., 2017; Marty et al., 1993; Pinti and Marty, 1998).

5.5.2 Ar, Ne, and Xe isotope constraints

The Ne isotopic signature of SP4 is dominated by a nucleogenic production within the continental crust, however, the data point lies slightly above the typical crust-air mixing line (Figure 5.4), which could be due to either (i) simple two component mixing between air and a Ne endmember between modern crustal values and Archean terrains, or (ii) a limited contribution of mantle Ne to crustal and atmospheric Ne. The fact that there is only a single data point does not allow us to draw mixing line(s) and therefore precludes a definitive conclusion about a possible contribution of mantle Ne.

The argon isotopic composition of SP4 gas (Table 5.3) indicates either atmospheric or mantle origin for the ^{38}Ar/^{36}Ar ratio and a significant contribution of radiogenic ^{40}Ar produced by the decay of ^{40}K over long periods of time (T1/2 = 1.25 Ga). Indeed, the ^{40}Ar/^{36}Ar ratios of 2866 are one order of magnitude higher than the atmospheric value of 298.6. High ^{40}Ar/^{36}Ar values are observed in both crustal and mantle rocks and gases, so it is not possible a priori to decipher the origin of such radiogenic Ar, but the continental environment of the gas reservoir and the low ^{3}He/^{4}He ratio compared to typical mantle He values suggests a strong crustal contribution.

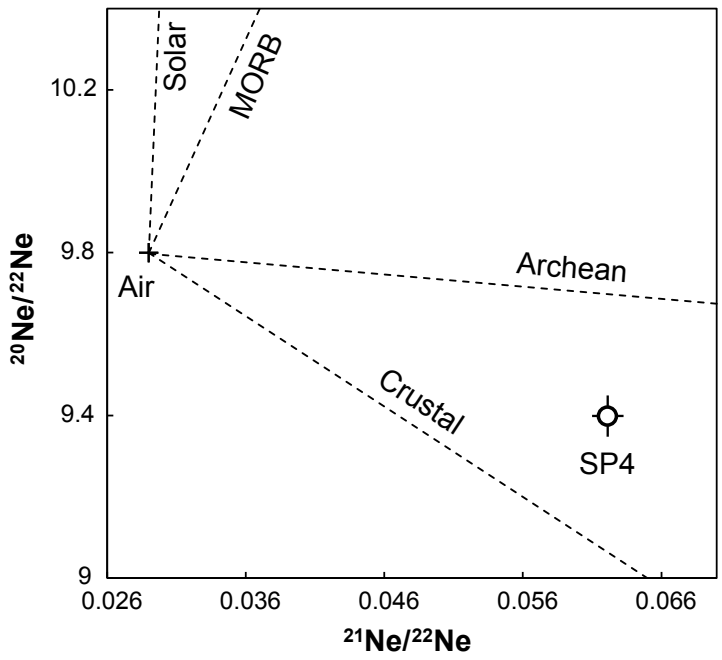

Figure 5.4: Three isotope diagram of neon. Mixing between air and solar, MORB (Sarda et al., 1988), Archean terrains (Lippmann-Pipke et al., 2011), crustal (Kennedy et al., 1990) end-members are displayed. SP4 plots between the crustal and Archean mixing lines with air and errors shown in 1 sigma level.

At the level of ultra-high precision provided by dynamic mass spectrometry, the isotopic composition of SP7 xenon is shown to deviate from that of atmospheric Xe. High precision Xe analysis from SP7 (Figure 5.5) shows a small yet distinguishable ^{129}Xe excess (relative to the atmosphere). ^{129}Xe excess is linked to ^{129}I decay either by ^{238}U spontaneous fission, cosmogenic origin, or trapped in the mantle reservoir from production in the first $\sim$ 100 Myr of the Earth formation (Moreira, 2013; Mukhopadhyay and Parai, 2019). Although ^{129}Xe can be produced in the crust by ^{129}I decay from ^{238}U spontaneous fission, considering the ^{136}Xe/^{130}Xe is very low (corrected absolute ratio of 2.207) and the upper limit for ^{129}Xe/^{136}Xe of ^{238}U-fissiogenic Xe is 0.001 (Eikenberg et al., 1993), the ^{129}Xe/^{130}Xe originated from fissiogenic ^{238}U would be minimal ($< 1\%$).

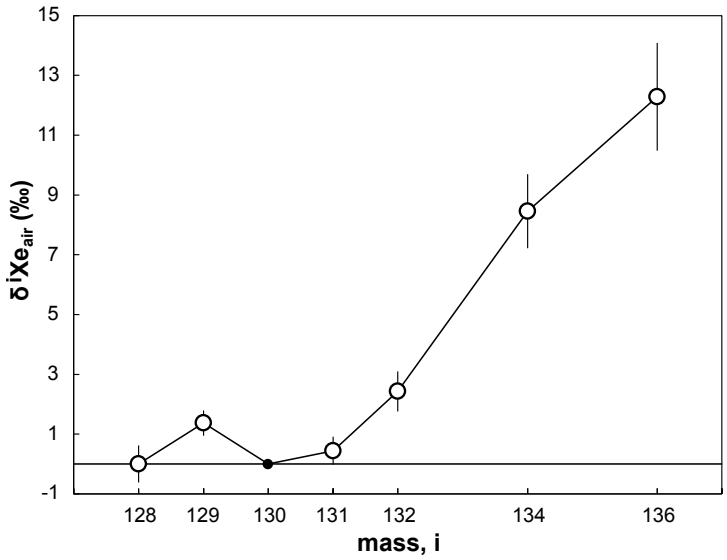

Figure 5.5: Xenon isotopic composition of SP7 gas corrected for physical fractionation. Data is expressed in δ (‰) of Xe ratios relative to atmospheric composition and normalised to 130Xe. Error bars are 2 sigma. The SP7 gas has a clear 129Xe excess that indicates mantle input.

Cosmogenic ^{129}I is concentrated in sediments enriched in carbon (Santos et al., 2007); Holland et al. (2013) attributed the 129Xe observed in the Timmins mine fluids to cosmogenic ^{129}I due to the age of the host rocks/fluids (Archean), presence of carbon-rich sediments, and absence of any evidence for mantle input since the ^{3}He/^{4}He ratios were within typical crustal ranges (up to 0.01 Ra). As discussed in section 5.5.1.1, Stephanian-Permian basins in the Massif Central region have coal levels (Mercuzot et al., 2021), however, the geology of the basin of our current study is not yet well established. Thus, in our study area, considering the helium isotope signature above typical crustal values (up to 0.22 Ra), ^{129}Xe excess is linked to mantle input.

Notably, heavy Xe isotopes are clearly enriched relative to the lighter ones (e.g., 130Xe). Such enrichment is likely to result from the contribution of fissiogenic Xe due to the spontaneous fission of long-lived ^{238}U (Mukhopadhyay and Parai, 2019). Thus, the isotopic composition of xenon confirms that SP7 hosts gas components derived from both the mantle and crust.

5.5.3 $CO_2/^3He$ and stable isotope constraints

The overall $\delta^{13}C$ of CO_2 signatures are outside the MORB range (-5 ± 2 ‰) and within range of non-marine carbonates, graphite, and marine plants (Favara et al., 2002). However, for the SP4 group, with exception of Fontaine des Vertus, $CO_2/^3He$ is close to the MORB values ($\sim$ 1 to 6 x 10^9; Marty and Zimmermann, 1999), ranging from 8 x 10^9 to 1 x 10^{10}. In a $CO_2/^3He$ versus δ13C plot (Sano and Marty, 1995; Figure 5.6), the CO_2-dominated samples show a mixing between three components, namely mid-ocean ridge basalts (MORB), organic sediments, and marine limestones (or slab carbonates). Considering that ^3He is mainly of mantle origin, the end-member contributions would range from 15% to 30% MORB, 40% to 55% limestones, and 25% to 30% sediments contribution to the source of CO_2. Secondary processes can still play an important role in the CO_2 and δ13C values (Supplementary material); Gilfillan et al (2009) propose that $CO_2/^3He$ variations in different gas fields are due to CO_2loss either from dissolution in groundwater or carbonate precipitation, and that the δ13C will vary according to the water pH in a negative correlation (Randazzo et al., 2021).

In the Massif Central, δ13C varies between -6.3 ‰ and -3.6 ‰ while $CO_2/^3He$ ranges from 3.9 x 10^9 to 1 x 10^{13} (Bräuer et al., 2017), which falls between upper mantle and marine limestone in Figure 5.6. This range can be interpreted as representing the composition of the typical regional mantle end-member. In this case, we might observe, for the SP4 group, the occurrence of a mantle-like component associated with CO_2 dissolution in water leading to more depleted $\delta^{13}C$ or a small contribution from organic sediments, and at Fontaines Salées and Bourbon-Lancy, an organic source. Alternatively, CO_2 in the SP4 group samples might originate from non-marine carbonates or graphite which can range, respectively, from $\sim$ -18 ‰ to 0 ‰ and $\sim$ -40 ‰ to 0 ‰ (Favara et al., 2002) that can still be associated with mixing with a MORB component. The history of CO_2 transport might be more complex for Fontaines Salées and Bourbon-Lancy and could reflect secondary processes.

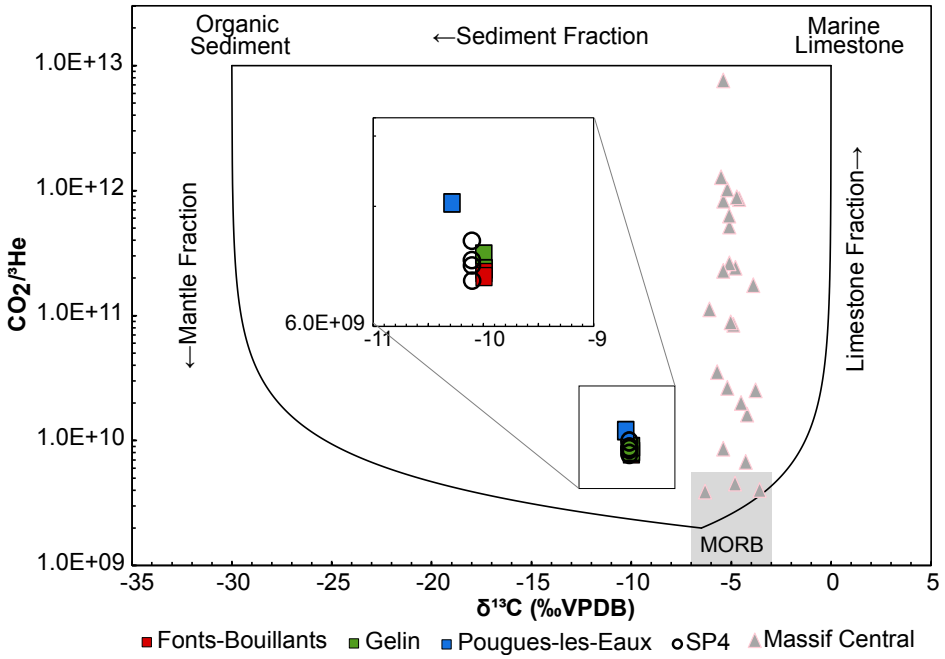

Figure 5.6: $CO_2/^3He$ versus $\delta^{13}C$ plot (Sano and Marty, 1995). The dataset shows mixing between the three components and plots close to the MORB value while Massif Central data (Bräuer et al., 2017) only shows mixing between MORB and marine limestone. The grey field represents the MORB range from Marty and Zimmermann (1999).

CO_2 reservoirs worldwide are generally interpreted as being magmatic in origin, with $\delta^{13}C$ ranging between - 5.7 to – 2.7 ‰ (Gilfillan et al., 2009); compared to them our dataset is atypical. However, in such reservoirs, water is the storage medium of CO_2 (Dubacq et al., 2012; Gilfillan et al., 2008) while in our study we did not identify water bodies at depth and no water manifested during the well tests. Nonetheless, in areas with no evidence of volcanism, CO_2 flow in the surface has already been reported for seismically active areas (e.g. Li Vigni et al., 2022), indicating that fault systems can lead to complex histories of CO_2 transport and entrapment.

For all samples, the $\delta^{15}N$ values show little variation, ranging from +6.1 to +8.4 ‰. This range is typical of continental or subduction-related gases and differs from that of MORB (around -5 ‰ in the convecting mantle; Marty and Dauphas, 2003). Mantle plumes also show lower $\delta^{15}N$ values, around 0 ± 3 ‰ (Labidi et al., 2020; Marty and Dauphas, 2003). In the Massif Central, $\delta^{15}N$ values around +2 ‰ (Bräuer et al., 2017) could potentially indicate the presence of a mantle plume or, alternatively, mixing between MORB-like and continental-like components. The near-constant $\delta^{15}N$ values of the present samples point to

a common nitrogen source despite large variations in the N_2 contents of the surveyed springs. Such variable N_2 contents might be relative to secondary physical/chemical processes in the crust since higher contents of N_2 and helium are associated with more depleted $\delta^{13}C$ values (Figure S1).

5.6 Conclusion

The main source of helium in the study area is the continental crust. $^3He/^4He$ ratios are independent of gas composition, given that $^3He/^4He$ is roughly the same for springs near SP4, including Fontaine des Vertus, while its helium and N_2 contents are much higher than for the other springs of the group. Local helium production alone is unlikely since the $^3He/^4He$ ratios (0.17-0.22 Ra) are in the same range across a 40 km area (Pougues-les-Eaux and Couy). To verify if ^3He and ^4He are produced and stored in the reservoir layers or if they are transported from a crustal flux, the U-Th-Li contents of the host rocks of the sites investigated is required, and a better understanding of the basin geometry and sources is necessary.

The decreasing $^3He/^4He$ gradient starting at the Massif Central towards the Paris Basin and the vertical $^3He/^4He$ gradient previously described in the literature at the Paris Basin aquifers (Marty et al., 1993; Pinti and Marty, 1995, 1998) point to a small mantle contribution limited to the N-S fault system, since laterally, few kilometres (50-80) east at Bourbon-Lancy and Fontaines Salées, $^3He/^4He$ ratios show typical crustal values ($\leq$ 0.04 Ra). The ^{129}Xe excess observed at SP7 confirms that excess ^3He relative to the crustal end-member composition is derived from the mantle. This indicates that either a deep-seated magmatic source is present, or deep fault systems reach the mantle and input ^3He via an improved permeability system (Kennedy and van Soest, 2007).

Considering that the $\delta^{13}C$ of CO_2 of our surveyed springs are distinct from the regional mantle value (Massif Central), CO_2 is probably mainly of crustal origin. However, mixing between crustal or biogenic components and mantle is expected, especially since CO_2 would most likely be the carrier phase of the mantle helium component and $CO_2/^3He$ ratios (between 8 x 10^9 and 1 x 10^{10}) are close to the MORB value and indicate a $\sim$ 15% mantle

contribution, in agreement with what is observed in He and Xe isotopes. Secondary processes in the crust are also possible given the low solubility of CO_2 in water, and potential carbonate precipitation can also explain the decrease of CO_2 contents associated with elevated concentrations of N_2 and helium at Fontaine des Vertus, Bourbon-Lancy, and Fontaines Salées. $\delta^{15}N$ results, for both sample groups, are comparable and point to a common crustal source.

Acknowledgment

We thank A. Caracausi for the insightful discussions. We are also thankful to L. Zimmermann and B. Tibari for helping with the analyses. We gratefully thank the two anonymous reviewers of this article and the Editor for his handling of our manuscript. This work was partially supported by the French PIA project "Lorraine Université d'Excellence", reference ANR-15-IDEX-04-LUE.

References

Andrews, J. N. (1985). The isotopic composition of radiogenic helium and its use to study groundwater movement in confined aquifers. Chemical Geology, 49(1–3), 339–351.

Ballentine, C. J., and Burnard, P. G. (2002). Production, release and transport of noble gases in the continental crust. Reviews in Mineralogy and Geochemistry, 47.

Baptiste, J. (2016). Cartographie structurale et lithologique du substratum du Bassin parisien et sa place dans la chaîne varisque de l'Europe de l'Ouest: approches combinées géophysiques, pétrophysiques, géochronologiques et modélisations 2D. Université d'Orléans.

Barruol, G., and Granet, M. (2002). A Tertiary asthenospheric flow beneath the southern French Massif Central indicated by upper mantle seismic anisotropy and related to the west Mediterranean extension. Earth and Planetary Science Letters, 202(1), 31–47.

Batard, F., Baubron, J. C., Bosch, B., Marcé, A., and Risler, J. J. (1982). Isotopic identification of gases of a deep origin in French thermomineral waters. Journal of Hydrology, 56(1–2), 1–21.

Battani, A., Deville, E., Faure, J. L., Jeandel, E., Noirez, S., Tocqué, E., Benoît, Y., Schmitz, J., Parlouar, D., and Sarda, P. (2010). Geochemical study of natural CO2 emissions in the French Massif Central: how to predict origin, processes and evolution of CO2 leakage. Oil and Gas Science and Technology–Revue de l'Institut Français Du Pétrole, 65(4), 615–633.

Beccaletto, L., Capar, L., Serrano, O., and Marc, S. (2015). Structural evolution and sedimentary record of the Stephano-Permian basins occurring beneath the Mesozoic sedimentary cover in the southwestern Paris basin (France). Bulletin de La Societe Geologique de France, 186(6), 429–450.

Bekaert, D. V, Barry, P. H., Broadley, M. W., Byrne, D. J., Marty, B., Ramírez, C. J., de Moor, J. M., Rodriguez, A., Hudak, M. R., and Subhas, A. V. (2023). Ultrahigh-precision noble gas isotope analyses reveal pervasive subsurface fractionation in hydrothermal systems. Science Advances, 9(15), eadg2566.

Bekaert, D. v, Broadley, M. W., Caracausi, A., and Marty, B. (2019). Novel insights into the degassing history of Earth's mantle from high precision noble gas analysis of magmatic gas. Earth and Planetary Science Letters, 525, 115766.

Boineau, R., and Maisonneuve, J. (1972). Les sources minérales du Massif Central français et leur cadre géologique. Rapport BRGM.

Bräuer, K., Kämpf, H., Niedermann, S., and Wetzel, H. U. (2017). Regional distribution pattern of carbon and helium isotopes from different volcanic fields in the French Massif Central: Evidence for active mantle degassing and water transport. Chemical Geology, 469(February), 4–18.

Broadley, M. W., Barry, P. H., Bekaert, D. v, Byrne, D. J., Caracausi, A., Ballentine, C. J., and Marty, B. (2020). Identification of chondritic krypton and xenon in Yellowstone gases and the timing of terrestrial volatile accretion. Proceedings of the National Academy of Sciences, 117(25), 13997–14004.

Broadley, M. W., Byrne, D. J., Ardoin, L., Almayrac, M. G., Bekaert, D. v, and Marty, B. (2022). High precision noble gas measurements of hydrothermal quartz reveal variable loss rate of Xe from the Archean atmosphere. Earth and Planetary Science Letters, 588, 117577.

Buikin, A., Trieloff, M., Hopp, J., Althaus, T., Korochantseva, E., Schwarz, W. H., and Altherr, R. (2005). Noble gas isotopes suggest deep mantle plume source of late Cenozoic mafic alkaline volcanism in Europe. Earth and Planetary Science Letters, 230(1–2), 143–162.

Čermák, V. (1982). Crustal temperature and mantle heat flow in Europe. Tectonophysics, 83(1–2), 123–142.

Clozier, L., and Turland, M. (1982). Notice explicative de la feuille Dornes a 1/50 000.

Coisy, P., and Nicolas, A. (1978). Regional structure and geodynamics of the upper mantle beneath the Massif Central. Nature, 274(5670), 429–432.

Craig, H., and Lupton, J. E. (1976). Primordial neon, helium, and hydrogen in oceanic basalts. Earth and Planetary Science Letters, 31(3), 369–385.

Dentzer, J., Lopez, S., Violette, S., and Bruel, D. (2016). Quantification of the impact of paleoclimates on the deep heat flux of the Paris Basin. Geothermics, 61, 35–45.

Dubacq, B., Bickle, M. J., Wigley, M., Kampman, N., Ballentine, C. J., and Sherwood Lollar, B. (2012). Noble gas and carbon isotopic evidence for CO 2-driven silicate dissolution in a recent natural CO 2 field. Earth and Planetary Science Letters, 341–344, 10–19.

Eikenberg, J., Signer, P., and Wieler, R. (1993). U-Xe, U-Kr, and U-Pb systematics for dating uranium

minerals and investigations of the production of nucleogenic neon and argon. Geochimica et Cosmochimica Acta, 57(5), 1053–1069.

Farjanel, G. (1989). Synthèse géologique des bassins permiens français (Issue 128). Editions BRGM.

Favara, R., Grassa, F., Inguaggiato, S., Pecoraino, G., and Capasso, G. (2002). A simple method to determine the δ13C content of total dissolved inorganic carbon. Geofisica Internacional, 41(3), 313–320.

Fonroche geothermie. (2019). Notice Technique du PER dit de "Bassin de Limagne."

Fontes, J. C., and Matray, J. M. (1993a). Geochemistry and origin of formation brines from the Paris Basin, France. 1. Brines associated with Triassic salts. Chemical Geology, 109(1–4), 149–175.

Fontes, J. Ch., and Matray, J. M. (1993b). Geochemistry and origin of formation brines from the Paris Basin, France: 2. Saline solutions associated with oil fields. Chemical Geology, 109(1), 177–200.

Froidevaux, C., Brousse, R., and Bellon, H. (1974). Hot spot in France? Nature, 248(5451), 749–751.

Gautheron, C., Moreira, M., and Allègre, C. (2005). He, Ne and Ar composition of the European lithospheric mantle. Chemical Geology, 217(1–2), 97–112.

Giggenbach, W. F., and Goguel, R. L. (1988). Methods for the collection and analysis of geothermal and volcanic water and gas samples. Chemistry Division, Department of Scientific and Industrial Research.

Gilfillan, S. M. V., Ballentine, C. J., Holland, G., Blagburn, D., Lollar, B. S., Stevens, S., Schoell, M., and Cassidy, M. (2008). The noble gas geochemistry of natural CO2 gas reservoirs from the Colorado Plateau and Rocky Mountain provinces, USA. Geochimica et Cosmochimica Acta, 72(4), 1174–1198.

Gilfillan, S. M. V., Lollar, B. S., Holland, G., Blagburn, D., Stevens, S., Schoell, M., Cassidy, M., Ding, Z., Zhou, Z., Lacrampe-Couloume, G., and Ballentine, C. J. (2009). Solubility trapping in formation water as dominant CO2 sink in natural gas fields. Nature, 458(7238), 614–618.

Gloaguen, E., Melleton, J., Lefebvre, G., Tourière, B., Yart, S., and Gourcerol, B. (2018). Ressources métropolitaines en lithium et analyse du potentiel par méthodes de prédictivité. Public report BRGM/RP-68321-FR, 126p.

Glueckauf, E. (1946). A micro-analysis of the helium and neon contents of air. Proceedings of the Royal Society of London. Series A. Mathematical and Physical Sciences, 185(1000), 98–119.

Gourcerol, B., Gloaguen, E., Melleton, J., Tuduri, J., and Galiegue, X. (2019). Re-assessing the European lithium resource potential – A review of hard-rock resources and metallogeny. Ore Geology Reviews, 109(April), 494–519.

Graham, D. W. (2002). Noble gas isotope geochemistry of mid-ocean ridge and ocean island basalts: Characterization of mantle source reservoirs. Reviews in Mineralogy and Geochemistry, 47, 247–317.

Griesshaber, E., O'Nions, R. K., and Oxburgh, E. R. (1992). Helium and carbon isotope systematics in crustal fluids from the Eifel, the Rhine Graben and Black Forest, F.R.G. Chemical Geology, 99(4), 213–235.

Guillocheau, F., Robin, C., Allemand, P., Bourquin, S., Brault, N., Dromart, G., Friedenberg, R., Garcia, J.-P., Gaulier, J.-M., and Gaumet, F. (2000). Meso-Cenozoic geodynamic evolution of the Paris Basin: 3D stratigraphic constraints. Geodinamica Acta, 13(4), 189–245.

Holland, G., Lollar, B. S., Li, L., Lacrampe-Couloume, G., Slater, G. F., and Ballentine, C. J. (2013). Deep fracture fluids isolated in the crust since the Precambrian era. Nature, 497(7449), 357–360.

Jolivet, L., Baudin, T., Calassou, S., Chevrot, S., Ford, M., Issautier, B., Lasseur, E., Masini, E., Manatschal, G., and Mouthereau, F. (2021). Geodynamic evolution of a wide plate boundary in the Western Mediterranean, near-field versus far-field interactions. BSGF-Earth Sciences Bulletin, 192(1), 48.

Joly, A. (2007). Relations plutons et discontinuités lithosphériques: approche pluridisciplinaire de la mise en place de plutons granitiques le long du Sillon Houiller (Massif Central Français): apports des études de terrain et des données gravimétriques, magnétiques et A. Orléans.

Kennedy, B. M., and van Soest, M. C. (2007). Flow of mantle fluids through the ductile lower crust: Helium isotope trends. Science, 318(5855), 1433–1436. https://doi.org/10.1126/science.1147537

Krauskopf, K. B., and Bird, D. K. (1967). Introduction to geochemistry (Vol. 721). McGraw-Hill New York.

Kulongoski, J. T., Hilton, D. R., Barry, P. H., Esser, B. K., Hillegonds, D., and Belitz, K. (2013). Volatile fluxes through the Big Bend : of the San Andreas Fault, California: Helium and carbon-dioxide systematics. Chemical Geology, 339, 92–102.

Kulongoski, J. T., Hilton, D. R., and Izbicki, J. A. (2005). Source and movement of helium in the eastern Morongo groundwater Basin: The influence of regional tectonics on crustal and mantle helium fluxes. Geochimica et Cosmochimica Acta, 69(15), 3857–3872.

Labidi, J., Barry, P. H., Bekaert, D. v., Broadley, M. W., Marty, B., Giunta, T., Warr, O., Sherwood Lollar, B., Fischer, T. P., Avice, G., Caracausi, A., Ballentine, C. J., Halldórsson, S. A., Stefánsson, A., Kurz, M. D., Kohl, I. E., and Young, E. D. (2020). Hydrothermal 15N15N abundances constrain the origins of mantle nitrogen. Nature, 580(7803), 367–371.

Lefort, J. P., and Agarwal, B. N. P. (1996). Gravity evidence for an Alpine buckling of the crust beneath the Paris Basin. Tectonophysics, 258(1–4), 1–14.

Li Vigni, L., Cardellini, C., Temovski, M., Ionescu, A., Molnár, K., Palcsu, L., Gagliano, A. L., Cappuzzo, S., and D'Alessandro, W. (2022). Duvalo "Volcano" (North Macedonia): A Purely Tectonic-Related CO2 Degassing System. Geochemistry, Geophysics, Geosystems, 23(4).

Mabry, J., Lan, T., Burnard, P., and Marty, B. (2013). High-precision helium isotope measurements in air. Journal of Analytical Atomic Spectrometry, 28(12), 1903–1910.

Manatschal, G., Chenin, P., Lescoutre, R., Miró, J., Cadenas, P., Saspiturry, N., Masini, E., Chevrot, S., Ford, M., and Jolivet, L. (2021). The role of inheritance in forming rifts and rifted margins and building collisional orogens: a Biscay-Pyrenean perspective. BSGF-Earth Sciences Bulletin, 192(1), 55.

Martel, D. J., O'Nions, R. K., Hilton, D. R., and Oxburgh, E. R. (1990). The role of element distribution in production and release of radiogenic helium: the Carnmenellis Granite, southwest England. Chemical Geology, 88(3–4), 207–221.

Marty, B., and Dauphas, N. (2003). The nitrogen record for crust-mantle interaction and mantle con-

vection from Archean to Present. Earth and Planetary Science Letters, 206(3–4), 397–410.

Marty, B., Dewonck, S., and France-Lanord, C. (2003). Geochemical evidence for efficient aquifer isolation over geological timeframes. Nature, 425(6953), 55–58.

Marty, B., O'Nions, R. K., Oxburgh, E. R., Martel, D., and Lombardi, S. (1992). Helium isotopes in Alpine regions. Tectonophysics, 206(1–2), 71–78.

Marty, B., Torgersen, T., Meynier, V., O'Nions, R. K., and de Marsily, G. (1993). Helium isotope fluxes and groundwater ages in the Dogger Aquifer, Paris Basin. Water Resources Research, 29(4), 1025–1035.

Marty, B., and Zimmermann, L. (1999). Volatiles (He, C, N, Ar) in mid-ocean ridge basalts: Assesment of shallow-level fractionation and characterization of source composition. Geochimica et Cosmochimica Acta, 63(21), 3619–3633.

Mazabraud, Y., Béthoux, N., and Deroussi, S. (2005). Characterisation of the seismological pattern in a slowly deforming intraplate region: Central and western France. Tectonophysics, 409(1–4), 175–192.

McKinney, C. R., McCrea, J. M., Epstein, S., Allen, H. A., and Urey, H. C. (1950). Improvements in mass spectrometers for the measurement of small differences in isotope abundance ratios. Review of Scientific Instruments, 21(8), 724–730.

Méjean, P., Pinti, D. L., Kagoshima, T., Roulleau, E., Demarets, L., Poirier, A., Takahata, N., Sano, Y., and Larocque, M. (2020). Mantle helium in Southern Quebec groundwater: A possible fossil record of the New England hotspot. Earth and Planetary Science Letters, 545, 116352.

Mercuzot, M., Bourquin, S., Beccaletto, L., Ducassou, C., Rubi, R., and Pellenard, P. (2021). Palaeoenvironmental reconstitutions at the Carboniferous–Permian transition south of the Paris Basin, France: implications on the stratigraphic evolution and basin geometry. International Journal of Earth Sciences, 110(1), 9–33.

Merle, O., and Michon, L. (2001). The formation of the West European Rift; a new model as exemplified by the Massif Central area. Bulletin de La Societé Géologique de France, 172(2), 213–221.

Millot, R., Guerrot, C., Innocent, C., Négrel, P., and Sanjuan, B. (2011). Chemical, multi-isotopic (Li-B-Sr-U-H-O) and thermal characterization of Triassic formation waters from the Paris Basin. Chemical Geology, 283(3–4), 226–241.

Millot, R., Négrel, P., and Petelet-Giraud, E. (2007). Multi-isotopic (Li, B, Sr, Nd) approach for geothermal reservoir characterization in the Limagne Basin (Massif Central, France). Applied Geochemistry, 22(11), 2307–2325.

Moreira, M. (2013). Noble Gas Constraints on the Origin and Evolution of Earth's Volatiles. Geochemical Perspectives, 2(2), 229–230.

Moreira, M., Rouchon, V., Muller, E., and Noirez, S. (2018). The xenon isotopic signature of the mantle beneath Massif Central. Geochem. Perspect. Lett, 6, 28–32.

Morrison, P., and Pine, J. (1955). Radiogenic Origin of the Helium Isotopes in Rock. Annals of the New York Academy of Sciences, 62(3), 71–92.

Mukhopadhyay, S., and Parai, R. (2019). Noble gases: A record of earth's evolution and mantle dynamics. Annual Review of Earth and Planetary Sciences, 47, 389–419.

Nehlig, P., Boivin, P., Goër, A., Mergoil, J., Prouteau, G., Sustrac, G., and Thiéblemont, D. (2003). Les volcans du Massif Central. Geologues, 130–131.

Oxburgh, E. R., O'Nions, R. K., and Hill, R. I. (1986). Helium isotopes in sedimentary basins. Nature, 324(6098), 632–635.

Pasquet, G., Houssein Hassan, R., Sissmann, O., Varet, J., and Moretti, I. (2021). An Attempt to Study Natural H2 Resources across an Oceanic Ridge Penetrating a Continent: The Asal–Ghoubbet Rift (Republic of Djibouti). Geosciences, 12(1), 16.

Petit, C., de Barros, L., Duclaux, G., and Mazabraud, Y. (2019). Why are there no earthquakes in the intracratonic paris basin? Insights from flexural models. Geosciences (Switzerland), 9(12).

Pinti, D. L., and Marty, B. (1995). Noble gases in crude oils from the Paris Basin, France: Implications for the origin of fluids and constraints on oil-water-gas interactions. Geochimica et Cosmochimica Acta, 59(16), 3389–3404.

Pinti, D. L., and Marty, B. (1998). The origin of helium in deep sedimentary aquifers and the problem of dating very old groundwaters. Geological Society Special Publication, 144, 53–68.

Prijac, C., Doin, M. P., Gaulier, J. M., and Guillocheau, F. (2000). Subsidence of the Paris Basin and its bearing on the late Variscan lithosphere evolution: A comparison between Plate and Chablis models. Tectonophysics, 323(1–2), 1–38.

Qin, S., Zhao, C., Li, Y., and Zhang, Y. (2015). Review of coal as a promising source of lithium. International Journal of Oil, Gas and Coal Technology, 9(2), 215–229.

Raimbault, L., Cuney, M., Azencott, C., Duthou, J. L., and Joron, J. L. (1995). Geochemical evidence for a multistage magmatic genesis of Ta-Sn-Li mineralization in the granite at Beauvoir, French Massif Central. Economic Geology, 90(3), 548–576.

Randazzo, P., Caracausi, A., Aiuppa, A., Cardellini, C., Chiodini, G., D'Alessandro, W., Li Vigni, L., Papic, P., Marinkovic, G., and Ionescu, A. (2021). Active Degassing of Deeply Sourced Fluids in Central Europe: New Evidences From a Geochemical Study in Serbia. Geochemistry, Geophysics, Geosystems, 22(11), 1–17.

Regorda, A., Lardeaux, J.-M., Roda, M., Marotta, A. M., and Spalla, M. I. (2020). How many subductions in the Variscan orogeny? Insights from numerical models. Geoscience Frontiers, 11(3), 1025–1052.

Risler, J. J. (1974). Description et classification géologique des sources minérales et thermales du Massif Central. BRGM Report, 74.

Roger, J., Gaudry, F., Marteau, P., Quesnel, F., Chevremont, P., and Jauffret, D. (2010). Notice explicative, Carte géol. France (1/50 000), feuille Decize (549). Orléans, BRGM, 185.

Sano, Y., and Marty, B. (1995). Origin of carbon in fumarolic gas from island arcs. Chemical Geology, 119(1–4), 265–274.

Santos, F. J., López-Gutiérrez, J. M., García-León, M., Synal, H. A., and San Miguel, E. G. (2007). 129I record in a sediment core from Tinto River (Spain). Nuclear Instruments and Methods in Physics Research, Section B: Beam Interactions with Materials and Atoms, 259(1), 503–507.

Seltzer, A. M., and Bekaert, D. v. (2022). A unified method for measuring noble gas isotope ratios in air, water, and volcanic gases via dynamic mass spectrometry. International Journal of Mass Spectrometry, 478, 116873.

Shuster, D. L., Farley, K. A., Sisterson, J. M., and Burnett, D. S. (2004). Quantifying the diffusion kinetics and spatial distributions of radiogenic 4He in minerals containing proton-induced 3He. Earth and Planetary Science Letters, 217(1–2), 19–32.

Sun, B., Zeng, F., Moore, T. A., Rodrigues, S., Liu, C., and Wang, G. (2022). Geochemistry of two high-lithium content coal seams, Shanxi Province, China. International Journal of Coal Geology, 260, 104059.

Tolstikhin, I., Kamensky, I., Tarakanov, S., Kramers, J., Pekala, M., Skiba, V., Gannibal, M., and Novikov, D. (2010). Noble gas isotope sites and mobility in mafic rocks and olivine. Geochimica et Cosmochimica Acta, 74(4), 1436–1447.

Torgersen, T. (1993). Defining the role of magmatism in extensional tectonics: Helium 3 fluxes in extensional basins. Journal of Geophysical Research, 98(B9), 16257.

Vanderhaeghe, O., Laurent, O., Gardien, V., Moyen, J. F., Gébelin, A., Chelle-Michou, C., Couzinié, S., Villaros, A., and Bellanger, M. (2020). Flow of partially molten crust controlling construction, growth and collapse of the Variscan orogenic belt: The geologic record of the French Massif Central. BSGF - Earth Sciences Bulletin, 191.

Wang, K., Brodholt, J., and Lu, X. (2015). Helium diffusion in olivine based on first principles calculations. Geochimica et Cosmochimica Acta, 156, 145–153.

Weinlich, F. H. (2005). Isotopically light carbon dioxide in nitrogen rich gases: The gas distribution pattern in the French Massif Central, the Eifel and the western Eger Rift. Annals of Geophysics, 48(1), 19–31.

Chapter 6

Lake Abhe geothermal field, Djibouti

Contents

6.1 The "Geothermal Village" project

The East African Rift System (EARS) has a vast geothermal untapped resource, especially in remote regions where social challenges require it the most. The "Geothermal Village" project (LEAP-RE european project, managed by Yves Géraud University of Lorraine and Jacques Varet Geo2D) arises from this need, with the objective of identifying and characterizing geothermal areas with potential for electric and thermal energy systems in the EARS for future implementation of independent geothermal power plants. One of the areas with such potential is Lake Abhe (Djibouti).

This site is isolated, 50 km from the National Grid and Electrical High Voltage line linking Ethiopia and Djibouti. The local population is pastoralist and semi-nomadic as the shore of the lake allow for permanent pastureland. Since the opening of a school in October 2020, the families tend to group around it. The objectives of this project were to identify potential for: (i) medium-high temperature resource for electricity production with an ORC (Organic Rankine Cycle); (ii) Hot water production for direct uses applications including SPA and (iii) drinking water production for the village, the school and touristic installations. The other members of the project investigated the structural geology, volcanic petrology, hydrothermal mineralogy, and petrophysics, as well as associated social impact and acceptability. Our contribution was with the geochemical model via a survey (mainly stable and helium isotopes) in order to establish the source of gas/heat and water dynamics. For this study, we took the opportunity to complement the data and associated discussions with additional available measures in the Ethiopian part of the Afar depression, acquired in the framework of a project on CO_2 and volatile flux founded by the Lounsbarry Fundation and sampled by Bernard Marty, Antonio Caracausi, and Raphaël Pik in 2017.

Previous studies modelled the reservoir temperature at 110-154°C (Awaleh et al., 2015; Hersir et al., 2016) indicating that the low enthalpy geothermal system at Lake Abhe has

potential for electricity production, although, according to Hersir et al. (2016), it would require large amounts of water for power production, which is a challenge for this arid region. The Lake Abhe geothermal area is $\sim$ 30 km from the Dama Ale volcano and $\sim$ 80 km from Lake Asal. Hot springs are located along WNW-ESE faults, emanating from carbonate chimneys (Figure 1.18).

6.2 Hydrochemical background

In the EARS, the hydrological setting is complex due to its tectonic history leading to aquifer heterogeneity both laterally and vertically, and to its topographic variability that results in heterogeneous rainfall and consequently of groundwater recharge distribution (Mechal et al., 2017).

The Awash River drains the central part of the Main Ethiopian Rift (MER) and ends in Lake Abhe in Afar; the aquifers are cut off by a series of NE–SW and E–W normal faults that dictate the flow direction of the Awash River in Southern Afar (Abiye, 2010). In the Republic of Djibouti, as a result of the fracture network, product of extensional tectonics, a groundwater flow from the highest basins (Lake Abhe) towards the lowest ones north-eastward (Dobi-Hanle and Asal) renders them interconnected (Gasse and Street, 1978). Hot springs and fumaroles occur in these basins, near the lakes Abhe, Hanle, and Asal (Houssein et al., 2014).

The hot springs at Lake Abhe are located along carbonate chimneys which are oriented WNW-ESE (Figure 6.3). Lake Abhe experienced fluctuations in water level throughout the Quaternary (Gasse, 1977), and the carbonate chimneys were formed underwater, when the Lake Abhe water level was higher, with its interaction with hydrothermal fluids from sublacustrine springs, facilitated by faults (Dekov et al., 2014; DeMott et al., 2021). DeMott et al. (2021) found δ^{18}O of chimney calcite to be in the range between the hot springs and Lake Abhe water endmembers. The springs range from 71 to 99.7 °C with pH from 7.61 to 8.80 and TDS of 1918 to 3795 mg/L (Awaleh et al., 2015). The salinity of these hot springs is high ($\sim$3,000 to 6,000 μS/cm Awaleh et al., 2015), unlike the ranges observed in the Djibouti volcanic aquifer system (1.2 to 9.9 μS/cm Awaleh et al., 2018), which supplies

the capital city of Djibouti with drinking water. In this aquifer system, Awaleh et al. (2018) identified three main water groups, two affected by salinization and one with water suitable for drinking, which includes the Awrlofoul geothermal field (50-70°C).

Awaleh et al. (2015) investigated the source of water in Lake Abhe (Djibouti) and its surrounding hot springs. These authors identified two main sources: one corresponding to young meteoric water from the surface and another from a deeper and older source, based on tritium ages. The latter suggesting the presence of a regional groundwater system.

In the Afar Depression, Ayenew et al. (2008) identified at least four groundwater regimens: (1) fresh and shallow groundwater associated with alluvial deposits recharged by isotopically depleted recent highland rainfall and the evaporated Awash River; (2) cold and relatively younger groundwater within localized fractured volcanics showing mixed origin in axial fault zones; (3) old groundwater with very high ionic concentration and low isotopic signature localized in deep volcanic aquifers; and (4) old and hot saline groundwaters connected to geothermal systems. The dataset from Awaleh et al. (2015), for the hot springs at Lake Abhe, fit the two latter groups since at Lake Abhe they found even higher ionic concentrations, salinity, and very depleted tritium values ($<$0.6 T.U.) compatible with the old component Ayenew et al. (2008) found for deeper systems in the Awash River basin.

Awaleh et al. (2015) proposed a model for the Lake Abhe geothermal area in which heat transport towards the surface mainly occurs due to circulation of meteoric water through faults (Figure 6.9). Helium isotopes can shed light into the sources of deep fluids that could be associated with the hot springs emanations and potentially into the source of heat. An additional dataset from other regions in SW Afar and Tendaho Grabben is also used for contextualizing the Lake Abhe geothermal systems within a regional scale.

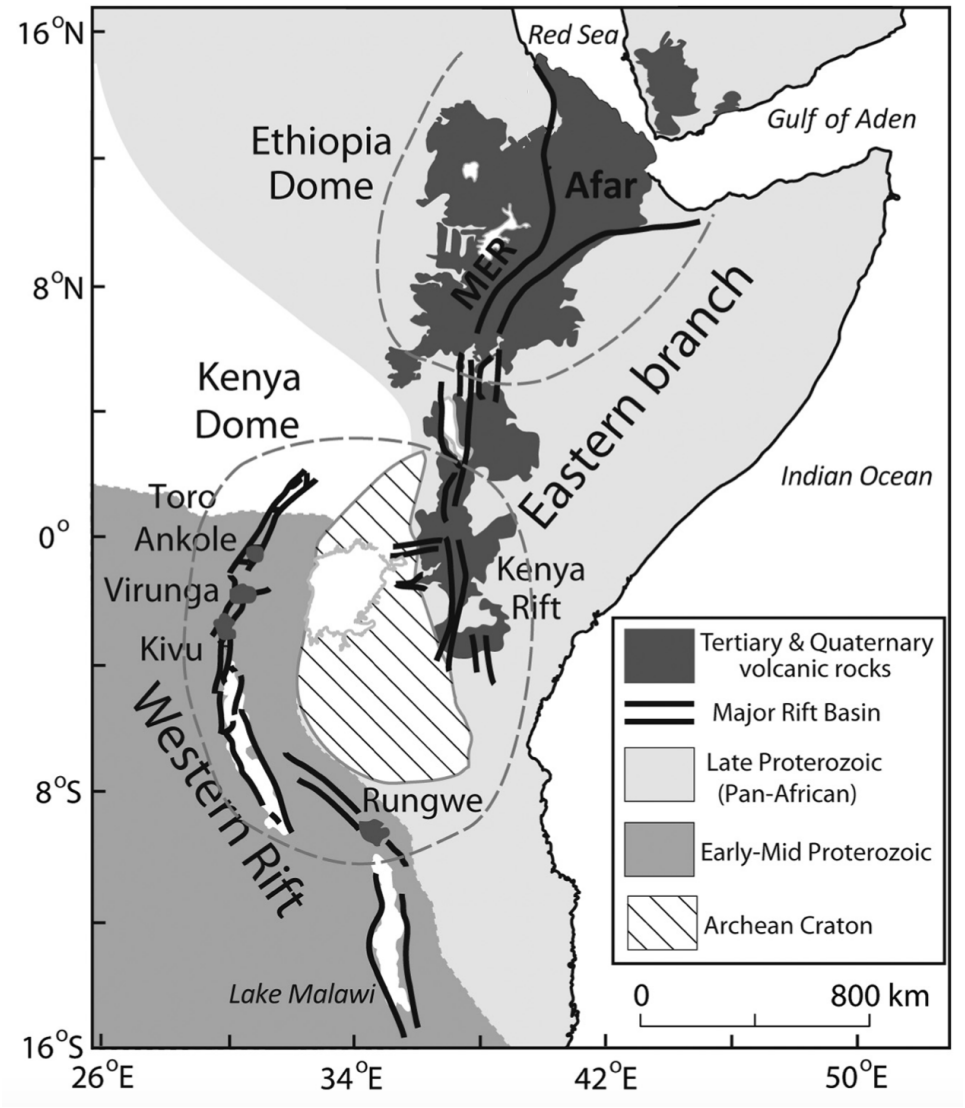

Figure 6.1: East African Rift System subdivisions and main structures. Modified from Castillo et al. (2020).

6.3 Geological setting

Lake Abhe is located in the SW border of Djibouti with Ethiopia, inserted in the context of the East African Rift System (EARS), at the triple junction of the Red Sea and Gulf of Aden mid-oceanic ridges and the MER (Figure 6.1). The lake is inserted in the western portion of the Gob Aad tectonic basin; this basin was formed under an extension regimen and is composed of Quaternary lacustrine deposits which top the Stratoid basalts (4 to

1 Ma) at Lake Abhe (Gasse and Street, 1978). These sediments are mainly composed of montmorillonite silt and clay with levels of calcareous sediments (Gasse and Street, 1978).

The EARS is the largest active intra-continental rift and includes, in its eastern branch, the Kenya Rift in its southernmost portion, the MER, and the Afar triple junction (Figure 6.1). Continental breakup already occurred in the Red Sea and Gulf of Aden where oceanic basins are under formation (Leroy et al., 2013). Seismic tomography (e.g., Ritsema et al., 1999; Zhao, 2004) identified the presence of an extensive low-velocity anomaly starting at the core-mantle boundary and deflected north-eastward below the whole Eastern African plate, called the African Superswel. This anomaly is attributed to the presence of one or multiple mantle plumes (e.g., Marty et al., 1993, 1996; Ebinger and Sleep, 1998; George et al., 1998; Pik et al., 2006; Furman, 2007) under the African continent, which, coupled to the mid-ocean spreading ridge lead to rifting in Afar and East Africa (Min and Hou, 2018), as well as to important associated volcanic activity.

Extension started in the Red Sea and EARS around 29-23 Ma (Wolfenden et al., 2005; Pik et al., 2008; Torres Acosta et al., 2015; Stab et al., 2016; Szymanski et al., 2016) and 34-33 Ma in the Gulf of Aden (Leroy et al., 2013). Oceanic spreading started, in the Gulf of Aden, 17.6 Ma ago and 2 Ma ago in the Gulf of Tadjoura (Leroy et al., 2013). In the Ethiopian province, magmatism started in the Eocene in the south and by the generation of flood basalts in the late Oligocene in the North ($\sim$ 30 Ma), lasting $\sim$ 1 Ma (Zumbo et al., 1995; Baker et al., 1996; Hofmann et al., 1997; Pik et al., 1998) associated with the Red Sea and Gulf of Aden rifting initiation (e.g., Pik et al., 1999, 2003; Furman, 2007; Leroy et al., 2013). Along the Western Afar Margin, continuous extension has been developed in the hearth of the volcanic province for the last 25 Ma (Stab et al., 2016), that lead to the present day Afar depression geo-tectonic configuration. The Afar depression is characterized by the emplacement of a second massive pulse of volcanism 4-2 Ma ago, that emplaced the thick (500 – 1500 m) Stratoid formation. This formation has been dissected recently by more localized tectonic and volcanic activity along en echelon active magmatic segments 6.2.

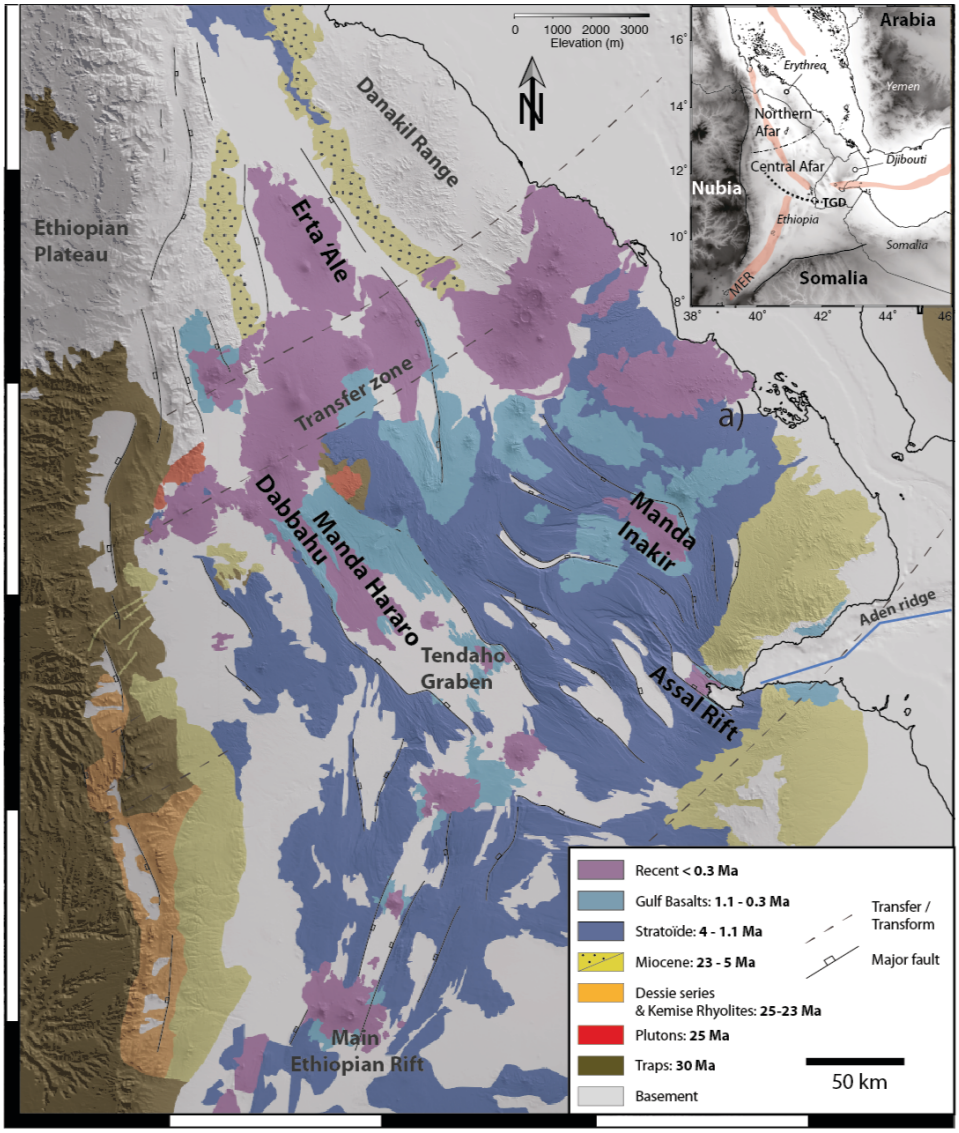

Figure 6.2: Geological map of Afar. Modified from Stab et al. (2016).

In the north of the EARS, helium isotopic signature of volcanic products separate two main domains: one represented by the Kenya Rift with 6-9 Ra and another including the Afar and MER with ∼ 9-20 Ra (Marty et al., 1993, 1996; Scarsi and Craig, 1996; Pik et al., 2006; Natali et al., 2016), with the highest ratios of about 20 Ra measured in the Ethiopian Flood Basalts (Marty et al., 1996; Natali et al., 2016). Those observations were at the base for the proposition of the existence of two geochemically distinct mantle plumes, one beneath Afar/Ethiopia and another beneath the Kenya Rift to explain the distinct volcanic hot spots (Pik et al., 2006; Rogers et al., 2000; Min and Hou, 2018). Recent detection of

a high ^{3}He component at the southern termination of the EARS in the Rungwe volcanic province (Halldórsson et al., 2014), allowed to generalize the model at the scale of the entire superswell and conceptualized it as one single plume with heterogeneous composition (Halldórsson et al., 2014; Castillo et al., 2020). At the scale of the Ethiopian volcanic province in the north of the EARS, the Afar plume head was proposed to be centred near Lake Abhe based on geochemical studies (Rooney et al., 2011; Schilling et al., 1992) which is disputed by Castillo et al. (2020) that defend one African superplume with geochemical and isotopic heterogeneities (Halldórsson et al., 2014) to explain the different chemical compositions observed between the MER and the Afar active volcanic segments . According to both studies, the variability in helium isotopic ratios in the EARS results from mixing between a (heterogeneous) superplume and MORB or the metasomatized sub-lithospheric mantle.

6.4 Methodology

In October 2021, at the Lake Abhe geothermal area, we collected samples from springs for gas chromatography, $^{3}He/^{4}He$, $^{4}He/^{20}Ne$, $\delta^{13}C_{CO_2}$, and $\delta^{15}N$, and Ar isotopes. When possible, we sampled the water for $\delta^{18}O$, $\delta^{2}H$, $\delta^{34}S_{SO_4}$, $\delta^{33}S_{SO_4}$, $\delta^{34}S_{H_2S}$, and $\delta^{33}S_{H_2S}$. Only gas chromatography was performed outside CRPG, at INGV Palermo. Free gas samples from SW Afar (Gewane border lake) and Tendaho grabben (Allalobad pools and Ayrolaf-Dubti wells) geothermal sites have been collected during two dedicated field trips in March 2015 and November 2017 in the framework of a more general project dedicated to CO_2 and volatile fluxes in the depression funded by the Lounsbarry Fundation. $^{3}He/^{4}He$, $^{4}He/^{20}Ne$ ratios have been measured at CRPG and (chromatography data) at INGV Palermo.

6.4.1 $\delta^{18}O$ and $\delta^{2}H$

All water samples were analysed at the CRPG UMR 7358 CNRS-UL (Nancy, France) using a CRDS L2140-i Picarro water isotope analyser coupled to a A0211 vaporization module. Water samples were transferred into 2 mL Pyrex vials with a 0.1 mL conic insert and sealed by an ultra-clean 9 mm septum. For each sample, 10 injections of 1.8 µL of water were performed. Only the 6 last injections were used for measurements to avoid any memory

Figure 6.3: Two of the hot springs we sampled near the carbonate chimneys. On the left, GVS6 and on the right GVS9.

effect. Isotopic compositions are reported in δ notation relative to the V-SMOW-SLAP scale. All samples were adjusted to three internal references calibrated on the international standards SLAP, GISP, and SMOW. Instrument precision was better than 0.1 ‰ and 1 ‰ for $\delta^{18}O$ and $\delta^{2}H$, respectively.

6.4.2 Sulfur isotopes

We sampled water into 15 ml HDPE bottles containing 0.15 ml of 1M $ZnCl_2$ solution to precipitate sulfide as ZnS. In the lab, samples were centrifugated to separate the precipitated ZnS. The liquid phase was removed and a 1 ml aliquot of the liquid phase was taken for sulfate extraction. The ZnS was oxidized using 30% H_2O_2 for 24 hours, centrifugated again and the supernatant was removed, dried down and re-diluted in 1 ml of ultra-pure water. The 1 ml solution (supernatant from the original sulfate and sulfate from oxidized ZnS) is then introduced on 0.8 ml of Biorad AG1X8 resin for removing cations following the procedure described in Paris et al. (2014). Sulfur isotopes were measured on a ThermoScientific Neptune Plus Multiple Collector – Inductively Coupled Plasma Mass Spectrometry (MC-ICPMS) at the Centre de Recherches Pétrographiques et Géochimiques (CRPG) (Paris et al., 2013) using a standard-sample bracketing method. Errors (2σ) were estimated at $\pm$ 0.2‰ based on a seawater long-term consistency standard, which yields a $\delta^{34}S$ value of 21.09 ‰, fully consistent with published values (Paris et al., 2013).

6.4.3 Gas chromatography

Gas samples were collected in Pyrex bottles with vacuum valves at both ends and carefully to avoid air contamination. Analyses were performed at the Istituto Nazionale di Geofisica e Vulcanologia, sezione di Palermo (INGV Palermo). The chemical composition of He, H_2, O_2, N_2, CO, CH_4, CO_2 and C_2H_6 has been measured by a Perkin Elmer Clarus 500 gas chromatograph equipped with a 3.5-m Carboxen 1000 column and double detector (hot-wire detector and flame ionization detector), with analytical errors of $<3\%$.

6.4.4 Helium and neon isotopes

The analyses of $^4He/^{20}Ne$ and $^3He/^4He$ ratios of gases sampled in copper tubes were performed, respectively, on a MKS Microvision 2 quadrupole mass spectrometer (QMS) and a split flight tube noble gas mass spectrometer (Helix SFT - Thermo Fisher Scientific) at the Centre de Recherches Pétrographiques et Géochimiques (CRPG) noble gas analytical facility (Mabry et al., 2013). The standard deviation of the $^3He/^4He$ ratios ranged from 2.3 to 3.7 % based on the replicate analysis of standard He (atmospheric). Results are corrected for blanks, which contributed < 0.1 % of the total He abundances.

6.4.5 $\delta^{15}N$

Nitrogen isotope measurements were done using the non-condensable fraction of the Giggenbach bottles, which consists mainly of N_2, CO, and noble gases since CO_2 has been removed. Both CO and N_2 gases were transferred in a sealed pyrex tube containing CuO and Cu2O grains to be oxidized into N_2 and CO_2 at 450°C for 1 hour. Prior to being used, the CuO and Cu_2O grains have been heated few minutes under vacuum at 350°C and pumped overnight at room temperature to remove adsorbed gases. The produced CO_2 was then cryogenically trapped and N_2 was collecting using a Toepler pump. The nitrogen isotopic composition of N_2 was measured with a Thermo Scientific MAT 253 Mass Spectrometer at the Centre de Recherches Pétrographiques et Géochimiques (CRPG) stable isotopes analytical facility. All values are reported using the delta notation, in permil (‰) relative to air, with error (approximately) 0.5 ‰ calculated from the reproducibility of duplicates.

6.4.6 $\delta^{13}C_{CO_2}$

$\delta^{13}C_{CO_2}$ measurements of the CO_2 were carried out at CRPG and INGV Palermo. CO_2 and H_2O were trapped into liquid nitrogen and then cryogenically separated. At CRPG stable isotopes analytical facility, the carbon isotopic compositions of CO_2 was measured with a Thermo Scientific MAT 253 Mass Spectrometer. All values are reported in the delta notation in permil (‰) relative to V-PDB, with error below 0.5‰.

At INGV Palermo, $\delta^{13}C_{CO_2}$ (expressed in ‰ vs. V-PDB) was determined using a Thermo (Finningan) Delta Plus XP CF-IRMS, connected to a Trace GC gas chromatograph and a Thermo (Finningan) GC/C III interface. The gas chromatograph, equipped with a Poraplot-Q column (length 30 m, i.d. 0.32 mm), kept at a constant temperature of 50°C, uses He as the carrier gas. The analytical uncertainty was ±0.1‰.

6.4.7 CH_4 isotopes

Carbon and hydrogen isotopes of CH_4 were carried out at INGV Palermo on a Thermo (Finningan) Delta Plus XP CF-IRMS, connected to a Trace GC gas chromatograph and a Thermo (Finningan) GC/C III interface. GC III combustion interface was used to produce carbon dioxide from CH_4. GC-TC interface provides on-line high-temperature methane conversion into hydrogen suitable for isotope analyses. Typical reproducibility (1σ) for $\delta^{13}C_{CH_4}$ and $\delta^{2}H_{CH_4}$ measurements is better than 0.2‰ and 2.5‰, respectively.

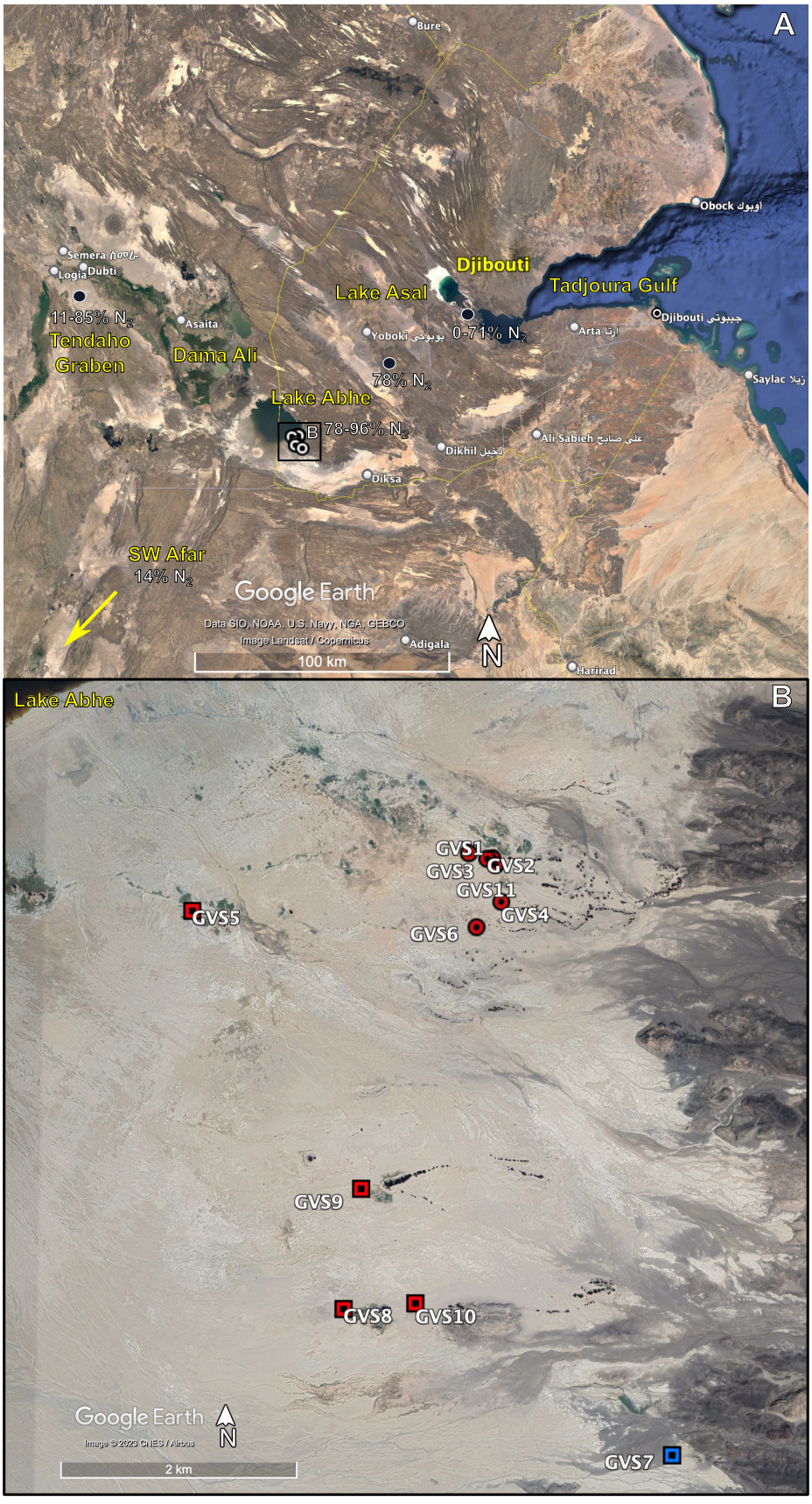

Figure 6.4: Location of samples. (a) N_2 content of fumaroles and hot springs in Djibouti are shown (this study; Darling and Talbot, 1991). (b) Location of samples in the Lake Abhe region; red represents hot springs and blue the cold spring whereas squares represent water samples and circles gas samples.

6.5 Results

6.5.1 Lake Abhe region

The hot springs occur near the carbonate chimneys which have been grouped previously as small and great chimneys (e.g., Awaleh et al., 2015). In terms of geochemical results, no distinction is evident between these two types, which is in agreement with observations from Awaleh et al. (2015).

Only one cold spring (GVS7) was sampled and, compared to the hot springs, the water only shows different signatures for δ^{18}O and δD (Table 6.1), which are heavier (-0.40 and -6.83 ‰, respectively) than all hot spring samples (δ^{18}O -3.22 to -2.41 ‰ and δD -24.28 to -21.21 ‰) and with values closer to modern precipitation (δD > - 10 ‰; Awaleh et al., 2015) and to the Lake Abhe signature (δ^{18}O 6.5 and δD 43.9 ‰; Awaleh et al., 2015). No geographical trend is clear (Figure 6.8), specially considering that the three great chimneys (GVS8, GVS9, and GVS10) are among the most depleted in δD and are also the closest to the cold spring with surface water signature (GVS7). Our dataset shows slightly heavier δD compared to those previously reported (-27.6 to -24 ‰; Awaleh et al., 2015).

SO_4 contents and sulfur isotopes of the water phase show little variation (Table 6.2). $\delta^{34}S_{SO_4}$ ranges from 11.45 to 15.89 ‰ and $\delta^{34}S_{H_2S}$ from 8.29 to 15.18‰. Awaleh et al. (2015) obtained similar values for $\delta^{34}S_{SO_4}$ (13.2 to 14.3‰) that they attributed to a gypsum-like endmember from Djibouti sediments (15.3 to 21.8‰; Gasse and Fontes). Our results might reflect mixing between basalt-leaching fluid and a sedimentary source or only the latter. The presence of H_2S highlights the occurrence of thermal surface reduction, however, the cold spring (GVS7) has the highest H_2S content (6.11).

^{3}He/^{4}He results (1.04 to 8.58 Ra, where Ra is the atmospheric ^{3}He/^{4}He ratio of 1.39 x 10^{-6}) and ^{4}He/^{20}Ne ratios (0.30 to 14.70) from water and gas samples (Table 6.4) show similar signatures for both small and great chimneys, and is comparable to results reported by Darling (1996) (3.8 and 7.9 Ra). The cold spring (GVS7) shows a signature (1.24 Ra) compatible with either surface water equilibrated with the atmosphere (ASW, 1 Ra) with minimal mantle contribution (< 16 %) or air contamination during sampling. Sample GVS2 is considered contaminated since its duplicate exhibits 8.58 Ra; samples GVS6 is also dis-

carded from future discussion since it appears contaminated by air during sampling. The helium isotopic signature indicates mixing between an air-like component and a magmatic endmember close to 9 Ra (Figure 6.6).

Gas chromatography data (Table 6.3) shows that the main phase is N_2 (77.65 to 96.27%), followed by O_2 (0.24 to 20.66%), CO_2 (0.10 to 10.43%), and CH_4 (0.01 to 1.56%). Helium varies from 27 to 260 ppm, CO from 1.3 to 69 ppm, H_2 from below detection limit to 61 ppm, C_2H_6 is only detected in two samples with 19 and 152 ppm. The gas composition is similar for both small and great chimneys. Samples GVS1 and GVS3 display an air-like composition that are most likely from the analytical stage since the remaining results, from other samples connected to same sampling train, show no evidence for atmospheric contamination.

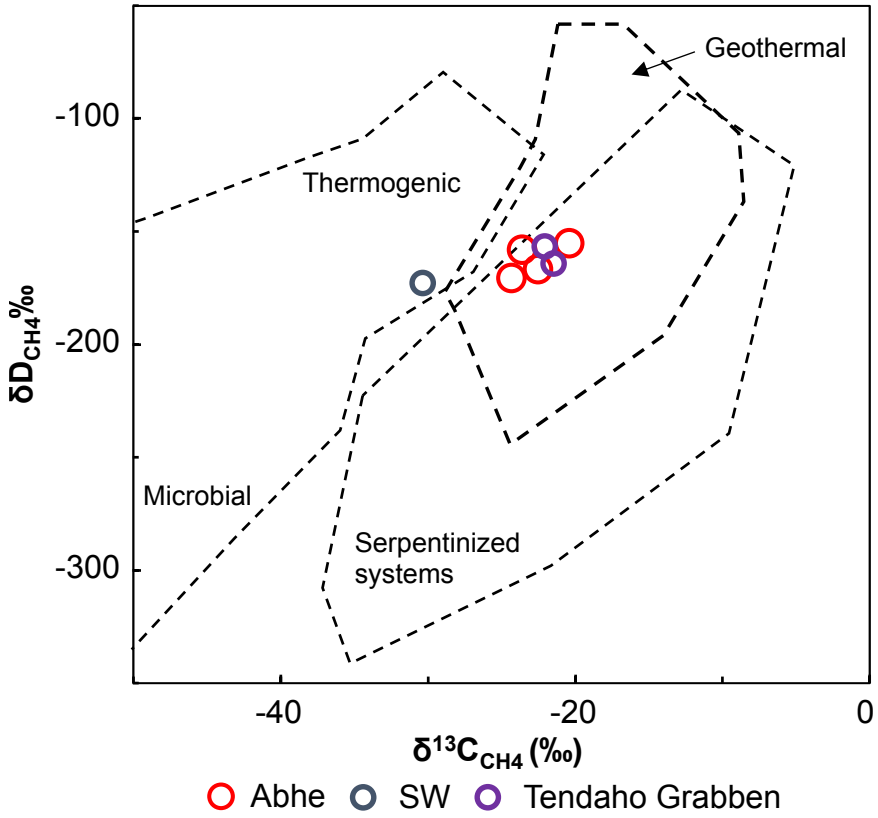

Figure 6.5: $\delta^{13}C_{CH_4}$ versus $\delta^{2}H_{CH_4}$ plot. Samples from Lake Abhe and Tendaho Graben are within range of geothermal CH_4 and the SW Afar sample plot in the field of thermogenic CH_4.

Regarding stable isotopes of the gas phase, $\delta^{13}C_{CO_2}$ results (Table 6.4) range from -8.18 to -4.82 ‰, mainly within range of typical values for volcanic gases (-7 to -3‰; Marty and Zimmermann, 1999). $\delta^{15}N$ results (Table 6.4) are close to a sedimentary signature (close to

7 ‰; Peters et al., 1978), except for sample DB1 (GVS1 site) (3.5 ‰). However, sample DB1 is most likely contaminated by air during sampling, as seen in the N_2/He versus $\delta^{15}N$ plot (Figure 6.11). $\delta^{13}C_{CH_4}$ and $\delta^{2}H_{CH_4}$ (Table 6.4) display a signature compatible with geothermal gas (Figure 6.5).

6.5.2 SW Afar and Tendaho Graben regions

Gas samples from the Gewane site in SW of Afar range from 8.0 to 11.5 Ra (Table 6.4), corresponding to corrected magmatic endmembers ranging from 10.0 to 11.5 Ra. Those two distinct values are a bit surprising for the same sampling site characterized by a unique source, but they have been sampled during two distinct surveys in 2015 and 2017 and could represent long-term compositional variations of degassing for this site (even if such a difference appears rather important). Overall, they are in agreement with published data from phenocrysts for this northern portion of the main Ethiopian Rift which enters in the Afar depression (6.7 to 12.1 Ra; Scarsi and Craig, 1996). For the Tendaho Graben, the two geothermal sites exhibit distinct isotopic signatures. For the western Allalobad site, water and gas samples exhibit values from 4.9 to 9.1 Ra (Table 6.4) which all plot along a coherent mixing line between ASW and a magmatic end-member of $\sim$ 9 Ra. Note that those data plot along a mixing line which is undistinguishable from the one of the lake Abhe gas and water samples. For the central Tendaho Dubti-Ayrolaf geothermal site, free gas samples from fumaroles around the old well-heads exhibit grouped values between 10.5 and 10.7 Ra for the two distinct surveys in 2017 and 2015 respectively (Table 6.4). Those $^3He/^4He$ results indicate mixing between an air-like component and a magmatic endmember close to 12 Ra (Figure 6.6) in agreement, even if slightly lower, than the results from Marty et al. (1996) for geothermal fluids and fumaroles of this central Tendaho geothermal site (12.8 to 13.1 Ra). Those data are also in agreement with the magmatic component of mafic phenocrysts of the adjacent Manda Hararo – Dabbahu magmatic segment (10 to 13.3 Ra; Medynski et al., 2013).

Gas chromatography data (Table 6.3) of one sample from the SW region has CO_2 as the main phase (78.58%), followed by N_2 (13.7%), O_2 (2.67%), and CH_4 (1.8%). Helium is 144 ppm, CO 9 ppm, H_2 204 ppm, C_2H_6 1490 ppm. Gas samples from Tendaho Graben range from 0.37 to 83.24% for CO_2, 10.5 to 84.9% for N_2, 2.9 to 19.28% for O_2, 0.08 to 5.2% for

CH_4, 17 to 251 pmm for He, 42 to 104 ppm for CO, 21 to 4423 ppm for H_2, and 255 to 1052 ppm for C_2H_6.

Regarding stable isotopes, $\delta^{13}C_{CO_2}$ results for SW Afar is of -4.32 ‰ (Table 6.4), consistent with a volcanic source whereas $\delta^{13}C_{CH_4}$ and δD_{CH_4} (Table 6.4) display a signature compatible with a thermogenic source (Figure 6.5). For the Tendaho Graben, $\delta^{13}C_{CO_2}$ is from -4.36 to -3.57 ‰, also within range of volcanic gases (Table 6.4). $\delta^{13}C_{CH_4}$ and δD_{CH_4} (Table 6.4) display a signature compatible with a geothermal gas (Figure 6.5).

Table 6.1: All sampled sites with coordinates, physical parameters of water, and stable isotopes results. Sample type "water-HS" refers to water samples from hot springs and "water-CS" from cold springs. *Data from Awaleh et al. (2015). Stable isotope results from this study. Errors in 1 sigma.

Site	region	type	LAT	LONG	T (°C)*	pH*	EC (μs/cm)*	δ^{18}O (‰)	δ^{2}H (‰)
Lake Abhe region									
GVS1	small Ch	free gas	11°08.926'	41°52.606'	98.8	8.33	5332	-3.19 ± 0.02	-23.63 ± 0.18
GVS2	small Ch	free gas	11°08.900'	41°52.693'	82.2	7.61	5866	-2.41 ± 0.17	-21.21 ± 1.04
GVS3	petite Ch	free gas	11°08.902'	41°52.718'	94.5	8.22	5495	-2.87 ± 0.06	-22.54 ± 0.43
GVS4	petite Ch	free gas	11°08.699'	41°52.759'	98.1	8.34	5576	-2.81 ± 0.11	-22.81 ± 0.56
GVS5	closer to lake	water-HS	11°08.657'	41°51.300'	-	-	-	-2.87 ± 0.16	-22.24 ± 0.67
GVS6	petite Ch	free gas	11°08.581'	41°52.642'	-	-	-	-2.75 ± 0.16	-22.44 ± 0.97
GVS7	petite Ch	water-CS	11°06.162'	41°53.546'	37.2	8.9	4476	-0.40 ± 0.02	-6.83 ± 0.20
GVS8	grande Ch	water-HS	11°06.824'	41°52.019'	92.5	8.62	3105	-3.22 ± 0.06	-24.28 ± 0.33
GVS9	grande Ch	water-HS	11°07.373'	41°52.100'	-	-	-	-3.19 ± 0.03	-24.28 ± 0.13
GVS10	grande Ch	water-HS	11°06.850'	41°52.354'	92.1	8.6	3224	-3.21 ± 0.03	-24.06 ± 0.32
GVS11	petite Ch	free gas	11°08.870'	41°52.732'	98.5	8.49	5610	-3.13 ± 0.06	-23.66 ± 0.26
SW Afar region									
Gawani 2015	-	free gas	9°59.496'	40°32.868'	-	-	-	-	-
Gawani 2015	-	free gas	9°59.496'	40°32.868'	-	-	-	-	-
Gawani 2017 AC	-	free gas	9°59.496'	40°32.868'	-	-	-	-	-
Tendaho Graben									
Ayrolaf geothermal pool 1V	-	free gas	11°46.819'	41°7.779'	-	-	-	-	-

Table 6.1: All sampled sites with coordinates, physical parameters of water, and stable isotopes results. Sample type "water-HS" refers to water samples from hot springs and "water-CS" from cold springs. *Data from Awaleh et al. (2015). Stable isotope results from this study. Errors in 1 sigma.

Site	region	type	LAT	LONG	T (°C)*	pH*	EC (μs/cm)*	δ^{18}O (‰)	δ^{2}H (‰)
Ayrolaf geothermal pool 2V	-	free gas	11°46.819'	41°7.779'	-	-	-	-	-
Ayrolaf 2015	-	free gas	11°46.819'	41°7.779'	-	-	-	-	-
Ayrolaf 2015	-	free gas	11°46.819'	41°7.779'	-	-	-	-	-
Ayrolaf soil 2017 AC	-	free gas	11°46.819'	41°7.779'	-	-	-	-	-
Ayrolaf soil 2017 AC	-	free gas	11°46.819'	41°7.779'	-	-	-	-	-
Alalo Bad 1V 2017 AC	-	free gas	11°38.551'	41°0.856'	-	-	-	-	-
Alalo Bad 2V 2017 AC	-	free gas	11°38.551'	41°0.856'	-	-	-	-	-
Alalo Bad 2015	-	free gas	11°38.551'	41°0.856'	-	-	-	-	-
Alalo bad water 2015	-	water (hot?)	11°38.551'	41°0.856'	-	-	-	-	-
Alalo bad water 2015	-	water (hot?)	11°38.551'	41°0.856'	-	-	-	-	-
Alalo bad gas 2015	-	free gas	11°38.551'	41°0.856'	-	-	-	-	-
Alalo bad gas 2015	-	free gas	11°38.551'	41°0.856'	-	-	-	-	-

Table 6.2: Sulfur isotopes results of water samples. Errors in 2 sigma.

Site	SO_4 (mmol/L)	H_2S (assuming 50 ml)	$\delta^{34}S_{SO_4}$ (‰)	$\delta^{33}S_{SO_4}$ (‰)	$\delta^{34}S_{H_2S}$ (‰)	$\delta^{33}S_{H_2S}$ (‰)
GVS1	3.29	0.09	14.04 ± 0.05	0.03 ± 0.06	-	-

Table 6.2: Sulfur isotopes results of water samples. Errors in 2 sigma.

Site	SO_4 (mmol/L)	H_2S (assuming 50 ml)	$\delta^{34}S_{SO_4}$ (‰)	$\delta^{33}S_{SO_4}$ (‰)	$\delta^{34}S_{H_2S}$ (‰)	$\delta^{33}S_{H_2S}$ (‰)
GVS2	3.38	3.40	14.23 ± 0.03	0.01 ± 0.07	-	-
GVS3	3.28	0.09	14.16 ± 0.05	0.04 ± 0.03	-	-
GVS4	3.36	0.04	13.92 ± 0.04	0.01 ± 0.17	-	-
GVS5	3.56	3.40	15.89 ± 0.08	0.06 ± 0.02	15.18 ± 0.03	-0.05 ± 0.07
GVS6	3.18	1.63	14.13 ± 0.04	0.00 ± 0.08	12.75 ± 0.04	-0.01 ± 0.13
GVS7	4.66	6.11	11.45 ± 0.08	0.00 ± 0.11	10.72 ± 0.05	0.03 ± 0.04
GVS8	3.05	0.27	12.93 ± 0.04	-0.01 ± 0.16	11.79 ± 0.28	0.03 ± 0.30
GVS9	3.14	0.03	13.03 ± 0.01	0.00 ± 0.09	-	-
GVS10	3.17	0.22	12.97 ± 0.07	0.00 ± 0.10	8.29 ± 0.18	-0.02 ± 0.30
GVS11	3.30	0.26	14.00 ± 0.05	0.03 ± 0.14	13.15 ± 0.26	0.07 ± 0.30

Table 6.3: Gas chromatography results. b.d.l.: below detection limit. Analyses performed at INGV Palermo.

Sample	N_2(%)	O_2(%)	CO_2(%)	CH_4(%)	He(ppmV)	CO(ppmV)	H_2(ppmV)	C_2H_6(ppmV)
Lake Abhe region								
GVS1	79.54	18.70	0.58	0.17	27	31	13	19
GVS2	96.27	0.24	0.21	1.56	260	1.3	71	b.d.l.
GVS3	77.65	20.66	0.98	0.01	b.d.l.	10	b.d.l.	b.d.l.
GVS4	93.42	2.24	1.01	1.43	240	20	37	b.d.l.

Table 6.3: Gas chromatography results. b.d.l.: below detection limit. Analyses performed at INGV Palermo.

Sample	N_2(%)	O_2(%)	CO_2(%)	CH_4(%)	He(ppmV)	CO(ppmV)	H_2(ppmV)	C_2H_6(ppmV)
GVS6	91.58	6.10	0.10	0.85	175	69	59	b.d.l.
GVS11	81.69	4.80	10.43	1.47	152	38	61	152
SW Afar region								
Gawani 2017 AC	13.70	2.67	78.58	1.80	144	9	204	1490
Tendaho Graben								
Ayrolaf geothermal pool 1V	10.50	2.90	83.24	1.90	51	64.3	4423	255
Ayrolaf soil 2017 AC	74.40	19.28	1.23	0.08	17	42	63	-
Alalo Bad 1V 2017 AC	84.90	7.90	0.37	5.20	251	104	21	1052

Table 6.4: Results for helium, nitrogen, CO_2, and CH_4 isotopes. G refers to gas samples and W to water samples. Analysed at [a]Woods Hole and [b]INGV Palermo, respectively. Remaining results from CRPG

Sample	Type	$^4He/^{20}Ne$	Rm/Ra	Rc/Ra	$\delta^{15}N$ (‰)	$\delta^{13}C_{CO_2}$ (‰)	$\delta^{13}C_{CH_4}$ [b] (‰)	$\delta^{2}H_{CH_4}$ [b] (‰)
Lake Abhe region								
GVS1B	G	11.56 ± 0.22	8.03 ± 0.18	8.23	5.8	-8.18	-25.2	-
DB1 (GVS1 site)	G	-	-		3.5[a]	-	-	-
GVS2	G	0.37 ± 0.01	1.04 ± 0.02	1.34	5.8	-4.82	-	-
GVS2 (gigg)	G	16.23 ± 0.84	8.58 ± 0.31	8.58	-	-	-	-
GVS3	G	-	-	-	5.8	-6.85	-24.3	-171.0

Table 6.4: Results for helium, nitrogen, CO_2, and CH_4 isotopes. G refers to gas samples and W to water samples. Analysed at [a]Woods Hole and [b]INGV Palermo, respectively. Remaining results from CRPG

Sample	Type	$^4He/^{20}Ne$	Rm/Ra	Rc/Ra	$\delta^{15}N$ (‰)	$\delta^{13}C_{CO_2}$ (‰)	$\delta^{13}C_{CH_4}$ [b] (‰)	$\delta^{2}H_{CH_4}$ [b] (‰)
GVS4B	G	3.90 ± 0.13	7.29 ± 0.16	7.85	5.4	-5.82	-23.6	-158.0
GVS5	W	5.55 ± 0.17	8.07 ± 0.18	8.51	-	-	-	-
GVS6	G	0.33 ± 0.01	1.26 ± 0.03	10.97	-	-	-20.4	-155.0
GVS7	W	0.34 ± 0.02	1.24 ± 0.03	4.87	-	-	-	-
GVS8B	W	0.87 ± 0.03	4.00 ± 0.09	5.71	-	-	-	-
GVS9	W	2.68 ± 0.12	6.70 ± 0.15	7.47	-	-	-	-
GVS10	W	0.71 ± 0.03	3.98 ± 0.09	6.39	-	-	-	-
GVS11	G	9.27 ± 0.17	8.48 ± 0.19	8.75	-	-	-22.5	-167.0
SW Afar region								
Gawani 2015	G	1.3 ± 0.1	8.0 ±0.1	10.3	-	-	-	-
Gawani 2015	G	324.0 ±16.0	9.8 ± 0.1	9.8	-	-	-	-
Gawani 2017 AC	G	61.0 ± 6.1	11.5 ± 0.0	11.6	-	-4.32[b]	-30.4	-173.0
Tendaho Graben								
Ayrolaf geothermal pool 1V	G	23.6 ± 3.0	11.5 ± 0.1	11.7	-	-3.57[b]	-21.5	-164.2
Ayrolaf geothermal pool 2V	G	12.6 ± 1.3	11.5 ± 0.1	11.8	-	-	-	-
Ayrolaf 2015	G	47.0 ± 2.0	11.7 ± 0.2	11.8	-	-	-	-
Ayrolaf 2015	G	1.1 ± 3.0	1.4 ± 0.2	1.5	-	-	-	-
Ayrolaf soil 2017 AC	G	0.4 ± 0.0	2.8 ± 0.6	14.0	-	-	-	-

Table 6.4: Results for helium, nitrogen, CO_2, and CH_4 isotopes. G refers to gas samples and W to water samples. Analysed at [a]Woods Hole and [b]INGV Palermo, respectively. Remaining results from CRPG

Sample	Type	$^4He/^{20}Ne$	Rm/Ra	Rc/Ra	$\delta^{15}N$ (‰)	$\delta^{13}C_{CO_2}$ (‰)	$\delta^{13}C_{CH_4}$ [b] (‰)	$\delta^{2}H_{CH_4}$ [b] (‰)
Ayrolaf soil 2017 AC	G	1.2 ± 0.1	0.6 ± 0.1	0.5	-	-	-	-
Alalo Bad 1V 2017 AC	G	17.4 ± 1.7	9.1 ± 0.1	9.3	-	-4.36[b]	-22.1	-156.5
Alalo Bad 2V 2017 AC	G	9.0 ± 0.9	9.1 ± 0.1	9.3	-	-	-	-
Alalo Bad 2015	G	1.5 ± 0.1	7.3 ± 0.2	8.9	-	-	-	-
Alalo bad water 2015	W	0.5 ± 0.0	4.9 ± 0.3	13.6	-	-	-	-
Alalo bad water 2015	W	1.0 ± 0.1	5.6 ± 0.4	7.7	-	-	-	-
Alalo bad gas 2015	G	8.3 ± 0.4	8.5 ± 0.1	8.8	-	-	-	-
Alalo bad gas 2015	G	6.7 ± 0.3	7.6 ± 0.1	7.9	-	-	-	-

6.6 Discussion

6.6.1 Helium isotopic signature and the local Afar plume composition

The helium isotopic signature indicates mixing between an air-like component and a magmatic endmember close to 9 Ra at the Lake Abhe and Allalobad geothermal springs and close to 12 Ra at Ayrolaf in Central Tendaho Graben and SW Afar (Figure 6.6).

In the Afar volcanic province, $^{3}He/^{4}He$ ratios can reach up to 20 Ra, indicating the presence of a deep ^{3}He-rich mantle plume (Marty et al., 1996; Pik et al., 2006; Scarsi and Craig, 1996; Rooney et al., 2011; Natali et al., 2016). However, the results from the Lake Abhe and Western Tendaho region (up to 8.58 Ra; Table 6.4) appear in the range of upper mantle composition (8 $\pm$ 2 Ra) and above the range of the continental lithospheric mantle (5 $\pm$ 2 Ra). Such values have already been observed south-westward in the MER system where they are cohabitating, along distinct magmatic segments, with lavas exhibiting the typical deep-mantle signature as well as along the connection between the Asal Rift and the gulf of Tadjoura (Figures 6.6 and 6.7). However, such new results are below those typically expected for the Afar region (10.0-13.5 Ra) as it has been described previously in SW Afar (Scarsi and Craig, 1996), Tendaho Graben (Marty et al., 1996), Manda Hararo – Dabbahu (Medynski et al., 2013) and Alayta-Erta Ale (Scarsi and Craig, 1996) active magmatic segments, and also confirmed by our new data on geothermal fluids from those sites (Table 6.4).

The typical upper mantle (MORB) signature for $^{3}He/^{4}He$ in the Lake Abhe and Allalobad Western Tendaho geothermal fields definitely contradicts previous hypothesis of a plume centre in this area (Rooney et al., 2011; Schilling et al., 1992) and represents stronger arguments for the position of Castillo et al. (2020) and Pik et al. (in prep.) who already refuted this hypothesis. Both sites are located along a tectonic discontinuity represented by the western edge of the Tendaho Grabben which from North to south hosts the Manda Hararo, Manda Gargory magmlatic segments and Dama Ali central volcano. For a better understanding and interpretation of this low-^{3}He mantle component it will be important in the future to investigate the helium isotopic signature of the Manda Gargory and Dama

Ali volcano, $\sim$ 30 km away from Lake Abhe, which is the closest volcanic system and best candidates for the source of helium and heat of the Lake Abhe geothermal system (see next section). Although the Afar and Ethiopian Rift basalts exhibit the same $^{3}He/^{4}He$ range (up to 20 Ra; e.g., Marty et al., 1996; Scarsi and Craig, 1996; Pik et al., 2006), their radiogenic isotopes signatures are distinct, mainly for $^{206}Pb/^{204}Pb$, which is higher in some of the Afar basalts investigated by Castillo et al. (2020), but not significantly for the one typical of the Central Afar volcanics from the Stratoid formation to the active Manda Hararo segment (Pik et al., in prep.). According to Castillo et al. (2020), the isotopic and geochemical variability in the Afar and Ethiopian basalts is due to the heterogeneity of its source - mixing of the common, most voluminous superplume component (variable $^{3}He/^{4}He$ up to 20 Ra) with Continental Lithospheric Mantle ($^{3}He/^{4}He$ = 6 Ra) beneath eastern Africa produces the observed 6 to 9 Ra range of $^{3}He/^{4}He$ in many EARS lavas, and led to a spatial puzzling of lavas exhibiting alternatively plume or anomalous upper mantle helium (and associated other chemical) signatures along the EARS. Lavas exhibiting a clear depleted trace element and Sr-Nd isotopes signature have been however described in the southern part of the Manda Hararo segment (close to the Allalobad geothermal site) (Barrat et al., 2003) and could represent an independent depleted low-^{3}He component (embedded in the plume head, Pik et al., in prep.) that will not require the implication of the CLM. It will then also be extremely important in the future to identify in the Tendaho Grabben volcanic products exhibiting such a low-^{3}He component and confront their full range of trace element and radiogenic isotopes to the various geochemical proposed scenarios.

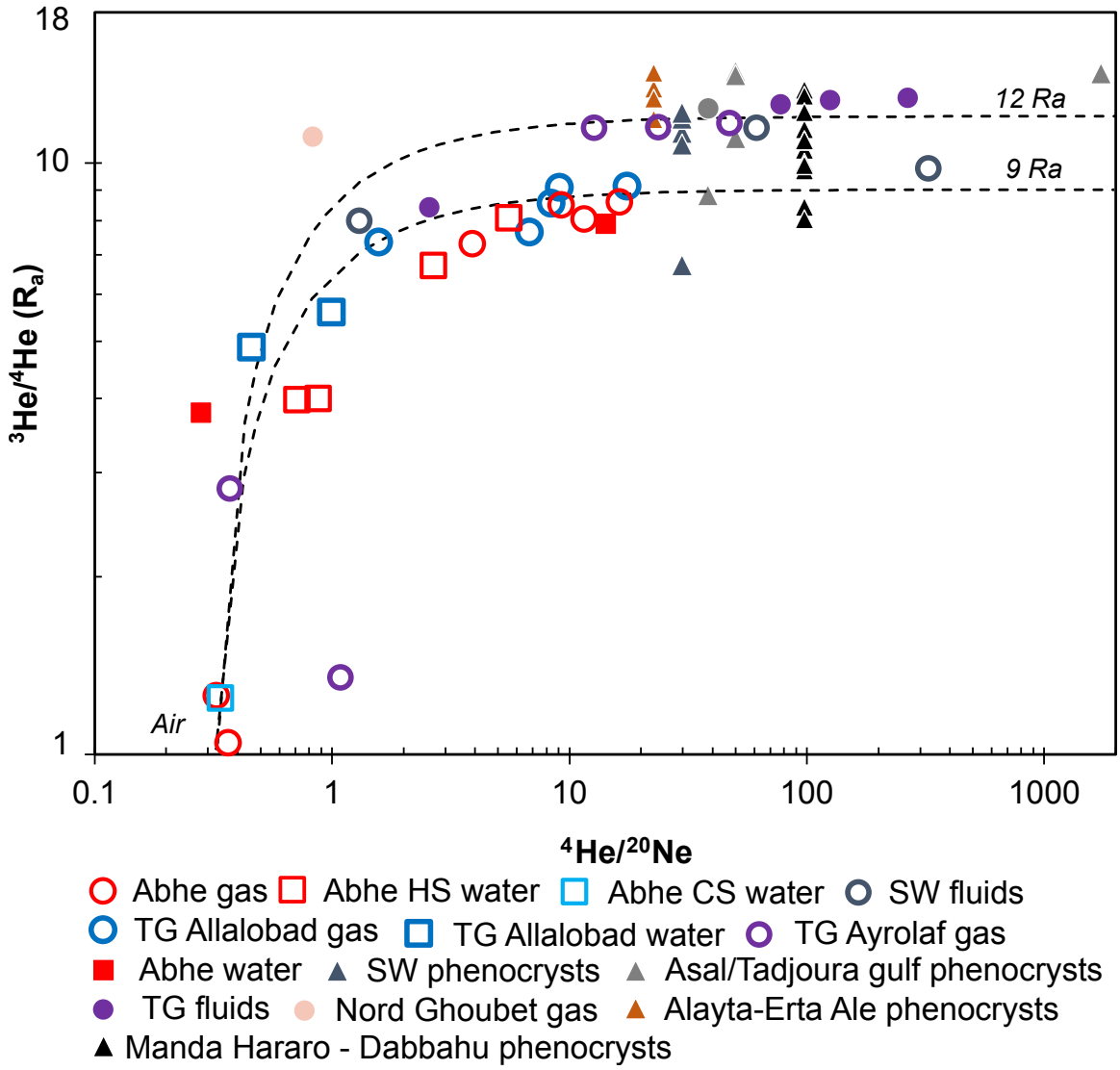

Figure 6.6: $^3He/^4He$ versus $^4He/^{20}Ne$ plot. Open symbols represent samples from the current study and filled symbols published data. Samples from Lake Abhe hot (HS) and cold (CS) springs plot along the Air and 9 Ra mixing line with samples from Allalobad (Tendaho Graben) whereas samples from Ayrolaf (Tendaho Graben), SW Afar, and Asal/Tadjoura gulf plot along mixing lines between ASW and an enriched mantle component (up to 14 Ra). Published data from Marty et al. (1993, 1996), Scarsi and Craig (1996), Darling (1996), and Medynski et al. (2013) for glass (basalts) and geothermal fluids.

Figure 6.7: Air-corrected $^3He/^4He$ values (Rc/Ra) for Lake Abhe and nearby regions. Results from this study are represented by circles and published data by triangles. Data for SW Afar, Tendaho Graben, Nord Ghoubet (between lakes Abhe and Asal) and Asal/Tadjoura gulf from Marty et al. (1993, 1996), Scarsi and Craig (1996), Darling (1996), for glass (basalts) and geothermal fluids.

6.6.2 Implications for groundwater source and transport near Lake Abhe

At the Lake Abhe hot springs, Awaleh et al. (2015) found very low tritium contents (< 0.6 TU) and low deuterium values (< -10 ‰) compatible with an older and deeper water source than that of surface waters (δ^2H > -10 ‰). According to the new helium isotopes data we provide in this study, the main sources of fluids in the groundwater are a deep component (mantle) and air-saturated water (ASW) (Figures 6.6 and 6.8). This is partially in agreement with the model previously proposed by Awaleh et al. (2015), based on water chemistry and stable isotope analyses, in which the authors propose a common regional reservoir fed by meteoric water. These authors also estimate the Lake Abhe geothermal reservoir between 117 and 154°C based on quartz geothermometers and the depth of the main heat reservoir is estimated at $\sim$ 1 km (Geophysical report, Centre d'Etudes et de Recherche de Djibouti, CERD, 2012). Heat transport towards the surface is mainly due to circulation of meteoric

water through faults (Awaleh et al., 2015).

Moreover, the water from Lake Abhe itself has a geochemical signature ($\delta^{34}S_{SO_4}$ 20.6 $\pm$ 0.5 ‰; Awaleh et al., 2015) compatible with seawater ($\delta^{34}S_{SO_4}$ 21 ‰; Rees et al., 1978) resultant of evaporation in arid environments ($\delta^{18}O$ shift, Figure 6.8a). The lake does not seem to influence the regional aquifer system directly, as no evidence of mixing is clear (Figure 6.8). $^{4}He/^{20}Ne$ ratios are low and close to the air-saturated value, indicating that the clear mantle signal observed in the $^{3}He/^{4}He$ ratios is most likely transported via groundwater in the context of a regional aquifer, rather than from local direct origin via vertical transfers between surface recharge and heat transfer zones at depth. Indeed, along the extremely active extensional zones of Central and southern Afar, the flux of magmatic volatiles carried by the groundwater is more likely to originate from fresh magma bodies intruded into the crust rather than to a flux initiating in the mantle from passive cryptic magmas. In such a framework, the closest active volcanic zone with underlying magma stored into the crust, is the Dama Ali volcanic system, situated on the same structural basin than the geothermal site, $\sim$ 30 km NW on the other side of Lake Abhe, in the alignment of the Tendaho Graben (Figure 6.2). Such a connection with a distant magmatic source is therefore the more logical to explain the volatiles carried by the groundwater system (Figure 6.9). Feeding of the hydrothermal system by a regional and chemically homogeneous groundwater body is also in agreement with the identical signatures measured at both great and small chimney spring systems. However, in the absence of helium isotopic ratios measured on the volcanic products of the Dama Ali system, this origin cannot be strictly confirmed. The structure of the Lake Abhe basin at the southern termination of the Tendaho Graben is not well known, but northward the Manda Harao and Dabbahu magmatic segments are typically organized with a central system of volcanic reservoirs, which periodically inject dyke swarms laterally for tens of kilometers along the axis of the segment (Medynski et al., 2016), as it has been observed during the seismo-volcanic crisis of 2005-2010 (Grandin et al., 2009, 2010). The distance between the magmatic source of volatiles and the hydrothermal system itself ,with associated heat exchanges, could therefore be closer to the springs site than the absolute distance between the central volcano itself. At a wider regional scale, this regional aquifer is most likely isolated from the Tendaho Graben underlying aquifers fed by the Awash river,

even if the helium isotopic signature at Lake Abhe is very close in isotopic composition with the one of the western geothermal site of the Tendaho Graben at Allalobad.

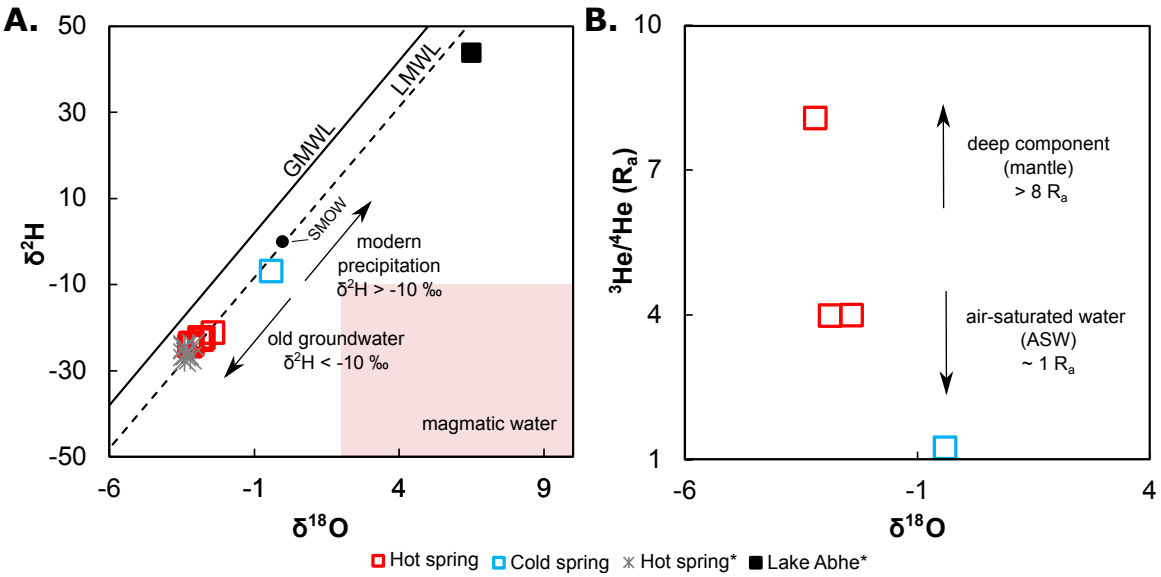

Figure 6.8: Relationships between $\delta^{18}O$, $\delta^{2}H$, and $^{3}He/^{4}He$ in the Lake Abhe geothermal area. (a) $\delta^{2}H$ versus $\delta^{18}O$ plot showing an older and deeper groundwater system more depleted in $\delta^{2}H$ than modern water; the water samples follow the local meteroric water line (Fontes et al., 1980), indicating water is mainly from precipitation. (b) $^{3}He/^{4}He$ versus $\delta^{2}H$ plot displaying mixing of a deeper fluid source and superficial water (ASW). *Data from Awaleh et al. (2015). Magmatic water field from Sheppard et al. (1971); White (1974).

6.6.3 Origin of gas in the Lake Abhe geothermal field

$\delta^{13}C_{CO_2}$ and $^{3}He/^{4}He$ results indicate that the main source of CO_2 and helium at Lake Abhe is the mantle, whereas CH_4 isotopes exhibit a geothermal signal. Considering the mantelic and geothermal signatures of most gas phases (CO_2, He, and CH_4), it is striking that N_2 is the main phase. In gas of volcanic origin, N_2 and helium can be concentrated in the gas phase due to preferential dissolution of CO_2 into the water. However, this is not the case since helium contents are relatively low and the $\delta^{13}C_{CO_2}$ are in a narrow range (-8.18 to -4.82 ‰) that do not indicate secondary processes were involved. Thus, N_2 has an alternative source than that of helium and CO_2.

Minissale et al. (2002) attributed the source of N_2 and He in N_2-rich gas emanations through limestones in Central Italy to shallow water (air-saturated water) since the highest N_2 were associated with the highest He contents; however, these gas samples also exhibit the

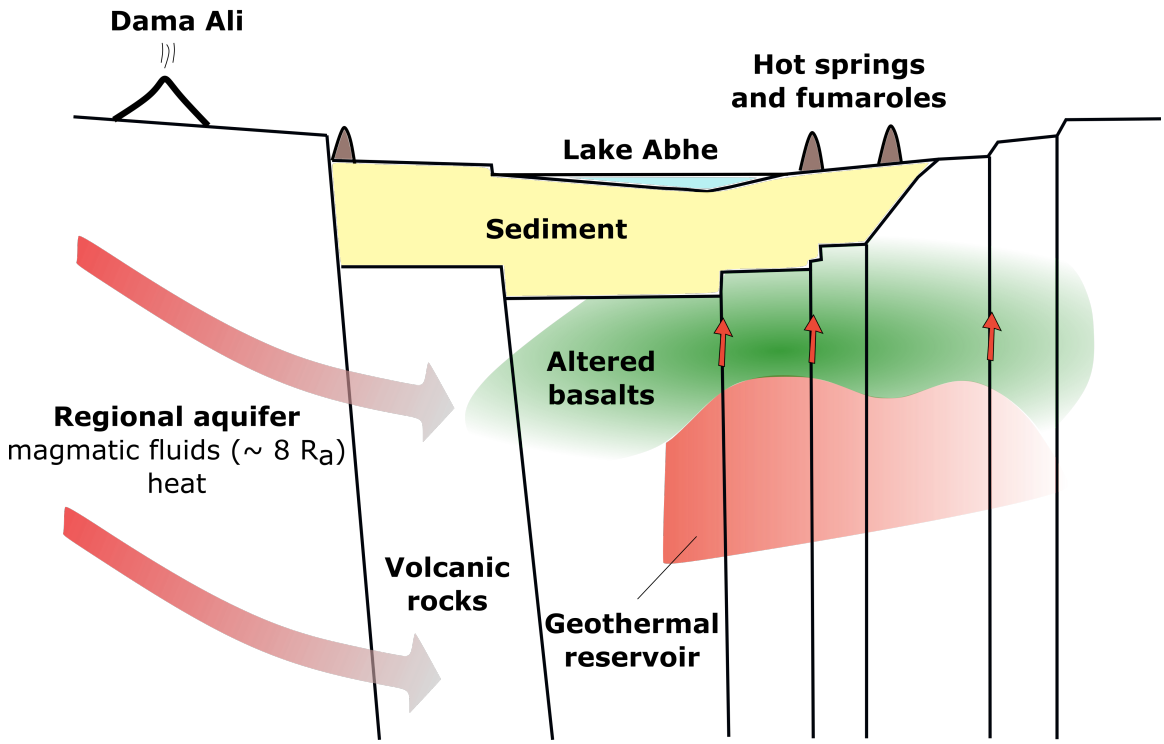

Figure 6.9: Simplified model for water circulation in the Lake Abhe geothermal field. Modified from Awaleh et al. (2015), excluding the local recharge and adding the Dama Ali volcanic system as the distal source of heat.

highest O_2 values that could indicate air contamination from sampling. Their study did not include $\delta^{15}N$ of these fluids and $^3He/^4He$ of only one site displaying crustal signature (0.08 Ra); thus the atmospheric source of N_2 is not confirmed. The Lake Abhe samples with lowest N_2 and He contents are the ones with higher O_2 that indicate air contamination. The ones with highest N_2 and He have variable $^3He/^4He$ (1.04 to 8.58 Ra); the $^3He/^4He$ range is most likely due to air contamination during sampling with the copper tubes since the Giggenbach bottle of the GVS2 site showed mantle signature (8.58 Ra). Thus, helium seems to be of mantle origin in every gas emanation in Lake Abhe, and not atmospheric.

In the N_2/He versus $\delta^{15}N$ plot (Figure 6.11), a mixing between sediments, mantle, and air-like sources is shown. The sample showing most air contribution is the only sample with Ar isotope analyses that indicated an atmospheric source. This sample is considered contaminated and will not be discussed further. The $\delta^{15}N$ signature is thus consistent with sediments, organic matter, and oceanic crust (Marty and Humbert, 1997). $\delta^{15}N$ is in a narrow range (5.4 to 5.8 ‰) which aligns with $\delta^{15}N$ of NH_4 in the crystal-lattice of clays, micas, and

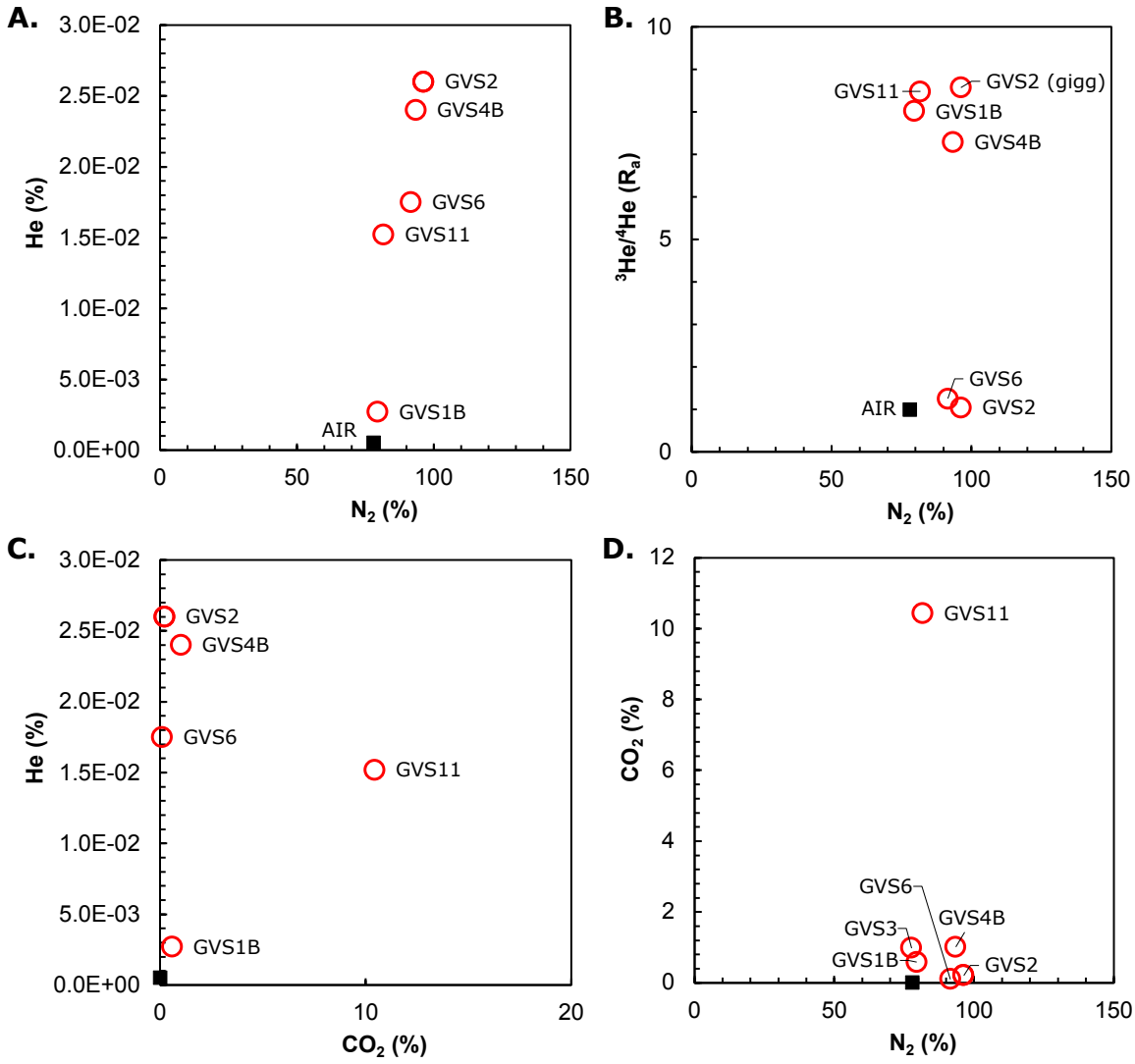

Figure 6.10: Relationships between N_2, He, $^3He/^4He$, CO_2. N_2 and He exhibit a positive relationship (a) whereas the other species are mainly scattered (b, c, and d).

feldspars (5.6 to 5.8 ‰) under unoxidized conditions and unaffected by diagenetic effects (Scholten et al., 1991). Clay minerals such as illite and smectite can hold NH_4 in their lattice (e.g., Sucha et al., 2007). Such minerals can resist up to 300°C (Kristmannsdóttir, 1979) and the deeper in the hydrothermal system, the more extensive basalt alteration is expected (e.g., Wu et al., 2021) which could indicate the fracture systems emanate volcanic/mantelic gas along with N_2 from potentially thicker altered basalt levels at depth. To confirm the source of N_2, the composition of secondary minerals and NH_4 of the water are necessary.

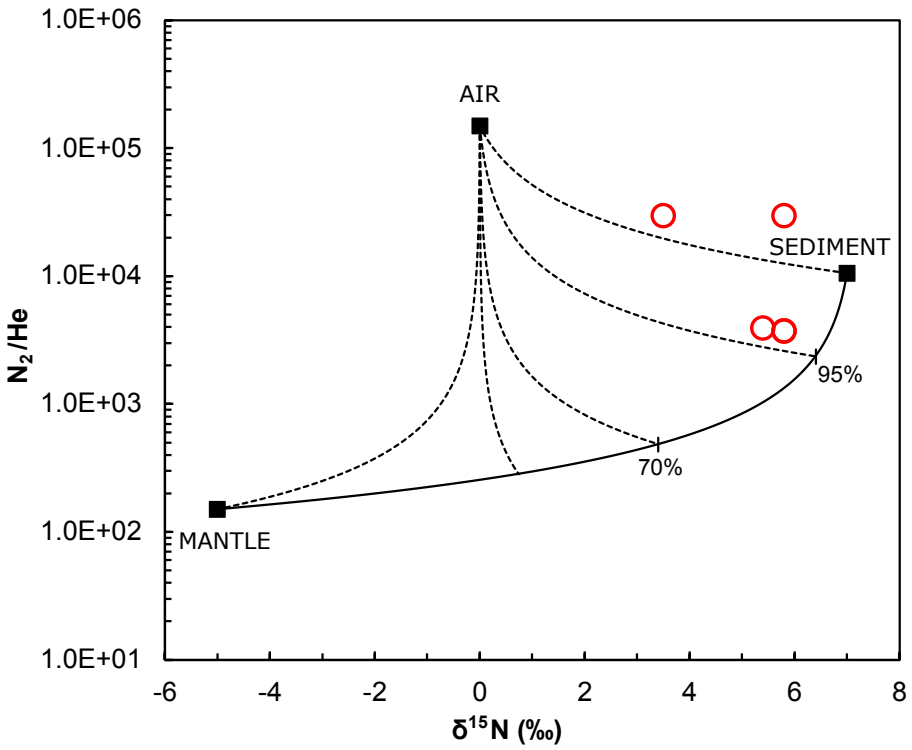

Figure 6.11: N_2/He versus δ^{15}N plot. Samples exhibit mainly a sedimentary source with small air contribution. The sample closest to the air component, with lowest δ^{15}N, is considered to be contaminated by atmosphere during sampling.

6.7 Conclusion

In the Lake Abhe geothermal field, degassing occurs in two domains commonly referred as "small chimneys" and "great chimneys"; however, both display similar gas compositions and isotopic signatures that indicate a common homogeneous hydrothermal system at depth, dominated by a magmatic source. This result agrees with the model previously proposed by Awaleh et al. (2015), in which the authors propose a common reservoir for both areas based on the transport of heat from depth with the hydrothermal system being fed by meteoric water from the regional aquifer. These authors found very low tritium contents and low deuterium values compatible with an older and deeper water source than that of surface waters.The deeper groundwater has a signature compatible with mixing between a mantle component (close to 9 Ra) and ASW, without clear evidence of influence of a ^{3}He-rich plume-like component. The source of heat of the Abhe geothermal system is most likely the Dama Ali volcanic system, $\sim$ 30 km W of Lake Abhe's hot springs, since the geothermal system is

fed by a regional-scale aquifer rather than a local and superficial one. Investigation of the Dama Ali volcanic system is crucial to better constrain the local endmember at the Lake Abhe geothermal system. Concerning the other gas phases, only N_2 is inconsistent with a geothermal and/or volcanic signature and is probably produced locally by sediments and/or hydrothermal alteration of the basement rocks.

Chapter 7

Conclusions and remaining questions

The main goal of this thesis was to detect the sources of crustal and geothermal fluids in different geological and geotectonic settings with a specific emphasis on precising transport processes in the crust – this, in order to optimize the use of noble gas isotopic geochemistry for monitoring fluids associated to seismic/volcanic contexts in Northern Iceland (Chapter 4) or for direct societal implications linked to helium (Chapter 5) and geothermal (Chapter 6) exploitation projects. From the results reported in this thesis, helium isotopes show that mantle input is present in different geotectonic contexts, not necessarily linked to active volcanism or extension, such as the case of the Paris Basin (Chapter 5) and Pyrenees (Annex), both inserted in continental crust settings, or from off-rift zones in Iceland (Chapter 4) which also require identical processes of direct vertical transfer from the mantle.

Although the main source of helium in the study area near the Paris Basin is the continental crust, there is evidence of a small mantle contribution (∼2.5%) highlighted by the combination of helium and xenon isotopes. In principle, nucleogenic ^{3}He can be produced in the crust via thermal neutron capture on ^{6}Li via the reaction ^{6}Li(n,α)^{3}H (β^{-}) $\rightarrow$ ^{3}He (Morrison and Pine, 1955). Since the surrounding areas in Central France are prone to high Li contents (Beauvoir granite with 367-5,220 ppm; Raimbault et al., 1995) relative to the continental crust average values (∼30 ppm), the ambiguity in the source of ^{3}He would remain until the contents of U-Th-Li in the lithologies hosting and surrounding the gas reservoirs could be established. However, thanks to high resolution Xe analysis, the ^{129}Xe excess observed at SP7 confirms that the excess ^{3}He relative to the crustal end-member composition

is derived from the mantle. Thus, the decreasing $^{3}He/^{4}He$ gradient starting at the Massif Central towards the Paris Basin and the vertical $^{3}He/^{4}He$ gradient previously described in the literature at the Paris Basin aquifers (Marty et al., 1993; Pinti and Marty, 1995, 1998) point to a small mantle contribution limited to the N-S fault system, since laterally, few kilometres (50-80) east at Bourbon-Lancy and Fontaines Salées, $^{3}He/^{4}He$ ratios show typical crustal values ($\leq$ 0.04 Ra). This evidence indicates that vertical transport occurs either from an unknown deep-seated magmatic source, or more likely through deep fault systems that reach the mantle and input ^{3}He via an improved permeability system (Kennedy and van Soest, 2007) and potential presence of cryptic non-collected melts in the mantle. From those results, local helium production alone is unlikely since the $^{3}He/^{4}He$ ratios (0.17-0.22 Ra) are in the same range across a 40 km area (Pougues-les- Eaux and Couy), indicating that helium is probably transported from a crustal flux and accumulated in the reservoir layers, experiencing at some point slight input from the mantle. However, this launches the question of efficient volatiles transport in the crust without associated carrying fluids. For a global and better understanding of the sources of helium and associated volatiles, as well as the potentiality of gas accumulations in crustal reservoirs, it is still relevant to obtain the U-Th-Li contents of the host rocks of the sites investigated to compute precise potential radiogenic/nucleogenic production ratios, along with a better understanding of the basin geometry and geological model of such potential gas reservoirs. A key question that could remain in the global model for this site is the potential connection/causality between the accumulation of crustal radiogenic helium and the presence of a slight mantle component.

High helium contents and isotopic ratios of geothermal fluids along fault zones in North Iceland (Chapter 4) also require the presence of a global magmatic flux that can only be explained by vertical transport of a plume-like component through the crust directly from the mantle. The estimated value for such a flux (1×10^{-7} $cm^{3}STPcm^{-2}yr^{-1}$ ^{4}He) is comparable to the ones of neighbouring active rift zones in Iceland, where melts intruded in the crust are still actively degassing. Because lateral transport of the magmatic component from those active rift zones or leaching of local magmatic country rocks are not satisfactory hypothesis to explain such a flux, the only alternative process that can be envisaged is direct transfer from the mantle itself. The helium ratios above typical upper mantle values ($\sim$ 8 Ra) for

these off-rift zones may therefore be associated to a mantle flux originating from degassing of a ^{3}He-rich mantle source influenced by the Iceland mantle plume via cryptic and incipient melting. The presence of a low velocity anomaly zone $\sim$ 56 km under North Iceland (Celli et al., 2021) supports this interpretation.

For the Iceland geothermal fluids the origin of volatiles could also be complex and multi-sourced. Along the Dalvík Lineament, the helium isotopic signature indicates additional release of radiogenic ^{4}He (*^{4}He) from the host rocks, which is not compatible with continuous release coupled with the mantle flux. This *^{4}He input is rather associated with additional short timescales processes, potentially linked to the tectonic earthquakes experienced along this major transfer zone between the mid-Atlantic ridge and the Northern Rift Zone of Iceland. In seismically active regions, release of noble gases, produced in rocks, can be increased due dilatancy resultant of shear deformation and fracturing (Buttitta et al., 2020; Caracausi and Paternoster, 2015; Honda et al., 1982). According to Torgersen and O'Donnell (1991), this process can occur in short timescales ($<$ 1500 years) and fracturing can increased the helium flux by a factor of 10^2 to 10^4 times higher the steady state model. Precise understanding of such mechanisms and their potential variations with time and general field constraints evolutions are important for hydrogeochemical monitoring in Northern Iceland and other seismic zones. Regarding the local isotopic variations and their potential association with seismicity, although we found no evidence for groundwater mixing at the regional scale, from the highlands towards the north, such a lateral transport seems to occur at local scale in the Aðaldalur valley, between Hafralækur and the NRZ western border. This process appears partially controlled or enhanced by high magnitude tectonic earthquakes (M $\geq$ 5), as shown by our helium isotope time series (2020 to 2022), confirming what Skelton et al. (2019, 2014) previously reported from stable isotopes shifts during the 2002, 2012, and 2012 M $>$ 5 events. To confirm these observations, monitoring of borehole HA-01 should continue until capturing a major event, and associated new monitoring initiative(s) along the Dalvík Lineament should be envisaged.

In the Lake Abhe geothermal field (Chapter 6), the system characteristics and physical-chemical processes are different than at the Paris Basin region and North Iceland. This low temperature ($<$ 150°C) geothermal field occurs in proximity to an active volcanic system

(Dama Ali, $\sim$ 30 km W), which is most likely its source of volatiles, and thus mantle input is expected. Transport of this component, unlike what we observed for Paris Basin region and North Iceland fluids, seems to occur laterally via groundwater flow since the Lake Abhe system is fed by a regional aquifer. In this geothermal system, degassing occurs in two domains commonly referred as "small chimneys" and "great chimneys"; however, both display similar gas compositions and isotopic signatures that indicate a common homogeneous hydrothermal system at depth, dominated by a magmatic source, which is an important information for the objectives of the Geothermal Village project and the issue for the future exploitation well location. This result agrees with the model previously proposed by Awaleh et al. (2015), in which the authors propose a common reservoir for both areas based on the transport of heat from depth with the hydrothermal system being fed by meteoric water from the regional aquifer. Moreover, the deep groundwater has a signature compatible with mixing between a mantle component (close to 9 Ra) and ASW, without clear evidence of influence of a ^{3}He-rich plume-like component. The source of those volatiles being most probably the Dama Ali volcanic system, $\sim$ 30 km W of Lake Abhe's hot springs, investigation of this volcanic system is crucial to better constrain the local endmember at the Lake Abhe geothermal system and the origin of the 7-9 Ra component in Central Afar associated to the plume component.

Although helium isotopes allied with other isotopic systems can provide answers to the source of fluids, often ambiguities remain. It is the case of the source of N_2 and CO_2 in the gas reservoir in the Nièvre, since they can originate from biogenic processes (N_2), organic matter (CO_2) or be susceptible to secondary processes (CO_2) (e.g., Favara et al., 2002; Wada et al., 1975). ^{3}He/^{4}He ratios are independent of gas composition, given that ^{3}He/^{4}He is roughly the same for springs near SP4, including Fontaine des Vertus, whereas its helium and N_2 contents are much higher than for the other springs of the group. δ^{15}N results, for all sample groups, are comparable and point to a common crustal source. Nitrogen in the crust mainly occurs in silicate minerals as NH_4 (clay minerals, mica, feldspar, garnet, wadsleyite, and bridgmanite; Mysen, 2019). A common source indicates that the variation in N_2 contents is related to secondary processes such as carbonate precipitation and CO_2 dissolution. These processes lead to CO_2 fractionation between the water and gas phase.

Preferential dissolution of CO_2 in the water relative to N_2 and helium cause lower contents of the former in the gas phase, which explains the elevated concentrations of N_2 and helium at Fontaine des Vertus, Bourbon-Lancy, and Fontaines Salées. Establishing the source of CO_2 is more challenging. Considering that the $\delta^{13}C$ of CO_2 of our surveyed springs near the Paris Basin are distinct from the regional mantle value (Massif Central), CO_2 is probably mainly of crustal origin. However, mixing between crustal or biogenic components and mantle is expected, especially since CO_2 would most likely be the carrier phase of the mantle helium component and $CO_2/^3He$ ratios (between 8 x 10^9 and 1 x 10^{10}) are close to the MORB value.

In the case of the Lake Abhe geothermal area, N_2 is the main gas phase but unlike for the Nièvre region, it is not concentrated in the gas phase due to preferential dissolution of CO_2 in the water phase but most likely due to local production from NH_4 present in clay silicates from sediments or formed from hydrothermal alteration of basalts at depth (Chapter 6). Thus, the likely carrier phase of mantle helium appears to be CO_2 as for the other study areas investigated in this thesis.

Bibliography

Abiye, T. A. (2010), 'An overview of the transboundary aquifers in east africa', *Journal of African Earth Sciences* **58**(4), 684–691.

Andrews, J. N. (1985), 'The isotopic composition of radiogenic helium and its use to study groundwater movement in confined aquifers', *Chemical Geology* **49**(1-3), 339–351.

Andrén, M., Stockmann, G., Skelton, A., Sturkell, E., Mörth, C.-M., Guðrúnardóttir, H. R., Keller, N. S., Odling, N., Dahrén, B., Broman, C., Balic-Zunic, T., Hjartarson, H., Siegmund, H., Freund, F. and Kockum, I. (2016), 'Coupling between mineral reactions, chemical changes in groundwater, and earthquakes in iceland', *Journal of Geophysical Research: Solid Earth* **121**(4), 2315–2337.
URL: *https://agupubs.onlinelibrary.wiley.com/doi/abs/10.1002/2015JB012614*

Awaleh, M. O., Boschetti, T., Soubaneh, Y. D., Kim, Y., Baudron, P., Kawalieh, A. D., Ahmed, M. M., Daoud, M. A., Dabar, O. A., Kadieh, I. H. et al. (2018), 'Geochemical, multi-isotopic studies and geothermal potential evaluation of the complex djibouti volcanic aquifer (republic of djibouti)', *Applied Geochemistry* **97**, 301–321.

Awaleh, M. O., Hoch, F. B., Boschetti, T., Soubaneh, Y. D., Egueh, N. M., Elmi, S. A., Mohamed, J. and Khaireh, M. A. (2015), 'The geothermal resources of the republic of djibouti — ii: Geochemical study of the lake abhe geothermal field', *Journal of Geochemical Exploration* **159**, 129–147.
URL: *https://www.sciencedirect.com/science/article/pii/S037567421530056X*

Ayenew, T., Kebede, S. and Alemyahu, T. (2008), 'Environmental isotopes and hydrochemical study applied to surface water and groundwater interaction in the awash river basin', *Hydrological Processes: An International Journal* **22**(10), 1548–1563.

Baker, J., Snee, L. and Menzies, M. (1996), 'A brief oligocene period of flood volcanism in yemen: implications for the duration and rate of continental flood volcanism at the afro-arabian triple junction', *Earth and Planetary Science Letters* **138**(1-4), 39–55.

Ballentine, C. J., Burgess, R. and Marty, B. (2002), 'Tracing Fluid Origin, Transport and Interaction in the Crust', *Reviews in Mineralogy and Geochemistry* **47**(1), 539–614.
URL: *https://doi.org/10.2138/rmg.2002.47.13*

Ballentine, C. J. and Burnard, P. G. (2002), 'Production, Release and Transport of Noble Gases in the Continental Crust', *Reviews in Mineralogy and Geochemistry* **47**(1), 481–538.
URL: *https://doi.org/10.2138/rmg.2002.47.12*

Ballentine, C. and O'Nions, R. (1992), 'The nature of mantle neon contributions to vienna basin hydrocarbon reservoirs', *Earth and Planetary Science Letters* **113**(4), 553–567.
URL: *https://www.sciencedirect.com/science/article/pii/0012821X9290131E*

Baptiste, J. (2016), Cartographie structurale et lithologique du substratum du Bassin parisien et sa place dans la chaîne varisque de l'Europe de l'Ouest: approches combinées géophysiques, pétrophysiques, géochronologiques et modélisations 2D, PhD thesis, Université d'Orléans.

Barbieri, M., Franchini, S., Barberio, M. D., Billi, A., Boschetti, T., Giansante, L., Gori, F., Jónsson, S., Petitta, M., Skelton, A. et al. (2021), 'Changes in groundwater trace element concentrations before seismic and volcanic activities in iceland during 2010–2018', *Science of the Total Environment* **793**, 148635.

Barrat, J., Joron, J., Taylor, R., Fourcade, S., Nesbitt, R. and Jahn, B. (2003), 'Geochemistry of basalts from manda hararo, ethiopia: Lree-depleted basalts in central afar', *Lithos* **69**(1-2), 1–13.

Barry, P. H., Hilton, D. R., Tryon, M. D., Brown, K. M. and Kulongoski, J. T. (2009), 'A new syringe pump apparatus for the retrieval and temporal analysis of helium in groundwaters and geothermal fluids', *Geochemistry, Geophysics, Geosystems* **10**(5).
URL: *https://agupubs.onlinelibrary.wiley.com/doi/abs/10.1029/2009GC002422*

Batard, F., Baubron, J., Bosch, B., Marcé, A. and Risler, J. (1982), 'Isotopic identification of gases of a deep origin in french thermomineral waters', *Journal of Hydrology* **56**(1-2), 1–21.

Battani, A., Deville, E., Faure, J., Jeandel, E., Noirez, S., Tocqué, E., Benoît, Y., Schmitz, J., Parlouar, D., Sarda, P. et al. (2010), 'Geochemical study of natural co2 emissions in the french massif central: how to predict origin, processes and evolution of co2 leakage', *Oil & Gas Science and Technology–Revue de l'Institut Français du Pétrole* **65**(4), 615–633.

Boineau, R. and Maisonneuve, J. (1972), 'Les sources minérales du massif central français et leur cadre géologique', *Rapport BRGM* .

Boschetti, T., Cortecci, G., Barbieri, M. and Mussi, M. (2007), 'New and past geochemical data on fresh to brine waters of the salar de atacama and andean altiplano, northern chile', *Geofluids* **7**(1), 33–50.

Brandon, A. D., Graham, D. W., Waight, T. and Gautason, B. (2007), '186os and 187os enrichments and high-3he/4he sources in the earth's mantle: evidence from icelandic picrites', *Geochimica et Cosmochimica Acta* **71**(18), 4570–4591.

Bräuer, K., Kämpf, H., Niedermann, S. and Wetzel, H.-U. (2017), 'Regional distribution pattern of carbon and helium isotopes from different volcanic fields in the french massif central: Evidence for active mantle degassing and water transport', *Chemical Geology* **469**, 4–18.

Breddam, K., Kurz, M. D. and Storey, M. (2000), 'Mapping out the conduit of the iceland mantle plume with helium isotopes', *Earth and Planetary Science Letters* **176**(1), 45–55.

Brown, A. (2019), 'Origin of helium and nitrogen in the Panhandle–Hugoton field of Texas, Oklahoma, and Kansas, United States', *AAPG Bulletin* **103**(2), 369–403.
URL: *https://doi.org/10.1306/07111817343*

Burnard, P. and Harrison, D. (2005), 'Argon isotope constraints on modification of oxygen isotopes in iceland basalts by surficial processes', *Chemical Geology* **216**(1-2), 143–156.

Burnard, P., Stuart, F., Turner, G. and Oskarsson, N. (1994), 'Air contamination of basaltic magmas: implications for high 3he/4he mantle ar isotopic composition', *Journal of Geophysical Research: Solid Earth* **99**(B9), 17709–17715.

Burnard, P., Zimmermann, L. and Sano, Y. (2013), The noble gases as geochemical tracers: History and background, *in* 'The noble gases as geochemical tracers', Springer, pp. 1–15.

Caracausi, A., Italiano, F., Martinelli, G., Paonita, A. and Rizzo, A. (2005), 'Long-term geochemical monitoring and extensive/compressive phenomena: case study of the umbria region (central apennines, italy)', *Annals of Geophysics* **48**(1).
URL: *https://www.annalsofgeophysics.eu/index.php/annals/article/view/3178*

Castillo, P. R., Liu, X. and Scarsi, P. (2020), 'The geochemistry and Sr-Nd-Pb isotopic ratios of high 3He/4He Afar and MER basalts indicate a significant role of the African Superplume in EARS magmatism', *Lithos* **376-377**.

Claesson, L., Skelton, A., Graham, C. and Mörth, C.-M. (2007), 'The timescale and mechanisms of fault sealing and water-rock interaction after an earthquake', *Geofluids* **7**(4), 427–440.
URL: *https://onlinelibrary.wiley.com/doi/abs/10.1111/j.1468-8123.2007.00197.x*

Craig, H. (1961), 'Isotopic Variations in Meteoric Waters', *Science* **133**(3465), 1702–1703.
URL: *https://doi.org/10.1126/science.133.3465.1702*

Craig, H. (1978), 'A mantle helium component in circum-pacific volcanic gases: Hakone, the marianas and mt. lassen', *Terriestrial Rare Gases* pp. 3–16.

Craig, H. and Lupton, J. (1976), 'Primordial neon, helium, and hydrogen in oceanic basalts', *Earth and Planetary Science Letters* **31**(3), 369–385.

Danabalan, D. (2017), Helium: Exploration Methodology for a strategic resource, PhD thesis, Durham University.

Darbyshire, F. A., White, R. S. and Priestley, K. F. (2000), 'Structure of the crust and uppermost mantle of iceland from a combined seismic and gravity study', *Earth and Planetary Science Letters* **181**(3), 409–428.
URL: *https://www.sciencedirect.com/science/article/pii/S0012821X00002065*

Darling, W. G. (1996), *The geochemistry of fluid processes in the eastern branch of the east African rift system*, Open University (United Kingdom).

Darling, W. and Talbot, J. (1991), 'Evaluation and development of gas geothermometry for geothermal exploration in the east african rift system'.

Dekov, V., Egueh, N., Kamenov, G., Bayon, G., Lalonde, S., Schmidt, M., Liebetrau, V., Munnik, F., Fouquet, Y., Tanimizu, M., Awaleh, M., Guirreh, I. and Le Gall, B. (2014), 'Hydrothermal carbonate chimneys from a continental rift (afar rift): Mineralogy, geochemistry, and mode of formation', *Chemical Geology* **387**, 87–100.
URL: *https://www.sciencedirect.com/science/article/pii/S0009254114003945*

DeMott, L. M., Scholz, C. A. and Awaleh, M. O. (2021), 'Lacustrine carbonate towers of lake abhe, djibouti: Interplay of hydrologic and microbial processes', *Sedimentary Geology* **424**, 105983.

Dixon, E. T., Honda, M., McDougall, I., Campbell, I. H. and Sigurdsson, I. (2000), 'Preservation of near-solar neon isotopic ratios in icelandic basalts', *Earth and Planetary Science Letters* **180**(3-4), 309–324.

Eason, D. E., Sinton, J. M., Grönvold, K. and Kurz, M. D. (2015), 'Effects of deglaciation on the petrology and eruptive history of the western volcanic zone, iceland', *Bulletin of Volcanology* **77**, 1–27.

Eberhardt, P., Eugster, O. and Marti, K. (1965), 'A redetermination of the isotopic composition of atmospheric neon', *Zeitschrift für Naturforschung A* **20**(4), 623–624.

Ebinger, C. and Sleep, N. (1998), 'Cenozoic magmatism in africa: One plume goes a long way', *Nature* **395**, 788–791.

Einarsson, P. (2008), 'Plate boundaries, rifts and transforms in iceland', *Jökull* **58**(12), 35–58.

Ellam, R. and Stuart, F. (2004), 'Coherent he–nd–sr isotope trends in high 3he/4he basalts: implications for a common reservoir, mantle heterogeneity and convection', *Earth and Planetary Science Letters* **228**(3-4), 511–523.

Favara, R., Grassa, F., Inguaggiato, S., Pecoraino, G. and Capasso, G. (2002), 'A simple method to determine the δ13c content of total dissolved inorganic carbon', *Geofísica Internacional* **41**(3), 313–320.

Fontes, J. C. and Gonfiantini, R. (1967), 'Comportement isotopique au cours de l'evaporation de deux bassins sahariens', *Earth and Planetary Science Letters* **3**(C), 258–266.

Fontes, J. C., Pouchon, P., Saliege, J., Zuppi, G. et al. (1980), 'Environmental isotope study of groundwater systems in the republic of djibouti.', *Environmental isotope study of groundwater systems in the Republic of Djibouti.* .

Furman, T. (2007), 'Geochemistry of east african rift basalts: an overview', *Journal of African Earth Sciences* **48**(2-3), 147–160.

Füri, E., Hilton, D., Halldórsson, S., Barry, P., Hahm, D., Fischer, T. and Grönvold, K. (2010), 'Apparent decoupling of the he and ne isotope systematics of the icelandic mantle: The role of he depletion, melt mixing, degassing fractionation and air interaction', *Geochimica et Cosmochimica Acta* **74**(11), 3307–3332.
URL: *https://www.sciencedirect.com/science/article/pii/S001670371000150X*

Gasse, E. and Street, F. (1978), 'Late quaternary lake-level fluctuations and environments of the northern rift valley and afar region (ethiopia and djibouti)', *Palaeogeography, Palaeoclimatology, Palaeoecology* **24**(4), 279–325.
URL: *https://www.sciencedirect.com/science/article/pii/0031018278900111*

Gasse, F. (1977), 'Evolution of lake abhé (ethiopia and tfai), from 70,000 bp', *Nature* **265**(5589), 42–45.

George, R., Rogers, N. and Kelley, S. (1998), 'Earliest magmatism in ethiopia: evidence for two mantle plumes in one flood basalt province', *Geology* **26**(10), 923–926.

Giggenbach, W. F. and Goguel, R. (1988), *Methods for the collection and analysis of geothermal and volcanic water and gas samples*, Chemistry Division, Department of Scientific and Industrial Research.

Gilfillan, S. and Haszeldine, S. (2011), *Report on Noble Gas, Carbon Stable Isotope and HCO3: measurements from the Kerr Quarter and surrounding area, Goodwater, Saskatchewan.*, IPAC CO2 Research Incorporated.

Gilfillan, S. M., Ballentine, C. J., Holland, G., Blagburn, D., Lollar, B. S., Stevens, S., Schoell, M. and Cassidy, M. (2008), 'The noble gas geochemistry of natural co2 gas reservoirs from the colorado plateau and rocky mountain provinces, usa', *Geochimica et Cosmochimica Acta* **72**(4), 1174–1198.
URL: *https://www.sciencedirect.com/science/article/pii/S0016703707005807*

Gilfillan, S. M., Wilkinson, M., Haszeldine, R. S., Shipton, Z. K., Nelson, S. T. and Poreda, R. J. (2011), 'He and ne as tracers of natural co2 migration up a fault from a deep reservoir', *International Journal of Greenhouse Gas Control* **5**(6), 1507–1516.

Glueckauf, E. (1946), 'A micro-analysis of the helium and neon contents of air', *Proceedings of the Royal Society of London. Series A. Mathematical and Physical Sciences* **185**(1000), 98–119.

Graham, D. W. (2002), 'Noble Gas Isotope Geochemistry of Mid-Ocean Ridge and Ocean Island Basalts: Characterization of Mantle Source Reservoirs', *Reviews in Mineralogy and Geochemistry* **47**(1), 247–317.
URL: *https://doi.org/10.2138/rmg.2002.47.8*

Grandin, R., Socquet, A., Binet, R., Klinger, Y., Jacques, E., De Chabalier, J.-B., King, G., Lasserre, C., Tait, S., Tapponnier, P. et al. (2009), 'September 2005 manda hararo-dabbahu rifting event, afar (ethiopia): constraints provided by geodetic data', *Journal of Geophysical Research: Solid Earth* **114**(B8).

Grandin, R., Socquet, A., Jacques, E., Mazzoni, N., De Chabalier, J.-B. and King, G. (2010), 'Sequence of rifting in afar, manda-hararo rift, ethiopia, 2005–2009: Time-space evolution and interactions between dikes from interferometric synthetic aperture radar and static stress change modeling', *Journal of Geophysical Research: Solid Earth* **115**(B10).

Halford, D., Karolytė, R., Barry, P., Whyte, C., Darrah, T., Cuzella, J., Sonnenberg, S. and Ballentine, C. (2022), 'High helium reservoirs in the four corners area of the colorado plateau, usa', *Chemical Geology* **596**, 120790.
URL: *https://www.sciencedirect.com/science/article/pii/S0009254122000845*

Halldórsson, S. A., Hilton, D. R., Barry, P. H., Füri, E. and Grönvold, K. (2016), 'Recycling of crustal material by the iceland mantle plume: new evidence from nitrogen elemental and isotope systematics of subglacial basalts', *Geochimica et Cosmochimica Acta* **176**, 206–226.

Halldórsson, S. A., Hilton, D. R., Scarsi, P., Abebe, T. and Hopp, J. (2014), 'A common mantle plume source beneath the entire east african rift system revealed by coupled helium-neon systematics', *Geophysical Research Letters* **41**(7), 2304–2311.

Hardarson, B., Fitton, J., Ellam, R. and Pringle, M. (1997), 'Rift relocation — a geochemical and geochronological investigation of a palaeo-rift in northwest iceland', *Earth and Planetary Science Letters* **153**(3), 181–196.
URL: *https://www.sciencedirect.com/science/article/pii/S0012821X97001453*

Harðardóttir, S., Halldórsson, S. A. and Hilton, D. R. (2018), 'Spatial distribution of helium isotopes in icelandic geothermal fluids and volcanic materials with implications for location, upwelling and evolution of the icelandic mantle plume', *Chemical Geology* **480**, 12–27. The noble gases as geochemical tracers – in celebration of Pete Burnard.
URL: *https://www.sciencedirect.com/science/article/pii/S0009254117302991*

Hauksson, E. and Goddard, J. G. (1981), 'Radon earthquake precursor studies in iceland', *Journal of Geophysical Research: Solid Earth* **86**(B8), 7037–7054.

Hersir, G. P., Thorbjornsson, D., Kristinsson, S. G., Eyjolfsdottir, E. I., Magnusson, I. T., Vilhjalmsson, A. M., Arnason, K., Khaireh, A., Magareh, H. M., Ibrahim, N.-A. and Hassan, S. Y. (2016), 'Djibouti – lake abhe. surface exploration studies in 2015 conceptual model', *ISOR* .

Hilton, D., Grönvold, K., O'Nions, R. and Oxburgh, E. (1990), 'Regional distribution of 3he anomalies in the icelandic crust', *Chemical Geology* **88**(1-2), 53–67.

Hilton, D., Gronvold, K., Sveinbjornsdottir, A. and Hammerschmidt, K. (1998), 'Helium isotope evidence for off-axis degassing of the icelandic hotspot', *Chemical Geology* **149**(3), 173–187.
URL: *https://www.sciencedirect.com/science/article/pii/S0009254198000448*

Hilton, D. R. (1996), 'The helium and carbon isotope systematics of a continental geothermal system: results from monitoring studies at long valley caldera (california, u.s.a.)', *Chemical Geology* **127**(4), 269–295.
URL: *https://www.sciencedirect.com/science/article/pii/0009254195001344*

Hilton, D. R., Grönvold, K., Macpherson, C. G. and Castillo, P. R. (1999), 'Extreme 3he/4he ratios in northwest iceland: constraining the common component in mantle plumes', *Earth and Planetary Science Letters* **173**(1-2), 53–60.

Hofmann, C., Courtillot, V., Feraud, G., Rochette, P., Yirgu, G., Ketefo, E. and Pik, R. (1997), 'Timing of the ethiopian flood basalt event and implications for plume birth and global change', *Nature* **389**(6653), 838–841.

Holland, G. and Gilfillan, S. (2013), 'Application of noble gases to the viability of CO2 storage', *Advances in Isotope Geochemistry* pp. 177–223.

Houssein, B., Chandrasekharam, D., Chandrasekhar, V. and Jalludin, M. (2014), 'Geochemistry of thermal springs around lake abhe, western djibouti', *International Journal of Sustainable Energy* **33**(6), 1090–1102.
URL: *https://doi.org/10.1080/14786451.2013.813027*

James, T. (1967), 'Thermal springs in tanzania', *Inst. Min. Metall., Trans., Sect. B;()* **76**(729).

Kipfer, R., Aeschbach-Hertig, W., Peeters, F. and Stute, M. (2002), 'Noble Gases in Lakes and Ground Waters', *Reviews in Mineralogy and Geochemistry* **47**(1), 615–700.
URL: *https://doi.org/10.2138/rmg.2002.47.14*

Kononov, V. and Polak, B. (1976), '. indicators of abyssal heat recharge of recent hydrothermal phenomena.'.

Kristmannsdóttir, H. (1979), Alteration of basaltic rocks by hydrothermal-activity at 100-300 c, *in* 'Developments in sedimentology', Vol. 27, Elsevier, pp. 359–367.

Kurz, M. D., Meyer, P. S. and Sigurdsson, H. (1985), 'Helium isotopic systematics within the neovolcanic zones of iceland', *Earth and Planetary Science Letters* **74**(4), 291–305.

Lafortune, S., Moreira, M., Agrinier, P., Bonneville, A., Schneider, H. and Catalette, H. (2009), 'Noble gases as tools for subsurface monitoring of co2 leakage', *Energy Procedia* **1**(1), 2185–2192. Greenhouse Gas Control Technologies 9.
URL: *https://www.sciencedirect.com/science/article/pii/S1876610209002859*

Leroy, S., Razin, P., Autin, J., Bache, F., d'Acremont, E., Watremez, L., Robinet, J., Baurion, C., Denèle, Y., Bellahsen, N. et al. (2013), From rifting to oceanic spreading in the gulf of aden: a synthesis, *in* 'Lithosphere dynamics and sedimentary basins: The Arabian plate and analogues', Springer, pp. 385–427.

Licciardi, J. M., Kurz, M. D. and Curtice, J. M. (2007), 'Glacial and volcanic history of icelandic table mountains from cosmogenic 3he exposure ages', *Quaternary Science Reviews* **26**(11-12), 1529–1546.

Lollar, B. S. and Ballentine, C. J. (2009), 'Insights into deep carbon derived from noble gases', *Nature Geoscience* **2**(8), 543–547.

Lollar, B. S., O'Nions, R. K. and Ballentine, C. J. (1994), 'Helium and neon isotope systematics in carbon dioxide-rich and hydrocarbon-rich gas reservoirs', *Geochimica et Cosmochimica Acta* **58**(23), 5279–5290.

Lupton, J. E. (1983), 'Terrestrial inert gases: Isotope tracer studies and clues to primordial components in the mantle', *Annual Review of Earth and Planetary Sciences* **11**(1), 371–414.
URL: *https://doi.org/10.1146/annurev.ea.11.050183.002103*

Mabry, J., Lan, T., Burnard, P. and Marty, B. (2013), 'High-precision helium isotope measurements in air', *J. Anal. At. Spectrom.* **28**, 1903–1910.
URL: *http://dx.doi.org/10.1039/C3JA50155H*

Macpherson, C. G., Hilton, D. R., Day, J. M., Lowry, D. and Grönvold, K. (2005), 'High-3he/4he, depleted mantle and low-δ18o, recycled oceanic lithosphere in the source of central iceland magmatism', *Earth and Planetary Science Letters* **233**(3-4), 411–427.

Marty, B., Appora, I., Barrat, J.-A. A., Deniel, C., Vellutini, P. and Vidal, P. (1993), 'He, ar, sr, nd and pb isotopes in volcanic rocks from afar: Evidence for a primitive mantle component and constraints on magmatic sources', *GEOCHEMICAL JOURNAL* **27**(4-5), 219–228.

Marty, B., Dewonck, S. and France-Lanord, C. (2003), 'Geochemical evidence for efficient aquifer isolation over geological timeframes', *Nature* **425**(6953), 55–58.

Marty, B., Gunnlaugsson, E., Jambon, A., Oskarsson, N., Ozima, M., Pineau, F. and Torssander, P. (1991), 'Gas geochemistry of geothermal fluids, the hengill area, southwest rift zone of iceland', *Chemical geology* **91**(3), 207–225.

Marty, B. and Humbert, F. (1997), 'Nitrogen and argon isotopes in oceanic basalts', *Earth and Planetary Science Letters* **152**(1-4), 101–112.

Marty, B., O'Nions, R. K., Oxburgh, E. R., Martel, D. and Lombardi, S. (1992), 'Helium isotopes in Alpine regions', *Tectonophysics* **206**(1-2), 71–78.

Marty, B., Pik, R. and Gezahegn, Y. (1996), 'Helium isotopic variations in ethiopian plume lavas: nature of magmatic sources and limit on lower mantle contribution', *Earth and Planetary Science Letters* **144**(1), 223–237.
URL: *https://www.sciencedirect.com/science/article/pii/0012821X96001586*

Marty, B. and Zimmermann, L. (1999), 'Volatiles (He, C, N, Ar) in mid-ocean ridge basalts: Assesment of shallow-level fractionation and characterization of source composition', *Geochimica et Cosmochimica Acta* **63**(21), 3619–3633.

Mechal, A., Birk, S., Dietzel, M., Leis, A., Winkler, G., Mogessie, A. and Kebede, S. (2017), 'Groundwater flow dynamics in the complex aquifer system of gidabo river basin (ethiopian rift): a multi-proxy approach', *Hydrogeology Journal* **25**(2), 519.

Medynski, S., Pik, R., Burnard, P., Dumont, S., Grandin, R., Williams, A., Blard, P.-H., Schimmelpfennig, I., Vye-Brown, C., France, L. et al. (2016), 'Magmatic cycles pace tectonic and morphological expression of rifting (afar depression, ethiopia)', *Earth and Planetary Science Letters* **446**, 77–88.

Medynski, S., Pik, R., Burnard, P., Williams, A., Vye-Brown, C., Ferguson, D., Blard, P.-H., France, L., Yirgu, G., Seid, J. et al. (2013), 'Controls on magmatic cycles and development of rift topography of the manda hararo segment (afar, ethiopia): Insights from cosmogenic 3he investigation of landscape evolution', *Earth and Planetary Science Letters* **367**, 133–145.

Min, G. and Hou, G. (2018), 'Geodynamics of the east african rift system 30 ma ago: A stress field model', *Journal of Geodynamics* **117**, 1–11.

Minissale, A., Vaselli, O., Tassi, F., Magro, G. and Grechi, G. (2002), 'Fluid mixing in carbonate aquifers near rapolano (central italy): chemical and isotopic constraints', *Applied Geochemistry* **17**(10), 1329–1342.

Moreira, M. (2013), 'Noble gas constraints on the origin and evolution of earth's volatiles', *Geochemical Perspectives* **2**(2), 229–230.

Moreira, M., Breddam, K., Curtice, J. and Kurz, M. D. (2001), 'Solar neon in the icelandic mantle: new evidence for an undegassed lower mantle', *Earth and Planetary Science Letters* **185**(1-2), 15–23.

Morrison, P. and Pine, J. (1955), 'Radiogenic origin of the helium isotopes in rock', *Annals of the New York Academy of Sciences* **62**(3), 71–92.

Mtili, K., Byrne, D., Tyne, R., Kazimoto, E., Kimani, C., Kasanzu, C., Hillegonds, D., Ballentine, C. and Barry, P. (2021), 'The origin of high helium concentrations in the gas fields of southwestern tanzania', *Chemical Geology* **585**, 120542.

Mukhopadhyay, S. (2012), 'Early differentiation and volatile accretion recorded in deep-mantle neon and xenon', *Nature* **486**(7401), 101–104.

Mysen, B. (2019), 'Nitrogen in the earth: abundance and transport', *Progress in Earth and Planetary Science* **6**(1), 1–15.

Natali, C., Beccaluva, L., Bianchini, G., Ellam, R. M., Savo, A., Siena, F. and Stuart, F. M. (2016), 'High-mgo lavas associated to cfb as indicators of plume-related thermochemical effects: The case of ultra-titaniferous picrite–basalt from the northern ethiopian–yemeni plateau', *Gondwana Research* **34**, 29–48.

Nicholson, K. (2012), *Geothermal fluids: chemistry and exploration techniques*, Springer Science & Business Media.

Oxburgh, E. R., O'Nions, R. K. and Hill, R. I. (1986), 'Helium isotopes in sedimentary basins', *Nature* **324**(6098), 632–635.

Ozima, M. and Podosek, F. A. (2002), *Noble gas geochemistry*, Cambridge University Press.

Paonita, A., Caracausi, A., Iacono-Marziano, G., Martelli, M. and Rizzo, A. (2012), 'Geochemical evidence for mixing between fluids exsolved at different depths in the magmatic system of mt etna (italy)', *Geochimica et Cosmochimica Acta* **84**, 380–394.
URL: *https://www.sciencedirect.com/science/article/pii/S0016703712000518*

Paonita, A., Caracausi, A., Martelli, M. and Rizzo, A. L. (2016), 'Temporal variations of helium isotopes in volcanic gases quantify pre-eruptive refill and pressurization in magma reservoirs: The mount etna case', *Geology* **44**(7), 499–502.

Paris, G., Adkins, J. F., Sessions, A. L., Webb, S. M. and Fischer, W. W. (2014), 'Neoarchean carbonate-associated sulfate records positive δ^{33}s anomalies', *Science* **346**(6210), 739–741.
URL: *https://www.science.org/doi/abs/10.1126/science.1258211*

Paris, G., Sessions, A. L., Subhas, A. V. and Adkins, J. F. (2013), 'Mc-icp-ms measurement of δ^{34}s and δ^{33}s in small amounts of dissolved sulfate', *Chemical Geology* **345**, 50–61.
URL: *https://www.sciencedirect.com/science/article/pii/S0009254113000818*

Peters, K., Sweeney, R. and Kaplan, I. (1978), 'Correlation of carbon and nitrogen stable isotope ratios in sedimentary organic matter 1', *Limnology and Oceanography* **23**(4), 598–604.

Pik, R., Deniel, C., Coulon, C., Yirgu, G., Hofmann, C. and Ayalew, D. (1998), 'The northwestern ethiopian plateau flood basalts: classification and spatial distribution of magma types', *Journal of Volcanology and Geothermal Research* **81**(1-2), 91–111.

Pik, R., Deniel, C., Coulon, C., Yirgu, G. and Marty, B. (1999), 'Isotopic and trace element signatures of ethiopian flood basalts: evidence for plume–lithosphere interactions', *Geochimica et Cosmochimica Acta* **63**(15), 2263–2279.

Pik, R., Marty, B., Carignan, J. and Lavé, J. (2003), 'Stability of the upper nile drainage network (ethiopia) deduced from (u–th)/he thermochronometry: implications for uplift and erosion of the afar plume dome', *Earth and Planetary Science Letters* **215**(1-2), 73–88.

Pik, R., Marty, B., Carignan, J., Yirgu, G. and Ayalew, T. (2008), 'Timing of east african rift development in southern ethiopia: Implication for mantle plume activity and evolution of topography', *Geology* **36**(2), 167–170.

Pik, R., Marty, B. and Hilton, D. (2006), 'How many mantle plumes in africa? the geochemical point of view', *Chemical Geology* **226**(3), 100–114. Special Issue in Honour of R.K. O'Nions.
URL: *https://www.sciencedirect.com/science/article/pii/S0009254105004225*

Pinti, D. L. and Marty, B. (1995), 'Noble gases in crude oils from the paris basin, france: Implications for the origin of fluids and constraints on oil-water-gas interactions', *Geochimica et Cosmochimica Acta* **59**(16), 3389–3404.

Pinti, D. L. and Marty, B. (1998), 'The origin of helium in deep sedimentary aquifers and the problem of dating very old groundwaters', *Geological Society Special Publication* **144**, 53–68.

Polak, B., Kononov, V., Tolstikhin, I., Mamyrin, B. and Khabarin, L. (1975), The helium isotopes in thermal fluids, *in* 'Thermal and Chemical Problems of Thermal Waters, Proceedings of the Grenoble Symposium, August/September 1975. p 17-33, 5 fig, 3 tab, 12 ref.'.

Porcelli, D., Ballentine, C. J. and Wieler, R. (2002), 'An overview of noble gas geochemistry and cosmochemistry', *Reviews in mineralogy and geochemistry* **47**(1), 1–19.

Porcelli, D. and Turekian, K. (2014), 6.16 - the history of planetary degassing as recorded by noble gases, *in* H. D. Holland and K. K. Turekian, eds, 'Treatise on Geochemistry (Second Edition)', second edition edn, Elsevier, Oxford, pp. 353–382.
URL: *https://www.sciencedirect.com/science/article/pii/B9780080959757004113*

Poreda, R., Craig, H., Arnorsson, S. and Welhan, J. (1992), 'Helium isotopes in icelandic geothermal systems: I. 3he, gas chemistry, and 13c relations', *Geochimica et Cosmochimica Acta* **56**(12), 4221–4228.

Rees, C., Jenkins, W. and Monster, J. (1978), 'The sulphur isotopic composition of ocean water sulphate', *Geochimica et Cosmochimica Acta* **42**(4), 377–381.

Risler, J. (1974), 'Description et classification géologique des sources minérales et thermales du massif central', *BRGM Report* **74**.

Ritsema, J., Heijst, H. J. v. and Woodhouse, J. H. (1999), 'Complex shear wave velocity structure imaged beneath africa and iceland', *Science* **286**(5446), 1925–1928.

Rizzo, A., Caracausi, A., Favara, R., Martelli, M., Paonita, A., Paternoster, M., Nuccio, P. M. and Rosciglione, A. (2006), 'New insights into magma dynamics during last two eruptions of mount etna as inferred by geochemical monitoring from 2002 to 2005', *Geochemistry, Geophysics, Geosystems* **7**(6).
URL: *https://agupubs.onlinelibrary.wiley.com/doi/abs/10.1029/2005GC001175*

Rizzo, A., Grassa, F., Inguaggiato, S., Liotta, M., Longo, M., Madonia, P., Brusca, L., Capasso, G., Morici, S., Rouwet, D. and Vita, F. (2009), 'Geochemical evaluation of observed changes in volcanic activity during the 2007 eruption at stromboli (italy)', *Journal of Volcanology and Geothermal Research* **182**(3), 246–254. The 2007 Eruption of Stromboli.
URL: *https://www.sciencedirect.com/science/article/pii/S0377027308004435*

Rogers, N., Macdonald, R., Fitton, J. G., George, R., Smith, M. and Barreiro, B. (2000), 'Two mantle plumes beneath the east african rift system: Sr, nd and pb isotope evidence from kenya rift basalts', *Earth and Planetary Science Letters* **176**(3-4), 387–400.

Rooney, T. O., Hanan, B. B., Graham, D. W., Furman, T., Blichert-Toft, J. and Schilling, J.-G. (2011), 'Upper Mantle Pollution during Afar Plume–Continental Rift Interaction',

Journal of Petrology **53**(2), 365–389.
URL: *https://doi.org/10.1093/petrology/egr065*

Saby, M., Pinti, D. L., van Hinsberg, V., Gautason, B., Sigurðardóttir, Á., Castro, C., Hall, C., Óskarsson, F., Rocher, O., Hélie, J. F. and Méjean, P. (2020), 'Sources and transport of fluid and heat at the newly-developed Theistareykir Geothermal Field, Iceland', *Journal of Volcanology and Geothermal Research* **405**, 107062.
URL: *https://doi.org/10.1016/j.jvolgeores.2020.107062*

Sæmundsson, K. (1991), 'Geology of the krafla system', *The Natural History of Lake Myvatn* pp. 24–95.

Sano, Y., Furukawa, Y. and Takahata, N. (2010), 'Atmospheric helium isotope ratio: Possible temporal and spatial variations', *Geochimica et Cosmochimica Acta* **74**(17), 4893–4901.
URL: *https://www.sciencedirect.com/science/article/pii/S0016703710003248*

Sano, Y. and Marty, B. (1995), 'Origin of carbon in fumarolic gas from island arcs', *Chemical Geology* **119**(1-4), 265–274.

Sano, Y., Takahata, N., Igarashi, G., Koizumi, N. and Sturchio, N. C. (1998), 'Helium degassing related to the kobe earthquake', *Chemical Geology* **150**(1), 171–179.
URL: *https://www.sciencedirect.com/science/article/pii/S0009254198000552*

Sano, Y., Urabe, A., Wakita, H., Chiba, H. and Sakai, H. (1985), 'Chemical and isotopic compositions of gases in geothermal fluids in iceland', *Geochemical journal* **19**(3), 135–148.

Sarda, P. and Graham, D. (1990), 'Mid-ocean ridge popping rocks: implications for degassing at ridge crests', *Earth and Planetary Science Letters* **97**(3), 268–289.
URL: *https://www.sciencedirect.com/science/article/pii/0012821X90900472*

Scarsi, P. and Craig, H. (1996), 'Helium isotope ratios in ethiopian rift basalts', *Earth and Planetary Science Letters* **144**(3), 505–516.
URL: *https://www.sciencedirect.com/science/article/pii/S0012821X96001859*

Schilling, J.-G., Kingsley, R. H., Hanan, B. B. and McCully, B. L. (1992), 'Nd-sr-pb isotopic variations along the gulf of aden: Evidence for afar mantle plume-continental lithosphere interaction', *Journal of Geophysical Research: Solid Earth* **97**(B7), 10927–10966.

Scholten, S. O. et al. (1991), *The distribution of nitrogen isotopes in sediments*, Faculteit Aardwetenschappen.

Sheppard, S. M., Nielsen, R. L. and Taylor, H. P. (1971), 'Hydrogen and oxygen isotope ratios in minerals from porphyry copper deposits', *Economic Geology* **66**(4), 515–542.

Sherwood Lollar, B., Ballentine, C. J. and O'Nions, R. K. (1997), 'The fate of mantle-derived carbon in a continental sedimentary basin: Integration of C/He relationships and stable isotope signatures', *Geochimica et Cosmochimica Acta* **61**(11), 2295–2307.

Sigmundsson, F., Hooper, A., Hreinsdóttir, S., Vogfjörd, K., Ófeigsson, B., Rafn Heimisson, E., Dumont, S., Parks, M., Spaans, K., Gudmundsson, G. et al. (2015), 'Rut hjartardóttir á', *Pedersen R., Bennett RA, Geirsson H., La Femina PC, Björnsson H., Pálsson F., Sturkell E., Bean CJ, Möllhoff M., Braiden AK, Eibl EPS, Segmented lateral dyke growth in a rifting event at Bárðarbunga volcanic system, Iceland. Nature* **517**, 191–195.

Skelton, A., Andrén, M., Kristmannsdóttir, H., Stockmann, G., Mörth, C.-M., Sveinbjörnsdóttir, Á., Jónsson, S., Sturkell, E., Guðrúnardóttir, H. R., Hjartarson, H. et al. (2014), 'Changes in groundwater chemistry before two consecutive earthquakes in iceland', *Nature Geoscience* **7**(10), 752–756.

Skelton, A., Liljedahl-Claesson, L., Wästeby, N., Andrén, M., Stockmann, G., Sturkell, E., Mörth, C.-M., Stefansson, A., Tollefsen, E., Siegmund, H., Keller, N., Kjartansdóttir, R., Hjartarson, H. and Kockum, I. (2019), 'Hydrochemical changes before and after earthquakes based on long-term measurements of multiple parameters at two sites in northern iceland—a review', *Journal of Geophysical Research: Solid Earth* **124**(3), 2702–2720.
URL: *https://agupubs.onlinelibrary.wiley.com/doi/abs/10.1029/2018JB016757*

Stab, M., Bellahsen, N., Pik, R., Quidelleur, X., Ayalew, D. and Leroy, S. (2016), 'Modes of rifting in magma-rich settings: Tectono-magmatic evolution of central afar', *Tectonics* **35**(1), 2–38.

Stefansson, R., Gudmundsson, G. B. and Halldorsson, P. (2008), 'Tjörnes fracture zone. new and old seismic evidences for the link between the north iceland rift zone and the mid-atlantic ridge', *Tectonophysics* **447**(1), 117–126. Plate movement and crustal processes in and around Iceland.
URL: *https://www.sciencedirect.com/science/article/pii/S0040195107003794*

Stuart, F. M., Lass-Evans, S., Fitton, J. G. and Ellam, R. M. (2003), 'High 3 he/4 he ratios in picritic basalts from baffin island and the role of a mixed reservoir in mantle plumes', *Nature* **424**(6944), 57–59.

Sucha, V., Uhlík, P., Madejová, J., Petit, S., Kraus, I. and Puskelová, L. (2007), 'Particle properties of hydrothermal ammonium-bearing illite-smectite', *Clays and Clay Minerals* **55**(1), 36–44.

Szymanski, E., Stockli, D., Johnson, P. and Hager, C. (2016), 'Thermochronometric evidence for diffuse extension and two-phase rifting within the central arabian margin of the red sea rift', *Tectonics* **35**(12), 2863–2895.

Thordarson, T. and Larsen, G. (2007), 'Volcanism in iceland in historical time: Volcano types, eruption styles and eruptive history', *Journal of Geodynamics* **43**(1), 118–152. Hotspot Iceland.
URL: *https://www.sciencedirect.com/science/article/pii/S0264370706000652*

Tolstikhin, I., Mamyrin, B., Khabarin, L. and Erlikh, E. (1974), 'Isotope composition of helium in ultrabasic xenoliths from volcanic rocks of kamchatka', *Earth and Planetary*

Science Letters **22**(1), 75–84.
URL: *https://www.sciencedirect.com/science/article/pii/0012821X74900661*

Torgersen, T. (1993), 'Defining the role of magmatism in extensional tectonics: Helium 3 fluxes in extensional basins', *Journal of Geophysical Research: Solid Earth* **98**(B9), 16257–16269.

Torgersen, T. and Clarke, W. (1985), 'Helium accumulation in groundwater, i: An evaluation of sources and the continental flux of crustal 4he in the great artesian basin, australia', *Geochimica et Cosmochimica Acta* **49**(5), 1211–1218.

Torgersen, T. and Jenkins, W. (1982), 'Helium isotopes in geothermal systems: Iceland, the geysers, raft river and steamboat springs', *Geochimica et Cosmochimica Acta* **46**(5), 739–748.

Torres Acosta, V., Bande, A., Sobel, E. R., Parra, M., Schildgen, T. F., Stuart, F. and Strecker, M. R. (2015), 'Cenozoic extension in the kenya rift from low-temperature thermochronology: Links to diachronous spatiotemporal evolution of rifting in east africa', *Tectonics* **34**(12), 2367–2386.

Trieloff, M., Kunz, J., Clague, D. A., Harrison, D. and Allègre, C. J. (2000), 'The nature of pristine noble gases in mantle plumes', *Science* **288**(5468), 1036–1038.

USGS (2023), 'Helium statistics and information'.
URL: *http://minerals.er.usgs.gov/minerals/pubs/commodity/helium/*

Wada, E., Kadonaga, T. and Matsuo, S. (1975), '15n abundance in nitrogen of naturally occurring substances and global assessment of denitrification from isotopic viewpoint', *Geochemical Journal* **9**(3), 139–148.

Walter, B., Géraud, Y., Favier, A., Chibati, N. and Diraison, M. (2023), 'Hydrothermal activity of the lake abhe geothermal field (djibouti): Structural controls and paths for further exploration', *EGUsphere* **2023**, 1–24.
URL: *https://egusphere.copernicus.org/preprints/2023/egusphere-2023-397/*

White, D. E. (1974), 'Diverse origins of hydrothermal ore fluids', *Economic Geology* **69**(6), 954–973.

Wilkinson, M., Gilfillan, S. M., Haszeldine, R. S. and Ballentine, C. J. (2009), 'Plumbing the depths: Testing natural tracers of subsurface co2 origin and migration, utah'.

Wittenberg, L., Cameron, E., Kulcinski, G., Ott, S., Santarius, J., Sviatoslavsky, G., Sviatoslavsky, I. and Thompson, H. (1992), 'A review of 3he resources and acquisition for use as fusion fuel', *Fusion Technology* **21**(4), 2230–2253.

Wolfenden, E., Ebinger, C., Yirgu, G., Renne, P. R. and Kelley, S. P. (2005), 'Evolution of a volcanic rifted margin: Southern red sea, ethiopia', *Geological Society of America Bulletin* **117**(7-8), 846–864.

Wu, J., Liu, Z. and Yu, X. (2021), 'Plagioclase-regulated hydrothermal alteration of basaltic rocks with implications for the south china sea rifting', *Chemical Geology* **585**, 120569.

Zhao, D. (2004), 'Global tomographic images of mantle plumes and subducting slabs: insight into deep earth dynamics', *Physics of the Earth and Planetary Interiors* **146**(1-2), 3–34.

Zimmermann, L. and Bekaert, D. (2020), 'Analyse des gaz rares par spectrométrie de masse statique-théorie et instrumentation', *Techniques de l'ingénieur* .

Zumbo, V., Féraud, G., Vellutini, P., Piguet, P. and Vincent, J. (1995), 'First 40ar39ar dating on early pliocene to plio-pleistocene magmatic events of the afar—republic of djibouti', *Journal of Volcanology and Geothermal Research* **65**(3-4), 281–295.

Annex

Draft of manuscript to be submitted to *Terra Nova*

Origin of helium in crustal fault hydrothermal system: the case of the Eastern part of the Pyrenees

Gaétan Milesi[1], Carolina Dantas Cardoso[2], Raphaël Pik[2], Delphine Charpentier[3], Julien Mercadier[1]

[1] GeoRessources, CNRS, Université de Lorraine, CREGU, 54506 Vandœuvre-lès-Nancy, France

[2] Université de Lorraine, CNRS, CRPG, UMR7358, F-5400, Nancy, France

[3] Chrono-Environnement, UMR 6249-CNRS, Université Bourgogne Franche-Comté, Besançon, France

ABSTRACT

The Eastern Pyrenees have undergone an important crustal thinning associated to major extensional tectonic link to the Gulf of Lion opening. The largest number of hot springs is reported in this part of the Pyrenees, mostly along regional tectonic structures. In this study, we investigated the helium isotopic ratio ($^3He/^4He$) in different hot springs along the Têt and Tech crustal faults. The difference of isotopic ratios observed along the Têt (0.03 and 0.10 Ra) and the Tech fault (0.17 to 0.37 Ra) is indicative of different geothermal reservoirs. $^3He/^4He$ ratios in hydrothermal fluids for the different hot spring clusters show

an increase toward the East and the Gulf of Lion, consistent with the observed thinning of the continental crust in this region. The comparison with helium dataset from the Alps questioned on the role of the seismicity on the helium isotopic ratios in hydrothermal water.

1. INTRODUCTION

The helium isotopes ($^3He/^4He$) allow to reveal source of water in various geological context (e.g. Craig and Lupton, 1976; Andrews, 1985; Marty et al., 1993; Pinti and Marty, 1995,1998; Moreira et al., 2019; Pinti et al., 2022). The two isotopes have different origins, ^3He is primordial from the Earth's mantle (Craig and Lupton, 1976); whereas ^4He originates from U and Th radiogenic decay in minerals present in the continental crust (Ballentine and Burnard, 2002; Moreira, 2013). The helium isotopic signature is therefore a proxy of the original fluid sources in which they were dissolved (e.g. Pinti et al., 2022).

In geothermal systems, fluids reservoirs can be regional (Roche et al., 2018; Kong et al., 2020) or the scale of a massif (Taillefer et al., 2018) or a fault (Duwiquet et al., 2019; Guillou-Frottier et al., 2020). The largest number of hot springs is reported in the eastern part of the Pyrenees, mostly along regional crustal scale faults (Taillefer et al., 2017). This area is also marked by an important thinning of the continental crust from 45 km to 25 km from West to East (Lacan and Ortuno, 2012; Chevrot et al., 2018; Diaz et al., 2018), associated to the Oligocene and earlier extensional tectonic (e.g. Taillefer et al., 2021). In this study, we measured helium isotopes in hot springs along the Têt and Tech faults which are major crustal scale faults. We aim to characterize the geothermal reservoir(s) along these faults but also the impact of regional crustal thinning on the helium isotopic ratios. In the discussion, data obtained in the Eastern Pyrenees are compared to the helium dataset from the Alps obtained by Marty et al. (1992) to discuss the different parameters that can explain the helium isotopic ratios obtained in fault hydrothermal systems.

2. GEOLOGICAL SETTING

2.1 Geological context of the Eastern Pyrenees

In the Pyrenees, the fault network is inherited of a multiple tectonic event with (i) Hercynian ductile deformation highlighted by important mylonitic deformation as visible along the Têt fault (e.g. Cochelin et al., 2017). (ii) Late Cretaceous to the Middle Miocene collision associated to the displacement of the European and Iberic plates (Muñoz, 1992; Vergés et al., 2002). During this period, the Pyrenean Axial Zone has undergone a stack of crustal nappes essentially during the main Eocene-early Oligocene orogenic build up (Jolivet et al., 2007; Mouthereau et al., 2014; Labaume et al., 2016; Vacherat et al., 2016; Waldner et al., 2021). The Eastern part of the Axial Zone (Fig. 1) is characterized by the emplacement of south-verging nappes rooted in the northern part of the Axial Zone (Laumonier et al., 2015; Sibuet et al., 2004; Vergès et al., 1995; Teixell et al., 2016). (iii) Late Priabonian to the Quaternary regional extensional tectonic, particularly well expressed in the Eastern Pyrenes associated to the (re-)activation of major structures as normal faults in response to the Gulf of Lion opening (e.g. Jolivet et al., 2021; Milesi et al., 2022). This regional-scale extension has led to an important crustal thinning at the scale of the Eastern Pyrenees (Fig.1) with a marked thinning of the crust from 45 km to 25 km from West to East (Lacan and Ortuno, 2012; Chevrot et al., 2018; Diaz et al., 2018). A link between crustal thinning and post-Oligocene mantle flow due to the Apennine slab retreat is proposed (Jolivet et al., 2020; 2021; Romagny et al., 2020), that could be expressed by the syn-rift Plio-quaternary volcanism observed along NW-SE faults of El Emporda or Transverse ranges (Fig.1) and high topographic supported by thick crust (Gunnell et al., 2008; Huyghe et al., 2020). In the Eastern Pyrenees, the Têt and Tech faults are the two main NE-SW crustal faults (Fig. 1). These structures display offsets in the Moho (Calvet et al., 2021) and are marked by a polyphased tectonic with Hercynian deformation as suggested by Ar-Ar ages on biotite (300 Ma) obtained in mylonite bordering the Têt fault (Milesi, 2020). Balanced cross-sections from Ternois et al., (2019) suggest an Eocene activity of the Têt fault with the thrusting of the Aspres-Mont-Louis massifs onto the Canigou massif, Tech fault activity during the south-verging nappes displacement is also proposed (Calvet et al., 2021). Thermochronological acquisitions show puri-kilometric displacement accommodated by these faults during the Gulf of Lion opening (Milesi et al., 2022; Maurel, 2003). These observations are also supported by the presence of 2 km thick of sediment in the Roussillon basin (Clauzon et

al., 2015).

2.2 Hydrothermal circulation along the Têt and Tech crustal faults

The Têt and the Tech fault localize active hydrothermal circulations that have been widely studied. The hot spring clusters are essentially localized in the footwall fault damage zone (Taillefer et al., 2017; Milesi et al., 2019). Figure 2 shows a schematic view of hydrothermal circulations; the fluids have a meteoric origin for both faults (Krimissa, 1995; Taillefer et al. 2018). For the Têt fault hydrothermal system altitude of infiltration is above 2000 m for Thuès/Canaveilles (TH) and St-Thomas-les-Bains/Prats-Balaguer (ST) hot spring clusters, between 1800 and 2000 m for Llo and Vernet-les-Bains (VB) hot spring clusters (Taillefer et al., 2018). For Amélie-les-Bains (AM) hot spring cluster, along the Tech fault, a lower altitude of infiltration between 1100 and 1200 m (Krimissa, 1995). For these hydrothermal systems, fluids reached at depth temperature between 80°C and 135°C, variable according to the hot spring cluster (Figure 2). Water residence times based on 14C are similar for the Têt and Tech faults between 5 and 13 ka (Krimissa, 1995). Taillefer et al. (2018) proposed a numerical model of hydrothermal circulations along the Têt fault, main results shows that the (i) topography appears to be the main parameter to initiate hydrothermal circulation and control maximum fluid temperature at depth. (ii) Proposed a model for hydrothermal circulation where the Têt fault hydrothermal system is divided into three parts. The hydrothermal fluids at TH and ST hot spring clusters come from the Carança range and geothermal activity is maximum. The presence of hot springs in the hanging wall of the Têt fault (Rivière, Table 1) questioned on potential thermal fluids from the hanging wall massifs. The negative thermal anomaly along the fault plane between ST and Llo hot spring clusters is interpreted as a fluid recharge area. different origin for Llo and VB hydrothermal fluids is suspected from Puigmal and the Canigou range, repectively.

3. SAMPLING AND ANALYTICAL METHOD 3.1 Sampling

For this study, hydrothermal fluids of Têt and Tech crustal NE-SW faults with similar tectonic history have been investigated. 11 hot springs have been sampled (Table 1), and

those located in the damage zone of the major fault have been favored. 4 hot spring clusters along the Têt fault have been sampled from the West to the East: Llo (1 spring), ST (2), TH (3) and VB (1). Further East, AM (3) hot spring cluster along the Tech fault have been investigated, this sampling is also consistent with the crustal thinning of the eastern Pyrenees (Fig. 1).

3.2 Helium measurement

The analyses of $^{4}He/^{20}Ne$ and $^{3}He/^{4}He$ ratios of gases sampled in copper tubes were performed, respectively, on a MKS Microvision 2 quadrupole mass spectrometer (QMS) and a split flight tube noble gas mass spectrometer (Helix SFT - Thermo Fisher Scientific) at the Centre de Recherches Pétrographiques et Géochimiques (CRPG) noble gas analytical facility (Mabry et al., 2013). The standard deviation of the $^{3}He/^{4}He$ ratios ranged from 2.0 to 3.7 % based on the replicate analysis of standard He (atmospheric). Results are corrected for blanks, which contributed < 0.1 % of the total He abundances (Table 1).

4. RESULTS

$^{4}He/^{20}Ne$ ratios against R/Ra ratios (Craig et al., 1988) obtained on the Eastern Pyrenees hot springs are plotted in Figure 3. For these samples the textsuperscript$^{4}He/^{20}Ne$ ratios range from 1.63 to 85.78, higher than the expected ASW value at 10 ∘C (0.276; Smith and Kennedy, 1983). $^{4}He/^{20}Ne$ ratios of hot spring of the Têt fault are different between clusters but similar inside each; in contrast this ratio is variable (1.63 to 85.78) for AM cluster along the Têch fault (Fig. 3). The textsuperscript$^{4}He/^{20}Ne$ ratio is not correlated with water temperature at the surface (Table 1). The helium isotopic ratios ($^{3}He/^{4}He$) measured in our studied water range from 0.03 to 0.37 Ra, where Ra is the atmospheric $^{3}He/^{4}He$ (1.39×10^{-6}, Graham, 2002). Two distinct groups of samples can be distinguished (i) Têt fault samples ranging between 0.03 and 0.10 Ra and (ii) Tech fault samples between 0.17 and 0.37 Ra (Fig. 3). Along the Têt fault an increase of helium isotopic ratios towards the East is observable. Helium isotopic ratio are 0.03 Ra for Llo hot spring, 0.04 Ra for the 2 hot springs from ST, 0.05 Ra for the 3 hot springs at TH and 0.10 Ra for the hot spring analyzed at VB. $^{3}He/^{4}He$

obtained in the AM hot spring cluster (4 hot springs) along the Tech fault, are more variable at the scale of the cluster between 0.17 to 0.37 Ra compared to the Têt fault, however, this range plots along the mixing line with ASW (Fig. 3).

5. DISCUSSION

5.1 Implications for hydrothermal systems of the Eastern Pyrenees

In this study, helium isotopic ratios obtained are lower for the Têt 0.025-0.05 Ra than the Tech fault hydrothermal system ∼0.17 Ra suggesting a different geothermal reservoir (Fig.4). The hydrothermal fluids have therefore a specific isotopic signature from the massif in which they circulate, the Canigou-Carança-Puigmal massifs for the Têt fault and the Albères for the Tech fault (Fig.1). These results are in agreement with fault-hosted orogenic geothermal systems and fluid reservoirs associated at the scale of a massif and a fault (e.g. Diamond et al., 2018; Taillefer et al., 2018; Wanner et al., 2019). In this part of the Pyrenees, the difference in helium isotopic ratio can be explained by (i) the difference of continental crust thickness <32 km for the Tech fault and between 36 and 40 km for the Têt fault (Fig. 4) and/or (ii) The influence of Tortonian to Plio-quaternary volcanism along NW-SE grabens formed in the transitional area between the Pyrenees and the Catalan Coastal Ranges, visible at the South of the Tech fault (Cebrià et al., 2000; Maillard et al., 2020; Fig. 1).

At the scale of the Têt fault, the increase of helium isotopic ratios toward the East for the different hot spring clusters (Fig. 4) seems more correlated to the crustal thinning than a different geological context along the fault. The differences of helium isotopic ratios between LLo (0.03 Ra), ST (0.04 Ra), TH (0.05 Ra) and VB (0.1 Ra) could mark a difference of geothermal reservoir between VB hot spring cluster than the other hot spring clusters, this result must be interpreted carefully due to the lower $^{4}He/^{20}Ne$ ratio compared to the other samples along the Têt fault. This difference appears consistent with a fluid contribution of the Canigou massif (Fig. 1) as suggested by Taillefer et al. (2018) and the crustal thinning observed. The differences of isotopic ratios observed on less than 30 km for Llo, ST and Th (Fig. 4) hot spring clusters can sign a various water residence time for the different hot spring clusters. The contrast tends to indicate different geothermal reservoirs at the scale of this

fault segment even for very close hot spring clusters like TH and ST clusters as proposed by Milesi et al. (2020). Moreover, the similar isotopic signature for hot spring from the hanging wall (Rivière) seems in favor of footwall origin of fluids rather than a hanging wall fluid contribution. Close $^{4}He/^{20}Ne$ ratios from 28.1 to 61.2 observed suggest low impact of fluid mixing with ASW. These results can be due to a compartmentalization of hydrothermal circulation even at the scale of the fault (Duwiquet et al., 2019; Guillou-Frottier et al., 2020).

5.2 Comparison with helium data from the Alps and Massif Central

Previous helium isotopic data from Marty et al. (1992) obtained on water samples from the Alps and peripherical sites and the Massif Central have been synthetized (Fig. 5, Appendix 1) with crustal thickness associated to each site (after European crustal map of Grab et al., 2009). The main results indicated a first order correlation between isotopic helium ratio and crustal thickness, with the highest ratio for the Massif Central springs (Fig. 5a). These results are consistent with the crustal thickness observed in this region (Fig. 5b) and major mantle dynamic (Granet et al., 1995; Goes et al., 1999). For continental crusts $>$ 30 km, the isotopic helium ratio is below 0.02 R/Ra, except for 4 sites: 3 in the Alps and 1 in the Eastern Pyrenees (Fig. 5b). In the Alps, Pyrawarth (1.6 Ra) and Bad Vôslau (0.45 Ra) springs are located in the Vienna Basin (Austria), the water are a mixture of an old thermal component and a young meteoric component in karst and water level and temperature variation has been correlated with seismicity (Hardege et al., 2019). This is consistent with the presence of the seismically active Vienna Basin Transfer fault (Barõn et al. 2019; Atanackov et al., 2021). The third site is Villach in the Eastern Alps for which the 3 hot springs show isotopic ratio between 0.59 and 0.61 Ra, for a continental crust of 45 km. On this site, the spring of Urquelle has the highest net heat flux of the Alps of 7.0 to 11 MW (Luijendijk et al., 2020), suggesting extremely pronounced hydrothermal activity. This site localized also active faults (Atanackov et al., 2021) and the largest historical regional earthquakes (M$>$6, Galadini et al., 2005; Hammerl, 2017). In the Alps, helium isotopic signature seems influenced by seismically active faults as proposed by Toutain and Baubron (1999), this isotopic record in fault hydrothermal systems appear possible even for thick continental crust.

In the Eastern Pyrenees, the Tech fault shows isotopic values of >0.2 Ra, despite the wide range in textsuperscript4He/^{20}Ne due to mixing with surface water, could be explained by recent volcanism or crustal thinning (see Section 5.2). Regarding the Alps dataset, the helium isotopic signature associated to a moderate seismic activity along this fault cannot be excluded, even if no clear evidence is recorded along this fault (Souriau and Pauchet, 1998; Sylvander et al., 2022).

CONCLUSIONS

Helium isotopic data obtained on fault hydrothermal system of the Eastern Pyrenees show the potential of the method to discuss the geothermal sytems and the scale of hydrothermal circulations. The results obtained on the Têt fault show that it can be possible to distinguished different geothermal circulation at the scale of a fault. The combination with previous data from the Alps and the Massif Central reminds the first order correlation with crustal thickness and demonstrates the importance of the fault activity on helium isotopic ratio that questioned on the origin of helium isotopic ratio (>0.2 Ra) obtained along the Tech fault. Further data on worldwide fault hydrothermal systems are needed to better understand the different processes associated to helium mobility.

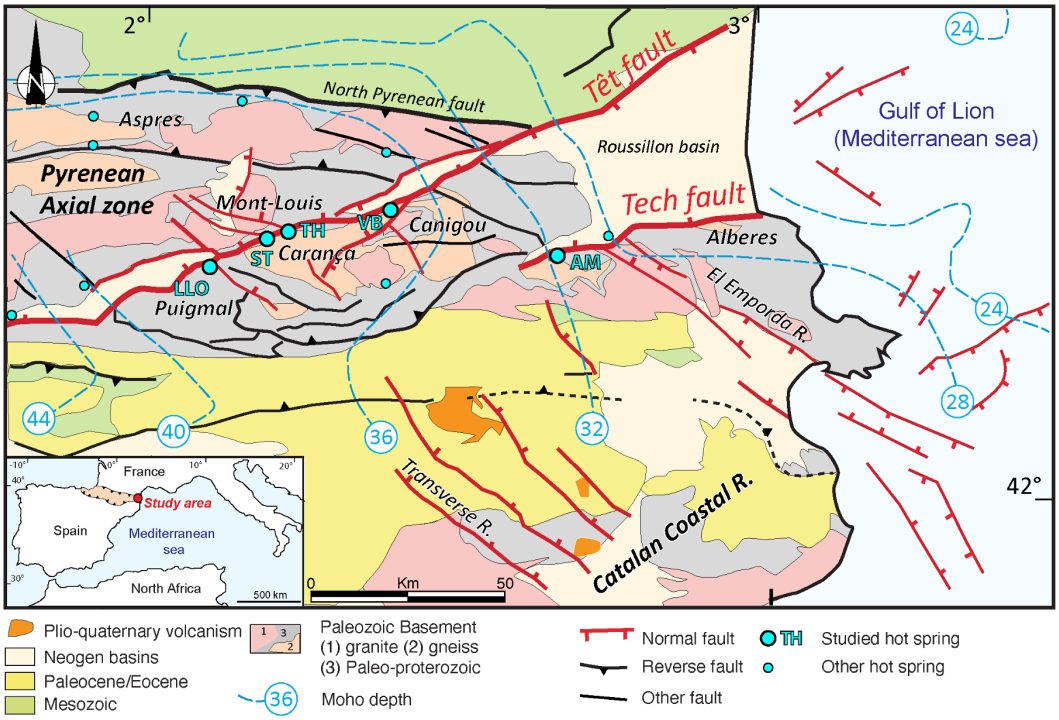

Figure 1: Structural map of Eastern Pyrenees modified after Taillefer et al. (2021). The name of the hot spring clusters studied are indicated: Llo, St-Thomas-les-Bains/Prats-Balaguer (ST), Thuès-les-Bains/Canaveilles (TH), Vernet-les-Bains (VB), Amélie-les-Bains (AM). Moho depth isocontours are modified from Goula et al. (1999), Mauffret et al. (2001) and Nercessian et al. (2001).

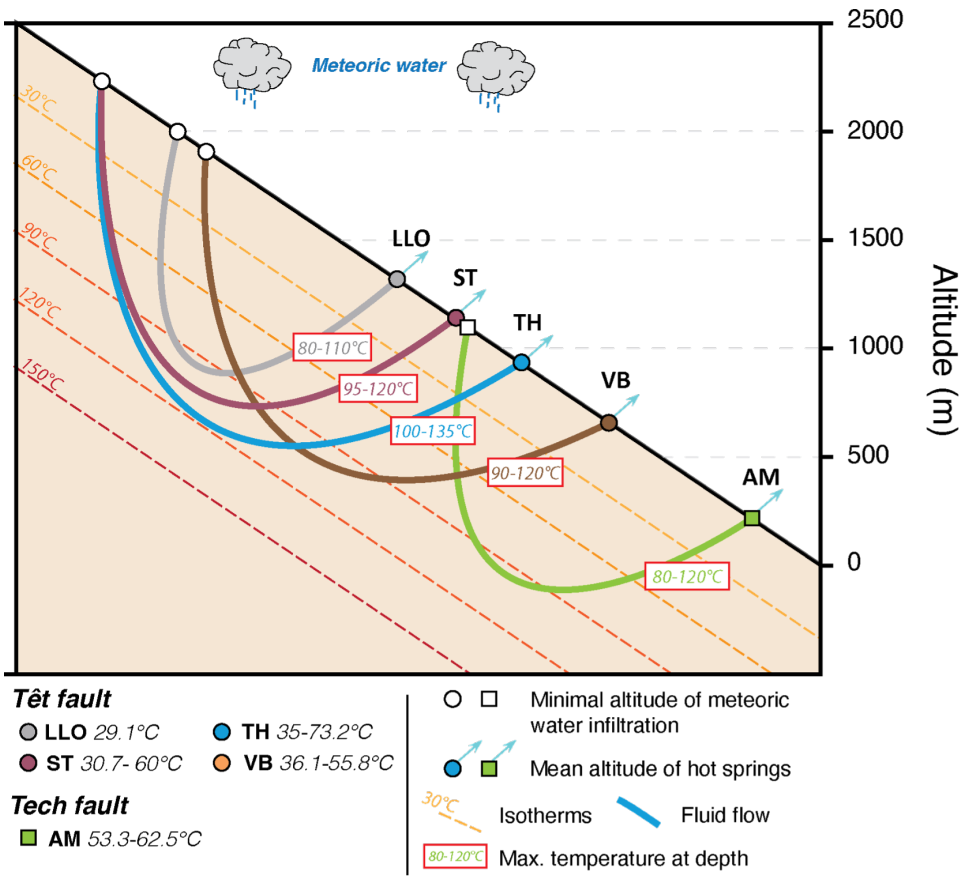

Figure 2: Conceptual model of hydrothermal circulation along the Têt fault for the LLO, ST, TH, VB hot spring clusters and the Tech fault for AM hot spring cluster, modified after Krimissa (2003). The altitude of infiltration and maximum temperature at depth are issued from Taillefer et al. (2018) for the Têt fault and Krimissa (1995) for the Tech fault. The maximal depth of fluid flow paths is not to scale, and we considered a constant geothermal gradient.

	Hot spring cluster	Source name	Lat N	Lon E	Cond. µS/cm	T °C	pH	^{4}He mol	^{4}He mol/g	^{4}He/^{20}Ne	error	R/R$_a$	error
Têt fault	LLO	Llo	42.45113	2.06108	342	29.1	9.4	3.39E-09	5.47E-10	28.1	0.93	0.03	0.001
	ST	Baraquette	42.50079	2.16746	303	46.8	9.3	3.90E-09	4.88E-10	60.7	2.15	0.04	0.001
	ST	Aigues	42.50425	2.18247	317	60.0	9.2	-	-	61.2	1.79	0.04	0.001
	TH	Cascade bas	42.52726	2.24521	323	72.5	9.0	1.13E-09	1.45E-10	46.4	1.49	0.05	0.002
	TH	Lukas	42.52678	2.24156	291	43.2	9.4	1.78E-09	2.22E-10	38.5	1.20	0.05	0.002
	TH	Rivière	42.53142	2.25015	324	60.1	9.1	3.45E-09	4.37E-10	34.9	1.04	0.05	0.002
	VB	Du parc	42.54451	2.38911	299	54.8	9.1	6.94E-10	1.12E-10	5.8	0.16	0.10	0.003
Tech fault	AM	Escaladou	42.46868	2.66789	444	62.5	8.7	9.91E-10	4.50E-10	11.38	0.33	0.22	0.004
	AM	Amélie	42.46999	2.66735	442	55.5	8.9	1.02E-09	5.36E-10	1.63	0.05	0.37	0.008
	AM	En Comes	42.46868	2.66789	444	52.6	8.9	2.49E-09	1.13E-09	22.76	0.75	0.19	0.004
	AM	Petit Monjollet	42.46868	2.66789	441	57.6	8.8	1.15E-08	5.22E-09	85.78	2.71	0.17	0.003

Table 1. Helium isotopic data for Eastern Pyrenees hot springs along the Têt and Tech fault. R is the ^{3}He/^{4}He ratio and Ra is the atmospheric ^{3}He/^{4}He ratio (1.39.10^{-6}, e.g. Graham, 2002)

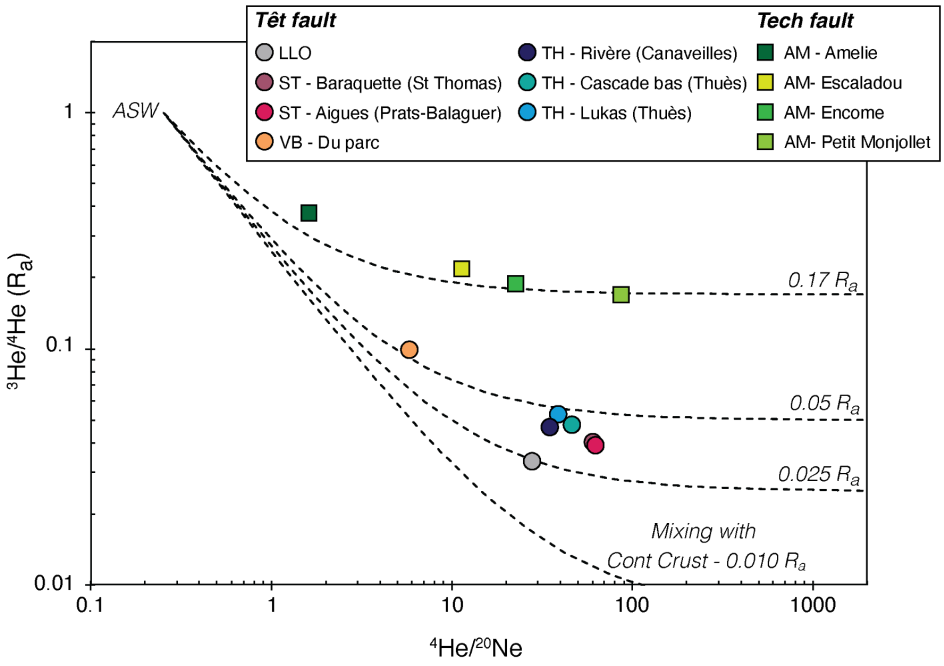

Figure 3: Mixing diagram showing the $^{3}He/^{4}He$ ratio reported against $^{4}He/^{20}Ne$ with the results obtained on the hot springs along the Têt and Tech faults (ASW: Air Saturated Water). Hot springs along Tech fault show are almost 2 times higher $^{3}He/^{4}He$ ratio compared to samples of the Têt fault.

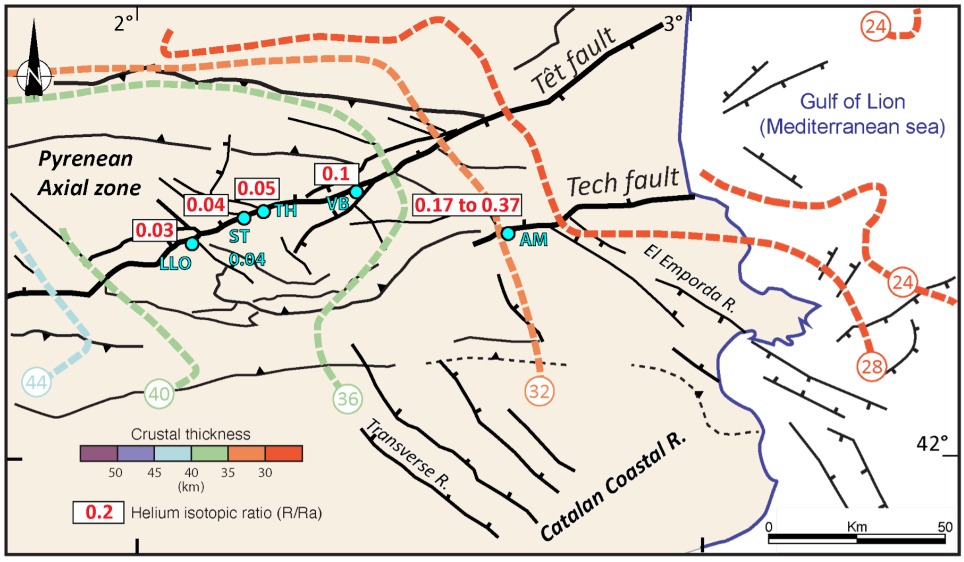

Figure 4: Simplified structural map of Eastern Pyrenees showing helium isotopic ratio obtained and Moho depth isocontours. The map shows the increase of helium isotopic ratio consistent with the crustal thinning towards the West.

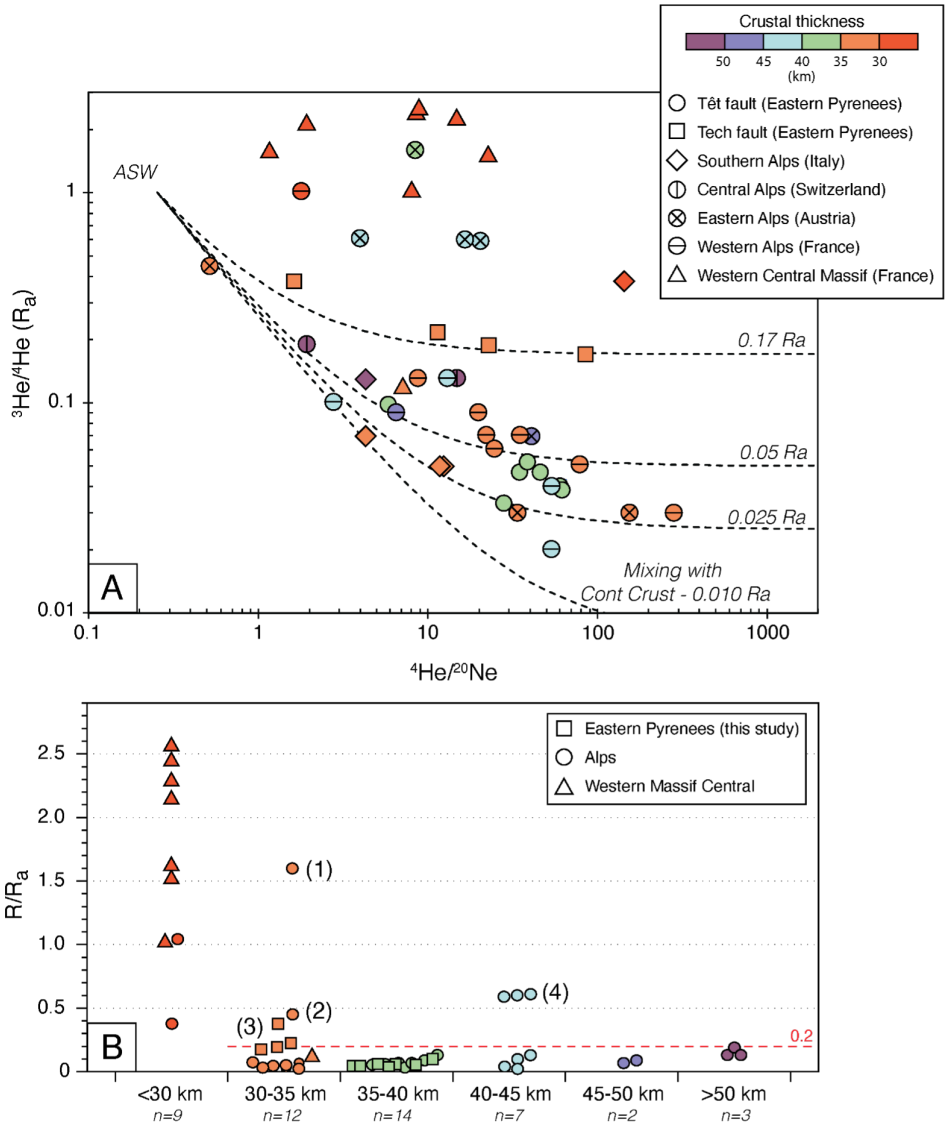

Figure 5: Synthesis of helium data on hydrothermal water from the Eastern Pyrenees (this study), Alps and Massif Central (Marty et al., 1992). The Alps and Massif Central data are available in Appendix 1. A) Mixing diagram showing the $^{3}He/^{4}He$ ratio reported against $^{4}He/^{20}Ne$. B) R/Ra for the different crust thickness. Crustal thickness for the Alps and Massif Central is issued of Grab et al. (2009). Points with R/Ra above 0.2 for normal or thickened continental crust ($>$ 30 km) are from Pyrawarth, Austria (1), Bad Vôslau, Austria (2), Tech fault hot springs (3), Villach hot springs, Austria (4).

References

Andrews, J.N., 1985. The isotopic composition of radiogenic helium and its use to study groundwater movement in confined aquifers: Chemical Geology, 49, p. 339–351,

Atanackov, J., Jamšek Rupnik, P., Jež, J., Celarc, B., Novak, M., Milanič, B., Markelj, A., Bavec, M. and Kastelic, V., 2021. Database of Active Faults in Slovenia: Compiling a New Active Fault Database at the Junction Between the Alps, the Dinarides and the Pannonian Basin Tectonic Domains: Frontiers in Earth Science, 9, p. 604388

Baroň, I., Plan, L., Sokol, L., Grasemann, B., Melichar, R., Mitrovic, I. and Stemberk, J., 2019. Present-day kinematic behaviour of active faults in the Eastern Alps: Tectonophysics, 752, p. 1-23

Calvet, M., Gunnell, Y. and Laumonier, B., 2021. Denudation history and palaeogeography of the Pyrenees and their peripheral basins: an 84-million-year geomorphological perspective: Earth-Science Reviews, 215, p. 103436

Cebriá, J.M., López-Ruiz, J., Doblas, M., Oyarzun, R., Hertogen, J. and Benito, R., 2000a. Geochemistry of the Quaternary alkali basalts of Garrotxa (NE Volcanic Province, Spain): a case of double enrichment of the mantle lithosphere: Journal of Volcanology and Geothermal Research, 102, p. 217-235

Cebriá, J.M., López-Ruiz, J., Doblas, M., Oyarzun, R., Hertogen, J. and Benito, R., 2000b. Geochemistry of the Quaternary alkali basalts of Garrotxa (NE Volcanic Province, Spain): a case of double enrichment of the mantle lithosphere: Journal of Volcanology and Geothermal Research, 102, p. 217-235

Chevrot, S., Sylvander, M., Diaz, J., Martin, R., Mouthereau, F., Manatschal, G., Masini, E., Calassou, S., Grimaud, F., Pauchet, H. and Ruiz, M., 2018. The non-cylindrical crustal architecture of the Pyrenees: Scientific Reports, 8

Clark, I.D., Al, T., Jensen, M., Kennell, L., Mazurek, M. and Mohapatra, R. 2 Paleozoic-age brine preserved in an Ordovician shale aquiclude: Clauzon, G., Le Strat, P., Duvail, C., Do Couto, D., Suc, J.-P., Molliex, S., Bache, F., Besson, D., Lindsay, E.H., Opdyke, N.D., Rubino, J.-L., Popescu, S.-M., Haq, B.U. and Gorini, C., 2015. The Roussillon Basin (S. France): A case-study to distinguish local and regional events between 6 and 3 Ma: Marine and Petroleum Geology, 66, p. 18-40

Cochelin, B., Chardon, D., Denèle, Y., Gumiaux, C. and Le Bayon, B., 2017. Vertical strain partitioning in hot Variscan crust: Syn-convergence escape of the Pyrenees in the Iberian-Armorican syntax: Bulletin de la Société géologique de France, 188, p. 39

Craig, H., Lupton, J.E., Welhan, J.A. and Poreda, R., 1978. Helium isotope ratios in Yellowstone and Lassen Park volcanic gases: Geophysical Research Letters, 5, p. 897-900

Diamond, L.W., Wanner, C. and Waber, H.N., 2018. Penetration depth of meteoric water in orogenic geothermal systems: Geology, 46, p. 1063-1066

Diaz, J., Vergés, J., Chevrot, S., Antonio-Vigil, A., Ruiz, M., Sylvander, M. and Gallart, J., 2018. Mapping the crustal structure beneath the eastern Pyrenees: Tectonophysics, 744, p. 296-309

Galadini, F., Poli, M.E. and Zanferrari, A., 2005. Seismogenic sources potentially responsible for earthquakes with M $\geq$ 6 in the eastern Southern Alps (Thiene-Udine sector, NE Italy): Geophysical Journal International, 161, p. 739-762

Goes, S., Spakman, W. and Bijwaard, H., 1999. A Lower Mantle Source for Central European Volcanism:

Science, 286, p. 1928-1931

Goula, X., Olivera, C., Fleta, J., Grellet, B., Lindo, R., Rivera, L.A., Cisternas, A. and Carbon, D., 1999. Present and recent stress regime in the eastern part of the Pyrenees: Tectonophysics, 308, p. 487-502

Grad, M., Tiira, T., and ESC Working Group, 2009. The Moho depth map of the European Plate: Geophysical Journal International, 176, p. 279-292

Graham, D. W. 2002. Noble gas isotope geochemistry of mid-ocean ridge and ocean island basalts: Characterization of mantle source reservoirs. Reviews in Mineralogy and Geochemistry, 47, 247317

Granet, M., Wilson, M. and Achauer, U., 1995. Imaging a mantle plume beneath the French Massif Central: Earth and Planetary Science Letters, 136, p. 281-296

Guillou-Frottier, L., Duwiquet, H., Launay, G., Taillefer, A., Roche, V. and Link, G., 2020. On the morphology and amplitude of 2D and 3D thermal anomalies induced by buoyancy-driven flow within and around fault zones: Solid Earth, 11, p. 1571-1595

Gunnell, Y., Zeyen, H. and Calvet, M., 2008. Geophysical evidence of a missing lithospheric root beneath the Eastern Pyrenees: Consequences for post-orogenic uplift and associated geomorphic signatures: Earth and Planetary Science Letters, 276, p. 302-313

Hammerl, C., 2017. Historical earthquake research in Austria: Geoscience Letters, 4, p. 7

Hardege, J., Plan, L., Winkler, G., Grasemann, B. and Baroň, I., 2019. Is hydrotectonics influencing the thermal spring in Eisensteinhöhle (Bad Fischau, Lower Austria)? Austrian Journal of Earth Sciences, 112, p. 166-181

Huyghe, D., Mouthereau, F., Ségalen, L. and Furió, M., 2020. Long-term dynamic topographic support during post-orogenic crustal thinning revealed by stable isotope (δ18O) paleo-altimetry in eastern Pyrenees: Scientific Reports, 10

Jolivet, L., Baudin, T., Calassou, S., Chevrot, S., Ford, M., Issautier, B., Lasseur, E., Masini, E., Manatschal, G., Mouthereau, F., Thinon, I. and Vidal, O., 2021. Geodynamic evolution of a wide plate boundary in the Western Mediterranean, near-field versus far-field interactions (O. Lacombe, S. Tavani, A. Teixell, D. Pedreira and S. Calassou, Eds.): BSGF - Earth Sciences Bulletin, 192, p. 48

Jolivet, M., Labaume, P., Monié, P., Brunel, M., Arnaud, N. and Campani, M., 2007. Thermochronology constraints for the propagation sequence of the south Pyrenean basement thrust system (France-Spain): PROPAGATION OF THE SOUTH PYRENEAN PRISM: Tectonics, 26

Jolivet, L., Romagny, A., Gorini, C., Maillard, A., Thinon, I., Couëffé, R., Ducoux, M. and Séranne, M., 2020. Fast dismantling of a mountain belt by mantle flow: Late-orogenic evolution of Pyrenees and Liguro-Provençal rifting: Tectonophysics, 776, p. 228312

Kong, Y., Pang, Z., Pang, J., Li, J., Lyu, M. and Pan, S., 2020. Fault-Affected Fluid Circulation Revealed by Hydrochemistry and Isotopes in a Large-Scale Utilized Geothermal Reservoir: Geofluids, 2020, p. 1-13

Krimissa, M., 1992. Application des méthodes isotopiques a l'étude des eaux thermales en milieu gran-

itique (Pyrénées, France): Orsay Paris-Sud, 237 p. Labaume, P., Meresse, F., Jolivet, M., Teixell, A. and Lahfid, A., 2016. Tectonothermal history of an exhumed thrust-sheet-top basin: An example from the south Pyrenean thrust belt: JACA THRUST-SHEET-TOP BASIN: Tectonics, 35, p. 1280-1313

Lacan, P. and Ortuño, M., 2012. Active Tectonics of the Pyrenees: A review: Journal of Iberian Geology, 38, doi: 10.5209/rev_JIGE.2012.v38.n1.39203. Laumonier, B. Les Pyrénées alpines sud-orientales (France, Espagne) – essai de synthèse: , p. 44

Luijendijk, E., Winter, T., Köhler, S., Ferguson, G., Hagke, C. and Scibek, J., 2020. Using Thermal Springs to Quantify Deep Groundwater Flow and Its Thermal Footprint in the Alps and a Comparison With North American Orogens: Geophysical Research Letters, 47

Mabry, J., Lan, T., Burnard, P. and Marty, B., 2013. High-precision helium isotope measurements in air: Journal of Analytical Atomic Spectrometry, 28, p. 1903

Maillard, A., Jolivet, L., Lofi, J., Thinon, I., Couëffé, R., Canva, A. and Dofal, A., 2020. Transfer zones and associated volcanic province in the eastern Valencia Basin: Evidence for a hot rifted margin? Marine and Petroleum Geology, 119, p. 104419

Marty, B., O'Nions, R.K., Oxburgh, E.R., Martel, D. and Lombardi, S., 1992. Helium isotopes in Alpine regions: Tectonophysics, 206, p. 71-78

Marty, B., Torgersen, T., Meynier, V., O'Nions, R.K. and de Marsily, G., 1993. Helium isotope fluxes and groundwater ages in the Dogger Aquifer, Paris Basin: Water Resources Research, 29, p. 1025-1035

Mauffret, A., de Grossouvre, B.D., Dos Reis, A.T., Gorini, C. and Nercessian, A., 2001. Structural geometry in the eastern Pyrenees and western Gulf of Lion (Western Mediterranean): Journal of Structural Geology, 23, p. 1701-1726

Maurel, O., 2003. L'exhumation de la Zone Axiale des Pyrénées orientales : Une approche thermo-chronologique multi-méthodes du rôle des failles.: , p. 264

Maurel, O., Monièˋ, P., Pik, R., Arnaud, N., Brunel, M. and Jolivet, M., 2008. The Meso-Cenozoic thermo-tectonic evolution of the Eastern Pyrenees: an 40Ar/39Ar fission track and (U-Th)/He thermochronological study of the Canigou and Mont-Louis massifs: International Journal of Earth Sciences, 97, p. 565-584

Milesi, G. Analyse thermochronologique, géochimique et structurale du système hydrothermal de la faille de la Têt (Pyrénées, France), un nouvel outil d'exploration géothermique

Milesi, G., Monié, P., Münch, P., Soliva, R., Taillefer, A., Bruguier, O., Bellanger, M., Bonno, M. and Martin, C., 2020. Tracking geothermal anomalies along a crustal fault using (U-Th)/He apatite thermochronology and rare-earth element (REE) analyses: the example of the Têt fault (Pyrenees, France): Solid Earth, 11, p. 1747-1771

Milesi, G., Monié, P., Soliva, R., Münch, P., Valla, P.G., Brichau, S., Bonno, M., Martin, C. and Bellanger, M., 2022. Deciphering the Cenozoic Exhumation History of the Eastern Pyrenees Along a Crustal-Scale Normal Fault Using Low-Temperature Thermochronology: Tectonics, 41

Milesi, G., Soliva, R., Monié, P., Münch, P., Bellanger, M., Bruguier, O., Bonno, M., Taillefer, A. and

Mayolle, S., 2019. Mapping a geothermal anomaly using apatite (U-Th)/He thermochronology in the Têt fault damage zone, eastern Pyrenees, France: Terra Nova, 31, p. 569-576

Moreira, M., Escartin, J., Scelin, L., Ruzié-Hamilton, L., Nomikou, P., Mével, C. and Andreani, M., 2019. New insights into the plumbing system of Santorini using helium and carbon isotopes: Geochemical Perspectives Letters, p. 46-50

Mouthereau, F., Filleaudeau, P.-Y., Vacherat, A., Pik, R., Lacombe, O., Fellin, M.G., Castelltort, S., Christophoul, F. and Masini, E., 2014. Placing limits to shortening evolution in the Pyrenees: Role of margin architecture and implications for the Iberia/Europe convergence: Plate convergence in the Pyrenees: Tectonics, 33, p. 2283-2314

Muñoz, J. A. (1992). Evolution of a continental collision belt: ECORS-Pyrenees crustal balanced cross-section. Thrust tectonics, 235-246

Nercessian, A., Mau, A., Gallart, J. and Diaz, J., 2001. Deep reflection seismic images of the crustal thinning in the eastern Pyrenees and western Gulf of Lion: Journal of Geodynamics,. Pinti, D.L. and Marty, B., 1995. Noble gases in crude oils from the Paris Basin, France: Implications for the origin of fluids and constraints on oil-water-gas interactions: Geochimica et Cosmochimica Acta, 59, p. 3389-3404

Pinti, D.L. and Marty, B., 1998. The origin of helium in deep sedimentary aquifers and the problem of dating very old groundwaters: Geological Society, London, Special Publications, 144, p. 53-68

Romagny, A., Jolivet, L., Menant, A., Bessière, E., Maillard, A., Canva, A., Gorini, C. and Augier, R., 2020. Detailed tectonic reconstructions of the Western Mediterranean region for the last 35 Ma, insights on driving mechanisms (O. Lacombe, S. Tavani, A. Teixell, D. Pedreira and S. Calassou, Eds.): BSGF - Earth Sciences Bulletin, 191, p. 37

Sibuet, J.-C., Srivastava, S.P. and Spakman, W., 2004. Pyrenean orogeny and plate kinematics: PYRENEAN OROGENY AND PLATE KINEMATICS: Journal of Geophysical Research: Solid Earth, 109

Smith, S.P. and Kennedy, B.M., 1983. The solubility of noble gases in water and in NaCl brine: Geochimica et Cosmochimica Acta, 47, p. 503-515

Souriau, A. and Pauchet, H., 1998. A new synthesis of Pyrenean seismicity and its tectonic implications: Tectonophysics, 290, p. 221-244

Sylvander, M., Rigo, A., Sénéchal, G., Battaglia, J., Benahmed, S., Calvet, M., Chevrot, S., Douchain, J.-M., Grimaud, F., Letort, J. and Pauchet, H., 2022. Seismicity patterns in southwestern France: Comptes Rendus. Géoscience, 353, p. 79-104

Taillefer, A., Guillou-Frottier, L., Soliva, R., Magri, F., Lopez, S., Courrioux, G., Millot, R., Ladouche, B. and Le Goff, E., 2018. Topographic and Faults Control of Hydrothermal Circulation Along Dormant Faults in an Orogen: Geochemistry, Geophysics, Geosystems

Taillefer, A., Milesi, G., Soliva, R., Monnier, L., Delorme, P., Guillou-Frottier, L. and Le Goff, E., 2021. Polyphased brittle deformation around a crustal fault: A multi-scale approach based on remote sensing and field data on the mountains surrounding the Têt hydrothermal system (Eastern Pyrénées, France):

Tectonophysics, 804, p. 228710

Taillefer, A., Soliva, R., Guillou-Frottier, L., Le Goff, E., Martin, G. and Seranne, M., 2017. Fault-Related Controls on Upward Hydrothermal Flow: An Integrated Geological Study of the Têt Fault System, Eastern Pyrénées (France): Geofluids, 2017, p. 1-19

Teixell, A., Labaume, P., Ayarza, P., Espurt, N., de Saint Blanquat, M. and Lagabrielle, Y., 2018. Crustal structure and evolution of the Pyrenean-Cantabrian belt: A review and new interpretations from recent concepts and data: Tectonophysics, 724–725, p. 146-170

Ternois, S., Odlum, M., Ford, M., Pik, R., Stockli, D., Tibari, B., Vacherat, A. and Bernard, V., 2019. Thermochronological Evidence of Early Orogenesis, Eastern Pyrenees, France: Tectonics, 38, p. 1308-1336

Toutain, J.-P. and Baubron, J.-C., 1999. Gas geochemistry and seismotectonics: a review: Tectonophysics, 304, p. 1-27

Vacherat, A., Mouthereau, F., Pik, R., Bellahsen, N., Gautheron, C., Bernet, M., Daudet, M., Balansa, J., Tibari, B., Pinna Jamme, R. and Radal, J., 2016. Rift-to-collision transition recorded by tectonothermal evolution of the northern Pyrenees: COOLING HISTORY OF THE NORTHERN PYRENEES: Tectonics, 35, p. 907-933

Vergés, J., Fernàndez, M. and Martìnez, A., 2002. The Pyrenean orogen: pre-, syn-, and post-collisional evolution: Journal of the Virtual Explorer, 08

Vergés, J., Millán, H., Roca, E., Muñoz, J.A., Marzo, M., Cirés, J., Bezemer, T.D., Zoetemeijer, R. and Cloetingh, S., 1995. Eastern Pyrenees and related foreland basins: pre-, syn- and post-collisional crustal-scale cross-sections: Marine and Petroleum Geology, 12, p. 903-915

Waldner, M., Bellahsen, N., Mouthereau, F., Bernet, M., Pik, R., Rosenberg, C.L. and Balvay, M., 2021. Central Pyrenees Mountain Building: Constraints From New LT Thermochronological Data From the Axial Zone: Tectonics, 40

Wanner, C., Diamond, L.W. and Alt-Epping, P., 2019. Quantification of 3-D Thermal Anomalies From Surface Observations of an Orogenic Geothermal System (Grimsel Pass, Swiss Alps): Journal of Geophysical Research: Solid Earth, 124, p. 10839-10854